Tumor Targeting of the Human Epidermal Growth Factor Receptor 2 with Designed Ankyrin Repeat Proteins

DISSERTATION

zur Erlangung der naturwissenschaftlichen Doktorwürde

(Dr. sc. nat.)

vorgelegt der

Mathematisch-naturwissenschaftlichen Fakultät der Universität Zürich

von

Christian Jost

aus Deutschland

Promotionskomitee

Prof. Dr. Andreas Plückthun (Vorsitz)

Prof. Dr. Nancy Hynes

Prof. Dr. Peter Sonderegger

Prof. Dr. Uwe Zangemeister-Wittke

Zürich 2013

Die vorliegende Arbeit wurde von der Mathematisch-Naturwissenschaftlichen Fakultät der Universität Zürich auf Antrag von Prof. Dr. Andreas Plückthun als Dissertation angenommen.

Publications

Jost, C.; Tamaskovic, R.; Morrison, S.; Plückthun, A. (2013).
"Designed Ankyrin Repeat Proteins engineered to cause cytostatic effects on HER2-addicted cancer cells",
Manuscript

Jost, C.; Schilling, J.; Tamaskovic, R.; Schwill, M.; Honegger, A.; Plückthun, A. (2013).
"Structural Basis for eliciting a cytotoxic effect in HER2-addicted cancer cells via binding to the extracellular domain of HER2",
submitted Manuscript

Tamaskovic, R.; Schwill, M.; Jost, C.; Schaefer, D.C.; Nagy-Davidescu, G.; Göranson, M.; Honegger, A.; Plückthun, A. (2013).
"Intermolecular Bi-epitopic Trapping of ErbB2 Disables ErbB Network and Induces Apoptosis in ErbB2-Addicted Tumors",
submitted Manuscript

Friedrich, K.; Hanauer, J.R.; Prüfer, S.; Münch, R.C.; Völker, I.; Filippis, C.; Jost, C.; Hanschmann, K.M.; Cattaneo, R.; Peng, K.W.; Plückthun, A.; Buchholz, C.J.; Cichutek, K.; Mühlebach, M.D. (2013).
"DARPin-targeting of Measles Virus: Unique Bispecificity, Effective Oncolysis, and Enhanced Safety",
Molecular Therapy

Gu, G.J.; Friedman, M.; Jost, C.; Johnsson K.; Kamali-Moghaddam, M.; Plückthun, A.; Landegren, U.; Söderberg, O. (2012).
"Protein tag-mediated conjugation of oligonucleotides to recombinant affinity binders for proximity ligation",
New Biotechnology

Frei, A.P.; Jeon, O.Y.; Kilcher, S.; Moest, H.; Henning, L.M.; Jost, C.; Plückthun, A.; Mercer, J; Aebersold, R.; Carreira, E.M.; Wollscheid, B. (2012).
"Direct identification of ligand-receptor interactions on living cells and tissues",
Nature Biotechnology 30:997-1001.

Münch, R.C.; Mühlebach, M.D.; Schaser, T.; Kneissl, S.; Jost, C.; Plückthun, A.; Cichutek, K.; Buchholz, C.J. (2011).
"DARPins: An Efficient Targeting Domain for Lentiviral Vectors",
Molecular Therapy 19:686-693.

Epa, V.C.; Dolezal, O.; Doughty, L.; Xiao, X.; Jost, C.; Plückthun, A.; Adams, T.E. (2013)
"Structural Model for the Interaction of a Designed Ankyrin Repeat Protein with the Human Epidermal Growth Factor Receptor 2"
PLOS ONE

PDB-entries

4HRL (HER2_I–9_29)
Authors: Jost, C.; Schilling, J.; Plückthun, A.

4HRM (HER2_I–9_26)
Authors: Jost, C.; Schilling, J.; Plückthun, A.

4HRN (HER2_IV–G3)
Authors: Jost, C.; Schilling, J.; Plückthun, A.

Patent

Tamaskovic, R.; Jost, C.; Schwill, M.; Plückthun, A. (2012) "Bispecific HER2 ligands for cancer therapy"
Application No. 12192465.8 – 2406 (date of filing 13.11.12)

Erklärung

Diese Dissertation im Fach Biochemie wurde von Prof. Dr. Andreas Plückthun betreut.

Die Dissertation wurde selbstständig, ohne unerlaubte Hilfe angefertigt. Bei der Abfassung der Dissertation wurden im Sinne von § 3 lit. 1 der Promotionsverordnung vom 08. Juli 2002 keine anderen als die angegebenen Hilfsmittel verwendet.

Zürich, im Juni 2013

Christian Jost

To my parents

Acknowledgments

I would like to express my gratitude to Prof. Dr. Andreas Plückthun for consigning me to continue working on the HER2-binding DARPins characterized during my Diploma thesis. It is still amazing to me, how many different questions and side projects could be (and still are) tackled from this great starting point on. I am thankful for Andreas' clever suggestions – great starting points to think and work, and for giving the freedom to implement own ideas at any time and to later on profit from his valuable feedback. Andreas' faith in his staff in combination with his well equipped lab environment allowed me to gain insight into many different aspects of science and various lab techniques on state-of-the-art level.

I would also like to thank Prof. Dr. Nancy Hynes, Prof. Dr. Peter Sonderegger and Prof. Dr. Uwe Zangemeister-Wittke for serving as my thesis committee and for their helpful advice during our meetings. Further thanks to Dr. Eric Sedlak, Marco Schütz and Pascal Eglof for creating a brilliant atmosphere in our lab M82.

I also wish to thank Johannes Schilling for our excellent collaboration on X-ray crystallography and for his constant support as a reliable friend. Further thanks to Karola Schlinkmann and Marc-Simon Schwer for moral support and to my former Master students Hannes Richter, Jakob Stüber, Rahel Schnellmann and Ye Xie – it was fun to work with you and I learned a lot!

Of course, special thanks go to Dr. Peter Lindner for taking care of everything necessary to keep our laboratory running and to all present and former colleagues in the Plückthun lab for creating such a nice working atmosphere. Great thanks also to Petra Vogt and Ilse Plückthun for a great administration job, Dr. Stefan Klauser and Steve Rast for IT support, Adrian Schmid & Sascha Weidner for technical support and Sibylle Strassmann for material supply.

I wish to thank the Krebsliga Schweiz and the Swiss National Science Foundation for financial support by consecutive grants and the Swiss Society for Biochemistry and the Molecular Life Science PhD Program Zurich for providing generous travel grants.

My biggest thank goes to Steffi, my sisters Katrin and Lisa and my parents, who I can always count on. Thank you for your understanding, support, tolerance and love.

Contents in Brief

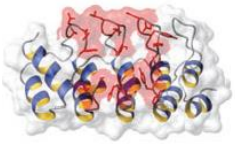

Chapter 1
Introduction **1**

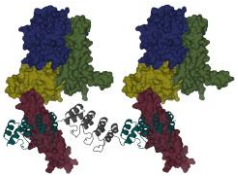

Chapter 2
Designed Ankyrin Repeat Proteins engineered to cause cytostatic effects on HER2-addicted cancer cells **19**

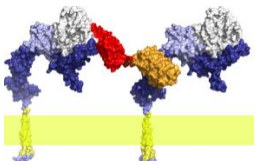

Chapter 3
Structural Basis for eliciting a cytotoxic effect in HER2-addicted cancer cells via binding to the extracellular domain of HER2 **42**

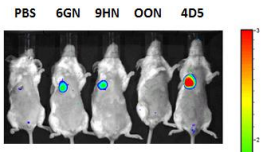

Chapter 4
Intermolecular Bi-epitopic Trapping of ErbB2 Disables ErbB Network and Induces Apoptosis in ErbB2-Addicted Tumors **XX**

Chapter 5 **XX**
Further Methods and Results

Chapter 6 **XX**
Discussion, Conclusions and Outlook

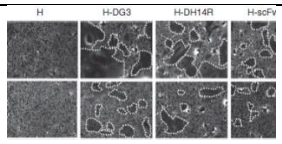

Appendix 1
DARPins: An Efficient Targeting Domain for Lentiviral Vectors **XX**

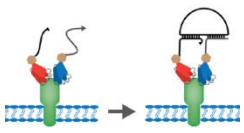

Appendix 2
Protein-tag mediated conjugation of oligonucleotides to recombinant affinity binders for proximity ligation **XX**

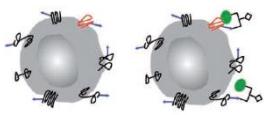

Appendix 3
Direct identification of ligand-receptor interactions on living cells and tissues **XX**

Appendix 4
Structural Model for the Interaction of a DARPin with the Human Epidermal Growth Factor Receptor 2 **XX**

Appendix 5 **XX**
Abbreviations, Lists, Curriculum vitae

Contents

Chapter 1 Introduction 19

1 General Introduction 2

1.1 Targeted tumor therapy 2

1.2 ErbB receptors: architecture and mode of action 4

1.3 Peculiarities of ErbB receptor family members 6

1.4 ErbB receptors and cancer 7

1.5 Different routes of ErbB tumor targeting 8

1.6 Trastuzumab – the first mAb FDA approved for α-HER2 tumor targeting 8

1.7 Modes of action of trastuzumab 9

1.8 New models of ErbB receptor activation 10

1.9 New therapeutic modalities 11

1.10 Designed Ankyrin Repeat Proteins (DARPins) 12

2 The Project 14

3 References 16

Chapter 2 Designed Ankyrin Repeat Proteins engineered to cause cytostatic effects on HER2-addicted cancer cells 19

1 Abstract 21

2 Introduction 22

3 Results and Discussion 24

3.1 Screening HER2-binding DARPins for antitumor activity 24

3.2 Epitope-mapping of DARPin H14 25

3.3 Competition with trastuzumab and evaluation of ectodomain-shedding 26

3.4 Importance of epitope and bivalent binding for antitumor activity 26

3.5 H14 in flexibly linked bivalent format promotes BT474 cell proliferation 27

3.6 Engineering of H14-constructs for improved antitumor activity 27

3.7 Transfering the inflexible linker format to DARPin G3 28

4 Materials and Methods 29

4.1 Cell culture 29

4.2 Cell-proliferation assays (XTT assays) 29

4.3 Cloning, Expression and Purification of DARPins 29

4.4 ELISA 30

4.5 Surface Plasmon Resonance (SPR, Biacore) 30

4.6 Epitope characterization via flow cytometry competition 31

4.7 Receptor Shedding assays 31

4.8 Receptor recycling assay via flow cytometry 31

4.9 Expression and purification of scFv 4D5 32

5 Conclusions 32

6 References 35

Chapter 3 Structural Basis for eliciting a cytotoxic effect in HER2-addicted cancer cells via binding to the extracellular domain of HER2 .. 41

1 Summary 44

2 Highlights 44

3 Introduction 44

4 Results 48

4.1 Epitope-mapping of HER2-binding DARPins 48

4.2 Construction of bispecific binders targeting different epitopes 48

4.3 Effects of mono- and bivalent constructs on cell proliferation and cell death 49

4.4 X-Ray Crystal Structures of complexes HER2_I:9_29, HER2_I:9_26 and HER2_IV:G3 50

4.5 Molecular modeling of full HER2 and DARPin-inhibited states 52

5 Discussion 55

5.1 Monomeric DARPins do not interfere with HER2 signaling 55

5.2 Activity depends on linker length 56

5.3 The linker length is too short for both DARPins to bind to the same HER2 monomer or dimer 57

5.4 Orientation of HER2 on the cell surface 57

5.5 Conformational flexibility of the HER2 extracellular domain 58

5.6 Interference with HER2 dimerization and activation 58

6 Conclusions 59

7 Experimental Procedures 61

7.1 Cloning, Expression and Purification of DARPins 61

7.2 Cell culture 61

7.3 Flow cytometry 61

7.4 Cell viability assays (XTT assays) 62

7.5 Expression in insect cells 62

7.6 X-ray crystallography 62

8 Acknowledgements....63

9 References....65

10 Supplementary Material....73

Chapter 4 Intermolecular Bi-epitopic Trapping of ErbB2 Disables ErbB Network and Induces Apoptosis in ErbB2-Addicted Tumors.... 85

1 Summary....89

2 Significance....89

3 Highlights....90

4 Introduction....90

5 Results....94

5.1 Bispecific DARPins crosslink two HER2 Molecules on the Surface of BT474 Cells....95

5.2 Molecular Models of Bispecific DARPins in Complex With Full-Length ErbB2 Explain their Activity....95

5.3 Anti-proliferative Activity of Bispecific DARPins In Vitro....98

5.4 Induction of G1 Arrest and Apoptosis....99

5.5 Anti-Tumor Activity of Bispecific DARPins In Vivo....100

5.6 Active Bispecific DARPins do not Influence ErbB2 Internalization....102

5.7 Inhibition of ErbB2 Heterodimerization by Bispecific DARPins in the Presence and Absence of Ligands....103

5.8 Bispecific DARPins Retain Anti-proliferative Activity in the Presence of HRG....104

5.9 Inhibition of Three-Dimensional Spheroid Growth and Morphogenesis....104

5.10 Bispecific DARPins Inhibit Cell Migration after Ligand Stimulation....105

5.11 Bispecific DARPins but not Trastuzumab Inhibit ErbB2 Phosphorylations....105

5.12 Bispecific DARPins Inhibit ErbB3 Phosphorylation by ErbB2 106

5.13 Bispecific DARPins also Inhibit ErbB3 Activation after HRG Stimulation 107

5.14 Bispecific DARPins Efficiently Inhibit the PI3K/PKB Pathway 107

5.15 Bispecific DARPins Efficiently Inhibit the MAPK Pathway 108

5.16 Downstream Effects of Bispecific DARPins on the Cell Cycle 109

5.17 Downstream Effects of Bispecific DARPins on Apoptosis 109

5.18 Plasticity of ErbB2 Signaling Network and Resistance against Anti-ErbB2 Treatments 109

6 Discussion 110

6.1 The Pathway of Apoptosis Induction by bispecific DARPins 111

6.2 Non-liganded ErbB2–ErbB3 Heterodimers 111

6.3 Ligand-induced Heterodimers 112

6.4 ErbB2 Homodimers 113

6.5 3D Model and Mechanism 114

6.6 Interconnection of ERK and PKB Pathway 115

6.7 Overcoming Clinical Resistance 116

7 Conclusions 117

8 Experimental Procedures 117

8.1 Cell Culture 117

8.2 XTT Cell Proliferation Assay 117

8.3 Clonogenic Assay 118

8.4 Cell Migration Assay 118

8.5 Three-dimensional Growth Assay 118

8.6 Flow cytometery: Cell Cycle, TUNEL and Annexin V 119

8.7 Mouse Xenograft Studies 119

9 Acknowledgements 120

10 References 121

Chapter 5 Further Methods and Results 155

1 Introduction 156

2 Construction of bivalent DARPins 157

2.1 Construction of vectors coding for flexible linkers with various lengths 157

2.2 Construction of vectors coding for various rigid DARPin linkers 158

2.3 Construction of pQi_scZIP and pQi_scdHLX 162

3 Approaches to gain insight into the DARPins' epitopes 163

3.1 Refolding of HER2_IV 164

3.2 Refolding of further extracellular HER2-subdomains 171

3.3 Chemical Linkage of Peptides onto Scaffolds (CLiPS) 173

3.4 Xtal- conditions screened 175

3.5 Preliminary work and cloning for Sf9-expression 192

3.6 Immunoprecipitation with DARPins 194

3.7 Cell proliferation assays with further interesting constructs 197

4 References 201

Chapter 6 Discussion, Conclusions and Outlook 203

1 Discussion and Conclusions 204

2 Outlook 206

3 References 209

Appendix 1 DARPins: An Efficient Targeting Domain for Lentiviral Vectors 211

Appendix 2 Protein tag-mediated conjugation of oligonucleotides to recombinant affinity binders for proximity ligation..... 221

Appendix 3 Direct indentification of ligand-receptor interactions on living cells and tissues..... 231

Appendix 4 Structural Model for the Interaction of a Designed Ankyrin Repeat Protein with the Human Epidermal Growth Factor Receptor 2 247

Appendix 5 259

1 Abbreviations 260

2 Relevant *E. coli* strains..... 262

2.1 *E. coli* XL1-blue 262

2.2 *E. coli* DH10 EmBacY.....262

3 Curriculum vitae..... 264

Abstract

Binding molecules recognizing their target molecules with high affinity and specificity are important tools for many biotechnological and pharmaceutical applications. Especially in targeted tumor therapy, where specific recognition of cancer cells via their particular oncogenes is used as starting point for the selective treatment of these cells, such binding molecules are indispensable.

The development of new generations of binding molecules within the last years has fostered novel strategies and approaches of targeted tumor therapy. One example of such alternative binders are Designed Ankyrin Repeat Proteins (DARPins). The focus of this thesis lies on the exploration of DARPins binding the oncogene HER2 (human epidermal growth factor receptor 2) for tumor targeting approaches.

Since HER2 functions via dimerization, and since HER2-overexpressing cancer cells – so called HER2-addicted cells – are dependent on the pro-proliferative signals that are elicited by HER2-dimerization, the overall idea pusued in this project was to use HER2-binding DARPins to prevent HER2-dimerization.

In the first part of this project, screening via cell proliferation assays with monovalent HER2-binding DARPins previously selected by ribosome or phage display identified one DARPin with an anti-proliferative effect on the HER2-overexpressing cell line BT474.

The second part of the project then focussed on the development of bivalent and bispecific DARPin-formats which elicit stronger anti-proliferative, in the best case even cytotoxic effects on such cells.

The mechanism of action by which the developed bispecific constructs cause their cytotoxic effects can be described, mainly with the aid of three crystal structures of DARPin-target complexes that were solved in this work.

In conclusion, this work describes the development of new tumor targeting reagents which act via a so far undescribed mechanism. We envision that the generic structure of the presented binding reagents might allow to apply the drawn conclusions onto other oncogenes that act via dimerization.

Zusammenfassung

Bindemoleküle, die Zielmoleküle mit hoher Affinität und Spezifität erkennen, sind wichtige Werkzeuge für viele biotechnologische und pharmazeutische Anwendungen. Speziell in der tumorgerichteten Therapie, in der die spezifische Erkennung von Krebszellen anhand spezieller Onkogene als Dreh- und Angelpunkt für die selektive Behandlung dieser Zellen genutzt wird, sind solche Bindemoleküle unverzichtbar.

Die Entwicklung neuer Generationen von Bindemolekülen innerhalb der letzten Jahre hat zu neuen Strategien und Ansätzen der tumorgerichteten Therapie geführt. Ein Beispiel für solche alternativen Binder sind *Designed Ankyrin Repeat Proteins* (DARPins). Der Fokus dieser Doktorarbeit liegt in der Erkundung von DARPins gegen das Onkogen HER2 (humaner epidermaler Wachstumsfaktor Rezeptor 2) für die gerichtete Tumortherapie.

Da HER2 via Dimerisierung aktiviert wird, und da HER2-überexprimierende Krebszellen – so genannte HER2-abhängige Zellen – abhängig von den wachstumsfördernden Signalen sind, die durch die HER2-Dimerisierung ausgelöst werden, lag die übergreifende Idee des Projekts darin, HER2-bindende DARPins zur Verhinderung der HER2-Dimerisierung einzusetzen.

Im ersten Teil des Projekts wurde mittels Zellwachstum-basiertem *Screening* mit DARPins aus *ribosome* und *phage display* Selektionen ein monovalentes DARPin identifiziert, das einen wachstumshemmenden Effekt auf die HER2-überexprimierende Zelllinie BT474 hat.

Der zweite Teil des Projekts richtete sich auf die Entwicklung von bivalenten und bispezifischen DARPin-Formaten, mit stärkeren wachstumshemmenden Effekten.

Der Wirkungsmechanismus, durch den die entwickelten bispezifischen Konstrukte ihre zytotoxischen Effekte auslösen, kann hauptsächlich mithilfe dreier Kristallstrukturen von Komplexen aus DARPin und Zielmolekül beschrieben werden, die in dieser Arbeit gelöst wurden.

Schlussendlich beschreibt diese Arbeit die Entwicklung eines neuen gerichteten Krebsmedikaments, das durch einen bislang unbeschriebenen Mechanismus wirkt. Wir erhoffen uns, dass die generische Struktur der präsentierten Reagenzien es ermöglichen wird, die gezogenen Schlussfolgerungen auf andere durch Dimerisierung wirkende Onkogene zu übertragen.

Chapter 1
Introduction

Contents

1 General Introduction 2

1.1 Targeted tumor therapy 2

1.2 ErbB receptors: architecture and mode of action 4

1.3 Peculiarities of ErbB receptor family members 6

1.4 ErbB receptors and cancer 7

1.5 Different routes of ErbB tumor targeting 8

1.6 Trastuzumab – the first mAb FDA approved for α-HER2 tumor targeting 8

1.7 Modes of action of trastuzumab 9

1.8 New models of ErbB receptor activation 10

1.9 New therapeutic modalities 11

1.10 Designed Ankyrin Repeat Proteins (DARPins) 12

2 The Project 14

3 References 16

1 General Introduction

According to the US-american National Institutes of Health (NIH), cancer is the leading cause of death in developed countries and the second leading cause of death in developing countries. Besides the rather traditional methods of surgery, chemo- and radiation therapy, progress in oncological treatment has also been made with other, more contemporary methods which make use of the increased understanding of the biological and biochemical properties of cancer cells. Unraveling of pathways and characteristics of different tumor entities like the description of tumor-associated proteins has led to new possibilities in tumor therapy. Since the overall aim of cancer therapy is to kill all tumor cells without interfering with any healthy cells, targeted tumor therapy has raised hope towards a better, because more directed, therapy.

1.1 Targeted tumor therapy

„Targeted tumor therapy“ also known as “Molecularly targeted therapy” encompasses a wide variety of different medication strategies to block the growth of cancer cells by interfering with tumor specific molecules (called “targets”) that constitute tumor growth. One way to classify the different approaches of targeted therapy is to divide them into “direct” and “indirect” approaches (Schrama *et al.* (2006)).

“Direct approaches” function through sole binding, meaning that the binding molecules achieve effects on tumor cells without being conjugated to e.g. a cytotoxic moietiy. The main category of molecules that belong to such direct approaches are the so called “small molecule drugs”. The largest subgroup within the group of “small molecule drugs” are kinase inhibitors (which is not surprising, as kinases are the biggest group of enzymes important for cell proliferation), but the “small molecule drugs” comprise furthermore molecules acting on other – normally intracellular – targets, like inhibitors of the proteasome (e.g. Bortezomib (Teicher *et al.* (1999))), estrogen receptor modulators (e.g. tamoxifen (Jordan and Koerner (1976))), binders to apoptosis regulator proteins (e.g. obatoclax binding Bcl-2 (Shore and Viallet (2005))) or PARP inhibitors (e.g. iniparib (Mendeleyev *et al.* (1995))).

"Indirect approaches" generally use the tumor-associated proteins expressed on the cell surface as a target device for fusion proteins containing different kinds of effector molecules. Here the possibilities for targeting are manifold. Delivery of conjugated cytokines to the tumor can, for example, activate the immune system or induce apoptosis. Specific degradation of tumor cells by induction of apoptosis can furthermore be achieved through conjugation of targeting molecules with toxins like cytotoxic drugs or radionuclides (Milenic *et al.* (2004)). In the case of antibody-directed enzyme prodrug therapy (ADEPT), an enzyme is targeted to the tumor cell and converts a subsequently injected non-toxic prodrug into its active cytotoxic form, effecting only the targeted tumor cells (Bagshawe (2006)).

The idea to use tumor-associated proteins – so-called tumor markers – in order to deliver a cytostatic or even cytotoxic effect depends on both the presence of such tumor markers on the cancer cell to treat and molecules specifically binding to this tumor marker.

The most prominent targeting binders are monoclonal antibodies (mAbs) and smaller versions of antibodies, such as single-chain scFv portion monomers (and their genetically linked dimers, trimers or tetramers). However, the arsenal of the targeting binders used nowadays is not restricted to the immunoglobulin fold but comprises furthermore so called engineered binders derived from other protein scaffolds like protein A, the lipocalins, a fibronectin domain, an ankyrin consensus repeat domain and thioredoxin (Skerra (2007)). Furthermore, the specific binding of the "target" might – at least in principle – of course be accomplished by non-protein molecules like e.g. DNA-aptamers.

The prominent tumor marker used in the here presented work is the receptor tyrosin kinase ErbB2, also refered to as Human Epidermal growth factor Receptor 2 (HER2).

The following introductory sections are aimed to introduce both the target and the targeting molecules used in this work.

1.2 ErbB receptors: architecture and mode of action

The four members of the family of human epidermal growth factor receptor tyrosine kinases (ErbB receptors, also known as HERs) are important mediators of cell growth, differentiation, migration and survival (Citri and Yarden (2006)). They have been shown to be overexpressed and involved in aberrant signaling in many cancers (Yarden (2001)) and are therefore often considered as target in tumor targeting approaches. In humans, there are four different homologous ErbB-receptors: epidermal growth factor receptor (EGFR, also refered to as HER1), HER2 (also known as ErbB2/neu), HER3 (ErbB3) and HER4 (ErbB4). These transmembrane receptors consist of a single polypeptide chain of about 1200 aa (e.g. 1186 aa for EGFR, equivalent to a M_r of 170 kDa (Carpenter and Cohen (1990))) and can be found in different concentrations and mixtures on the surface of the majority of somatic cells.

The receptor architecture can be divided into three regions, the extracellular ligand-binding region, the intracellular region with tyrosine kinase activity and a transmembrane region with a single hydrophobic anchor sequence by which the receptor traverses the cell membrane a single time. The extracellular aminoterminal end can be divided into four domains (termed extracellular domains (ECDs) I to IV (ECD_I to ECD_IV).

All members of the EGFR family belong to subclass I of receptor tyrosine kinases (Yarden and Ullrich (1988)) which generally means that receptor activation occurs by binding of monomeric ligands to the active site on the extracellular region of monomeric receptor molecules.

According to the present opinion, all ErbB-receptors except HER2 persist until activation through ligand-binding in a “closed” or “tethered” conformation with the dimerization arm in ECD_II interacting with modules 5 and 6 of ECD_IV (**Figure 1.1**). This ECD-conformation autoinhibits the receptor from dimerization, as the interacting regions on domains II and IV (the “dimerization arm” on ECD_II and the “tethering arm” on ECD_IV) are needed to form intermolecular contacts with the corresponding domains of the dimerization partner once two receptors dimerize (**Figure 1.2**)(Cho and Leahy (2002); Ferguson *et al.* (2003)).

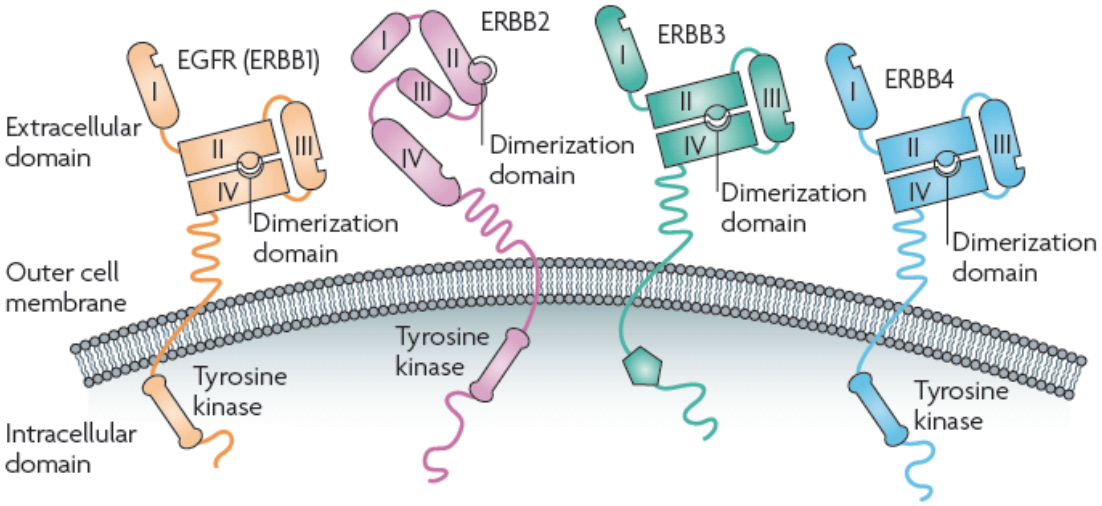

Figure 1.1: Schematic drawing of the four homologous ErbB receptors. The ErbB family contains four members (EGFR, ErbB2, ErbB3 and ErbB4) with similar topologies. Each receptor is composed of three functional modules: an extracellular domain (which can in turn be subdivided into 4 different subdomains), an α-helical transmembrane segment and an intracellular tyrosine kinase domain that also contains motifs that mediate interactions with intracellular signaling molecules. EGFR, ErbB3 and ErbB4 exist in a tethered ("closed") conformation in which the dimerization domain is not available to interact with partner ErbB receptors in the absence of ligand. There is no known natural ligand for ErbB2, this receptor exists in an active extended ("open") conformation and is permanently available for dimerization. Figure adapted from Baselga and Swain (2009).

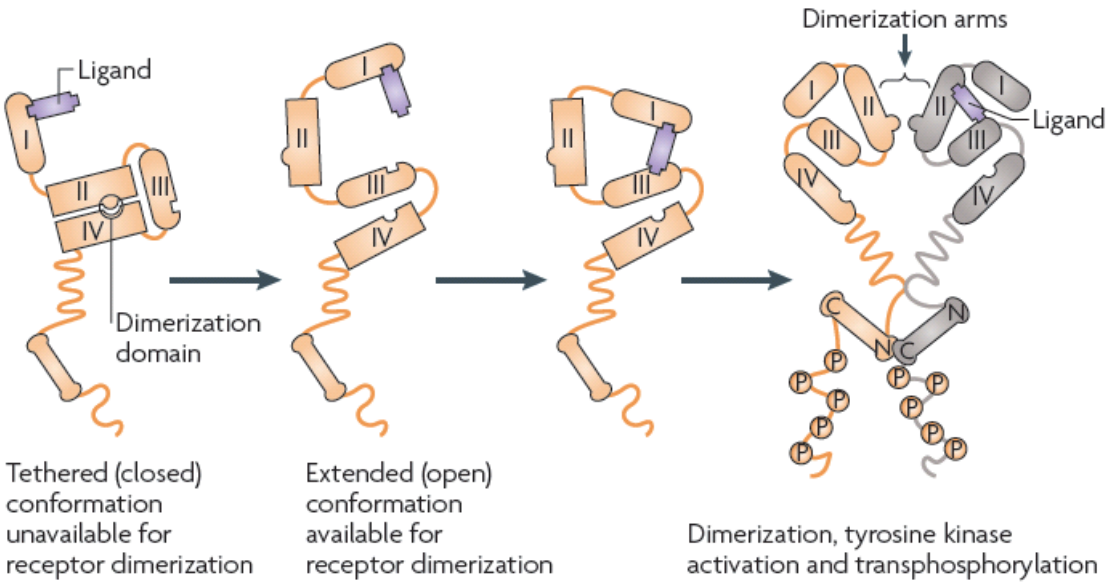

Figure 1.2:Conceptualization of the conformational change of the extracellular domain of EGFR, ErbB3 or ErbB4 induced by ligand binding to subdomains I and III. In the ligand-induced open conformation, the dimerization domain (the "dimerization arm") on subdomain II becomes exposed. Intermolecular interactions between subdomains II and IV of two receptors constitute dimerization. The kinase domain interaction is asymmetric, with the amino-terminal lobe of one tyrosine kinase interacting with the carboxy-terminal lobe of the other. Figure adapted from Baselga *et al.* (2009).

In the ligand-bound "open" or "non-tethered" state the dimerization arm on domain II protrudes out from the rest of the molecule and is therefore able to interact with residues from ECD II of the dimerization partner, which can be any other activated receptor (Ogiso *et al.* (2002)) leading to the formation of either homo- or heterodimers.

As a consequence of dimerization the kinase domains of the dimerization partners, that were in the inactive conformation in the monomeric receptors, transactivate each other (or to be more precise: one kinase activates the other): The close proximity of the two kinases allows the C lobe of one partner to bind to the N lobe of the other, resulting in the αC helix of the latter rotating to the position required for kinase activity (Zhang *et al.* (2006)). The activated kinase subsequently transphosphorylates tyrosine-residues within the intracellular part of the dimerization partner, especially within the very C-terminal "tail".

The thereby phosphorylated residues serve as docking sites for the recruitment and phosphorylation of a number of intracellular substrates that activate pro-proliferative and anti-apoptotic pathways.

Signalling is terminated partly through endocytosis and lysosomal degradation of the activated receptor/ligand complex (whereas the receptor may be recycled to the plasma membrane (French *et al.* (1994))), and partly by dephosphorylation.

1.3 Peculiarities of ErbB receptor family members

Within the ErbB receptor family, the two EGFR-homologues HER2 and HER3 carry interesting peculiarities:

HER2 does not bind to any of the 12 natural ligands known so far and is most likely to not have a natural ligand (Alvarado *et al.* (2009)). Its extracellular domains are supposed to be always in the open conformation due to the absence of the domain II-IV interaction (in detail discussed in (Hynes and Lane (2005)) which may explain why HER2 is the preferred dimerization partner for the other three receptor family members (Li *et al.* (2012)). In such heterodimers the affinity of HER2's dimerization partners for their ligands is enhanced by

slowing down the rate of ligand-receptor complex dissociation. In accordance with publications based on computer simulations, HER2 molecules might permanently be homodimerized when overexpressed on the cell surface (Fleishman *et al.* (2002); Garnier *et al.* (2003)). This model proposes an equilibrium between two states of the receptor dimer, one active and one inactive. The amount of active receptor dimers signalling for cell proliferation and -survival would therefore be related to the amount of HER2 molecules on the cell. At higher concentrations more and more receptor dimers would exist in the active state, driving cancerous growth. This concept aligns well with growth-data from HER2-overexpressing cells.

HER3 is a special family member as its kinase domain is catalytically inactive or only weakly active (Telesco *et al.* (2011)). However, HER3 plays an important role, especially in oncogenic HER3 signaling, as its intracellular part appears to readily serve both as activator and as substrate.

1.4 ErbB receptors and cancer

Although expressed as well in nonmalignant cells, the EGFR-family members, especially HER2, are highly expressed in a variety of tumors (Yarden and Sliwkowski (2001)) and their expression correlates with poor response to treatment, fast disease progression and poor survival (Baselga (2002)). ErbB receptor signaling impacts on many aspects of tumor biology including the promotion of proliferation, angiogenesis, invasion/metastasis and inhibition of apoptosis. Major routes for ErbB-related signalling are the Ras-Raf-mitogen-activated protein (MAP) kinase pathway, mainly responsible for proproliferative signaling (Alroy and Yarden (1997)) and the phosphatidylinositol 3-kinase and Akt (PI3K/Akt) pathway, which constitutes general tumor-cell survival (Burgering and Coffer (1995)).

However, the respective mechanisms affecting ErbB signaling differ in each particular tumor. Transformation might occur by mutation, overexpression or coexpression of different EGFR-family members with one or more of their ligands resulting in an autocrine loop leading to uncontrolled cell growth (Voldborg *et al.* (1997)). In order to employ ErbB-signalling for cancer

therapy by molecular targeted agents, one can generally treat the pathway at different stages (like ligand binding, receptor-dimerisation or downstream-signaling). The most promising arms and their respective drugs can be divided into two main groups, presented in the following section.

1.5 Different routes of ErbB tumor targeting

Tyrosine kinase inhibtors (TKIs) (also termed 'small-molecule inhibitors') have been developed to block the catalytic ability of protein tyrosine kinases. TKIs act by competing with ATP for binding to the kinase's active site. Unfortunately, low response rates have been reported from clinical trials (Gadgeel *et al.* (2007)) which might be explained by mutations in the ErbB genes that seem to impair TKI effects, leading to TKI resistance (Toschi and Cappuzzo (2007)).

Monoclonal antibodies (mAbs), mostly in the IgG-format, are used as experimental therapy in humans since the beginning of the 1980s (Houghton and Scheinberg (1986)). In selective anticancer therapy of ErbB-driven tumors, therapeutic mAbs work via manifold mechanisms:

Disruption of ErbB signaling can be archieved either through binding the ligand in order to prevent it from activating the receptor, binding the receptor in order to prevent it from being bound by the ligand (e.g. mAb cetuximab binding EGFR) or binding the receptor in order to prevent it from dimerization (e.g. mAb pertuzumab (Perjetta) binding HER2).

In general, binding of mAbs is furthermore able to induce antibody dependent cellular cytotoxicity (ADCC) and complement dependent cytotoxicity (CDC). A big advantage of mAbs is their long serum half-life, which has been shown to be in the range of days (Müller *et al.* (2007)).

1.6 Trastuzumab – the first mAb FDA approved for α-HER2 tumor targeting

Trastuzumab, better known under its tradename 'Herceptin', has been shown to effectively inhibit the growth of HER2-overexpressing cells *in vitro* and *in vivo* through binding to an epitope on HER2_IV (Cho *et al.* (2003)). Herceptin received FDA approval in 1998. It is indicated

for the treatment of patients with metastatic breast cancer whose tumors do overexpress HER2 (20-30% of all patients suffering from breast cancer) and clinically active in patients that have received prior anti-cancer therapy (Baselga *et al.* (1996)). The majority of HER2-positive tumors have nevertheless been found to be non-responding to the antibody therapy, e.g. 15% objective response rate in extensively pretreated patients, 26% of previously untreated patients, and 45% overall response rate for antibody- with chemotherapy vs. 29% after chemotherapy alone (Baselga (2001); Slamon *et al.* (2001)). Besides treatment of patients with HER2-overexpressing metastatic breast cancers, Herceptin is approved in combination with chemotherapy for use in patients with HER2-positive metastatic gastric cancer. Although Herceptin was the first FDA-approved HER2-targeting mAb, its mode of action gives still rise for discussion (cf. next section).

1.7 Modes of action of trastuzumab

Besides CDC and especially ADCC, which are by far the most important mechanisms of action *in vivo* and in the patient, the following effects of trastuzumab are discussed:

Binding of trastuzumab (in contrast to binding of cetuximab or pertuzumab) to HER2 has been shown to sterically block proteinases like matrix metalloproteinases (MMPs) from cleaving the extracellular parts of receptor dimers (Molina *et al.* (2001)). In the absence of trastuzumab, this 'receptor-shedding' leads to truncated but still dimerized receptors that stay as phosphorylated specimens in the membrane. Whether these truncated dimers, consisting of the phosphorylated intracellular domains, escape dephosphorylation or internalization or if the pro-proliferative signalling is maintained through other effects is not understood.

HER2 overexpression leads to ligand-independent HER2/HER3 interaction and HER3 phosphorylation. Trastuzumab sterically disrupts this ligand-independent interaction of HER2 with HER3 (Junttila *et al.* (2009)).

Another originally suggested mode of action, that trastuzumab induces some of its effect by down-regulation of HER2, leading to disruption of receptor dimerization and signaling, could be excluded by Austin *et al.* (2004).

When discussing trastuzumab's modes of action, one will always have to take care to not confuse the overall (phenotypic) effect caused by trastuzumab with the direct mode of action of trastuzumab.

For instance, it has clearly been shown that "trastuzumab triggers the accumulation of the cyclin-dependent kinase inhibitor $p27^{Kip1}$ in the nucleus and therefore initiates cell cycle arrest" (Le *et al.* (2005)). However, this accumulation of p27 in the nucleus is not more than one of the effects caused by trastuzumab binding through a long signaling cascade, but might not really be named direct "mode of action", as it just describes an effect that follows several steps from the initial mode of action.

1.8 New models of ErbB receptor activation

Besides the so called canonical receptor dimers schematically depicted in **Figure 1.2**, more recent publications have focused on alternative models of ErbB receptor activation.

One of such additional modes of ErbB receptor activation are "ligand-independent ErbB receptor interactions" that appear as a result of receptor overexpression. HER2 overexpression, for instance, leads to HER3 phosphorylation, that could be shown to be a result of ligand-independent HER2/HER3 interactions (Junttila *et al.* (2009)) that not necessarily resemble canonical receptor dimers.

Besides canonical dimers and ligand-independent receptor-interactions, there have also been reports on ligand-induced transient tetramers composed of side-by-side oriented canonical dimers (Clayton *et al.* (2008); Zhang *et al.* (2012)).

How exactly all those alternative models look like is by far not entirely solved. In principle, each way of bringing two ErbB-kinases in close proximity, could allow allosteric activation with all consequences discussed in **Chapter 2**.

The description of new models for ErbB receptor activation implies the possibility to search for new ErbB targeting binders, employing new mechanisms of action in ErbB tumor

targeting. This is a promising development, as, in the end, tumor targeting strategies employing HER2 and its relatives need to be as versatile as possible.

1.9 New therapeutic modalities

Monoclonal antibodies (mAbs), the assumed most potent molecular targeting agents for selective anticancer therapy, face several disadvantages. For instance, antibodies are comparatively diffcult and expensive to produce. Furthermore the huge size of an immunglobulin G (IgG) of approximately 150 kDa is rather large for therapeutic applications that require efficient tissue penetration (Binz *et al.* (2005)). As the *in vitro* mechanisms of action of e.g. cetuximab, pertuzumab and trastuzumab are caused by steric effects like blockage of ligand binding (cetuximab), inhibition of receptor dimerization (pertuzumab, trastuzumab) or prevention of receptor shedding (trastzumab), the question arises, if biological activity in terms of cytostatic effects can't just be achieved by specific binding through other molecules than mAbs.

For example, so called peptidomimetics, small protein-like amino acid sequences designed to mimic structural features of the antibody complementarity determining regions (CDRs), appear to have similar inhibitory properties as mAbs in experimental models (Pal and Pegram (2006)). Although peptidomimetics are attractive – because simple – candidates for stabilizing or disrupting protein-protein interactions, their efficacy as *in vivo*-reagents is severely compromised by their loss of secondary structure, susceptibility to proteolytic degradation and low serum half life.

During the last years several alternative binding proteins have been developed (for a review see (Binz *et al.* (2005))) including camelid antibodies ("Nanobodies" (Muyldermans and Lauwereys (1999))), protein scaffolds derived from protein A domains ("Affibodies" (Hansson *et al.* (1999))), fibronectin-domain based "Monobodies" (also known as "Adnectins" (Batori *et al.* (2002))), genetically engineered lipocalins ("Anticalins" (Schlehuber and Skerra (2005))), A-domains of several receptors ("Avimers" (Jeong *et al.* (2005))), PDZ domains (Kurakin *et al.*

(2007)), ubiquitin based scaffolds ("Affilins" (Ebersbach *et al.* (2007))), knottins (Smith *et al.* (1998)) or DARPins (recently reviewed in (Boersma and Plückthun (2011))).

These alternatives to antibodies have a completely different protein topology, associated with advantages like small size (for good tissue penetration) and single-chain buildup (allowing easy manufacturing and subsequent construction of fusion proteins). Furthermore the small single-chain character facilitates the application of powerful selection technologies like Phage Display (PD) and Ribosome Display (RD).

1.10 Designed Ankyrin Repeat Proteins (DARPins)

Repeat proteins can be found in all phyla mediating numerous key protein-protein interactions (Bork (1993)). They are characterized by consecutive homologous structural units ('repeats'), which stack to form an elongated protein domain with a continuous hydrophobic core (Kobe and Kajava (2000)).

The natural function of repeat proteins to assure specific binding to substrates like proteins and nucleic acids suggests using repeat proteins as binding molecules for diagnostic and therapeutic applications. The strategy of designing binding molecules that employ the modular nature of repeat proteins was evaluated on leucine-rich- (Stumpp *et al.* (2003)) and ankyrin repeat proteins (Binz *et al.* (2003)). The latter was named Designed Ankyrin Repeat Proteins ('DARPins'). In a combined approach of structure and sequence analysis a consensus repeat module of 33 amino acids with fixed framework residues and randomized positions as potential interaction surface was designed. Using this consensus design strategy, combinatorial libraries of ankyrin repeat proteins with varying repeat numbers and diversified binding surfaces were generated (Binz *et al.* (2004)).

DARPins are designed single-chain proteins that consist of varying numbers of repeat modules, held together in a fixed tertiary structure by a self-assembling hydrophobic core (**Figure 1.3**). Each repeat forms a structural unit consisting of a β-turn followed by two antiparallel α-helices. Addition of an N- and C-terminal module ('cap') shields the hydrophobic

areas of the first and the last repeat module and assures favorable behavior in solution. High expression level in *E. coli*, thermodynamic stability and the absence of disulfide bonds or free cysteins provide advantages in comparison to other novel frameworks.

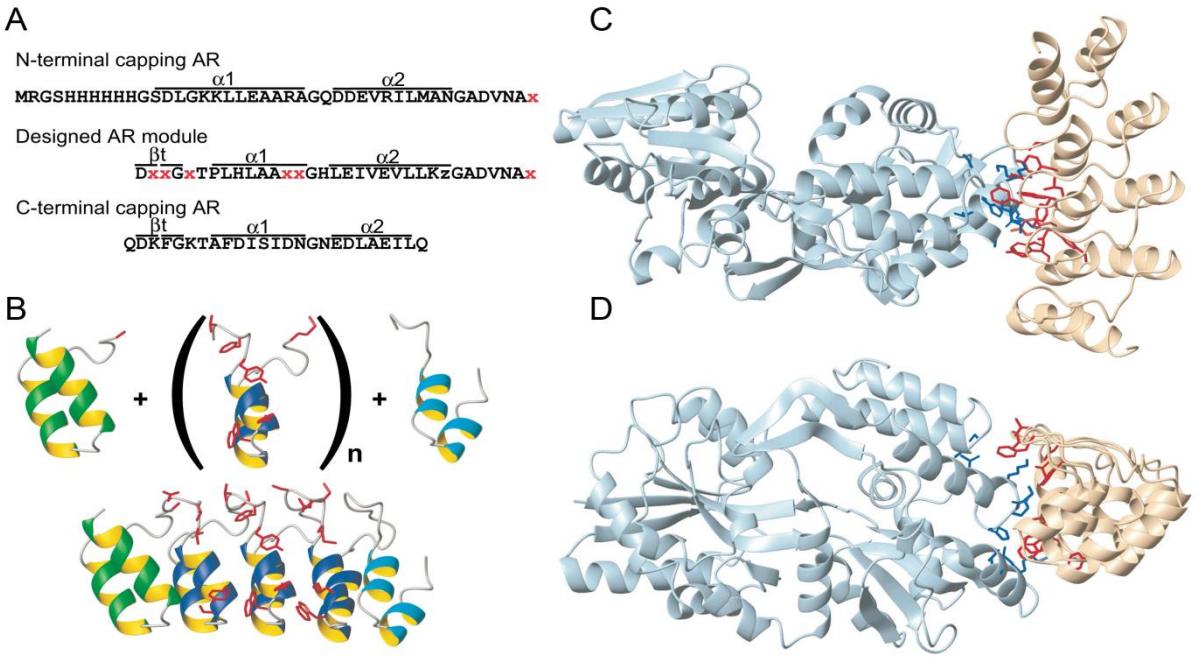

Figure 1.3: Architecture of Designed Ankyrin Repeat Proteins (DARPins). (A) Primary sequences of the N-terminal capping ankyrin repeat (AR), the internal designed AR module and the C-terminal capping AR. The secondary structure elements are indicated above the sequences. Each designed AR module consists of 26 defined framework residues, six randomized potential interaction residues (red x, any of the 20 natural amino acids except cysteine, glycine or proline) and one randomized framework residue (z, any of the amino acids asparagine, histidine or tyrosine). (B) Assembly of DARPins from N- and C-terminal capping repeats (green and cyan, respectively) and varying numbers of internal designed AR modules (blue) (side chains of the randomized residues are shown in stick mode in red). (C, D) Two perpendicular views of the crystal structure of the complex of DARPin off7 bound to MBP. MBP is on the left (blue), off7 on the right (ochre). The interaction residues are highlighted in stick-mode in red (off7) and blue (MBP), respectively. Figure adapted from (Binz *et al.* (2004)).

2 The Project

The initial question of my PhD-project had already been posed as initial question of my diploma project: Is it possible to use HER2-binding-DARPins – without cytotoxic fusions – to obtain anti-proliferative effects on HER2-overexpressing cells?

This question appears consequent when taking into consideration that the efficacy of the two most prominent non small molecule drugs engaged in tumor targeting of HER2-overexpressing cancer cells – trastuzumab (hu4D5, Herceptin) and pertuzumab (hu2C4, Omnitarg) – relies at least partially on the mere binding to the receptor.

After having screened and characterized DARPins binding to the extracellular part of HER2 during my diploma thesis, first screenings for effects on cell-proliferation and viability of BT474-cells had identified one DARPin – termed "H14" (H_14 in (Steiner *et al.* (2008))) – which displayed antitumor activity on this cell line.

In my PhD thesis, the developments to improve the antitumor activity of this DARPin are described. The main improvements during this development were achieved by switching from the monovalent to the bivalent format. Various DARPin-constructs ranging from simple monovalent up to hexavalent binders have been engineered, expressed, characterized and finally screened for their potential antitumor activity on different cancer cell lines. The majority of the constructs did not exhibit antitumor activity. However, several engineered binders could be shown to affect proliferation and viability of cancer cells with diverse gain in activity as compared to the initially identified monovalent H14. The exhibited mode of action ranges from cytostatic up to cytotoxic effects.

In the course of the project it became evident that knowledge on the epitopes of the HER2-binding DARPins would be essential to understand and explain the main achievements obtained in improving their tumoricidal activity.

This knowledge, at least for three of the most interesting binders, has finally been gained at atomic resolution by resolving crystal structures of the DARPins in complex with their target.

Therefore, the initial question, if DARPins binding the extracellular part of HER2 can be used to cause anti-proliferative effects on HER2-overexpressing cancer cells, is not only affirmed, but has been extended towards improving the observed effects. Furthermore, the answer given has even been extended: The knowledge gained on the DARPins' epitopes and the orientation of binding can be used as a blueprint for the construction of any HER2-binding reagent with anti-proliferative effects on HER2-dependent cancer cells.

3 References

1. Alroy I & Yarden Y (1997) The ErbB signaling network in embryogenesis and oncogenesis: signal diversification through combinatorial ligand-receptor interactions. *FEBS Lett.* 410:83-86.
2. Alvarado D, Klein DE, & Lemmon MA (2009) ErbB2 resembles an autoinhibited invertebrate epidermal growth factor receptor. *Nature* 461:287-291.
3. Austin CD*, et al.* (2004) Endocytosis and sorting of ErbB2 and the site of action of cancer therapeutics trastuzumab and geldanamycin. *Mol. Biol. Cell* 15:5268-5282.
4. Bagshawe KD (2006) Antibody-directed enzyme prodrug therapy (ADEPT) for cancer. *Expert Rev. Anticancer Ther.* 6:1421-1431.
5. Baselga J (2001) Herceptin alone or in combination with chemotherapy in the treatment of HER2-positive metastatic breast cancer: pivotal trials. *Oncology* 61 Suppl 2:14-21.
6. Baselga J (2002) Why the epidermal growth factor receptor? The rationale for cancer therapy. *Oncologist* 7 Suppl 4:2-8.
7. Baselga J & Swain SM (2009) Novel anticancer targets: revisiting ERBB2 and discovering ERBB3. *Nat. Rev. Cancer* 9:463-475.
8. Baselga J*, et al.* (1996) Phase II study of weekly intravenous recombinant humanized anti-p185HER2 monoclonal antibody in patients with HER2/neu-overexpressing metastatic breast cancer. *J. Clin. Oncol.* 14:737-744.
9. Batori V, Koide A, & Koide S (2002) Exploring the potential of the monobody scaffold: effects of loop elongation on the stability of a fibronectin type III domain. *Protein Eng.* 15:1015-1020.
10. Binz HK*, et al.* (2004) High-affinity binders selected from designed ankyrin repeat protein libraries. *Nat. Biotechnol.* 22:575-582.
11. Binz HK, Amstutz P, & Plückthun A (2005) Engineering novel binding proteins from nonimmunoglobulin domains. *Nat. Biotechnol.* 23:1257-1268.
12. Binz HK, Stumpp MT, Forrer P, Amstutz P, & Plückthun A (2003) Designing repeat proteins: well-expressed, soluble and stable proteins from combinatorial libraries of consensus ankyrin repeat proteins. *J. Mol. Biol.* 332:489-503.
13. Boersma YL & Plückthun A (2011) DARPins and other repeat protein scaffolds: advances in engineering and applications. *Curr. Opin. Biotechnol.* 22:849-857.
14. Bork P (1993) Hundreds of ankyrin-like repeats in functionally diverse proteins: mobile modules that cross phyla horizontally? *Proteins* 17:363-374.
15. Burgering BM & Coffer PJ (1995) Protein kinase B (c-Akt) in phosphatidylinositol-3-OH kinase signal transduction. *Nature* 376:599-602.
16. Carpenter G & Cohen S (1990) Epidermal growth factor. *J. Biol. Chem.* 265:7709-7712.
17. Cho HS & Leahy DJ (2002) Structure of the extracellular region of HER3 reveals an interdomain tether. *Science* 297:1330-1333.
18. Cho HS*, et al.* (2003) Structure of the extracellular region of HER2 alone and in complex with the Herceptin Fab. *Nature* 421:756-760.
19. Citri A & Yarden Y (2006) EGF-ERBB signalling: towards the systems level. *Nat. Rev. Mol. Cell Biol.* 7:505-516.
20. Clayton AH, Orchard SG, Nice EC, Posner RG, & Burgess AW (2008) Predominance of activated EGFR higher-order oligomers on the cell surface. *Growth Factors* 26:316-324.
21. Ebersbach H*, et al.* (2007) Affilin-novel binding molecules based on human gamma-B-crystallin, an all beta-sheet protein. *J. Mol. Biol.* 372:172-185.
22. Ferguson KM*, et al.* (2003) EGF activates its receptor by removing interactions that autoinhibit ectodomain dimerization. *Mol. Cell* 11:507-517.
23. Fleishman SJ, Schlessinger J, & Ben-Tal N (2002) A putative molecular-activation switch in the transmembrane domain of erbB2. *Proc. Natl. Acad. Sci. U. S. A.* 99:15937-15940.

24. French AR, Sudlow GP, Wiley HS, & Lauffenburger DA (1994) Postendocytic trafficking of epidermal growth factor-receptor complexes is mediated through saturable and specific endosomal interactions. *J. Biol. Chem.* 269:15749-15755.
25. Gadgeel SM*, et al.* (2007) Phase II study of gefitinib, an epidermal growth factor receptor tyrosine kinase inhibitor (EGFR-TKI), and celecoxib, a cyclooxygenase-2 (COX-2) inhibitor, in patients with platinum refractory non-small cell lung cancer (NSCLC). *J. Thorac. Oncol.* 2:299-305.
26. Garnier N, Crouzy S, & Genest M (2003) Molecular dynamics simulations of the transmembrane domain of the oncogenic ErbB2 receptor dimer in a DMPC bilayer. *J. Biomol. Struct. Dyn.* 21:179-200.
27. Hansson M*, et al.* (1999) An in vitro selected binding protein (affibody) shows conformation-dependent recognition of the respiratory syncytial virus (RSV) G protein. *Immunotechnology* 4:237-252.
28. Houghton AN & Scheinberg DA (1986) Monoclonal antibodies: potential applications to the treatment of cancer. *Semin. Oncol.* 13:165-179.
29. Hynes NE & Lane HA (2005) ERBB receptors and cancer: the complexity of targeted inhibitors. *Nat. Rev. Cancer* 5:341-354.
30. Jeong KJ, Mabry R, & Georgiou G (2005) Avimers hold their own. *Nat. Biotechnol.* 23:1493-1494.
31. Jordan VC & Koerner S (1976) Tamoxifen as an anti-tumour agent: role of oestradiol and prolactin. *J. Endocrinol.* 68:305-311.
32. Junttila TT*, et al.* (2009) Ligand-independent HER2/HER3/PI3K complex is disrupted by trastuzumab and is effectively inhibited by the PI3K inhibitor GDC-0941. *Cancer Cell* 15:429-440.
33. Kobe B & Kajava AV (2000) When protein folding is simplified to protein coiling: the continuum of solenoid protein structures. *Trends Biochem. Sci.* 25:509-515.
34. Kurakin A, Swistowski A, Wu SC, & Bredesen DE (2007) The PDZ domain as a complex adaptive system. *PLoS One* 2:e953.
35. Le XF, Pruefer F, & Bast RC, Jr. (2005) HER2-targeting antibodies modulate the cyclin-dependent kinase inhibitor p27Kip1 via multiple signaling pathways. *Cell Cycle* 4:87-95.
36. Li Y, Macdonald-Obermann J, Westfall C, Piwnica-Worms D, & Pike LJ (2012) Quantitation of the effect of ErbB2 on epidermal growth factor receptor binding and dimerization. *J. Biol. Chem.* 287:31116-31125.
37. Mendeleyev J, Kirsten E, Hakam A, Buki KG, & Kun E (1995) Potential chemotherapeutic activity of 4-iodo-3-nitrobenzamide. Metabolic reduction to the 3-nitroso derivative and induction of cell death in tumor cells in culture. *Biochem. Pharmacol.* 50:705-714.
38. Milenic DE, Brady ED, & Brechbiel MW (2004) Antibody-targeted radiation cancer therapy. *Nat. Rev. Drug Discov.* 3:488-499.
39. Molina MA*, et al.* (2001) Trastuzumab (herceptin), a humanized anti-Her2 receptor monoclonal antibody, inhibits basal and activated Her2 ectodomain cleavage in breast cancer cells. *Cancer Res.* 61:4744-4749.
40. Müller D*, et al.* (2007) Improved pharmacokinetics of recombinant bispecific antibody molecules by fusion to human serum albumin. *J. Biol. Chem.* 282:12650-12660.
41. Muyldermans S & Lauwereys M (1999) Unique single-domain antigen binding fragments derived from naturally occurring camel heavy-chain antibodies. *J. Mol. Recognit.* 12:131-140.
42. Ogiso H*, et al.* (2002) Crystal structure of the complex of human epidermal growth factor and receptor extracellular domains. *Cell* 110:775-787.
43. Pal SK & Pegram M (2006) Targeting HER2 Epitopes. *Semin. Oncol.* 33:386-391.
44. Schlehuber S & Skerra A (2005) Anticalins as an alternative to antibody technology. *Expert Opin. Biol. Ther.* 5:1453-1462.
45. Schrama D, Reisfeld RA, & Becker JC (2006) Antibody targeted drugs as cancer therapeutics. *Nat. Rev. Drug Discov.* 5:147-159.

46. Shore GC & Viallet J (2005) Modulating the bcl-2 family of apoptosis suppressors for potential therapeutic benefit in cancer. *Hematology Am. Soc. Hematol. Educ. Program.*:226-230.
47. Skerra A (2007) Alternative non-antibody scaffolds for molecular recognition. *Curr. Opin. Biotechnol.* 18:295-304.
48. Slamon DJ*, et al.* (2001) Use of chemotherapy plus a monoclonal antibody against HER2 for metastatic breast cancer that overexpresses HER2. *N. Engl. J. Med.* 344:783-792.
49. Smith GP*, et al.* (1998) Small binding proteins selected from a combinatorial repertoire of knottins displayed on phage. *J. Mol. Biol.* 277:317-332.
50. Steiner D, Forrer P, & Plückthun A (2008) Efficient selection of DARPins with sub-nanomolar affinities using SRP phage display. *J. Mol. Biol.* 382:1211-1227.
51. Stumpp MT, Forrer P, Binz HK, & Plückthun A (2003) Designing repeat proteins: modular leucine-rich repeat protein libraries based on the mammalian ribonuclease inhibitor family. *J. Mol. Biol.* 332:471-487.
52. Teicher BA, Ara G, Herbst R, Palombella VJ, & Adams J (1999) The proteasome inhibitor PS-341 in cancer therapy. *Clin. Cancer Res.* 5:2638-2645.
53. Telesco SE, Shih AJ, Jia F, & Radhakrishnan R (2011) A multiscale modeling approach to investigate molecular mechanisms of pseudokinase activation and drug resistance in the HER3/ErbB3 receptor tyrosine kinase signaling network. *Mol. Biosyst.* 7:2066-2080.
54. Toschi L & Cappuzzo F (2007) Understanding the new genetics of responsiveness to epidermal growth factor receptor tyrosine kinase inhibitors. *Oncologist* 12:211-220.
55. Voldborg BR, Damstrup L, Spang-Thomsen M, & Poulsen HS (1997) Epidermal growth factor receptor (EGFR) and EGFR mutations, function and possible role in clinical trials. *Ann. Oncol.* 8:1197-1206.
56. Yarden Y (2001) The EGFR family and its ligands in human cancer. signalling mechanisms and therapeutic opportunities. *Eur. J. Cancer* 37 Suppl 4:S3-8.
57. Yarden Y & Sliwkowski MX (2001) Untangling the ErbB signalling network. *Nat. Rev. Mol. Cell Biol.* 2:127-137.
58. Yarden Y & Ullrich A (1988) Growth factor receptor tyrosine kinases. *Annu. Rev. Biochem.* 57:443-478.
59. Zhang Q, Park E, Kani K, & Landgraf R (2012) Functional isolation of activated and unilaterally phosphorylated heterodimers of ERBB2 and ERBB3 as scaffolds in ligand-dependent signaling. *Proc. Natl. Acad. Sci. U. S. A.* 109:13237-13242.
60. Zhang X, Gureasko J, Shen K, Cole PA, & Kuriyan J (2006) An allosteric mechanism for activation of the kinase domain of epidermal growth factor receptor. *Cell* 125:1137-1149.

Chapter 2

Designed Ankyrin Repeat Proteins engineered to cause cytostatic effects on HER2-addicted cancer cells

Christian Jost, Rastislav Tamaskovic, Shane Morrison and Andreas Plückthun

Department of Biochemistry, University of Zürich, Winterthurerstrasse 190, 8057 Zürich, Switzerland

Content

1 Abstract 21

2 Introduction 22

3 Results and Discussion 24

3.1 Screening HER2-binding DARPins for antitumor activity 24

3.2 Epitope-mapping of DARPin H14 25

3.3 Competition with trastuzumab and evaluation of ectodomain-shedding 26

3.4 Importance of epitope and bivalent binding for antitumor activity 26

3.5 H14 in flexibly linked bivalent format promotes BT474 cell proliferation 27

3.6 Engineering of H14-constructs for improved antitumor activity 27

3.7 Transfering the inflexible linker format to DARPin G3 28

4 Materials and Methods 29

4.1 Cell culture 29

4.2 Cell-proliferation assays (XTT assays) 29

4.3 Cloning, Expression and Purification of DARPins 29

4.4 ELISA 30

4.5 Surface Plasmon Resonance (SPR, Biacore) 30

4.6 Epitope characterization via flow cytometry competition 31

4.7 Receptor Shedding assays 31

4.8 Receptor recycling assay via flow cytometry 31

4.9 Expression and purification of scFv 4D5 32

5 Conclusions 32

6 References 35

1 Abstract

The human epidermal growth factor receptor 2 (hErbB2, HER2) is implicated in the malignant growth of tumors from various human cancers, including an aggressive form of breast cancer. This high potential of HER2 to become an oncogene is explained by the mode of action of this cell surface protein: Receptor dimerization leads to trans-phosphorylation events at the intracellular part of the receptor that in turn serve as starting points for pro-proliferative and anti-apoptotic signaling cascades. HER2 overexpression therefore leads to transformation into malignant cells, but can be used as point of attack for diverse approaches of molecular tumor targeting as well. The prevention of HER2-dimerization in HER2 overexpressing tumor cells that have become addicted to the receptor might induce anti-proliferative effects in such cells. Such inhibition might be caused sterically through binding to the extracellular domain of HER2. Designed Ankyrin Repeat Proteins (DARPins) have been previously selected as high-affinity binders of HER2, so far being employed as reporters in diagnostic approaches or as targeting domains for gene vector delivery. We now aimed to engage our anti-HER2-DARPins to inhibit the in vitro growth of HER2 addicted cancer cells. Screening 22 monovalent anti-HER2 DARPins in cell proliferation assays on BT474 cells yielded one DARPin that exhibits an anti-proliferative effect through binding to the extracellular subdomain IV of HER2 (HER2_IV). Bivalent fusions of this DARPin, in which the two DARPin paratopes are held at a distance by an inert rigid linker DARPin, could be found to have pronounced cytostatic effects. Interestingly, the antiproliferative effects caused by the bivalent DARPins are comparable to those caused by the therapeutic antibody trastuzumab. Furthermore, the bivalent rigid linker format can be transferred to another DARPin binding another epitope on HER2_IV. We conclude that the observed effect on cell proliferation is a result of the “trapping” of HER2 monomers by the DARPin-constructs. The HER2 molecules are kept apart from each other by the intermolecular DARPin binding and thereby contribute to a lesser extent to the HER2 signaling than non-bound HER2 molecules that are free to undergo homo- and heterodimerization.

2 Introduction

The human epidermal growth factor receptor 2 (HER2, hErbB2) is an important and very well studied model system for the role that a receptor tyrosine kinase might play in oncogenesis. In the same manner as all other receptor tyrosine kinases, HER2 acts via homodimerization with other HER2-molecules and especially via heterodimerization with the homologous receptors EGFR, HER3 and HER4 (Sundaresan *et al.* (1999)). The so formed receptor dimers contribute to important signal transduction pathways, mainly by signaling onto the PI3K/Akt and the mitogen-activated protein (MAP) kinase cascades, leading to cell survival and proliferation, respectively (Craven *et al.* (2003)).

The amplified expression of a member of the EGFR-family therefore promotes tumorigenesis (Yarden and Sliwkowski (2001)). Especially amplification of HER2 is a hallmark of a number of different tumors, as HER2 is special in the sense that it does not require ligand binding for dimerization (reviewed in (Brennan *et al.* (2000))).

As HER2-overexpression is characteristic to many different types of cancer, it has provoked the development of molecular targeting reagents that specifically target this receptor. The monoclonal antibodies trastuzumab (Herceptin®) (Genentech, San Francisco, CA) and pertuzumab (Perjeta®) (Roche), humanized versions of the murine antibodies 4D5 and 2C4, are FDA-approved drugs that bind the extracellular part of HER2 (HER2_ECD or p110) and thereby mark HER2-overexpressing cells for the attack of cytotoxic T-cells. However, this antibody-dependent cellular cytotoxicity (ADCC) and the closely related complement-dependent cytotoxicity (CDC), that do mainly account for the antibodies' efficacy *in vivo* (Yan *et al.* (2008)), do not comprise the antibodies' whole mechanism of action. Both antibodies also have anti-proliferative effects on the growth of HER2-overexpressing cancer cell lines grown *in vitro*, where no immune- or complement system are present. It can be therefore concluded that a certain part of the anti-proliferative effect caused by HER2-binding proteins on HER2-overexpressing cancer cells is attributed to sole binding.

This steric effect can be explained in view of the epitopes on HER2_ECD that are bound by pertuzumab and trastuzumab. Both epitopes cover parts of the ECD that come close to the partnering receptor during dimerization. Pertuzumab blocks the receptor dimerization through binding its epitope next to the dimerization arm on subdomain II of HER2, while the epitope of trastuzumab is located on a region of subdomain IV. Both subdomain II and IV make contact with the corresponding subdomains of the dimerization partner in a receptor dimer. This is why binding to epitopes on subdomains II and IV that are facing the dimerization partner can sterically prevent dimerization.

A similar steric effect on HER2 dimerization potential obtained through binding to the ECD was reported by Chen *et al.* (2003). In this study, a biologically inert binder, the aptamer A30 binding to the ECD of HER3, was found to have an inhibitory effect on ligand-induced in vitro growth of MCF7 cells. Interestingly, the epitope of A30 is not located within the dimer interaction surface, but laterally situated on subdomain III (HER3_III). This epitope location, taken together with the observation that A30 inhibits HER2- but not HER3-phosphorylation, led to a model in which A30 disrupts ligand-induced transient tetramers composed of side-by-side oriented canonical dimers (Zhang *et al.* (2012)) that had already been proposed for EGFR in an earlier studies by Clayton and coworkers (Clayton *et al.* (2008)).

The described anti-proliferative *in vitro* effects on HER2-overexpressing cancer cell lines of both the HER2-binding monoclonal antibodies trastuzumab and pertuzumab, and the aptamer A30 binding to HER3, depict the potential that ECD-binding agents may have for disrupting HER2 dimerization.

One new class of such binding agents are designed ankyrin repeat proteins (DARPins) that have been recently developed in our lab. DARPins are binding scaffolds that can be selected to bind virtually any target-protein with high specificity and affinity (Binz *et al.* (2004)). Previously, DARPins binding the soluble recombinant ectodomain of HER2 (HER2_ECD) were selected by ribosome display (Zahnd *et al.* (2007)) or phage display (Steiner *et al.* (2008)). These

DARPins all show monomeric behavior in size exclusion chromatography and have (sub)nanomolar affinities.

Using the HER2-addicted BT474 cell line, a widely used model system for testing anti-HER2 activity, we investigated the biological activities of these monovalent DARPins and compared them to that of trastuzumab. We could identify one monovalent DARPin that elicits an anti-proliferative effect on BT474 cells. Interestingly, this DARPin competes with trastuzumab for binding and has a biological activity that is comparable to the anti-proliferative effect caused by the scFv 4D5, which is the scFv of trastuzumab.

In the course of our screening for biologically active DARPins, we further made use of an advantage that DARPins offer in comparison to other binding scaffolds: The facile generation of bivalent constructs by genetical fusion allowed us to engineer bivalent constructs with rigid protein linkers in between the two DARPin paratopes. This led to DARPins composed of two HER2_IV-binding DARPins per molecule, fused via a third non-binding DARPin as rigid linker moiety. The best rigid bivalent constructs were found to inhibit the *in vitro* growth of BT474 cells equally to trastuzumab, both in terms of concentration and efficacy. Notably, the effect is obtained by binding only and seems to rely on arresting HER2 molecules in fixed distances from each other. Our knowledge on the epitopes of the HER2-binding DARPins allows us to describe the molecular mechanism by which the rigid bivalent DARPin constructs cause their effect.

3 Results and Discussion

3.1 Screening HER2-binding DARPins for antitumor activity

In order to screen DARPins for antitumor activity on HER2-overexpressing cells, we choose 22 candidates that had previously been selected by ribosome display (Zahnd *et al.* (2007)) or phage display (Steiner *et al.* (2008)) to bind the recombinant ectodomain of HER2. The binders were chosen judging on exclusive monomeric running behavior in size exclusion chromatography and affinities to be at least in the nanomolar range. Screening 1 μM dilutions of all 22 candidates in cell-proliferation assays (XTT) identified one DARPin to have anti-proliferative activity: BT474

cells that had been grown for four days in presence of DARPin H14 showed a concentration-dependent decrease in cell viability of 25% compared to cells that had been grown without treatment, while treatment with trastuzumab decreased cell viability by 45% (**Figure 2.1**). It has to be noted that the indicated decreases in cell viability are calculated in comparison to the untreated control which grows over the four days. Since our XTT-assays were performed as endpoint measurement after four days of growth, and since the cell count of untreated cells doubles during this time, a signal decrease of ~50% after four days (comparing signals from treated cells with the signals from untreated control) equals the signal at the beginning of the assay. Therefore a decrease in cell viability of about 50% (like observed for trastuzumab) indicates a cytostatic effect.

3.2 Epitope-mapping of DARPin H14

As described previously, DARPin H14 had been originally selected using an epitope masking strategy employing high-affinity DARPin G3 to mask an epitope on HER2_IV that had proven to be very dominant in earlier selections on HER2_ECD (Steiner *et al.* (2008)). Already in the initial characterization, binder H14 had attracted our interest due to its exceptionally high binding signal in ELISA. Further analysis by surface plasmon resonance (SPR) revealed binder H14 to show an affinity in the picomolar range (**Figure 2.2**). Interestingly, besides its high affinity already after three rounds of selection, H14 proved to compete with DARPin G3 for binding, both in ELISA on recombinant target protein and in flow cytometry using BT474 cells (Jost et al., *submitted*, **Chapter 3**). Apparently, the epitope masking strategy had not resulted in directing the binder to another epitope, but to select for a binder targeting a similar epitope with comparably high affinity as DARPin G3, which underwent ten rounds of selection including affinity maturation steps (Zahnd *et al.* (2006); Zahnd *et al.* (2007)) to reach that affinity. Furthermore, the overlapping epitopes for binders G3 and H14 again highlight the fact that this particular region on HER2_ECD seems to be well suited for DARPin-binding.

3.3 Competition with trastuzumab and evaluation of ectodomain-shedding

To further characterize the epitope of the biologically active DARPin H14, we set up competition assays with trastuzumab. In analogy to DARPin G3, preincubation with trastuzumab competed binding of DARPin H14 in flow cytometry using BT474 cells (**Figure 2.3**). DARPin H14 therefore shares parts of its epitope with both DARPin G3 and the antibody trastuzumab. Both of these binders, DARPin G3 and antibody trastuzumab, do however not compete for binding among each other (Jost *et al.*, cf. **Chapter 3**).

As trastuzumab had previously been shown to inhibit HER2 ectodomain-shedding (Molina *et al.* (2001)) and given the fact that our biologically active DARPin H14 shares an overlapping epitope with trastuzumab, we were interested to investigate HER2 ectodomain-shedding in presence of H14. Proteins from BT474-supernatants after 48 hours of growth were therefore extracted by methanol/chloroform precipitation (Wessel and Flügge (1984)) and applied to anti-HER2 immunoblotting, detecting the N-terminus of HER2. Our results confirm the inhibitory effect of trastuzumab on ectodomain-shedding, but do not indicate any comparable effect of the DARPins H14 nor G3 (**Figure 2.4**).

3.4 Importance of epitope and bivalent binding for antitumor activity

To investigate the significance of bivalent binding for antitumor activity, we used further XTT-cell-proliferation assays comparing dilution series of trastuzumab, scFv 4D5 and DARPin H14. Interestingly, we found that the scFv 4D5 was only half as effective as trastuzumab in its anti-proliferative activity. This is striking, especially because the potential of H14 was found to be comparable to the one of scFv 4D5 both in terms of activity and concentration (**Figure 2.5**). The two monovalent binders to similar epitopes on HER2_IV – a scFv and a DARPin – showed comparable anti-proliferative activity, while the respective antibody trastuzumab was clearly more potent than the monovalent binders in inhibiting the cell proliferation of BT474 cells *in vitro*.

3.5 H14 in flexibly linked bivalent format promotes BT474 cell proliferation

Since biological activities of DARPin and scFv were comparable and since both proteins were able to achieve half the effect of the respective bivalent antibody format, it appeared reasonable to test bivalent constructs built up of H14 moieties linked by various protein-linkers. The first bivalent binders were constructed with flexible icosa-peptide linkers ($(G_4S)_4$). Testing of this bivalent DARPin construct, termed H_20_H, concerning its potential effects on cell viability in XTT assays on BT474 cells revealed, very much to our surprise, an *increased* cell proliferation as a result of H_20_H-treatment (**Figure 2.6**). The agonistic activity found for H14_20_H14 is however similar to the agonistic activity of a monospecific F(ab')2-like trastuzumab isomer reported by Scheer *et al.* (2012).

3.6 Engineering of H14-constructs for improved antitumor activity

The finding that the flexible fusion of H14 into bivalent constructs had turned the anti-proliferative effect of monovalent H14 into a pro-proliferative effect highlights the above-mentioned significance of bivalent binding to the HER2 ectodomain for achieving an effect on cellproliferation. However, flexible bivalent binding of HER2_ECD – at least when making use of binder H14 – did not prove to be beneficial and on the contrary could enhance cellular growth. In order to improve the anti-tumor effect of H14, we reasoned that an inflexible linker connecting the H14 moieties might strengthen the anti-proliferative effect of DARPin H14.

Inflexibly linked bivalent H14-constructs were obtained by replacing the flexible icosa-peptide linker in H_20_H through consensus DARPins of various sizes, ranging from one to ten internal repeat modules (see **Chapter 5** for vector design and construction of NXC-consensus-DARPins). A certain degree of flexibility between the HER2-binding H14-moieties and the linker-DARPin was ensured by introducing short tri-peptides (GGS) at the two boundaries. The resulting six inflexibly linked bivalent H14-constructs (with 3, 4, 6, 7, 8 or 10 consensus repeat modules in the linker-DARPin) were all tested regarding their potential effects on cell viability in XTT assays on BT474 cells. In contrast to the flexibly linked H_20_H, all tested inflexibly linked

bivalent H14-constructs showed anti-proliferative effects that exceeded the effect of monovalent H14 (**Figure 2.7**). The inhibitory effects slightly increased in strength with increasing linker length from N3C to N6C, whereas further linker elongation to N8C or N10C did not further improve the constructs' anti-proliferative potential. Notably, the most potent inflexible construct H_N6C_H proved to be comparable to trastuzumab both in terms of activity and EC_{50}.

3.7 Transfering the inflexible linker format to DARPin G3

Since our approach of engineering inflexible bivalent H14-constructs had resulted in H14-derivatives with clearly improved efficacy as compared to monovalent H14, we next wanted to address the importance of the targeted HER2-epitope for the bivalent targeting format. For this purpose, we chose DARPin G3 to be combined with the N6C-linker to form G3_N6C_G3 ("G_N6C_G"). Though sharing an overlapping epitope with DARPin H14 on HER2_IV, monovalent DARPin G3 had proven to show no effect on BT474 cell proliferation by itself (Jost et al. *submitted*). Interestingly, however, the inflexible bivalent construct G_N6C_G could be shown to inhibit cell proliferation comparable to H_N6C_H in terms of activity and EC_{50} (**Figure 2.8**).

4 Materials and Methods

4.1 Cell culture

BT-474 cells were obtained from the American Type Culture Collection (ATCC HTB-20). Cells were grown in complete RPMI 1640 medium (Sigma-Aldrich) supplemented with 10% (v/v) heat-inactivated FCS (PAA GmbH, Pasching, Austria) and 100 U/ml penicillin/streptomycin (Sigma) in a humidified incubator with 5% CO_2.

4.2 Cell-proliferation assays (XTT assays)

BT474 cells were seeded at a density of 10,000 cells/cm^2 in 96-well-plates (Nunc). After 24 h, DARPins (or trastuzumab as control) were added and cells were incubated for another 72 h. Cells were then incubated with 50 µl/well 2,3-bis(2-methoxy-4-nitro-5-sulfophenyl)-2H-tetrazolium-5-carboxanilide (XTT; Roche) for 4h at 37°C. Absorbance was measured at 450 nm and expressed as percentage of the untreated controls.

4.3 Cloning, Expression and Purification of DARPins

DARPin H14 is derived from H_14 (Steiner *et al.* (2008)) with a Cys→Arg mutation (C31R). DARPin G3 was originally termed H10-2-G3 (Zahnd *et al.* (2007)).

All DARPins were purified essentially as described previously (Zahnd *et al.* (2010)). Briefly, proteins were overexpressed in *E. coli* XL1-Blue and purified via their N-terminal $MRGSH_6$ tag with nickel-nitrilotriacetic acid superflow resin (Qiagen, Hilden, Germany). For cloning of bivalent constructs, the DARPin ORFs were digested with *Bam*HI and *Hin*dIII (New England Biolabs, Ipswich, Massachusetts) and ligated into compatible expression vectors pQiBi, coding for an flexible $(G_4S)_5$ linker or various inflexible NxC linkers (see **Supplementary Material** for vector design and construction of NXC-consensus-DARPins).

4.4 ELISA

HER2-domains (200 nM in PBS, 100 µl/well) were immobilized on MaxiSorp plates (Thermo Scientific) by overnight incubation at 4°C. For ELISAs, wells were blocked with 300 µl of PBSTB (PBS, 0.1% Tween-20, 0.2% BSA) for 1 h at room temperature. 50 nM of purified DARPins were incubated with the target domains for 1 h at room temperature followed by three washing steps with 300 µl of PBSTB. For detection of bound DARPins, an anti RGS-His IgG1 mouse antibody (Qiagen) was added (1:5,000 in PBSTB, 1 h at RT) which recognizes the N-terminal MRGS-His_6 tag of the DARPins and wells were washed as described above. After incubation with a secondary anti mouse-IgG antibody alkaline phosphatase conjugate (Sigma-Aldrich) (1:10,000 in PBSTB, 1 h at RT), pNPP substrate (Fluka) was added to measure alkaline phosphatase activity.

4.5 Surface Plasmon Resonance (SPR, Biacore)

SRP measurements were performed using a Biacore 3000 system (GE Healtcare). Biotinylated HER2_ECD was immobilized on Sensor Chips SA, that had been conditioned with three consecutive 1-minute injections of 1 M NaCl in 50 mM NaOH. One flow cell was left without immobilized ligand as reference flow cell. For interaction analysis and determination of kinetic data, the analyte (DARPin H14) was exchanged into HBS_T running buffer (20 mM HEPES, pH 7.4; 150 mM NaCl; 3 mM EDTA; 0.005% Tween20) via NAP5 columns (GE Healthcare). The concentrations of the rebuffered protein stock solution was determined by a spectrophotometer and diluted to different concentrations ranging from 1 nM to 40 nM for measuring on- and off-rates. Kinetic measurements were performed with a flow of 50 µl/min as follows: five minutes initial buffer blow, followed by a 2 min injection of DARPin at different concentrations. In between each single measurement the surfaces of the flow cells were regenerated with three 10 µl injections of 10 mM glycine-HCl, pH 3, as tested in preliminary studies. The signal of the uncoated reference cell and buffer response was always subtracted from the sonsograms (double referencing). Data were analysed with a global fit using “Scrubber-2” (BioLogic Software Ltd.).

4.6 Epitope characterization via flow cytometry competition

For flow cytometry competition assays, 1 × 10^5 BT474 cells were incubated with the respective AlexaFluor488-labeled binders binding at 100 nM in 100 µl PBS_BA (PBS, 0.2% NaN_3, 1% BSA) either alone or after preincubation with unlabeled binder at 1 µM to be tested for competition. After incubation, cells were harvested by centrifugation (800 × g, 30 sec, 4°C) and washed twice using 1 ml PBS_BA, each. Flow cytometry was performed on a Cyflow space system (Partec, Germany). Recorded events were gated for FSC/SSC of single viable cells. Fluorescence data were analyzed using FlowJo software.

4.7 Receptor Shedding assays

BT474 cells were grown in 6-well plates with 200,000 cells/cm^2 for 48 hours in presence or absence of the HER2 binders to be tested for inhibition of receptor shedding. After 48 hours of incubation, proteins from cell-supernatants were extracted by methanol/chloroform precipitation Wessel and Flügge (1984) and applied to anti-HER2 immunoblotting detecting the N-terminus of HER2 using primary antibody L87 (Thermo Scientific).

4.8 Receptor recycling assay via flow cytometry

For receptor recycling assays, aliquots of 1 × 10^5 cells in 100 µl DMEM were incubated with 100 nM of the respective AlexaFluor-488-labeled binder for 2 hours at 37°C in a thermal shaker to allow internalization. The cells were then washed twice with cold PBS and incubated with 100 nM anti-Alexa-488 quenching antibody (Invitrogen) and 1 µM unlabeled DARPin (chasing DARPin). The cells were put back to 37°C for 20, 40, 60 or 80 min to allow recycling. For each time point, receptor recycling was stopped by adding NaN_3 (0.1% final concentration) and putting the respective aliquots on ice. Prior to the detection of the remaining fluorescent signal by flow cytometry, cells were washed with cold PBS_BA. The percentage of unchased signal corresponding to non-recycled DARPins was calculated by comparison to aliquots of cells with internalized DARPins which had not been allowed to recycle.

4.9 Expression and purification of scFv 4D5

The scFv 4D5 was expressed and purified as described before (Willuda *et al.* (2001)). In brief, expression was performed in the periplasm of *E. coli* strain SB536. Freshly transformed cells grown overnight in 50 ml of 2YT medium containing 50 µg/ml ampicillin (2YT/Amp) were used to inoculate 1 litre of culture, shaking in baffled 5 l flasks. At an OD_{600} of 0.7, expression was induced with 1 mM IPTG (final concentration) and continued for 8 hours at 20°C. Cells were harvested by centrifugation (4000 g, 15min, 4°C) and lysed with an Emulsiflex-C5 homogenizer (Avestin, Canada). The scFv was purified via IMAC.

5 Conclusions

The screening of 22 monovalent DARPins binding to different extracellular HER2-epitopes led to the discovery of one DARPin, termed H14, which exhibits antiproliferative effects on the *in vitro* growth of BT474 cells. These antiproliferative effects are comparable, both in terms of activity and EC_{50}, with those caused by scFv 4D5, which is the monovalent single-chain fragment of the therapeutic antibody trastuzumab. Interestingly, DARPin H14 and scFv 4D5 bind to overlapping epitopes on HER2_IV, as could be concluded from competition experiments. Different than trastuzumab, DARPin H14 does not affect the receptor shedding of HER2.

Since both monovalent binders, DARPin H14 and scFv 4D5, cause their antiproliferative effect *in vitro*, where mechanisms like ADCC or CDC are excluded, and since alternative mechanisms of action like a putative effect on receptor shedding have been excluded, this antiproliferative effect seems to be of steric nature.

This hypothesis that binding of DARPin H14 and scFv 4D5 sterically interferes with HER2 homo- or heterodimerization is in line with previous reports, which named residues in the homologous region of EGFR_IV as being important for intermolecular contacts between dimerization partners (Adak *et al.* (2011)). In the publication by Adak *et al.* it was suggested that the tethering arm on EGFR_IV (residues 561-585), that is highly conserved among ErbB family receptors, contributes to intersubunit interactions within receptor homo- and heterodimers.

Interestingly, the region on HER2_IV that is homologous to the tether region of EGFR is part of the epitope bound by scFv 4D5, and thereby most likely part of the epitope of DARPin H14 as well. It is therefore very likely that binding to that particular epitope on HER2_IV, both by DARPin H14 or scFv 4D5, reduces the receptor's potential to undergo canonical dimerization.

In an attempt to improve the antiproliferative effect of DARPin H14 and inspired by the example of trastuzumab, which connects two monovalent 4D5 moieties to one bivalent IgG molecule, we engineered bivalent DARPin constructs which are composed of two H14 moieties, connected via inflexible, inert DARPin-linkers with various lengths ("H14_NxC_H14" with x being 3, 4, 6, 7, 8 or 10 internal repeat modules). In analogy to the immunoglobulin formats scFv 4D5 and IgG trastuzumab, these bivalent DARPins could be shown to have improved antiproliferative activity, with N6C (or longer) linkers being most effective.

In contrast to the monovalent format, where DARPin H14 was the only DARPin found to exhibit an effect on cell growth, the bivalent format could be applied to DARPin G3, another anti-HER2 DARPin binding subdomain IV, which lacks biological activity in the monovalent format. Testing the rigid linker format with different anti-HER2 DARPins binding subdomain I (HER2_I) yielded bivalent constructs that had only weak antiproliferative effects or completely lacked any effect on cell growth of HER2 overexpressing cells.

In summary, our investigations with monovalent and bivalent HER2 binding DARPins offer two new ways how to affect the cell proliferation of HER2-addicted cancer cells with protein binders to the extracellular part of the receptor. On the one hand, we identified an epitope region within the dimer interaction surface on HER2_IV, which seems to play a role for the HER2 dimerization potential, as binding of DARPin H14 or scFv 4D5 affect cell proliferation of cells that are dependent on HER2 dimerization. On the other hand, we have demonstrated another way to efficiently inhibit HER2's pro-proliferative influence in such cells: the inhibitory constructs act by keeping pairs of HER2 molecules in a fixed distance by bivalent binding of rigid DARPin constructs. As the receptor positioning induced by our rigid DARPin constructs leads to

strong anti-proliferative effects on HER2-addicted cancer cells, we propose that the bound receptor molecules are inhibited from contributing to HER2 signaling.

Interestingly, bivalent binding to the same epitope with flexible constructs led to an increased cell proliferation. This finding might propose a role of HER2 homodimers for cell proliferation. It is tempting to speculate that pairs of HER2, that are flexibly kept in close proximity by flexible bivalent binders, are prone to transphosphorylate each other and contribute thereby to proproliferative signaling.

6 References

1. Adak S, DeAndrade D, & Pike LJ (2011) The tethering arm of the EGF receptor is required for negative cooperativity and signal transduction. *J. Biol. Chem.* 286:1545-1455.
2. Binz HK*, et al.* (2004) High-affinity binders selected from designed ankyrin repeat protein libraries. *Nat. Biotechnol.* 22:575-582.
3. Brennan PJ, Kumagai T, Berezov A, Murali R, & Greene MI (2000) HER2/neu: mechanisms of dimerization/oligomerization. *Oncogene* 19:6093-6101.
4. Chen CH, Chernis GA, Hoang VQ, & Landgraf R (2003) Inhibition of heregulin signaling by an aptamer that preferentially binds to the oligomeric form of human epidermal growth factor receptor-3. *Proc. Natl. Acad. Sci. U. S. A.* 100:9226-9231.
5. Clayton AH, Orchard SG, Nice EC, Posner RG, & Burgess AW (2008) Predominance of activated EGFR higher-order oligomers on the cell surface. *Growth Factors* 26:316-324.
6. Craven RJ, Lightfoot H, & Cance WG (2003) A decade of tyrosine kinases: from gene discovery to therapeutics. *Surg. Oncol.* 12:39-49.
7. Molina MA*, et al.* (2001) Trastuzumab (herceptin), a humanized anti-Her2 receptor monoclonal antibody, inhibits basal and activated Her2 ectodomain cleavage in breast cancer cells. *Cancer Res.* 61:4744-4749.
8. Scheer JM*, et al.* (2012) Reorienting the Fab Domains of Trastuzumab Results in Potent HER2 Activators. *PLoS One* 7:e51817.
9. Steiner D, Forrer P, & Plückthun A (2008) Efficient selection of DARPins with sub-nanomolar affinities using SRP phage display. *J. Mol. Biol.* 382:1211-1227.
10. Sundaresan S, Penuel E, & Sliwkowski MX (1999) The biology of human epidermal growth factor receptor 2. *Curr. Oncol. Rep.* 1:16-22.
11. Wessel D & Flügge UI (1984) A method for the quantitative recovery of protein in dilute solution in the presence of detergents and lipids. *Anal. Biochem.* 138:141-143.
12. Willuda J*, et al.* (2001) Tumor targeting of mono-, di-, and tetravalent anti-p185(HER-2) miniantibodies multimerized by self-associating peptides. *J. Biol. Chem.* 276:14385-14392.
13. Yan L, Hsu K, & Beckman RA (2008) Antibody-based therapy for solid tumors. *Cancer J* 14:178-183.
14. Yarden Y & Sliwkowski MX (2001) Untangling the ErbB signalling network. *Nat. Rev. Mol. Cell Biol.* 2:127-137.
15. Zahnd C*, et al.* (2010) Efficient tumor targeting with high-affinity designed ankyrin repeat proteins: effects of affinity and molecular size. *Cancer Res.* 70:1595-1605.
16. Zahnd C, Pecorari F, Straumann N, Wyler E, & Plückthun A (2006) Selection and characterization of Her2 binding-designed ankyrin repeat proteins. *J. Biol. Chem.* 281:35167-35175.
17. Zahnd C*, et al.* (2007) A designed ankyrin repeat protein evolved to picomolar affinity to HER2. *J. Mol. Biol.* 369:1015-1028.
18. Zhang Q, Park E, Kani K, & Landgraf R (2012) Functional isolation of activated and unilaterally phosphorylated heterodimers of ERBB2 and ERBB3 as scaffolds in ligand-dependent signaling. *Proc. Natl. Acad. Sci. U. S. A.* 109:13237-13242.

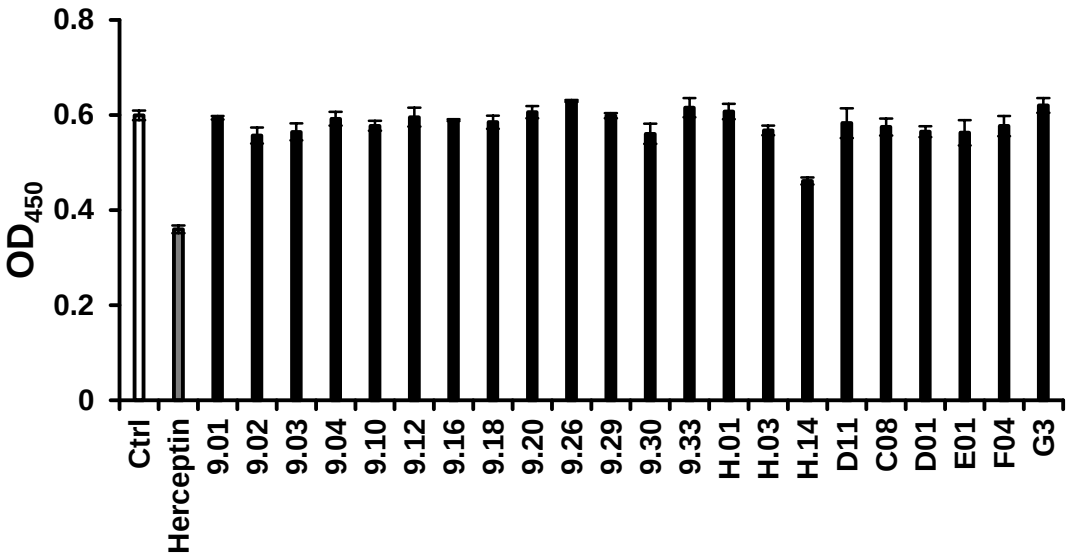

Figure 2.1: Cell proliferation assay with 1 µM concentrations of DARPins on BT474 cells. Cells were seeded with 10'000 cells × cm^{-2} and allowed to attach for 24 hours. Cell viability after additional four days of growth with or without treatment (Ctrl) was measured by XTT-assays (indicated as OD_{450}). Cells treated with 10 nM trastuzumab (Herceptin) served as positive control.

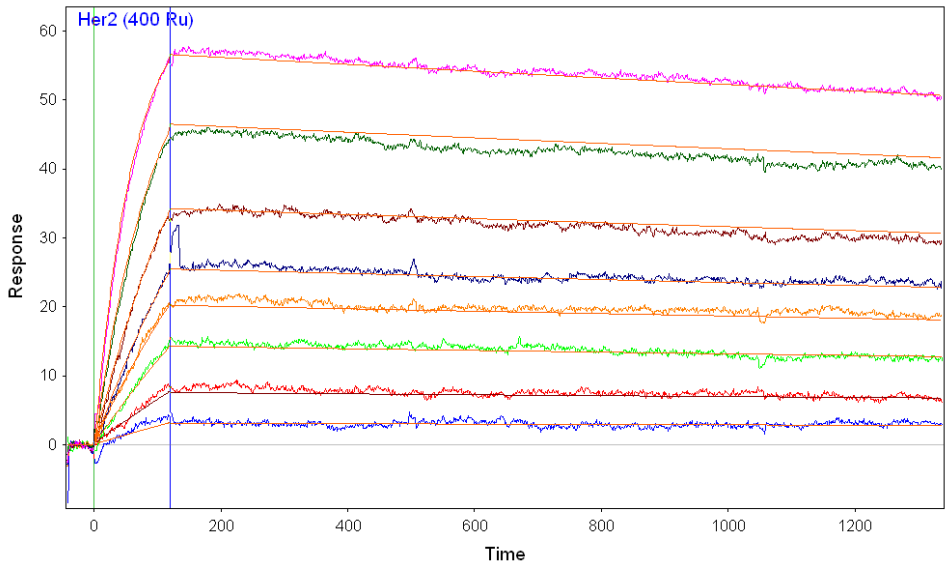

Figure 2.2: Quantitative affinity measurements (SPR) with DARPin H14. Measurements were performed in HBS-T buffer at a flow rate of 50 µl/min with increasing concentrations of H14 (nM 1, 2.5, 5, 7.5, 10, 15, 25, 40).

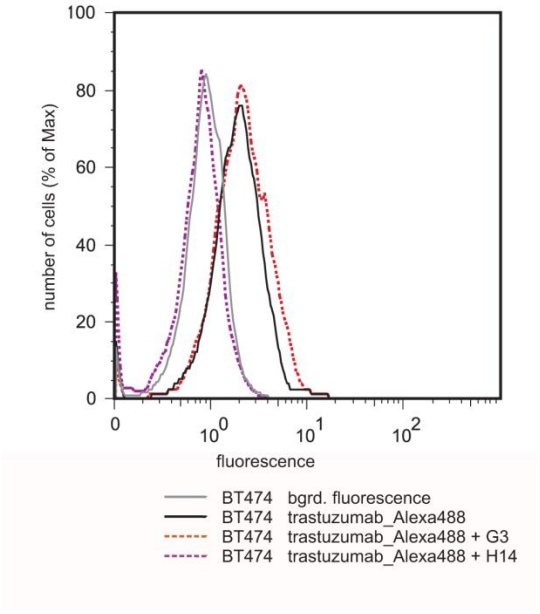

Figure 2.3: Epitope characterization of HER2-binding DARPins. Flow cytometry experiments with AlexaFluor488-labeled trastuzumab binding to BT474 cells at 100 nM either alone (continuous lines) or after preincubation with unlabeled DARPins to be tested at 1 µM for competition (dotted lines).

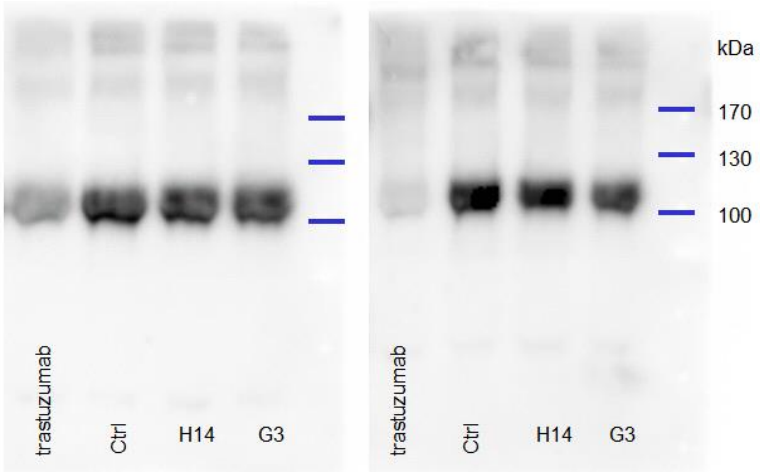

Figure 2.4: Effect of HER2 binders on receptor shedding. Proteins from BT474-cell supernatants after 48 hours of growth in the presence or absence (Ctrl) of HER2 binders were extracted by methanol/chloroform precipitation and applied to anti-HER2 immunoblotting, detecting the N-terminus of HER2. Each condition was performed in duplicates.

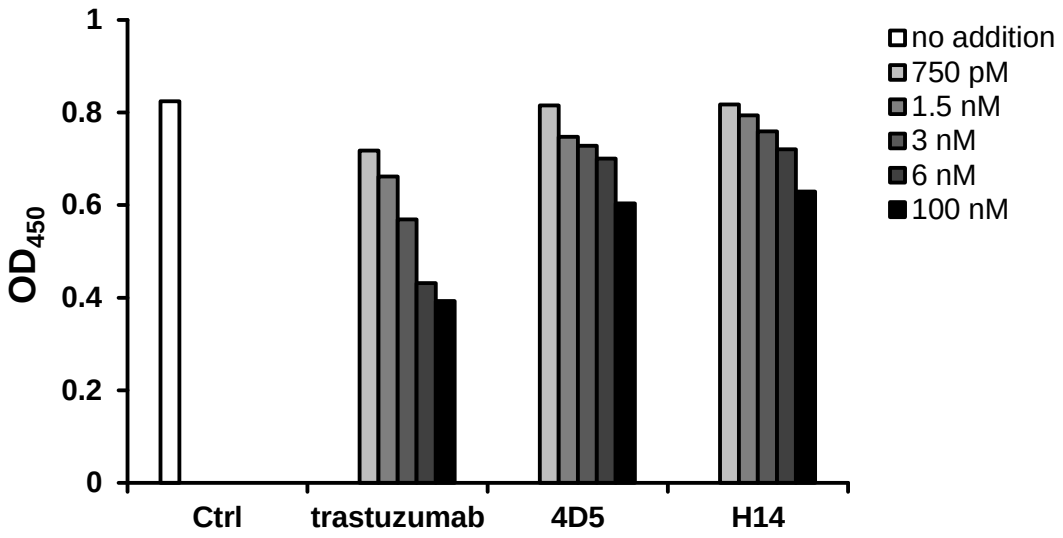

Figure 2.5: Cell proliferation assay with dilution series of different HER2-targeting proteins on BT474 cells. Cells were seeded with 10,000 cells × cm^{-2} and allowed to attach for 24 hours. Cell viability after an additional four days of growth with or without treatment (Ctrl) was measured by XTT-assays (indicated as OD_{450}).

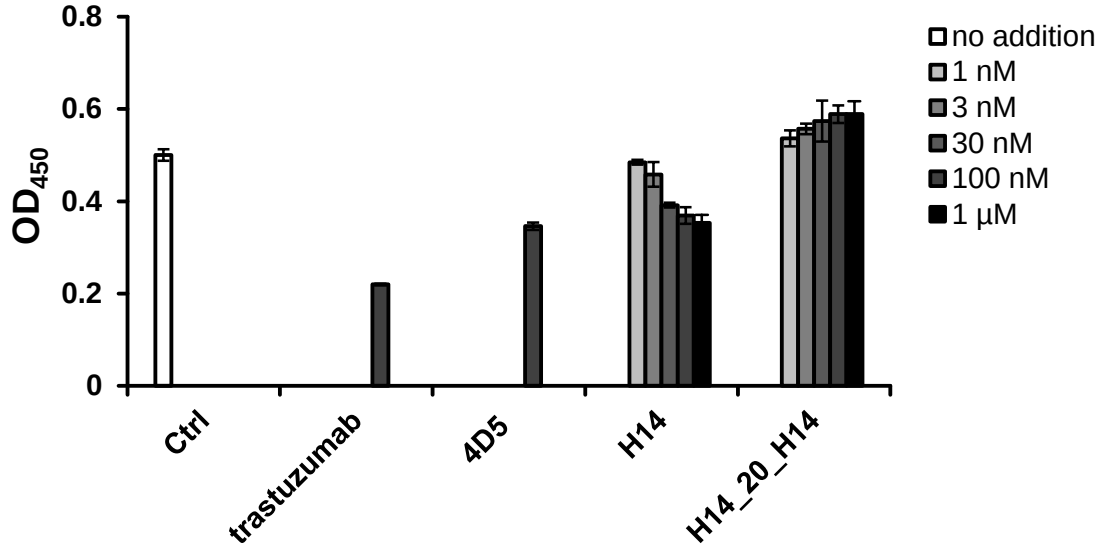

Figure 2.6: Cell proliferation assay with dilution series of DARPin H14 in monovalent (H14) or flexible bivalent (H14_20_H14) format. Cells were seeded with 10'000 cells × cm^{-2} and allowed to attach for 24 hours. Cell viability after additional four days of growth with or without treatment (Ctrl) was measured by XTT-assays (indicated as OD_{450}). Cells treated with 100 nM of trastuzumab or scFv 4D5 served as controls. Data points were recorded in triplicates.

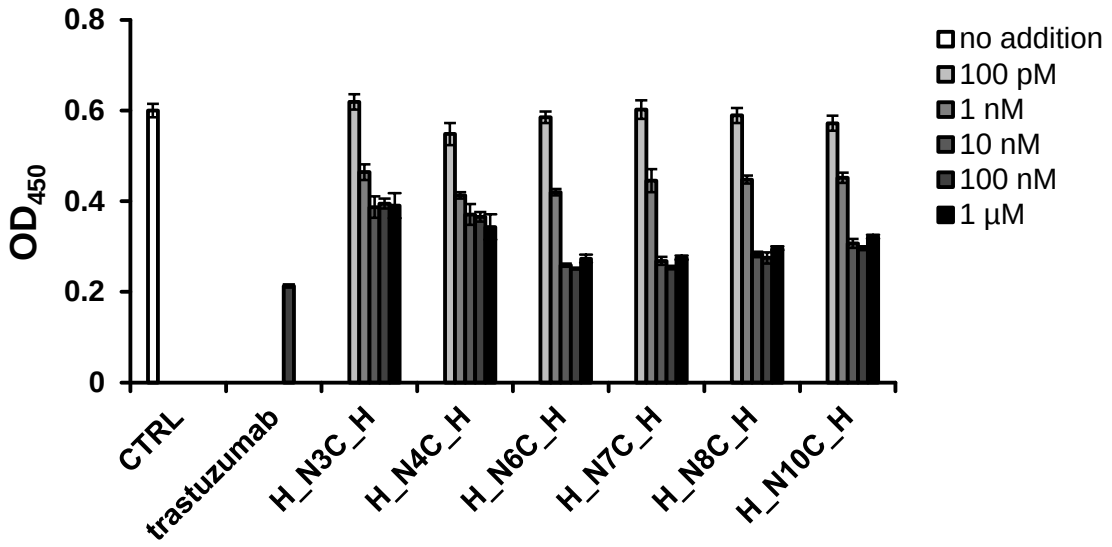

Figure 2.7: Cell proliferation assay with dilution series of inflexibly linked bivalent H14 constructs. Cells treated with 100 nM of trastuzumab or untreated cells (Ctrl) served as controls. Data points were recorded in triplicates.

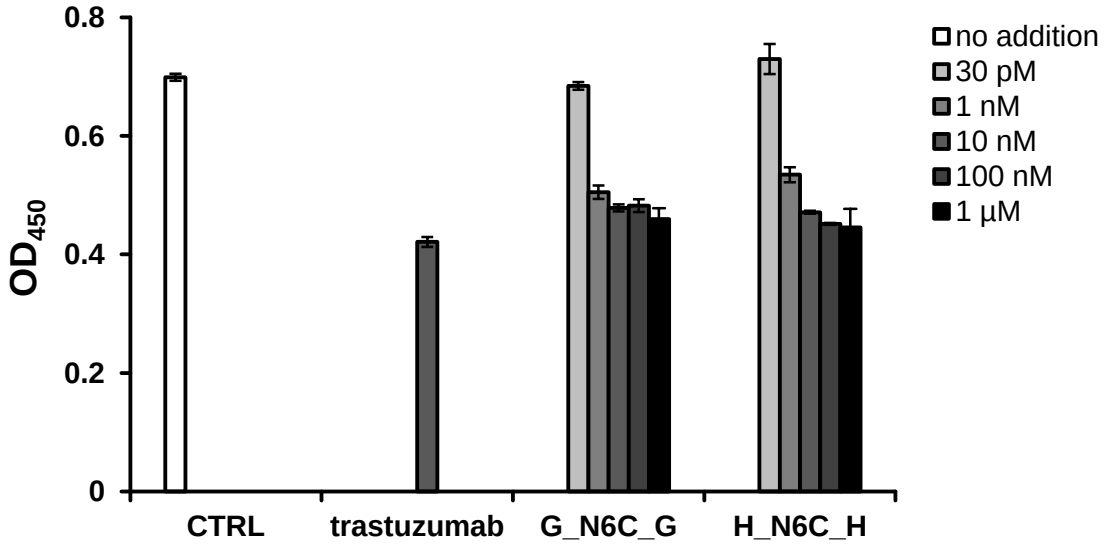

Figure 2.8: Cell proliferation assay with dilution series of inflexibly linked bivalent DARPin constructs composed of DARPin G3 (G_N6C_G) or H14 (H_N6C_H). Cells treated with 100 nM of trastuzumab or untreated cells (Ctrl) served as controls. Data points were recorded in triplicates.

Chapter 3

Structural Basis for eliciting a cytotoxic effect in HER2-addicted cancer cells via binding to the extracellular domain of HER2

Christian Jost, Johannes Schilling, Rastislav Tamaskovic, Martin Schwill, Annemarie Honegger and Andreas Plückthun

Department of Biochemistry, University of Zürich, Switzerland

Correspondence should be addressed to

Prof. Andreas Plückthun, Biochemisches Institut, Universität Zürich, Winterthurerstr. 190, 8057 Zürich, Switzerland, phone: +41-44-635 5570, plueckthun@bioc.uzh.ch.

Running Title: Structural Basis of cytotoxic HER2-binding DARPins

Content

1 Summary 44

2 Highlights 44

3 Introduction 44

4 Results 48

4.1 Epitope-mapping of HER2-binding DARPins 48

4.2 Construction of bispecific binders targeting different epitopes 48

4.3 Effects of mono- and bivalent constructs on cell proliferation and cell death 49

4.4 X-Ray Crystal Structures of complexes HER2_I:9_29, HER2_I:9_26 and HER2_IV:G350

4.5 Molecular modeling of full HER2 and DARPin-inhibited states 52

5 Discussion 55

5.1 Monomeric DARPins do not interfere with HER2 signaling 55

5.2 Activity depends on linker length 56

5.3 The linker length is too short for both DARPins to bind to the same HER2 monomer or dimer 57

5.4 Orientation of HER2 on the cell surface 57

5.5 Conformational flexibility of the HER2 extracellular domain 58

5.6 Interference with HER2 dimerization and activation 58

6 Conclusions 59

7 Experimental Procedures 61

7.1 Cloning, Expression and Purification of DARPins 61

7.2 Cell culture 61

7.3 Flow cytometry 61

7.4 Cell viability assays (XTT assays) 62

7.5 Expression in insect cells 62

7.6 X-ray crystallography 62

8 Acknowledgements 63

9 References 65

1 Summary

Human epidermal growth factor receptor-2 (HER2) is a receptor tyrosine kinase directly linked to the growth of malignancies from various origins and a validated target for monoclonal antibodies and kinase inhibitors. Utilizing a new approach with Designed Ankyrin Repeat Proteins (DARPins) as alternative binders, we show that binding of two DARPins connected by a short linker, one targeting extracellular subdomain I, the other subdomain IV, causes much stronger cytotoxic effects on the HER2-addicted breast cancer cell line BT474, surpassing the therapeutic antibody trastuzumab. We determined crystal structures of these DARPins in complex with the respective subdomains. Detailed models of the full-length receptor, constrained by its rigid domain structures and its membrane anchoring, explain how the bispecific DARPins connect two membrane-bound HER2 molecules, distorting them such that they cannot form signaling-competent dimers with any EGFR family member, preventing any kinase dimerization, and thus leading to a complete loss of signaling.

2 Highlights

- Particular Bispecific DARPins binding to the HER2 extracellular domain are cytotoxic
- Crystal structures of the DARPin:target complexes reveal mechanism of action
- Bivalent binding crosslinks HER2-monomeres in a signaling-incompetent state
- Bispecific DARPin-bound state prevents HER2 kinases from forming any complex

3 Introduction

The human epidermal growth factor receptor 2 (HER2, hErbB2) is a receptor tyrosine kinase expressed on the cell surface of nearly every cell in the human body. HER2 contributes to multiple signal transduction pathways, but mainly stimulates the HER3/PI3K/Akt pathway and the mitogen-activated protein (MAP) kinase cascades, leading to cell survival and proliferation (Craven *et al.* (2003); Yarden and Sliwkowski (2001)). HER2 amplification promotes tumorigenesis (Faber *et al.* (2010)), and human tumors and various tumor cell lines rely on

HER2-signaling for their survival. Such cancer cells are often referred to as "HER2-addicted" (Moasser (2007)).

Trastuzumab (Herceptin®, Genentech, San Francisco, CA), a humanized monoclonal antibody binding to the extracellular subdomain IV of HER2 (HER2_IV), is effectively used in the clinic to treat patients with HER2-overexpressing breast cancers (Cobleigh *et al.* (1999); Finn and Slamon (2003)). Besides exerting cytotoxic effects in vivo through antibody-dependent cellular cytotoxicity (ADCC) and complement-dependent cytotoxicity (CDC), trastuzumab mainly acts as a cytostatic agent inducing a G1 phase cell cycle arrest in HER2-amplified cancer cells (Sliwkowski *et al.* (1999)). Inhibition of HER2 homodimerization (Ghosh *et al.* (2011)) and of HER2/HER3 heterodimerization (Junttila *et al.* (2009)) is thought to be responsible for this anti-proliferative effect. Pertuzumab (Perjeta®, Genentech, San Francisco, CA), a humanized monoclonal antibody binding next to the dimerization arm on subdomain II of HER2, shows only moderate anti-tumor effects in vitro on HER2 overexpressing breast cancer cell lines (shown for SkBr-3 cells (Schaefer *et al.* (1997))). However, for cell lines with normal HER2 expression levels that are grown in the presence of the HER3-activating ligand Heregulin, which efficiently stimulates HER2/HER3 heterodimer formation (Sliwkowski *et al.* (1994)), the effect of pertuzumab exceeds the effect of trastuzumab (Schaefer *et al.* (1997)). This finding can be explained in that pertuzumab, bound next to the HER2 dimerization arm, sterically blocks the formation of back-to-back heterodimers that are induced by ligand stimulation of HER3 (Franklin *et al.* (2004)).

Recently, Trastuzumab emtansine (T-DM1) (Kadcyla®), a maytansinoid conjugate (Burris *et al.* (2011); Verma *et al.* (2012)), has become FDA-approved. It is thought to be endocytosed with the slow internalization and recycling rates intrinsic to ErbB2 and thus to release the toxin. These encouraging data stimulate the search for novel mechanisms of action, which may pave the way for agents not requiring a conjugated toxin.

Recent studies on the regulation of the homologous receptor EGFR have shown that receptor dimerization is required, but may not be sufficient for full receptor activation

(Arkhipov *et al.* (2013); Endres *et al.* (2013)). Dimerization of ECD, TM-helices and, as a consequence, the kinase domains have to take place in a well ordered mechanism, requiring, e.g., pairing the N- but not the C-terminal parts of the two TM-helices for functional dimerization of the kinase domains. Additional factors modifying the coupling between dimerization of the extracellular domain to the dimerization and activation of the kinase domain may contribute to the subtle regulation of receptor activity (Arkhipov *et al.* (2013); Endres *et al.* (2013)).

Tumor cells becoming refractory to trastuzumab treatment present a major clinical problem. This is not only caused by down-regulation or loss of HER2 expression, but also by various mutations bypassing the blocked HER2-signaling, including constitutive activation of the PI3K-signaling pathway, accumulation of a constitutively active HER2-kinase, and crosstalk of HER2 with other growth factor receptors (Sergina *et al.* (2007); Xia *et al.* (2004)). Acquisition of trastuzumab resistance might be promoted by the cytostatic effect of trastuzumab, which allows the tumor to undergo a directed evolution to escape treatment. Thus, an optimal drug against HER2-overexpressing cancer cells would have to be cytotoxic instead of cytostatic, but the cytotoxicity should not broadly aim at all HER2-expressing cells, but rather specifically target cancer cells that are dependent on HER2.

The concept that HER2 remains the active oncogenic driver in many cancer cells, e.g. by signaling through HER2-HER3-heterodimers, motivates further research for alternative molecular therapies targeting HER2 (Gajria and Chandarlapaty (2011)). To expand and complement existing anti-HER2 therapies beyond pertuzumab and trastuzumab or any toxin conjugates, such as T-DM1 (Burris *et al.* (2011)), further HER2-binders that employ alternative mechanisms should thus be developed for abolishing HER2-dependent signaling.

Designed ankyrin repeat proteins (DARPins) are binding scaffolds that have recently been developed to expand the range of formats and applications beyond what is possible with immunoglobulin-based proteins (Binz *et al.* (2004); Boersma and Plückthun (2011)). Because of their small size, high stability and efficient folding, DARPins can easily be fused to each other in different orientation and geometries and to different protein domains, to generate multivalent

or multispecific constructs or to provide targeting specificity to effector proteins. They are highly suitable for site-specific chemical modification (Simon *et al.* (2012)), e.g. coupling to polyethylene glycol (PEGylation) to increase the hydrodynamic radius and thus serum half-life and thereby promote tumor uptake (Zahnd *et al.* (2010)) or conjugation of toxins. While they have been used for targeting toxins to a tumor (Martin-Killias *et al.* (2011)), it is of interest to investigate whether they can also exert a biological function by themselves. Thus, they appear predestined as binding moieties for novel approaches in targeted therapy. DARPins recognizing the soluble recombinant ectodomain of HER2 (HER2-ECD) with sub-nanomolar to low nanomolar affinities were selected by ribosome display (Zahnd *et al.* (2007)) and phage display (Steiner *et al.* (2008)). These HER2-specific DARPins have been used for histochemical staining (Theurillat *et al.* (2010)), for tumor targeting of toxins (Zahnd *et al.* (2010)) and for targeting adenoviral (Dreier *et al.* (2013)) and lentiviral vectors (Münch *et al.* (2011); cf. **Appendix 1**) to HER2-overexpressing cells.

In this paper, we demonstrate the cytotoxic activity of bispecific DARPin constructs against the HER2-addicted cell line BT474, a widely used model system for testing anti-HER2 activity in vitro. The bispecific DARPins do not only induce a cytostatic effect like trastuzumab, but rather act as specific cytotoxic agents. This cytotoxic effect does not rely on any conjugated toxin, but is intrinsic to the binding mechanism.

The results were confirmed on a broad panel of breast tumor cell lines and tumor models by (Tamaskovic et al. (2013), cf. **Chapter 4**), who proceeded to characterize in great detail the influence of these constructs on various aspects of downstream signaling, such as phosphorylation pattern, downstream kinase activity and apoptotic markers. They showed that the most potent of the bispecific DARPins cause a persistent inhibition of both the phosphatidyl-inositol-3-kinase (PI3K-AKT/PKB) and the RAS-RAF-MAPK pathway, leading to a strong apoptotic response. Based on the X-ray structures of three DARPins in complex with the cognate HER2-ECD subdomain we have determined here, we propose a model of how such a complete shutdown of HER2-dependent signaling is achieved.

4 Results

4.1 Epitope-mapping of HER2-binding DARPins

DARPins that had been selected by phage display (Steiner *et al.* (2008)) or ribosome display (Zahnd *et al.* (2007)) to target the full-length ectodomain of HER2 without showing any cross-specificity against other EGFR-family members were characterized concerning which of the four HER2-subdomains forms the epitope. Since DARPins typically recognize conformational epitopes, we expressed subdomains alone and in combination in insect cells using a baculovirus system (Supplementary Text, SI Text). To minimize glycosylation for subsequent crystallization, we replaced the Asn residues in predicted N-linked glycosylation sites by Asp. ELISAs on these proteins showed that the epitopes recognized by DARPins 9_26 and 9_29 are located on HER2-I, while DARPin G3 bound to HER2-IV (**Supplementary Fig. S1A**). Competition for binding to HER2-overexpressing cells measured by flow cytometry revealed that DARPins 9_26 and 9_29 compete for the same epitope (**Fig. S1B**). DARPin G3, which binds to HER2 subdomain IV, did not compete with trastuzumab but competed with a different HER2-specific DARPin, H.14, which in turn competed with trastuzumab.

4.2 Construction of bispecific binders targeting different epitopes

Various bivalent and bispecific constructs were generated by genetically fusing two DARPins by $(G_4S)_n$ linkers of different lengths. To target two non-overlapping epitopes with a single molecule, DARPins 9_29 or 9_26 were connected to DARPin G3 by a 20 amino acid linker, with either an ECD-I binder at the N-terminal end and the ECD-IV binder at the C-terminus or in opposite orientation. The four different bispecific binders (e.g., 9_26-$(G_4S)_4$-G3, abbreviated "6_20_G" for the two DARPins and the linker length of 20 amino acids) were tested regarding their binding to HER2-overexpressing cells. G3 with a K_D of 90 pM (Zahnd *et al.* (2007)) has the highest affinity of the three HER2-binders used in this study, compared to a K_D of 1 nM for 9_26 and 1 nM for 9_29 (Steiner *et al.* (2008)). Kinetic experiments on cells in the presence of a competing DARPin (to prevent rebinding) revealed that the off-rates of the bispecific binders

were 10 times lower than the off-rates of monovalent G3 (**Fig. 1A**, **Table S1**). The slower off-rate and higher K_D of the bispecific constructs, compared to their monovalent building blocks, can be attributed to an avidity effect and indicates bispecific binding to HER2 on the cell.

4.3 Effects of mono- and bivalent constructs on cell proliferation and cell death

We tested the influence of the different DARPin constructs on cell proliferation and cell survival in XTT assays, using BT474 cells as an example of a HER2-addicted cell line. MCF7-cells, which express HER2 at much lower levels than BT474 cells, were used as a control. Calibration experiments showed that a signal decrease by 60%, compared to untreated cells, corresponded to lack of cell proliferation over the 4 days of cell growth before the XTT assay — a larger decrease indicated cell death.

None of the monovalent DARPins characterized in this study affected the number of viable cells measured by the XTT assay (**Fig. 1B**). Mixtures of two different DARPins proved to be equally inert, as did control constructs in which one of the two DARPins in the bispecific molecule had been replaced by a non-HER2-binding DARPin (DARPin off7, targeting maltose-binding-protein (Binz *et al.* (2004))) (**Fig. 1C**). A monospecific bivalent DARPin G_20_G even stimulated cell proliferation (**Fig. 1C**).

Bispecific constructs composed of a subdomain I binder at the N- and the subdomain IV binder at the C-terminus (6_20_G or 9_20_G) showed a concentration-dependent decrease of cell viability by up to 75%, while treatment with trastuzumab decreased viability by ~50% (**Fig. 1D**). The constructs with reverse orientation (G_20_9) either lacked any effect on cell-growth (G_20_6) or even slightly promoted cell growth. Similar to trastuzumab, bispecific constructs did not affect the cell-proliferation of MCF7-cells (**Fig. 1E**), suggesting the restriction of the observed effects to HER2-addicted cells. Comparison of constructs with 5, 10, 20, 30 and 40 amino acid linkers showed that for 9_x_G constructs, specific activity and potency decreases with increasing linker length. The most potent constructs proved to be 6_5_G and 9_5_G, with (G4S)-linkers of only five amino acids. They decreased the cell viability in XTT-assays after four

days of growth by more than 80% as compared to untreated cells, and showed a half-maximal effect already at a concentration of less than 100 pM compared to ca. 1 nM for 6_20_G and 9_20_G. Conversely, increasing the linker length to forty amino acids, as in 6_40_G and 9_40_G, decreased the biological activity (growth reduction of only 40%) (**Fig. 1F**). The constructs with inverse orientation, G_x_6 and G_x_9, inactive or even stimulatory at a linker length of 20 amino acids, gained anti-proliferative activity at short linker lengths, but the best construct was found to be only as active as trastuzumab (**Fig. 1G**). Neither the single DARPins nor the bispecific constructs affected internalization or degradation of HER2, as determined by flow cytometry (Tamaskovic *et al.* (2013), cf. **Chapter 4**).

4.4 X-Ray Crystal Structures of complexes HER2_I:9_29, HER2_I:9_26 and HER2_IV:G3

The structures of the complexes of HER2_I with DARPin 9_29 and with 9_26 were determined at 2.55 Å and 3.2 Å resolution, respectively, the structure of HER2_IV in complex with G3 at 2.65 Å resolution. A summary of data collection statistics and refinement results is listed in **Table S2**. Unliganded 9_26 was solved to 2.9 Å (unpublished result), unliganded G3 (PDB ID: 2JAB) (Zahnd *et al.* (2007)) to 1.7 Å. G3 and unliganded 9_26 contain the original DARPin C-cap, which by NMR had been shown, to some percentage, to show some transient unfolding in solution (Wetzel *et al.* (2010)). For crystallization in complex with HER2_I, this C-cap was replaced by an optimized C-cap (Mut5) (Interlandi *et al.* (2008)) in DARPins 9_29 and 9_26, which does not give any sign of transient unfolding.

The asymmetric unit of HER2_I:9_29 contains one heterodimeric complex with 7 intermolecular hydrogen bonds (**Table S3**), and a buried surface area of 784 Å2 (**Fig. 2 A-C**). In the asymmetric unit of HER2_I:9_26, two heterodimers are present. Due to the limiting quality of the HER2_I:9_26 data set, slight differences are visible between the two complexes and parts of the complex are not resolved. Most of our analyses are therefore concentrated on the HER2_I:9_29 complex. The asymmetric unit of the HER2_IV:G3 structure contains two heterodimeric complexes with 7 and 5 intermolecular hydrogen bonds between DARPin G3 and

HER2_IV (**Table S4**), respectively, and a buried surface area of 818 Å2 (complexes A/D, **Fig. 2D-F**) or 759 Å2 (complex B/C).

The conformation of HER2_I and HER2_IV is essentially the same as that of the respective subdomain in structures of the whole extracellular domain of HER2 (Bostrom *et al.* (2009); Cho *et al.* (2003); Fisher *et al.* (2010); Franklin *et al.* (2004); Garrett *et al.* (2003)), with rmsd values for the Cα-backbone around 0.49 to 0.81 Å for HER2_I and 0.24 to 0.68 for HER2_IV (**Table S5**, **Fig. S2 A,B**), underlining the rigidity of the HER2 domains.

A comparison of the epitopes recognized by various HER2 binders in the Protein Data Bank (**Fig. 3**) shows that the regions recognized by the three DARPins do not overlap with epitopes recognized by any of the other binders: scFv A21 binding to domain I (Zhou *et al.* (2011)), therapeutic antibody pertuzumab recognizing subdomain II (Franklin *et al.* (2004)), Z-domain-derived affibody zHER2 (Eigenbrot *et al.* (2010)), recognizing the same epitope on domain III as Fab37 (Fisher *et al.* (2010)), and trastuzumab (Cho *et al.* (2003)) and its HER2/VEGF dual specific variant bH1 (Bostrom *et al.* (2009)) binding to subdomain IV.

DARPins 9_29 and 9_26 bind to the same epitope on HER2_I, involving residues from the N-cap and the first two internal repeats (**Fig. 4**). The third repeat and the C-cap make no contacts. The DARPin contacts two adjacent strands of HER2_I at the edge of this domain, including further interactions down the side perpendicular to the β-helix axis of domain I, which is a member of the L-domain family. The high-affinity binding of DARPin 9_29 to HER2_I is governed by six hydrogen bonds, pi-stacking and extended hydrophobic interactions described in detail in the SI Text (**Table S3**). Epitope and paratope residues are highlighted in the sequence alignments shown in **Fig. S3**. Comparison of the sequence differences between the two DARPins to this contact map shows that 14 out of 19 contact residues are conserved.

Construct HER2-IV spans residues 509-604 of the HER2-ECD, omitting the last two disulfide bonds. Residues 581-604 are disordered in the structure. DARPin G3 binds to an epitope on the N-terminal half of subdomain IV (residues 513-564). The structure of G3 in the complex is well maintained compared to its uncomplexed structure (rmsd 0.65 or 0.55 Å,

Fig. S2 C), demonstrating that the DARPin:HER2 complexes can, in a first approximation, be considered as rigid body interactions. The paratope comprises both internal repeats and the C-cap of the DARPin (**Fig. 2**, **Fig. S3**). The long axis of the DARPin is at nearly a right angle to the long axis of HER2_IV, the DARPin β-turns facing towards the membrane. The DARPin wraps around the rod shaped Cys-rich domain IV, its slight curvature is fitting the target shape very well, explaining the high affinity of 90 pM. It contacts two protrusions, formed by the loop spanned by Cys 523 and 539 and the adjacent pair of interlocked disulfide bond. Two of the four mutations introduced during affinity maturation are directly involved in binding interaction. Of the 14 randomized residues, 9 are involved in specific contacts, as are several framework residues. Six hydrogen bonds and extended hydrophobic interactions, altogether contributed by 13 residues (SI Text), are responsible for the picomolar affinity of G3. The atomic interactions are summarized in **Table S4**. Thus, although G3 possesses only two internal repeats, the perfectly matching hydrophobic and hydrogen bonding interactions, contributed by adapted curvature as a result of directed evolution (Zahnd *et al.* (2007)), account for its high affinity.

4.5 Molecular modeling of full HER2 and DARPin-inhibited states

Since the HER2 domains are very rigid, and their structure did not change between the DARPin complexes and the whole ECD, we could easily place the DARPins on the full HER2_ECD (residues 1-620). We also built models of putative HER2_ECD homo-and heterodimers (see SI Text for a detailed description of the modeling procedure), taking into account all available ErbB-family structures to make the models as realistic as possible. The DARPins bound to HER2_I and HER2_IV could be added to the HER2 monomer and dimer models without any clashes (**Fig. 5 A-D**).

To build a model of the whole receptor, the HER2-ECD model were combined with the NMR structures of transmembrane helices (PDB entry 2JWA (Bocharov *et al.* (2008))) and the X-ray structures of the kinase domains (PDB ID: 3PP0 for the active kinase dimer (Aertgeerts *et al.* (2011)), 3RCD for the inactive kinase (Ishikawa *et al.* (2011))), taking the EM-based models of

Mi *et al.* (2011) as a guide. Seven residues between the last disulfide bridge of ECD domain IV and the start of the transmembrane helix and 30 residues between TM domain and kinase were treated as flexible to connect the domains. The resulting models assume that initially both monomer and dimer stand upright on the membrane, and that the HER2-ECD is as rigid as suggested by Cho *et al.* (2003) and Dawson *et al.* (2007).

The distance between the C-term of the domain-I-binding DARPin and the N-term of the domain-IV-binding DARPin is 130 Å on the same HER2 molecule (**Fig. 5A**). For intramolecular binding to a HER2_ECD monomer in this orientation, 9_x_G, the linker would have to be even longer, as it needs to wrap around the monomer. However, the most active of our constructs has a linker length of a mere five amino acids, spanning no more than 17 Å, which thus excludes intramolecular binding (**Fig. S4**).

To connect two DARPins on the same side of the HER2 homodimer (**Fig. 5 C,D**), the linker would have to span at least 80 Å for the 9_x_G construct, and to connect DARPins on two independent monomers, the linker would have to span at least the difference in height above the membrane of the two termini, more than 50 Å. It follows that with the most active of our constructs, with a 17 Å linker, linking two HER2 molecules in either of these upright conformation is not possible, either.

Since the observed biological activity and increased binding avidity of the short-linkered constructs prove that the bispecific constructs do bind bivalently on cells, it follows that the HER2 molecules must arrange to accommodate this. For bivalent binding of 9-5-G to occur, the 9_29 epitope of HER2_I has to move closer to the membrane, and this requires either a major conformational change within the HER2_ECD (which is unlikely, as explained below), or a major change in the orientation of the HER2-ECD relative to the membrane.

Comparison of extracellular domain conformations in various different ErbB family crystal structures indicates that there are very few possibilities for major conformational changes within the HER2_ECD. The connection between subdomains I and II and between III and IV is quite rigid: the side chain of conserved Trp 183 of subdomain II inserting into the core of

subdomain I and the side chain of Trp 499 of subdomain IV inserting into the core of domain III severely limit the flexibility of these interfaces. Major conformational changes within ErbB receptor extracellular domains appear to be limited to a rigid-body movement of the domain I–II pair relative to the domain III–IV pair around a pivot between domains II and III (Cho *et al.* (2003)). EGFR/HER1, HER3 and HER4 occur in two conformational states: In the presence of an activating ligand, their extracellular domain assumes an "open" conformation, similar to the default conformation of the HER2_ECD (Liu *et al.* (2012); Ogiso *et al.* (2002)), while their default conformation in the absence of a ligand and/or dimerization partner is a "tethered" conformation (Bouyain *et al.* (2005); Cho and Leahy (2002); Ferguson *et al.* (2003)), which has so far not been observed for HER2. The HER2_ECD constitutively assumes an "open" conformation (Garrett *et al.* (2003)).

However, a rigid HER2_ECD could easily tilt relative to the membrane (**Fig. 6 D, G**). This would require flexibility in the short peptide segment between the last disulfide-bridged cysteine of the extracellular domain and the start of the transmembrane helix. Indeed, these residues are disordered in reported structures of the HER2 extracellular domain and in NMR structures of the transmembrane helix. Based on single-molecule Förster resonance energy transfer (FRET) analysis and fluorescence lifetime imaging microscopy, this region in EGFR has been proposed to be sufficiently flexible to allow the EGFR_ECD to equilibrate between an upright position and one lying flat on the membrane (Webb *et al.* (2008)). Thus, tilting the ECD in such a way that the dimerization loop points towards the membrane (**Fig. 6 D, G**) would lower the C-terminus of 9_29/9_26 and raise the N-terminus of G3 in such a way that the two can be connected by a short linker.

Alternatively, a hypothetical pseudo-tethered conformation of HER2, for which there is currently no direct evidence, would bring the 9_29 epitope into an ideal position relative to the G3 epitope of a second HER2 monomer for intermolecular crosslinking with short-linkered constructs (**Fig. 6 C, F**), while intra-molecular crosslinking within a tethered monomer would still require a 70 Å (G_x_9) to 80 Å (9_x_G) linker. Such a conformation would not interfere with

DARPin binding, but would prevent the formation of back-to-back HER2 homo- and heterodimers.

The most important deduction from these models is that linking domain I of one HER2 molecule to domain IV of another by a short linker, the transmembrane domains of the two HER2 are forced apart. This conclusion is independent of the pivot point utilized. The consequence of this movement is that it prevents the assembly of active kinase dimers.

5 Discussion

The results presented in this paper and the associated models of the induced inhibited states of HER2 allow us to propose a mechanism of the induction of cytotoxicity within the framework of activation and inhibition of the ErbB receptor family. We present the X-ray structures of three DARPin:target complexes, with DARPins 9_29 and 9_26 binding to the same epitope on subdomain I of HER2, and DARPin G3 recognizing subdomain IV. The structures of the DARPins in complex with the cognate receptor domain can be superimposed on the structure of the full-length HER2 extracellular domain without any evidence for conformational changes in the individual domain beyond some very small local flexibility, already apparent from the comparison of the various structures of HER2_ECD in the Protein Data Bank. Thus, the superposition of the DARPins on the whole HER2 ECD is unambiguous.

5.1 Monomeric DARPins do not interfere with HER2 signaling

All tested monovalent DARPins that were used for the construction of the bispecific binders, individually or as a mixture, have no effect on the cell survival and proliferation of cultured BT474 cells, indicating that the monovalent DARPins do not interfere with HER2 signaling in this HER2-addicted cell line. Models of the putative HER2 “back-to-back” homodimer (**Fig. 6B**) or of canonical heterodimers with EGFR or HER3 (not shown), which are generally thought to represent the active state of HER2, indicate indeed that the binding of unlinked, i.e. monovalent, DARPins should not interfere with homo- or heterodimerization, consistent with the

observation that the monovalent DARPins are not biologically active. Since the monovalent DARPins cover both sides of the dimer, they should interfere with the lateral association of receptor dimers to produce tetramers or higher oligomers formed by stacking the planes defined by domains I, II and III, as recently proposed (Zhang *et al.* (2012)). However, since the unlinked DARPins do not interfere with HER2 activity, higher oligomers associating in this specific manner cannot be required for the activity of HER2 measured in our assays.

5.2 Activity depends on linker length

When connected by short flexible linkers, the two DARPins 9_29 and G3 acquire biological activity: While monospecific bivalent constructs, in particular G_20_G, activate HER2 signaling and have a pro-proliferative effect on BT474 cells, presumably by stabilizing HER2-HER2 homodimers, the bispecific bivalent constructs described here inhibit HER2 signaling and decrease cell viability, without affecting the number of receptors displayed on the cell surface (Tamaskovic *et al.* (2013), cf. **Chapter 4**). Their activity is dependent on linker length and on domain orientation: Constructs with shorter linkers show higher activity than constructs with longer linkers, and constructs with N-terminal DARPin 9_29 and C-terminal DARPin G3 (9_x_G) show significantly higher activity than G_x_9 of the same linker length. While for the G_x_9 conformation the inhibitory activity already disappears with a linker length of 20 amino acids, in the 9_x_G orientation, even the construct equipped with a 40 amino acid linker shows some activity.

Constructs in which one of the DARPins has been replaced by the non-binding DARPin off7 are biologically inactive, demonstrating the need for bivalency. Therefore, we have to conclude that the biological activity of the bispecific constructs is indeed due to crosslinking of HER2 molecules and not to simple direct steric hindrance of HER2 homo- or heterodimerization by the DARPins.

5.3 The linker length is too short for both DARPins to bind to the same HER2 monomer or dimer

The linkers of the shortest and most potent of the bispecific constructs tested, 9_5_G, 9_10_G and 9_20_G, are too short to connect the C-terminus of 9_29 to the N-terminus of G3 bound to the same HER2 molecule, in either the open conformation seen in all crystal structures of the HER2 ectodomain (Bostrom *et al.* (2009); Cho *et al.* (2003); Eigenbrot *et al.* (2010); Fisher *et al.* (2010); Franklin *et al.* (2004)) or in a hypothetical pseudo-tethered conformation modeled in analogy to the tethered conformations of other members of the ErbB family (Bouyain *et al.* (2005); Cho and Leahy (2002); Ferguson *et al.* (2003); Hollmen *et al.* (2012); Li *et al.* (2005); Liu *et al.* (2012); Ramamurthy *et al.* (2012)). The linkers are also too short to connect DARPins bound to the two HER2 monomers in a putative "back-to-back" HER2 homodimer. The observed bivalent binding, therefore, can only be explained by crosslinking of two independent HER2 monomers, at least one of which has to bend down (see below).

5.4 Orientation of HER2 on the cell surface

On the surface of intact cells, the transmembrane domain of the receptor is constrained to the plane of the membrane, restricting translational and rotational freedom of the receptors. Conventionally, receptors of the ErbB2 family are depicted as standing upright on the cell surface, with their main axis about perpendicular to the plane of the membrane. However, it has been proposed that a small percentage of EGFR, providing high-affinity EGF sites, can lie flat on the surface (Webb *et al.* (2008)), underlining the flexibility of the few residues between the receptor ectodomain and the TM helices to allow this. Therefore, a tilting of the whole ectodomain of HER2 with a pivot close to the membrane has some precedent.

Nonetheless, a completely flat orientation of HER2 dimers is inconsistent with binding of DARPins, as in the bound state they would prevent a flat orientation, since DARPin epitopes would be located between receptor and membrane. Also, since the majority of receptors is standing upright in EGFR (Webb *et al.* (2008)), there must be a dynamic equilibrium, and any

bound DARPin will shift this equilibrium away from any flat orientation. Considering the data on EGFR, it follows for HER2 that a tilted orientation of HER2 molecules in the DARPin-linked state is possible, but not a completely flat one. This flat orientation, which we can exclude, would be the only one in which the TM helices would be able to come close enough for the kinases to form an active dimer.

5.5 Conformational flexibility of the HER2 extracellular domain

Our experiments show that even the shortest linker, spanning less than 17 Å in extended conformation, allows bivalent binding of the bispecific DARPins. Since such bivalent binding is not possible for the open, fully erect conformation of the extracellular domain, something has to bend. The interfaces between domain I and II and between domain III and IV are rigid: The side chain of Trp 183 in cysteine-rich domain II is buried in the core of domain I, and the side chain of Trp 499 of cysteine-rich domain IV is buried in the core of domain III, allowing only very limited flexibility. HER2_I_II and HER2_III_IV can therefore be regarded as structurally rigid units. Only two positions in the extracellular domain have the potential to act as a pivot for allowing large-scale conformational changes: Either a hinge motion around the boundary residue between domain II and III (a Lys in EGFR, HER3 and HER4, corresponding to Arg 317 in HER2), which relates the open to the tethered conformation in other ErbB family members (**Fig. 6 C, F**), or – more likely regarding the probable constitutively open confirmation of HER2_ECD – a tilting of the whole ECD relative to the membrane, relying on the flexibility of the residues between the last cysteine of domain IV and the transmembrane helix (**Fig. 6 D, G**).

5.6 Interference with HER2 dimerization and activation

Either of the two discussed conformational changes captured by the bispecific DARPins leads to a situation where the “back-to-back” dimerization interface of HER2 is obstructed. In a pseudo-tethered conformation, this obstruction is intramolecular, in the tilted conformation it is due to the enforced proximity of the dimerization interface to the membrane. Either model would

result in bringing the C-terminus of DARPin 9_29 closer to the N-terminus of DARPin G3. As the transmembrane helices cannot be pulled out of the plane of the membrane, this enforces the membrane insertion points, and therefore the transmembrane and intracellular kinase domains apart, independent of the pivot point.

For maximal inhibition, formation of larger oligomers formed by daisy-chaining may be required, where every receptor monomer is bound to two bispecific DARPins and both DARPin epitopes on HER2 are occupied. For linker lengths >> 20 amino acids, alternative, intramolecular binding modes may start to compete with the intermolecular binding modes enforced by the short linker, explaining their overall lower biological activity.

6 Conclusions

The contrast between the biological inertness of the monovalent DARPins alone or in combination, the stimulation of HER2 signaling by monospecific bivalent DARPin construct G_20_G and, on the other hand, the potent inhibition of HER2 signaling by bispecific DARPin constructs connected by a minimal linker is intriguing. Trivial explanations for the inhibitory activity of the bispecific constructs, such as receptor downregulation or direct steric hindrance of receptor dimerization could be excluded (Tamaskovic *et al.* (2013), cf. **Chapter 4**), leaving a model where the steric constraints imposed by the membrane anchoring of the receptors play an important role in forcing apart the transmembrane helices of two HER2 monomers connected by the bispecific DARPin constructs.

The large fraction of the HER2 dimer surface covered by the biologically inert monovalent DARPins challenges models which postulate a need for lateral tightly packed HER2-oligomers for certain aspects of HER2 signalling in the cell line described here. The strong inhibitory effect of the bispecific DARPin constructs makes them an interesting starting point for future tumor targeting constructs directed against HER2-addicted cancer cells. A detailed analysis of their effects on different aspects of downstream signaling is presented in a separate publication (Tamaskovic *et al.* (2013), cf. **Chapter 4**).

In summary, the engineering of binding molecules that bispecifically target HER2 at domains I and IV, connected by a linker not commensurate with intramolecular binding or binding to back-to-back complexes, has proven to be a very promising way to expand the arsenal of molecular targeting of cancer cells that are addicted to this receptor. In this context, DARPins might be particularly promising, as they can be easily engineered in a variety of molecular orientations, and equipped for prolonged systemic circulation in order to extend their outstanding in vitro potency for in vivo studies (Tamaskovic *et al.* (2013), cf. **Chapter 4**).

7 Experimental Procedures

7.1 Cloning, Expression and Purification of DARPins

All DARPins were purified essentially as described previously (Zahnd *et al.* (2010)). Proteins were overexpressed in *E. coli* XL1-Blue and purified via their N-terminal MRGSH6 tag with nickel-nitrilotriacetic acid superflow resin (Qiagen, Hilden, Germany). For cloning of bispecific constructs, the DARPin ORFs were digested with *Bam*HI and *Hind*III (New England Biolabs) and ligated into compatible expression vectors pQiBi, coding for different flexible $(G_4S)_n$ linkers. This results in the connecting sequence …AEILQKL$(G_4S)_n$RSDLGKKLL…, where the first underlined sequence is from the C-cap of the N-terminal DARPin, the second underlined sequence is from the N-cap of the C-terminal DARPin and n indicates the number of pentapeptides present in the flexible linker.

7.2 Cell culture

BT-474 cells were obtained from the American Type Culture Collection (ATCC HTB-20). Cells were grown in complete RPMI 1640 medium (Sigma-Aldrich) supplemented with 10% (v/v) heat-inactivated FCS (PAA GmbH, Pasching, Austria) and 100 U/ml penicillin/streptomycin (Sigma) in a humidified incubator with 5% CO_2.

7.3 Flow cytometry

Per assay, 1×10^6 cells were incubated with the respective fluorescently labeled DARPins at the indicated concentrations in 100 µl PBS_BA (PBS, 0.2% NaN_3, 1% BSA). After incubation, cells were harvested by centrifugation (800 g, 30 sec, 4°C) and washed twice using 1 ml PBS_BA, each. Flow cytometry was performed on a Cyflow space system (Partec, Germany). Recorded events were gated for FSC/SSC of single viable cells. Fluorescence data were analyzed using the FlowJo software.

Dissociation experiments were performed as described (Tamaskovic *et al.* (2012)). In brief, aliquots of 1×10^6 cells were preincubated with DARPin-AlexaFluor488-conjugates at 100

nM in PBS_BA for 1 h at room temperature. Cells were washed twice as described above and dissociation was allowed to proceed in the presence of unlabeled DARPin for the times indicated shaking at room temperature, followed by washes and flow cytometry measurements as described above.

7.4 Cell viability assays (XTT assays)

BT474 cells were seeded at a density of 10,000 cells/cm^2 in 96-well-plates (Nunc). After 24 h, DARPins (or trastuzumab as control) were added and cells were incubated for another 72 h. Cells were then incubated with 50 µl/well 2,3-bis(2-methoxy-4-nitro-5-sulfophenyl)-2H-tetrazolium-5-carboxanilide (XTT; Roche) for 4h at 37°C. Absorbance was measured at 450 nm and expressed as percentage of the untreated controls.

7.5 Expression in insect cells

Recombinant HER2-ectodomains carrying an N-terminal melittin signal sequence and an N-terminal His6 tag were expressed in *Spodoptera frugiperda* (Sf9) cells. Baculoviruses for infection of Sf9 cells were generated using the Multibac system as described (Fitzgerald *et al.* (2006)). Sf9 cells were grown to a density of 4×10^6 cells/mL and co-infected with the respective virus at a MOI of 1. 72 h post infection, cells were harvested by centrifugation (30 min, 5000 g, 4°C) and the cleared medium was subjected to immobilized metal ion affinity chromatography (IMAC) purification with Ni-NTA Superflow (Qiagen) purification resin.

7.6 X-ray crystallography

HER2_I and HER2_IV were expressed and purified as described above. After preincubation with DARPins 9_26_Mut5, 9_29_Mut5 or G3 at equimolar concentrations, complexes were purified via size exclusion chromatography on a Superdex 200 HiLoad 16/60 column equilibrated with TBS150 (PBS, 150 mM NaCl). Eluted protein was concentrated to 14 (9_26/HER2_I), 8 (9_29/HER2_I) or 9 (G3/HER2_IV) mg/ml using centrifugal concentrators (Millipore). Crystals

of the complexes formed in sitting drops mixed with two parts protein solution and one part mother liquor. The mother liquor contained 0.2 M NaCl, 0.1 M phosphate citrate (pH 4.2) and 20% PEG 8000 for 9_26/HER2_I; 0.2 M ammonium acetate (pH 5.6), 0.1 M sodium citrate, 30% (w/v) PEG 4000 for 9_29/HER2_I or 0.05 M succinic acid and 29% ammonium sulfate (pH 4.0) for G3/HER2_IV, respectively. Crystals grew within three days (9_29/HER2_I), three weeks (9_26/HER2_I) or four weeks (G3/HER2_IV), respectively. They were then transferred to a cryo-protectant solution containing 20% glycerol. Data were collected using the PILATUS 2 M detector system on the PXIII beam line at the Swiss Light Source (Paul Scherrer Institute, Villigen, Switzerland) and processed using the program XDS (Kabsch (2010)). The structures were solved by molecular replacement using PHASER MR (McCoy *et al.* (2007)) from within the CCP4 package (CCP4 (1994)). Model building was carried out by using the program COOT(Emsley *et al.* (2010)). The structures were refined using PHENIX (Adams *et al.* (2010)). Stereochemical properties were analyzed with MOLPROBITY (Davis *et al.* (2007)) and structure figures were generated in PYMOL (http://pymol.org).

8 Acknowledgements

We thank Céline Stutz-Ducommun and Beat Blattmann for help in protein crystallization and the staff of beamline PXIII at the Swiss Light Source for support during data collection. This work was supported by the Swiss National Center of Competence in Research in Structural Biology, Schweizerischer Nationalfonds grant No 3100A0-113720 and the Krebsforschung Schweiz grant No KFS-02448-08-2009.

Data deposition: The HER2_I/9_29, HER2_I/9_26, and HER2_IV/G3 structures have been deposited in the Protein Data Bank, www.pdb.org (PDB ID codes 4HRL, 4HRM, and 4HRN, respectively).

Author contributions: C.J., J.S., R.T., M.S. and A.P. designed research; C.J., J.S. and M.S. performed research; C.J., J.S., A.H. and A.P. analyzed data and C.J., J.S., A.H. and A.P. wrote the paper.

Conflict of interest statement: C.J., R.T., M.S. & A.P. have applied for a patent on findings related to this manuscript.

9 References

1. Adams PD*, et al.* (2010) PHENIX: a comprehensive Python-based system for macromolecular structure solution. *Acta Crystallogr. D. Biol. Crystallogr.* 66:213-221.
2. Aertgeerts K*, et al.* (2011) Structural analysis of the mechanism of inhibition and allosteric activation of the kinase domain of HER2 protein. *J. Biol. Chem.* 286:18756-18765.
3. Arkhipov A*, et al.* (2013) Architecture and membrane interactions of the EGF receptor. *Cell* 152:557-569.
4. Binz HK*, et al.* (2004) High-affinity binders selected from designed ankyrin repeat protein libraries. *Nat. Biotechnol.* 22:575-582.
5. Bocharov EV*, et al.* (2008) Spatial structure and pH-dependent conformational diversity of dimeric transmembrane domain of the receptor tyrosine kinase EphA1. *J. Biol. Chem.* 283:29385-29395.
6. Boersma YL & Plückthun A (2011) DARPins and other repeat protein scaffolds: advances in engineering and applications. *Curr. Opin. Biotechnol.* 22:849-857.
7. Bostrom J*, et al.* (2009) Variants of the antibody herceptin that interact with HER2 and VEGF at the antigen binding site. *Science* 323:1610-1614.
8. Bouyain S, Longo PA, Li S, Ferguson KM, & Leahy DJ (2005) The extracellular region of ErbB4 adopts a tethered conformation in the absence of ligand. *Proc. Natl. Acad. Sci. U. S. A.* 102:15024-15029.
9. Burris HA, 3rd, Tibbitts J, Holden SN, Sliwkowski MX, & Lewis Phillips GD (2011) Trastuzumab emtansine (T-DM1): a novel agent for targeting HER2+ breast cancer. *Clin Breast Cancer* 11:275-282.
10. CCP4 (1994) The CCP4 suite: programs for protein crystallography. *Acta Crystallogr. D. Biol. Crystallogr.* 50:760-763.
11. Cho HS & Leahy DJ (2002) Structure of the extracellular region of HER3 reveals an interdomain tether. *Science* 297:1330-1333.
12. Cho HS*, et al.* (2003) Structure of the extracellular region of HER2 alone and in complex with the Herceptin Fab. *Nature* 421:756-760.
13. Cobleigh MA*, et al.* (1999) Multinational study of the efficacy and safety of humanized anti-HER2 monoclonal antibody in women who have HER2-overexpressing metastatic breast cancer that has progressed after chemotherapy for metastatic disease. *J. Clin. Oncol.* 17:2639-2648.
14. Craven RJ, Lightfoot H, & Cance WG (2003) A decade of tyrosine kinases: from gene discovery to therapeutics. *Surg. Oncol.* 12:39-49.
15. Davis IW*, et al.* (2007) MolProbity: all-atom contacts and structure validation for proteins and nucleic acids. *Nucleic Acids Res.* 35:375-383.
16. Dawson JP, Bu Z, & Lemmon MA (2007) Ligand-induced structural transitions in ErbB receptor extracellular domains. *Structure* 15:942-954.
17. Dreier B*, et al.* (2013) Development of a generic adenovirus delivery system based on structure-guided design of bispecific trimeric DARPin adapters. *Proc. Natl. Acad. Sci. U. S. A.* 110:E869-877.
18. Eigenbrot C, Ultsch M, Dubnovitsky A, Abrahmsén L, & Härd T (2010) Structural basis for high-affinity HER2 receptor binding by an engineered protein. *Proc. Natl. Acad. Sci. U. S. A.* 107:15039-15044.
19. Emsley P, Lohkamp B, Scott WG, & Cowtan K (2010) Features and development of Coot. *Acta Crystallogr. D. Biol. Crystallogr.* 66:486-501.
20. Endres NF*, et al.* (2013) Conformational coupling across the plasma membrane in activation of the EGF receptor. *Cell* 152:543-556.

21. Faber AC, Wong KK, & Engelman JA (2010) Differences underlying EGFR and HER2 oncogene addiction. *Cell Cycle* 9:851-852.
22. Ferguson KM*, et al.* (2003) EGF activates its receptor by removing interactions that autoinhibit ectodomain dimerization. *Mol. Cell* 11:507-517.
23. Finn RS & Slamon DJ (2003) Monoclonal antibody therapy for breast cancer: herceptin. *Cancer Chemother. Biol. Response Modif.* 21:223-233.
24. Fisher RD*, et al.* (2010) Structure of the complex between HER2 and an antibody paratope formed by side chains from tryptophan and serine. *J. Mol. Biol.* 402:217-229.
25. Fitzgerald DJ*, et al.* (2006) Protein complex expression by using multigene baculoviral vectors. *Nat. Methods* 3:1021-1032.
26. Franklin MC*, et al.* (2004) Insights into ErbB signaling from the structure of the ErbB2-pertuzumab complex. *Cancer Cell* 5:317-328.
27. Gajria D & Chandarlapaty S (2011) HER2-amplified breast cancer: mechanisms of trastuzumab resistance and novel targeted therapies. *Expert Rev. Anticancer Ther.* 11:263-275.
28. Garrett TP*, et al.* (2003) The crystal structure of a truncated ErbB2 ectodomain reveals an active conformation, poised to interact with other ErbB receptors. *Mol. Cell* 11:495-505.
29. Ghosh R*, et al.* (2011) Trastuzumab has preferential activity against breast cancers driven by HER2 homodimers. *Cancer Res.* 71:1871-1882.
30. Hollmen M*, et al.* (2012) Proteolytic processing of ErbB4 in breast cancer. *PLoS One* 7:e39413.
31. Interlandi G, Wetzel SK, Settanni G, Plückthun A, & Caflisch A (2008) Characterization and further stabilization of designed ankyrin repeat proteins by combining molecular dynamics simulations and experiments. *J. Mol. Biol.* 375:837-854.
32. Ishikawa T*, et al.* (2011) Design and synthesis of novel human epidermal growth factor receptor 2 (HER2)/epidermal growth factor receptor (EGFR) dual inhibitors bearing a pyrrolo[3,2-d]pyrimidine scaffold. *J. Med. Chem.* 54:8030-8050.
33. Junttila TT*, et al.* (2009) Ligand-independent HER2/HER3/PI3K complex is disrupted by trastuzumab and is effectively inhibited by the PI3K inhibitor GDC-0941. *Cancer Cell* 15:429-440.
34. Kabsch W (2010) Xds. *Acta Crystallogr. D Biol. Crystallogr.* 66:125-132.
35. Li S*, et al.* (2005) Structural basis for inhibition of the epidermal growth factor receptor by cetuximab. (Translated from eng) *Cancer Cell* 7:301-311 (in eng).
36. Liu P, Bouyain S, Eigenbrot C, & Leahy DJ (2012) The ErbB4 extracellular region retains a tethered-like conformation in the absence of the tether. *Protein Sci.* 21:152-205.
37. Martin-Killias P, Stefan N, Rothschild S, Plückthun A, & Zangemeister-Wittke U (2011) A novel fusion toxin derived from an EpCAM-specific designed ankyrin repeat protein has potent antitumor activity. *Clin. Cancer Res.* 17:100-110.
38. McCoy AJ*, et al.* (2007) Phaser crystallographic software. *J. Appl. Crystallogr.* 40:658-674.
39. Mi LZ*, et al.* (2011) Simultaneous visualization of the extracellular and cytoplasmic domains of the epidermal growth factor receptor. *Nat Struct Mol Biol* 18:984-989.
40. Moasser MM (2007) The oncogene HER2: its signaling and transforming functions and its role in human cancer pathogenesis. *Oncogene* 26:6469-6487.
41. Münch RC*, et al.* (2011) DARPins: an efficient targeting domain for lentiviral vectors. *Mol. Ther.* 19:686-693.
42. Ogiso H*, et al.* (2002) Crystal structure of the complex of human epidermal growth factor and receptor extracellular domains. *Cell* 110:775-787.
43. Ramamurthy V*, et al.* (2012) Structures of adnectin/protein complexes reveal an expanded binding footprint. *Structure* 20:259-269.
44. Schaefer G, Fitzpatrick VD, & Sliwkowski MX (1997) Gamma-heregulin: a novel heregulin isoform that is an autocrine growth factor for the human breast cancer cell line, MDA-MB-175. *Oncogene* 15:1385-1394.

45. Sergina NV*, et al.* (2007) Escape from HER-family tyrosine kinase inhibitor therapy by the kinase-inactive HER3. *Nature* 445:437-441.
46. Simon M, Zangemeister-Wittke U, & Plückthun A (2012) Facile double-functionalization of designed ankyrin repeat proteins using click and thiol chemistries. *Bioconjug. Chem.* 23:279-286.
47. Sliwkowski MX*, et al.* (1999) Nonclinical studies addressing the mechanism of action of trastuzumab (Herceptin). *Semin. Oncol.* 26:60-70.
48. Sliwkowski MX*, et al.* (1994) Coexpression of erbB2 and erbB3 proteins reconstitutes a high affinity receptor for heregulin. *J. Biol. Chem.* 269:14661-14665.
49. Steiner D, Forrer P, & Plückthun A (2008) Efficient selection of DARPins with sub-nanomolar affinities using SRP phage display. *J. Mol. Biol.* 382:1211-1227.
50. Tamaskovic R*, et al.* (2013) Mechanism for eliciting apoptosis selectively in ErbB2-addicted tumor cells by bispecific binding proteins. *submitted*.
51. Tamaskovic R, Simon M, Stefan N, Schwill M, & Plückthun A (2012) Designed ankyrin repeat proteins (DARPins) from research to therapy. *Methods Enzymol.* 503:101-134.
52. Theurillat JP*, et al.* (2010) Designed ankyrin repeat proteins: a novel tool for testing epidermal growth factor receptor 2 expression in breast cancer. *Mod. Pathol.* 23:1289-1297.
53. Verma S*, et al.* (2012) Trastuzumab emtansine for HER2-positive advanced breast cancer. *N. Engl. J. Med.* 367:1783-1791.
54. Webb SE*, et al.* (2008) Single-molecule imaging and fluorescence lifetime imaging microscopy show different structures for high- and low-affinity epidermal growth factor receptors in A431 cells. *Biophys. J.* 94:803-819.
55. Wetzel SK*, et al.* (2010) Residue-resolved stability of full-consensus ankyrin repeat proteins probed by NMR. *J. Mol. Biol.* 402:241-258.
56. Xia W, Liu LH, Ho P, & Spector NL (2004) Truncated ErbB2 receptor (p95ErbB2) is regulated by heregulin through heterodimer formation with ErbB3 yet remains sensitive to the dual EGFR/ErbB2 kinase inhibitor GW572016. *Oncogene* 23:646-653.
57. Yarden Y & Sliwkowski MX (2001) Untangling the ErbB signalling network. *Nat. Rev. Mol. Cell Biol.* 2:127-137.
58. Zahnd C*, et al.* (2010) Efficient tumor targeting with high-affinity designed ankyrin repeat proteins: effects of affinity and molecular size. *Cancer Res.* 70:1595-1605.
59. Zahnd C*, et al.* (2007) A designed ankyrin repeat protein evolved to picomolar affinity to HER2. *J. Mol. Biol.* 369:1015-1028.
60. Zhang Q, Park E, Kani K, & Landgraf R (2012) Functional isolation of activated and unilaterally phosphorylated heterodimers of ERBB2 and ERBB3 as scaffolds in ligand-dependent signaling. *Proc. Natl. Acad. Sci. U. S. A.* 109:13237-13242.
61. Zhou H*, et al.* (2011) Structural insights into the down-regulation of overexpressed p185(her2/neu) protein of transformed cells by the antibody chA21. *J. Biol. Chem.* 286:31676-31683.

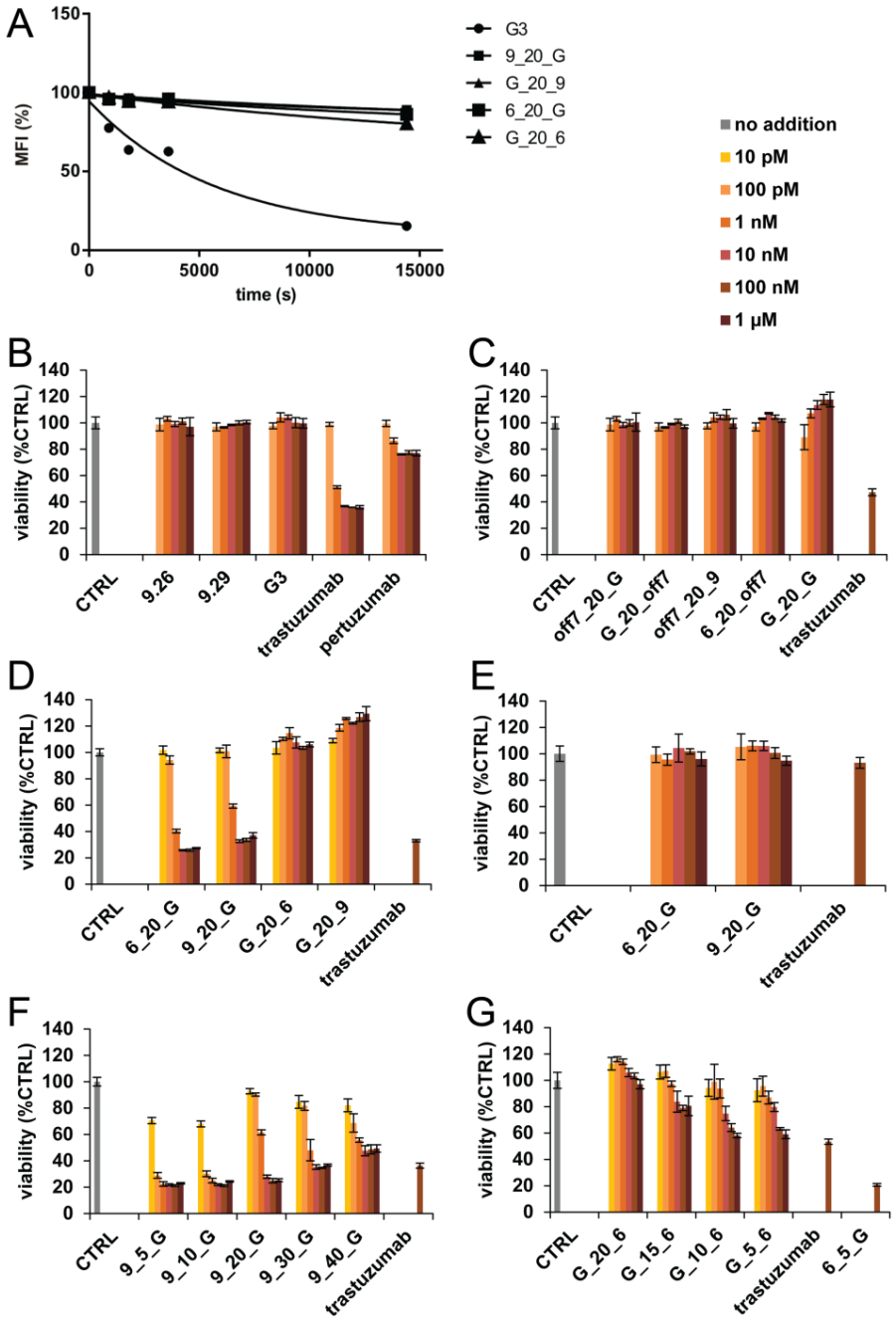

Figure 1: Biological activity of DARPin constructs

(A) Dissociation of monovalent and bispecific DARPins from the surface of BT474 cells. Median fluorescence intensities (MFI) of fluorescently labeled DARPins bound to the BT474 cell surface are plotted as a function of dissociation time. See **Table S1** for fitted off-rates, **Fig. S1A** for ELISA epitope mapping and **Fig. S2B** for binding competition on intact cells. **(B-G)** Inhibition of cell proliferation was determined by XTT assays with HER2-addicted BT474 cells. Cells grew for 72 h in the presence of different concentrations of DARPins. Bispecific DARPins 6_20_G and 9_20_G decreased the cell viability, whereas the reversely oriented constructs G_20_6 and G_20_9 did not. Cells that grew in the presence of 100 nM trastuzumab and cells growing without treatment served as control (CTRL). **(B)** Biological effects of monovalent DARPins. **(C)** Bispecific DARPins containing a non-binding DARPin. Off7 is a control DARPin recognizing maltose binding protein. G_20_G is homobivalent and contains twice the DARPin G3. **(D)** Biological effects of bispecific anti-HER2-DARPins on HER2-addicted BT474 cells and **(E)** on non-overexpressing MCF7 cells. **(F)** Effect of linker length on biological activity of bispecific DARPins in 9_x_G orientation or **(G)** in G_x_9 orientation.

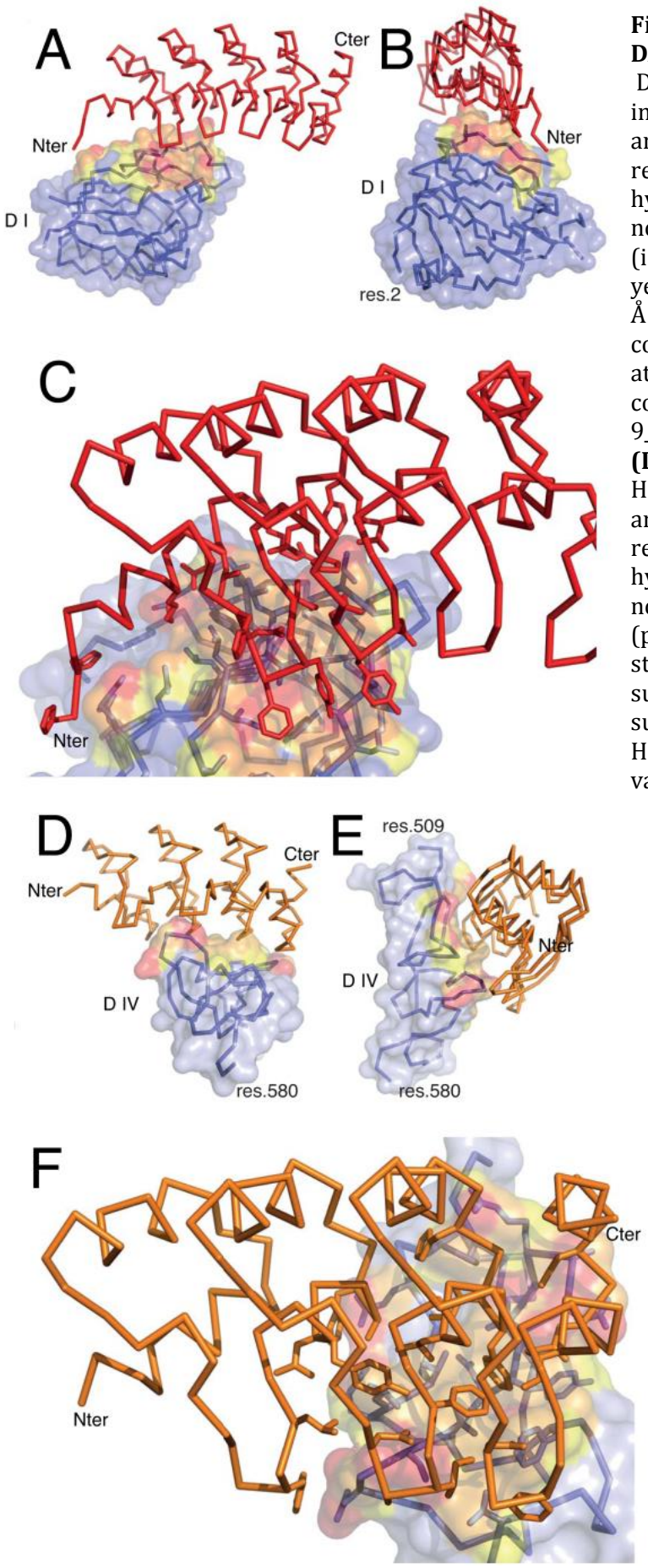

Figure 2: Structures of DARPin:HER2 complexes:
DARPins 9.29 (red) and G3 (orange) in complex with HER2 subdomain I and IV, respectively (blue). HER2 residues having at least one non-hydrogen atom within 5.0 Å of a non-hydrogen atom of the DARPin (i.e., epitope residues) are shown in yellow, those with atoms within 5.0 Å of the DARPin (solvent excluding contacts) in orange, and those with atoms within 3.6 Å (Van-der-Waals contacts) in red. **(A, B, C)** DARPin 9_29 in complex with HER2_I.
(D, E, F) DARPin G3 in complex with HER2_IV. **(C, F)** Close-up of epitope and paratope: side chains of residues having at least one non-hydrogen atom within 5.0 Å of a non-hydrogen atom of HER2 (paratope residues) are shown in stick representation. See Fig. S2 for superpositions of the HER2 subdomains on the full-length HER2_ECD, **Table S5** for rmsd-values.

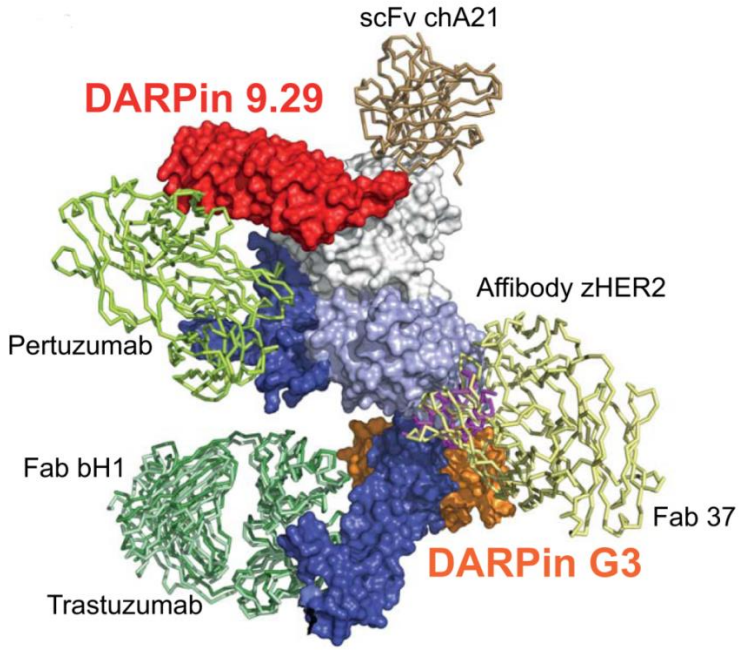

Figure 3: Superposition of HER2 complexes on the full-length HER2 ECD:
DARPin 9_29 (PDB ID: 4HRL, red) is binding to subdomain I, DARPin G3 (PDB ID: 4HRN, orange) to subdomain IV. In addition, Fab fragments of the therapeutic antibody trastuzumab (Herceptin®, PDB ID 1N8Z, pale green), its derived HER2/VEGF dual specific variant bH1 (PDB ID: 3BE1, forest green) and pertuzumab (Perjeta®, PDB ID: 1S78, lime) are shown, as well as Fab 37 (PDB ID: 3N85, pale yellow), scFv chA21 (PDB ID: 3H3B, sand) and Z-domain affibody zHER2 (PDB ID: 3MZW).

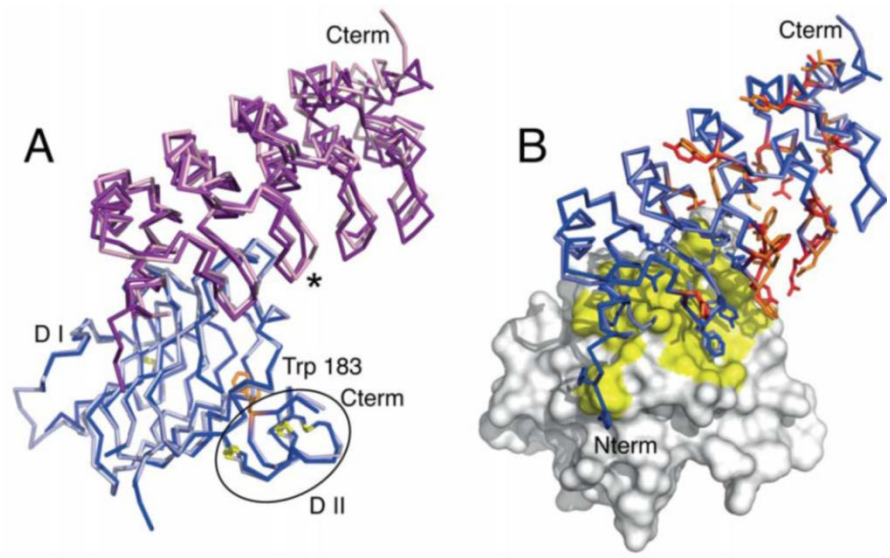

Figure 4: Comparison of DARPin 9_26 and 9_29 complexes with HER2-I:
(A) Superposition of the HER2_I:DARPin 9_29 complex structure (HER2_I: dark blue, 9_29: purple) onto the HER2_I:DARPin 9_26 complex structure (HER2_I: pale blue, 9_26: magenta). The two structures were superimposed by a least-squares fit of the Cα positions of HER2_I residues 21-96 and 116-152 (rmsd 0.53 Å). Unliganded DARPin 9_26 (2.9 Å resolution, pale pink) was superimposed on the DARPin in the HER2_I:9_26 complex. A one residue deletion in the second loop of DARPin 9_29 is indicated by (*). **(B)** Sequence differences between DARPins 9_29 (dark blue) and 9_26 (pale blue). DARPin 9_26 was superimposed on DARPin 9_29 in the HER2_I:DARPin 9_29 complex structure. Side chains of conserved paratope residues (blue) and divergent DARPin residues (9_29, red; 9_26, orange) are shown in stick representations. (See **Fig. S3** for a sequence alignment)

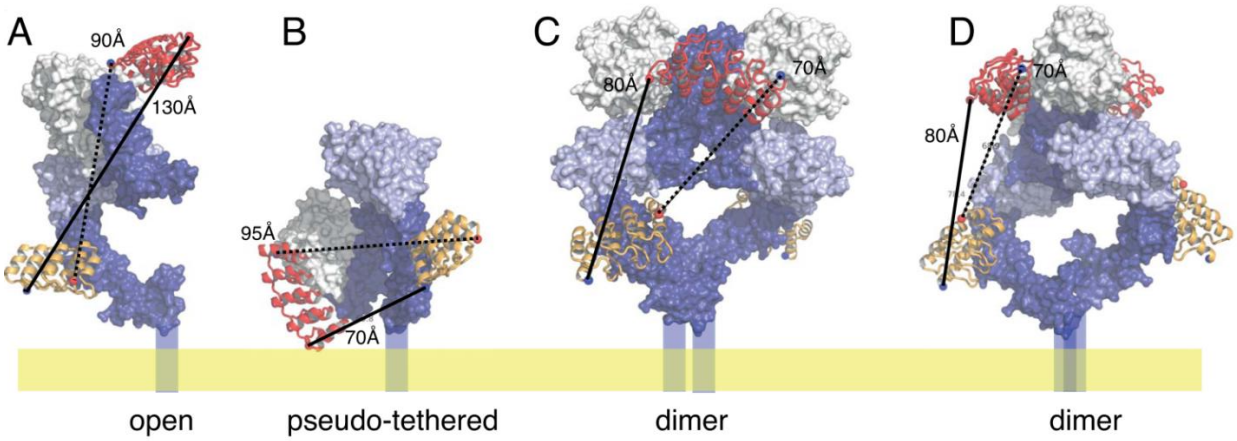

Figure 5: Distances between DARPin N- and C-termini
(A) For bivalent binding to a HER2 monomer, the linker in a 9_x_G construct would need to span a distance of 130 Å (solid line), with enough slack added to wrap around HER2. In a G-x-9 constructs, the two termini would need to span 90 Å (broken line). **(B)** To bind to a HER2 monomer in a pseudo-tethered conformation, 70 Å (9_x_G construct) or 95 Å (G_x_9 construct) would have to be bridged. **(C, D)** To connect two DARPins bound to the same side of a HER2 dimer, 80 Å would have to be bridged by a 9_x_G construct, 70 Å by a G_x_9 construct. **(C)** and **(D)** show the same dimer, rotated by 90° around the y-axis. Linker lengths in the various bispecific DARPins vary from 16.5 Å (9_5_G) to 132 Å (9_40_G). assuming a fully extended conformation (**Fig. S4**).

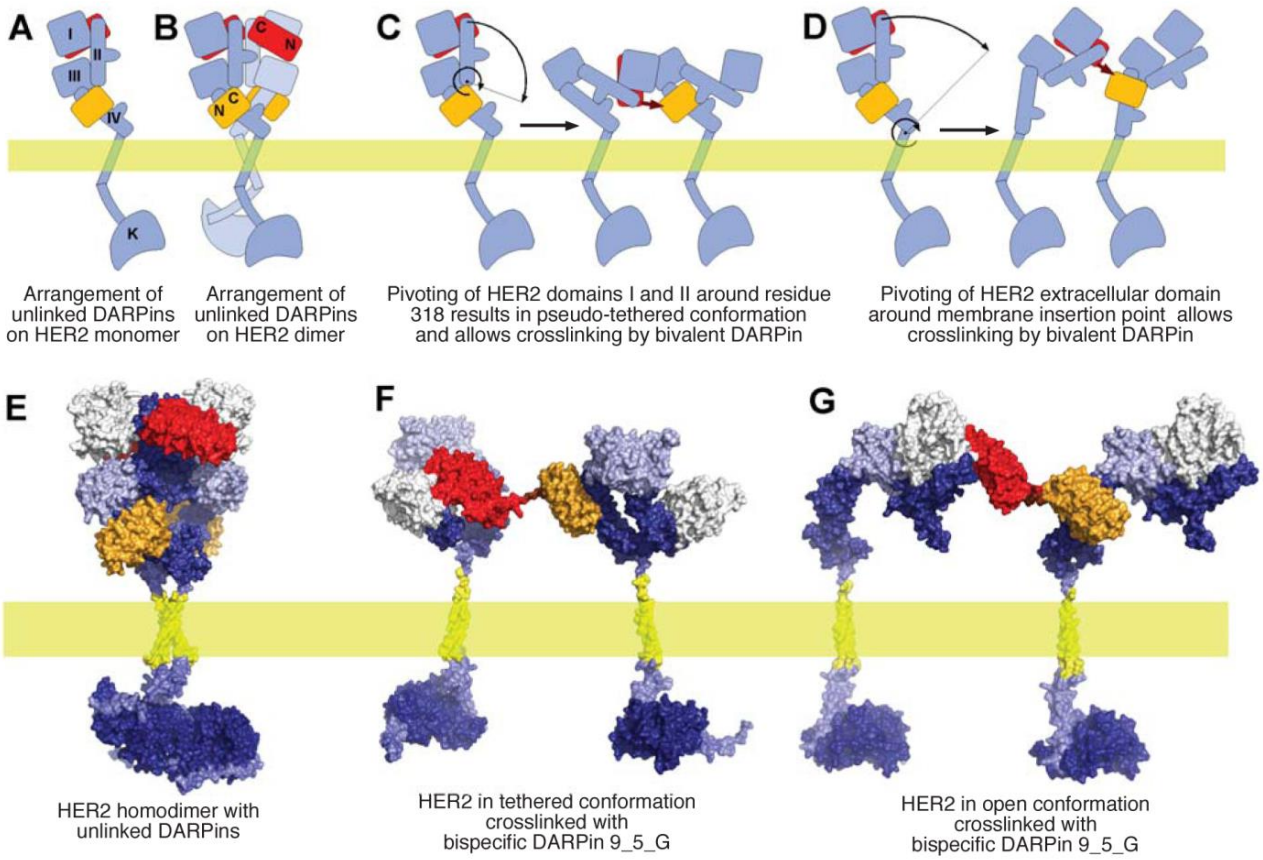

Figure 6: Models of full-length HER2 complexed by monovalent or bispecific DARPins.
A model of the complete structure of HER2 in complex with the two DARPins 9_29 and G3 was generated as described in the SI Text. **(A, B, E)**: Unlinked DARPins 9_29 (red) and G3 (orange) are modeled to bind to putative HER2 homo- and heterodimers and are predicted to not interfere with receptor dimerization. **(C,D,F,G)**: Bispecific DARPins with short linkers can only crosslink two HER2 molecules if domain I is brought closer to the membrane through binding of the DARPin. **(D, G)**: Domain I is brought closer to the membrane by pivoting the rigid extracellular domain (ECD) around a point in a short flexible peptide between the last disulfide bridge in domain IV and the start of the transmembrane helix. This would allow bispecific DARPin 9_5_G to bind two HER2 molecules with ECDs in the open conformation found in all structures. **(C,F)**: Alternatively, a rotation around the pivot point utilized in the transition between open and tethered conformation (Arg 317) of other ErbB members would yield a pseudo-tethered conformation that brings domain I closer to the membrane and allows bispecific DARPin 9_5_G to crosslink two HER2 molecules with ECDs in (putative) tethered conformation. Both models (**B/F** and **C/G**) enforce a large distance between the kinase domains, and both prevent further dimerization by the strong tilt of dimerization interfaces and/or making the dimerization loop inaccessible. Both models would also be compatible with daisy-chaining, forming higher order oligomers.

10 Supplementary Material

Supplemental Experimental Procedures

DARPin nomenclature

The full name of DARPin G3 in the original publication (Zahnd et al., 2007) is H10-2-G3.

ELISA

HER2-domains (200 nM in PBS, 100 µl/well) were immobilized on MaxiSorp plates (Thermo Scientific) by overnight incubation at 4°C. For ELISAs, wells were blocked with 300 µl of PBSTB (PBS, 0.1% Tween-20, 0.2% BSA) for 1 h at room temperature. 50 nM of purified DARPins were incubated with the target domains for 1 h at room temperature, followed by three washing steps with 300 µl of PBSTB. For detection of bound DARPins, an anti RGS-His IgG1 mouse antibody (Qiagen) was added (1:5,000 in PBSTB, 1 h at RT) which recognizes the N-terminal MRGS-His_6 tag of the DARPins, and wells were washed as described above. After incubation with a secondary anti mouse-IgG antibody alkaline phosphatase conjugate (Sigma-Aldrich) (1:10,000 in PBSTB, 1 h at RT), pNPP substrate (Fluka) was added to measure alkaline phosphatase activity.

HER2 subdomains produced in Sf9-cells.

The primary sequences of the HER2 subdomains produced in Sf9-cells are shown in Figure S1B. Note that the N-glycosylation sites (highlighted in red) were N->D-mutated for crystallization.

Crystal structures

The high-affinity binding of DARPin 9_29 to HER2_I is governed by six hydrogen bonds, pi-stacking and extended hydrophobic interactions. Starting from the N-terminus of the DARPin 9_29, 9_29:His8 is involved in pi-stacking interactions with Her2_I:Arg135. Hydrogen bonds between the side chains of 9_29:Lys16 and 9_29:Glu20 and the side chains of Her2_I:Glu87 and Her2_I:Tyr90 further contribute to the binding interface. Side-chain-backbone hydrogen bonds between 9_29 residues Arg23, Asp44 and Tyr46 and Her2_I residues Leu157, Thr160 and Trp147, and backbone-backbone hydrogen bonds between 9_29:Phe45 and Her2_I:Thr160 complete the vast hydrogen bonding network. 9_29 residues Lys16, Glu20 and Arg23 are not only involved in hydrogen bonds, but also contact HER2_I residues Leu132, Tyr90, Leu161 and Leu159 via hydrophobic interactions. The first internal repeat of 9_29 employs Phe45, Tyr46 and Ile48 and Leu53 in binding to a hydrophobic depression on HER2_I, which is formed by HER2_I residues Trp147, Thr160, Ile162, Leu161, Leu159, Leu157 and Lys148. Asn56 from the first and Tyr78 and Asp79 from the second internal repeat of 9_29 bind the protruding HER2_I residues Leu157 and Lys148 via hydrophobic interactions. The C-terminal part of 9_29 does not contribute to the interaction with HER2_I.

The 2 complexes in the asymmetric unit of the G3+HER2_IV structure possess practically identical interactions. Therefore, only the complex formed between chain A of G3 and chain D of HER2_IV will be described. Similar to the 9_29+HER2_I complex, the G3+HER2_IV complex contains six hydrogen bonds and extended hydrophobic interactions, which are responsible for the low picomolar affinity of G3. Starting from the N-terminus of the DARPin G3, G3:Tyr46 and G3:Leu48 bind via hydrophobic interactions

to protruding residues Asp49 and Gly50 on HER2_IV, whereas G3:Leu48 and G3:Tyr52 reach into a small hydrophobic groove on HER2_IV formed by Gly50 and Leu25. G3:Ala56 contacts HER2_IV:Leu25 through a hydrophobic interaction. G3:His57 on the other hand contributes the first hydrogen bond with HER2_IV:Glu21 to the interface. A backbone-backbone hydrogen bond and hydrophobic interactions between G3:Ala78 and HER2_IV:Gly50 are followed by hydrophobic interactions between G3 residues Ile79 and Phe81, which bind to a surface exposed hydrophobic patch formed by HER2_IV residues Ser51, Val52 and Phe55. G3:Phe89 perfectly reaches into a semi-circular hydrophobic depression involving Val52, Val24, Val33, Tyr32 and Phe55 on HER2_IV. Ile90 on G3 binds to an adjacent hydrophobic patch formed by HER2_IV residues Val24, Val33 and Phe12. These interactions are followed by hydrogen bonds between the backbone of G3 residues Gly91 and Gly122 with side chains of residues Arg36 and Asn34 on HER2_IV. The backbone-backbone hydrogen bond between G3:Asn123 and HER2_IV:Ala35 and the side-chain-backbone hydrogen bond between G3:Asn125 and HER2_IV:Ala35 complete the vast interaction network between G3 and HER2_IV.

Although G3 possesses only two internal repeats, the perfectly matching hydrophobic and hydrogen bonding interactions account for its extremely high affinity.

Certain residues in the 9_29/HER2_I and G3/HER2_IV complex structures at termini or connecting loops are flexible and therefore not visible in the electron density. In addition, some residues for which the backbone was clearly visible in the electron density, but side chains were partly or fully unresolved in the structure, were built as Alanines and are listed in Table S4.

Interestingly, electron density for HER2_IV is clearly visible for the stretch complexed with DARPin G3. It starts at residue 9 and suddenly becomes untraceable after residue 79 (in chain C; 78 in chain D). The resolved structure of Domains IV in complex with G3 compares very well with Domain IV from full length ECD (PDB ID: 1N8Z) (see Table S5 for $RMSD_{CA}$-values and Fig. S2*B* for overlays of the protein backbones).

The quality of the 9_26/HER2_I structure at a resolution of 3.25 Å is lower than the quality of the aforementioned two structures. Large parts of both, the DARPin 9_26 and Domain I, are unresolved in the structure. Affected residues are listed in Table S4. Interestingly, different parts of 9_26 are resolved in chain B and D and therefore complement each other.

Molecular modeling

To assess conformational differences between different HER2 domain I (HER2_I) structures, HER2 structures 1N8Y, 1N8Z, 1S78, 2A91, 3BE1, 3H3B, 3MZW and 3N85 were aligned by least-squares superposition of the Cα coordinates of residues 21-96 and 116-152 onto the aligned HER2_I-DARPin complexes.

In the structures HER2_I:9_29 and HER2_I:9_26, several HER2_I positions near the N-terminus, in loop 99-114 and near the C-terminus of the domain are missing. In a composite model, the majority of the residues was taken from structure 3N85, which covers the HER2 structure from residue 2 to 621, the last disulfide-linked Cys of domain IV. The missing loop residues were patched from structure 3H3B; the DARPin binding epitopes were patched from the structures of the DARPin complexes. Missing residues in positions 249-253 of 3N85 were patched in a similar manner. The coordinates of an unpublished X-ray

structure of unliganded DARPin 9_26 were used to provide the missing residues of the DARPin in the complex. However, for further modeling, the 9_29 complex was used, since the two DARPins recognize the same epitope. The DARPin G3–HER2_IV complex was fitted to domain IV of structure 3N85 by superposition of residues 510 to 563.

All models were built using the Homology module of InsightII (Accelrys, San Diego) to assign the coordinates from the aligned templates to the complete sequence, the "Discover" module to locally energy minimize the sites where different templates were spliced, and „Rosetta 3.4“ (www.rosettacommons.org) for constrained relaxation of the final model.

The best-resolved tethered structures of HER1, HER3 and HER4 were superimposed by a least-squares fit of domain III to assess the divergence. To build a model of the hypothetical tethered conformation of HER2, each domain of HER2 was superimposed separately on the corresponding domain of the template structure of HER4 (2AHX). HER2_I was superimposed on HER4_I by least-squares superposition of the Cα atoms of residues A32-A96 and A116-A141 of HER2 on A31-A95 and A106-A131 of HER4 (RSMD 0.65 Å). Domain II of a second copy of HER2 was superimposed on domain II of HER4 by least-squares superposition of the Cα atoms of residues A206-A247 and A268-A282 of HER2 on A196-A237 and A258-272 of HER4 (RSMD 0.56 Å). Domain III of HER2 was superimposed on domain III of HER4 by least-squares superposition of the Cα atoms of residues A321-A324, A337-A356, A371-A414 and A429-A454 of a third copy of HER2 on residues A309-A312, A325-A344, A359-A402 and A417-A442 HER4 (RSMD 0.55 Å). Domain IV of HER2 was superimposed on domain IV of HER4 by least-squares superposition of the Cα atoms of residues A510-A546 and A555-A579 of a fourth copy of HER2 on residues A498-A534 and A544-A568 of erbB4 (RMSD 0.57 Å) Coordinates were assigned to the model from the properly oriented HER2 domain templates using the Homology module of InsightII and the joining regions as well as the tethering loops were extensively energy-minimized, while the domains themselves were constrained to their initial conformation. Binding partners DARPin 9_29 and DARPin G3 were transferred in the correct relative orientation from the template model to the final model.

For the model of the HER2 homodimer, individual domains of HER2 were superimposed on the corresponding domains of the HER4 homodimer structure 3U7U. This was unproblematic for domains I, III, and IV. For domain II, however, no good fit of the entire domain could be found, and therefore, the N- and C-terminal half of the domain were fitted separately, the conformations of the tethering loop adjusted, and the entire domain minimized, constraining only the positions of the disulfide-linked Cys residues.

To include the transmembrane (TM) domain and the kinase domain into the models, extracellular domain, NMR models of the TM domain (PDB entry 2JWA) and kinase structures (PDB entry 3PP0 for the active kinase dimer, 3RCD for the inactive kinase) were oriented in space taking electron micrographs from Zhang et al. (2012) as a guide. Seven residues between the last disulfide bridge of HER2_IV and the start of the transmembrane helix and 30 residues between TM domain and the kinase were treated as flexible to connect the domains. Local minimization of flexible regions and patched loops using the „Discover“ module of InsightII were followed by constrained relaxation using Rosetta.

To explore the conformations that would allow crosslinking with the shortest (five-amino-acid) linker constructs, the models with attached unlinked DARPins were cut at the chosen pivot point and rotations around this pivot point were explored to identify conformations that would bring the termini

into a distance compatible with such a short linker without any overlap of the proteins. Fig. 6 in the main paper shows two such solutions for bispecific DARPin 9_5_G.

It should be pointed out that the bispecific DARPin 9_5_G can also link a HER2 molecule in the open conformation with one in the tethered conformation, leading to the same conclusions as shown in Fig. 6. In principle, more distorted conformations of HER2 are conceivable, but there is currently no evidence for those.

In the paper, we mainly discussed the more active 9_x_G orientation of the bivalent DARPins. In this orientation, short linkers would pull down subdomain I of the HER2 monomers in such a way that the dimerization interface is obstructed by the membrane and by the second HER2 monomer kept in an orientation unsuitable for dimerization with the first monomer. This obstruction by the second HER2 monomer, especially in the context of long daisy-chains of HER2 molecules, may become the main mechanism of inhibition in constructs with linkers that are too long to significantly tilt the ECD. Due to the spatial arrangement of the DARPin termini in the HER2 complex, the less active G_x_9 constructs would tilt the HER2-ECD sideways, in an orientation less suitable to obstruct the dimer interface. The resulting side-by-side arrangement of the HER2-ECDs is also less effective at obstructing the dimerization interface and preventing activating dimerization with an additional HER2 monomer in constructs with longer linkers.

Supplemental References

Zahnd, C., Wyler, E., Schwenk, J. M., Steiner, D., Lawrence, M. C., McKern, N. M., Pecorari, F., Ward, C. W., Joos, T. O., and Plückthun, A. (2007). A designed ankyrin repeat protein evolved to picomolar affinity to HER2. J. Mol. Biol. *369*, 1015-1028.

Zhang Q., Park E., Kani K., and Landgraf R. (2012) Functional isolation of activated and unilaterally phosphorylated heterodimers of ERBB2 and ERBB3 as scaffolds in ligand-dependent signaling. Proc Natl Acad Sci U S A *109*,13237-13242.

(subsequent page) Fig. S1: Sequence and binding specificity of DARPins
(A) ELISA of HER2 binding DARPins 9_26, 9_29 and G3. The respective DARPins were tested for binding to the immobilized target proteins HER2_I-IV, HER2_I or HER2_IV, respectively. **(B)** Sequence of ELISA targets. HER2_I-IV contains the entire extracellular part of HER2, whereas HER2_I and HER2_IV denote the respective single domains, and the sequences are given underneath. The N-glycosylation sites (highlighted in red) were mutated (N→D) for crystallization. **(C, D)** Competition experiments using flow cytometry with AlexaFluor488-conjugated HER2-binders. BT474 cells were incubated with the respective fluorescently labeled HER2 binder at 100 nM concentration, either without (solid lines) or with (dotted lines) prior preincubation of the cells with the indicated non-labeled competitor at 1 µM concentration. **(C)** DARPins, **(D)** trastuzumab control.

A

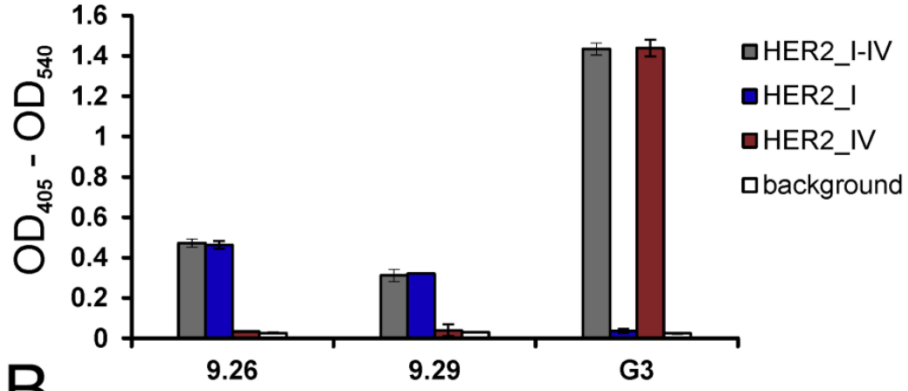

B

>HER2_I
HHHHHHQVCT GTDMKLRLPA SPETHLDMLR HLYQGCQVVQ GNLELTYLPT
DASLSFLQDI QEVQGYVLIA HNQVRQVPLQ RLRIVRGTQL FEDNYALAVL
DNGDPLDNTT PVTGASPGGL RELQLRSLTE ILKGGVLIQR NPQLCYQDTI
LWKDIFHKNN QLALTLIDTD RSRACHPCSP MCKGSRCWGE SSEDCQSLTR
TVA

>HER2_IV
HHHHHHVDCS QFLRGQECVE ECRVLQGLPR EYVNARHCLP CHPECQPQDG
SVTCFGPEAD QCVACAHYKD PPFCVARCPS GVKPDLSYMP IWKFPDEEGA
CQP

>HER2_I-IV
HHHHHHQVCT GTDMKLRLPA SPETHLDMLR HLYQGCQVVQ GNLELTYLPT
NASLSFLQDI QEVQGYVLIA HNQVRQVPLQ RLRIVRGTQL FEDNYALAVL
DNGDPLNNTT PVTGASPGGL RELQLRSLTE ILKGGVLIQR NPQLCYQDTI
LWKDIFHKNN QLALTLIDTN RSRACHPCSP MCKGSRCWGE SSEDCQSLTR
TVCAGGCARC KGPLPTDCCH EQCAAGCTGP KHSDCLACLH FNHSGICELH
CPALVTYNTD TFESMPNPEG RYTFGASCVT ACPYNYLSTD VGSCTLVCPL
HNQEVTAEDG TQRCEKCSKP CARVCYGLGM EHLREVRAVT SANIQEFAGC
KKIFGSLAFL PESFDGDPAS NTAPLQPEQL QVFETLEEIT GYLYISAWPD
SLPDLSVFQN LQVIRGRILH NGAYSLTLQG LGISWLGLRS LRELGSGLAL
IHHNTHLCFV HTVPWDQLFR NPHQALLHTA NRPEDECVGE GLACHQLCAR
GHCWGPGPTQ CVNCSQFLRG QECVEECRVL QGLPREYVNA RHCLPCHPEC
QPQNGSVTCF GPEADQCVAC AHYKDPPFCV ARCPSGVKPD LSYMPIWKFP
DEEGACQPA

C

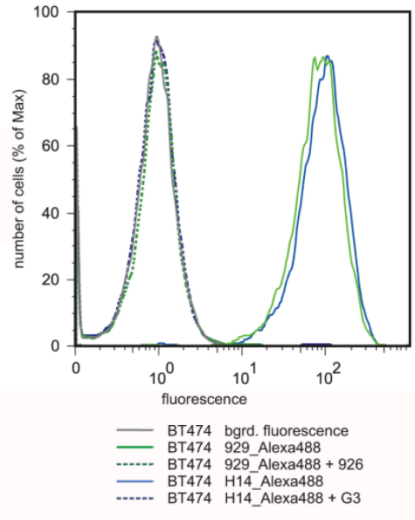

D

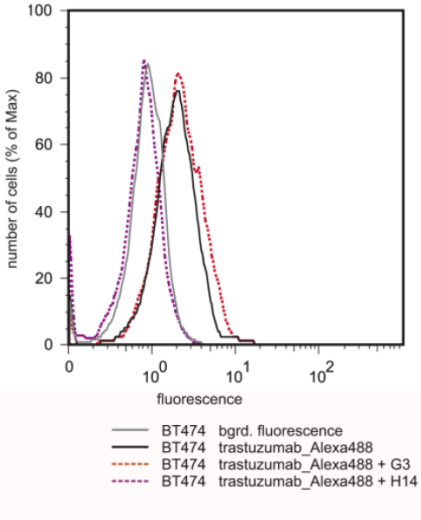

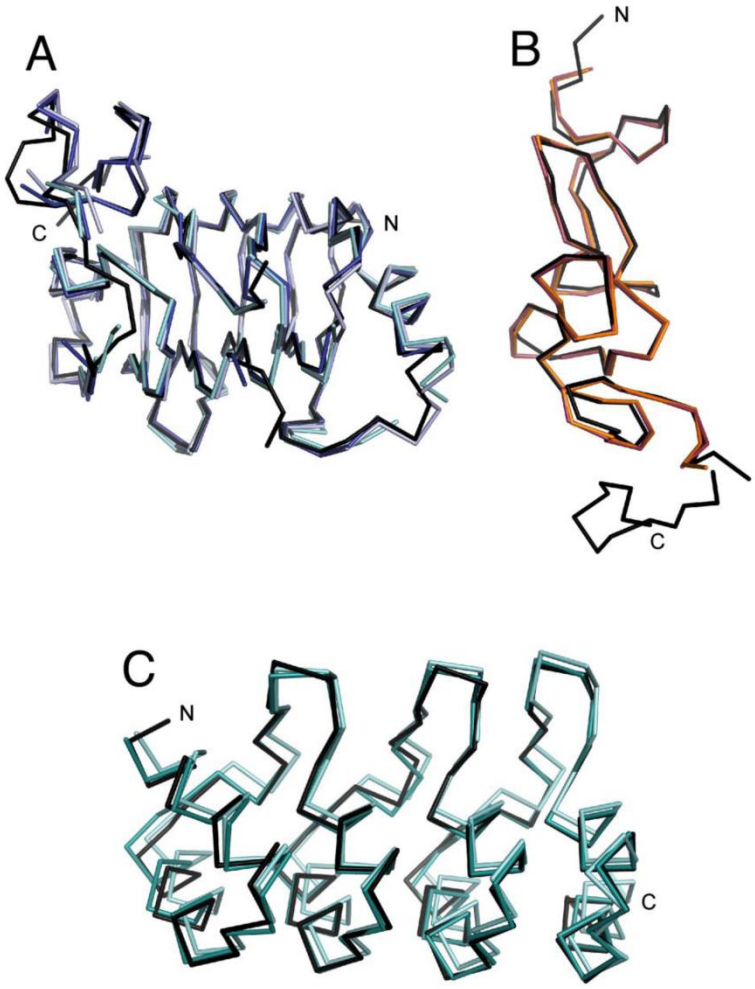

Fig. S2: Conservation of HER2 domain structures
(A) Overlay of the HER2_I-chains from the two DARPin-complex structures (chain A from HER2_I:9_29 in dark blue; chain A and C from HER2_I:9_26 in cyan and light blue, respectively) with the same domain from HER2_ECD (PDB ID: 1N8Z) (black).
(B) Overlay of HER2_IV from the complex structure with DARPin G3 (chain C in orange; chain D in raspberry) with the same domain from HER2_ECD (black).
(C) Overlay of the different X-ray structures of DARPin G3, either co-crystallized with HER2-subdomain IV or withou target (Zahnd *et al.* (2007)). The chains found in the complex structure (chain A in light blue; chain B in cyan) are very similar to the known structure of uncomplexed G3 (black) (PBD ID: 2JAB). See **Table S5** for a complete list of the corresponding RMSD values.

(subsequent page) Fig. S3: Sequence comparisons of ErbB domains and of DARPins
(A, B) Sequences of HER2_I and HER2_IV constructs in comparison to the sequences of HER1, HER3 and HER4. Residues that are identical to the HER2 sequence are shown in black on white background, sequence differences as white letters on black background, the cysteine residues on yellow background. HER2_I includes the first two interlocked disulfide bonds of the Cys-rich HER2_II. HER2 residues having at least one non-hydrogen atom within 5.0 Å of a non-hydrogen atom of the DARPin are considered part of the epitope and highlighted by a red background.
(C) Sequences of DARPins G3, 9_26 and 9_29. DARPin residues having at least one non-hydrogen atom within 5.0 Å of a non-hydrogen atom of HER2 are considered part of the paratope and highlighted by a red background. Sequence differences between 9_26 and 9_29 are shown in white on blue background. "r" indicates positions randomized in the DARPin libraries, "m" mutations acquired by G3 during affinity maturation, improving the K_D from 270 nM to 0.09 nM (Zahnd *et al.* (2007)) and "x" the mutations introduced into the C-cap to improve stability.

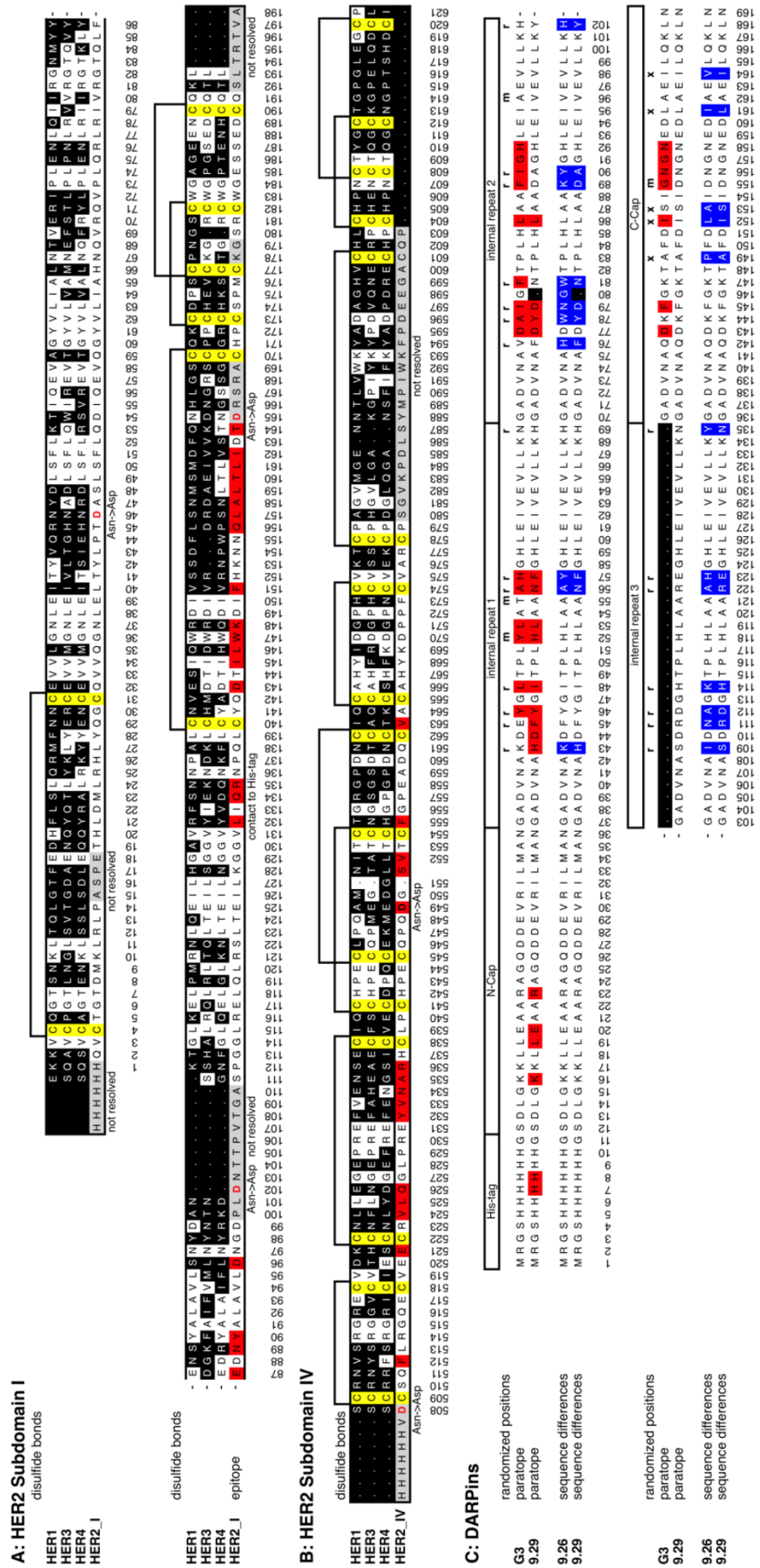
A: HER2 Subdomain I
B: HER2 Subdomain IV
C: DARPins
HER1
HER3
HER4
HER2_I
HER2_IV
disulfide bonds
epitope
not resolved
contact to His-tag
Asn->Asp
His-tag
N-Cap
internal repeat 1
internal repeat 2
internal repeat 3
C-Cap
randomized positions
paratope
sequence differences
G3
9.29
9.26

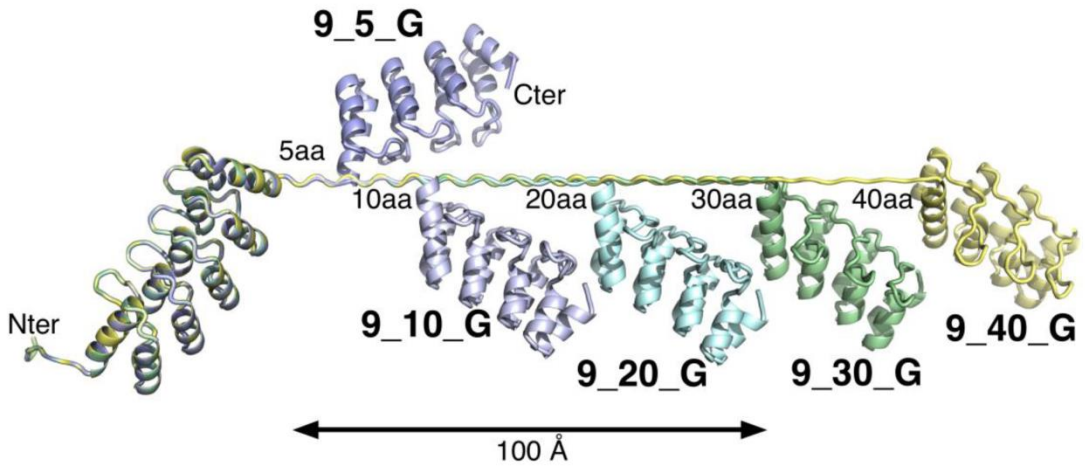

Fig. S4: Linker length of the bivalent DARPins
The linker was modeled in β-strand conformation to illustrate the maximal distance that could be bridged by such a linker. In reality, significantly longer linkers will be needed, as the mean end-to-end distance of a flexible polymer scales with the square root of the extended linker length, and the fully extended conformation of a long linker will be sampled very rarely.

Table S1: Fitted off-rates of mono- and bivalent DARPins

DARPin	k_{off} (s^{-1})
G3	1.76×10^{-4}
9_20_G	8.13×10^{-5}
G_20_9	4.46×10^{-5}
6_20_G	5.12×10^{-5}
G_20_6	4.80×10^{-5}

Table S2: Statistics for data collection and refinement

Complex	Statistics
HER2_I/9_29	
Data collection	
Space group	oP: $P2_12_12_1$
Cell dimensions, Å	a = 46.6, b = 80.5, c = 115.1
	$\alpha = \beta = \gamma = 90°$
AU content	1 complex
VM, Å³/Da	2.63
Resolution limits, Å	50 – 2.55
Observed reflections	Total 53167, unique 14553, possible 14772
Completeness, %	98.7 (99.4)*
R-merge	7.1 (40.7)*
I/σ	17.83 (4.01)*
Refinement	
Resolution range, Å	50-2.55
Final R-cryst, R-free, %	20.22, 25.39
Number of residues	331
Number of solvent molecules	31
Number of atoms	2559
Mean B-factor, Å²	32.99
rmsd (bonds), Å	0.008
rmsd (angles), °	1.293
Ramachandran analysis, %	97.2/2.8/0
HER2_I/9_26	
Data collection	
Space group	mC: C2
Cell dimensions, Å	a = 138.5, b = 60.7, c = 107.2
	$\alpha = 90°, \beta = 118.9°, \gamma = 90°$
AU content	2 complexes
VM, Å³/Da	2.40
Resolution limits, Å	50 – 3.2
Observed reflections	Total 37684, unique 12785, possible 13151
Completeness, %	97.2 (98.3)*
R-merge	7.1 (20.8)*
I/σ	14.37 (5.94)*
Refinement	
Resolution range, Å	50-3.2
Final R-cryst, R-free, %	31.31, 33.94
Number of residues	547
Number of solvent molecules	0
Number of atoms	3517
Mean B-factor, Å²	48.66
rmsd (bonds), Å	0.004
rmsd (angles), °	0.766
Ramachandran analysis, %	88.7/9.6/1.7
HER2_IV/G3	
Data collection	
Space group	hR: R32
Cell dimensions, Å	a = 195, b = 195, c = 112
	$\alpha = 90°, \beta = 90°, \gamma = 120°$
AU content	2 complex
VM, Å³/Da	1.95
Resolution limits, Å	50 – 2.65
Observed reflections	Total 120455, unique 23767, possible 23791
Completeness, %	99.9 (99.9)*
R-merge	4.1 (51.1)*
I/σ	26.42 (3.54)*
Refinement	
Resolution range, Å	50-2.65
Final R-cryst, R-free, %	21.32, 24.59
Number of residues	385
Number of solvent molecules	0
Number of atoms	2808
Mean B-factor, Å²	47.60
rmsd (bonds), Å	0.009
rmsd (angles), °	1.204
Ramachandran analysis, %	94.7/4.5/0.8

* Values in parentheses refer to the highest-resolution shell

TableS3: List of the major interaction contacts in the HER2_I/9_29 complex

9_29 interaction residue (repeat module)*			Chain	Interacting atoms (distance in Å, interaction)	HER2_I interaction residue*		Chain
HIS	7	(tag)	A		ARG	135	C
HIS	8	(tag)	A		ARG	135	C
LYS	6	(N-cap)	A	CG-OH (3.86, pi-stacking)	TYR	90	C
LYS	16	(N-cap)	A		LEU	161	C
LYS	16	(N-cap)	A		LEU	32	C
LYS	16	(N-cap)	A	NZ-OE (3.56, H-bond)	GLU	87	C
LYS	16	(N-cap)	A	NZ-OE (2.44, H-bond)	GLU	87	C
GLU	20	(N-cap)	A		ASN	89	C
GLU	20	(N-cap)	A		LEU	159	C
GLU	20	(N-cap)	A		GLU	87	C
GLU	20	(N-cap)	A	OE2-OH (2.51, H-bond)	TYR	90	C
ARG	23	(N-cap)	A		ASN	89	C
ARG	23	(N-cap)	A	NE-O (3.26, H-bond)	LEU	157	C
ARG	23	(N-cap)	A		ALA	158	C
ASP	44	(1)	A		LEU	161	C
ASP	44	(1)	A		LEU	159	C
ASP	44	(1)	A	OD2-N (3.03, H-bond)	THR	160	C
ASP	44	(1)	A		ALA	158	C
PHE	45†	(1)	A	N-O (2.67, H-bond)	THR	160	C
PHE	45†	(1)	A		ILE	162	C
PHE	45†	(1)	A		ASP	143	C
TYR	46†	(1)	A		LYS	148	C
TYR	46†	(1)	A		THR	160	C
TYR	46†	(1)	A	OH-N (3.19, H-bond)	TRP	147	C
TYR	46†	(1)	A		ILE	145	C
ILE	48†	(1)	A		ALA	158	C
LEU	53	(1)	A		LEU	159	C
LEU	53	(1)	A		LEU	157	C
ASN	56†	(1)	A		LEU	157	C
TYR	78†	(2)	A		LYS	148	C
ASP	79†	(2)	A		LYS	148	C

*A cutoff of 4 Å was applied for interactions.
†Amino acids are located in a randomized position of 9_29.

Table S4: List of the major interaction contacts in the HER2_IV/G3 complex

G3 interaction residue (repeat module)*			Chain	H-bond (Å)	HER2_IV interaction residue*		Chain
TYR	46†	(1)	A		ASP	49	D
LEU	48†	(1)	A		GLY	50	D
TYR	52‡	(1)	A		LEU	25	D
ALA	56†	(1)	A		LEU	25	D
HIS	57†	(1)	A	ND1-OE (2.90, 3.05)	GLU	21	D
HIS	57†	(1)	A		GLN	26	D
ASP	77	(2)	A		GLY	50	D
ASP	77	(2)	A		SER	51	D
ALA	78†	(2)	A	N-O (2.81)	GLY	50	D
ALA	78†	(2)	A		SER	51	D
ILE	79†	(2)	A		SER	51	D
ILE	79†	(2)	A		PHE	55	D
PHE	81†	(2)	A		PHE	55	D
PHE	89†	(2)	A		VAL	33	D
PHE	89†	(2)	A		CYS	54	D
PHE	89†	(2)	A		VAL	52	D
PHE	89†	(2)	A		TYR	32	D
ILE	90†	(2)	A		VAL	33	D
ILE	90†	(2)	A		PHE	12	D
ILE	90†	(2)	A		VAL	24	D
GLY	91	(2)	A	O-NH (3.14)	ARG	36	D
HIS	92	(2)	A		PHE	12	D
GLY	122‡	C-cap	A	O-ND (3.46)	ASN	34	D
ASN	123	C-cap	A		ASN	34	D
ASN	123	C-cap	A		VAL	33	D
ASN	123	C-cap	A	O-N (3.05)	ALA	35	D
ASN	123	C-cap	A		PHE	55	D
GLY	124	C-cap	A		ASN	34	D
GLY	124	C-cap	A		ALA	35	D
ASN	125	C-cap	A	OD1-N (3.27)	ALA	35	D
TYR	46†	(1)	B		GLY	50	C
TYR	46†	(1)	B		ASP	49	C
LEU	48†	(1)	B		LEU	25	C
LEU	48†	(1)	B		GLY	50	C
TYR	52‡	(1)	B		LEU	25	C
ALA	56†	(1)	B		LEU	25	C
HIS	57†	(1)	B	ND1-OE (2.61, 3.61)	GLU	21	C
HIS	57†	(1)	B		GLN	26	C
ASP	77	(2)	B		GLY	50	C
ASP	77	(2)	B		SER	51	C
ALA	78†	(2)	B	N-O (2.85)	GLY	50	C
ILE	79†	(2)	B		SER	51	C
ILE	79†	(2)	B		VAL	63	C
ILE	79†	(2)	B		PHE	55	C
PHE	81†	(2)	B		PHE	55	C
LEU	86	(2)	B		VAL	52	C
PHE	89†	(2)	B		VAL	33	C
PHE	89†	(2)	B		CYS	54	C
PHE	89†	(2)	B		TYR	32	C
ILE	90†	(2)	B		PHE	12	C
ILE	90†	(2)	B		VAL	33	C
HIS	92	(2)	B		PHE	12	C
PHE	112	C-cap	B		PHE	55	C
GLY	122‡	C-cap	B	O-ND (2.92)	ASN	34	C
ASN	123	C-cap	B		VAL	33	C
ASN	123	C-cap	B		ASN	34	C
ASN	123	C-cap	B	O-N (3.01)	ALA	35	C
GLY	124	C-cap	B		ASN	34	C

*A cutoff of 4 Å was applied for interactions.
† Positions randomized in DARPin library.
‡Amino acids were affinity matured (Zahnd, et al. 2007).

Table S5: List of $RMSD_{(CA)}$ values (Å) of all solved structures. The pairwise comparisons were calculated both for the solved structures among each other and in comparison with the respective PDB-entries.

	HER2_I (1N8Z)	HER2_I (9_29_C)	HER2_IV (1N8Z)	HER2_IV (G3_C)	G3 (2JAB)	G3 (G3_A)
HER2_I (9_29_C)	0.491					
HER2_I (9_26_A)	0.810	0.660				
HER2_I (9_26_C)	0.794	0.623				
HER2_IV (G3_C)			0.640			
HER2_IV (G3_D)			0.678	0.242		
G3 (G3_A)					0.645	
G3 (G3_B)					0.525	0.441

Chapter 4

Intermolecular Bi-epitopic Trapping of ErbB2 Disables ErbB Network and Induces Apoptosis in ErbB2-Addicted Tumors

Rastislav Tamaskovic[1,2], Martin Schwill[1,2], Christian Jost[2], Dagmar C. Schaefer[3], Gabriela Nagy-Davidescu[2], Mareike Göranson[2], Annemarie Honegger[2] and Andreas Plückthun[2,*]

[2] Department of Biochemistry, University of Zurich, Winterthurerstrasse 190, CH-8057 Zurich, Switzerland

[3] Institute of Laboratory Animal Science, University of Zurich, Winterthurerstrasse 190, CH-8057 Zurich, Switzerland

[1] These authors contributed equally

*corresponding author:

Phone: +41-44-635 5570

FAX: +41-44-625 5712

Email: plueckthun@bioc.uzh.ch

Content

1 Summary **89**

2 Significance **89**

3 Highlights **90**

4 Introduction **90**

5 Results **94**

5.1 Bispecific DARPins crosslink two HER2 Molecules on the Surface of BT474 Cells 95

5.2 Molecular Models of Bispecific DARPins in Complex With Full-Length ErbB2 Explain their Activity 95

5.3 Anti-proliferative Activity of Bispecific DARPins In Vitro 98

5.4 Induction of G1 Arrest and Apoptosis 99

5.5 Anti-Tumor Activity of Bispecific DARPins In Vivo 100

5.6 Active Bispecific DARPins do not Influence ErbB2 Internalization 102

5.7 Inhibition of ErbB2 Heterodimerization by Bispecific DARPins in the Presence and Absence of Ligands 103

5.8 Bispecific DARPins Retain Anti-proliferative Activity in the Presence of Heregulin 104

5.9 Inhibition of Three-Dimensional Spheroid Growth and Morphogenesis 104

5.10 Bispecific DARPins Inhibit Cell Migration after Ligand Stimulation 105

5.11 Bispecific DARPins but not Trastuzumab Inhibit ErbB2 Phosphorylations 105

5.12 Bispecific DARPins Inhibit ErbB3 Phosphorylation by ErbB2 106

5.13 Bispecific DARPins also Inhibit ErbB3 Activation after HRG Stimulation 107

5.14 Bispecific DARPins Efficiently Inhibit the PI3K/PKB Pathway 107

5.15 Bispecific DARPins Efficiently Inhibit the MAPK Pathway 108

5.16 Downstream Effects of Bispecific DARPins on the Cell Cycle 109

5.17 Downstream Effects of Bispecific DARPins on Apoptosis 109

5.18 Plasticity of ErbB2 Signaling Network and Resistance against Anti-ErbB2 Treatments 109

6 Discussion 110

6.1 The Pathway of Apoptosis Induction by bispecific DARPins 111

6.2 Non-liganded ErbB2–ErbB3 Heterodimers 111

6.3 Ligand-induced Heterodimers 112

6.4 ErbB2 Homodimers 113

6.5 3D Model and Mechanism 114

6.6 Interconnection of ERK and PKB Pathway 115

6.7 Overcoming Clinical Resistance 116

7 Conclusions 117

8 Experimental Procedures 117

8.1 Cell Culture 117

8.2 XTT Cell Proliferation Assay 117

8.3 Clonogenic Assay 118

8.4 Cell Migration Assay 118

8.5 Three-dimensional Growth Assay 118

8.6 Flow cytometery: Cell Cycle, TUNEL and Annexin V 119

8.7 Mouse Xenograft Studies 119

9 Acknowledgements 120

10 References..... 121

1 Summary

Intermolecular crosslinking of extracellular domains I and IV of ErbB2 by bi-paratopic Designed Ankyrin Repeat Proteins (DARPins) yields bent-down signaling-incompetent receptors, incapable of productive homo- or heterodimerization with any other EGFR family member. The ensuing dephosphorylation of both ErbB2 and ErbB3 results in a persistent attenuation of both PI3K/PKB and RAS/MAPK pathway, and elicits apoptosis in 2D- and 3D-cell culture models as well as in tumor-bearing mice via induction of the pro-apoptotic protein BIM and caspase-9. Furthermore, the interdomain ErbB2 trapping was shown to inhibit EGFR or ErbB3 ligand-induced cell motility, invasion and spheroid morphogenesis. We show that the sustained inhibition of both pathways has overcome feedback loops which otherwise reactivate the ErbB signaling network, robustly eliciting apoptosis.

2 Significance

We discovered and elucidated a new mechanism of sending ErbB2-dependent tumors to apoptosis. By creating a trap for ErbB2, in which the receptor is bent and kinases are unable to interact, all signaling from ErbB2 complexes is obstructed, leading to a pan-ErbB inhibition. This is necessary and sufficient to elicit apoptosis in ErbB2-addicted tumors. Our novel strategy is the first rational approach to engineer cell-specific apoptosis based on a structurally and mechanistically understood principle, and without using a toxin with potential off-tumor side effects. Our concept can add to the arsenal of monoclonal antibodies, kinase inhibitors and toxin conjugates, by molecularly designing novel ErbB2-targeted therapeutics, with the potential to avoid resistance because of their receptor-mediated cytotoxic and not cytostatic action.

3 Highlights

- Novel biparatopic proteins block productive homo- and heterodimerization of ErbB2
- Dephosphorylation of both ErbB2 and ErbB3 triggers the OFF-switch of ErbB network
- Sustained inhibition of both PKB and MAPK pathways and elicits apoptosis via BIM
- Apoptosis is elicited in vivo and causes tumor regression in mouse xenografts

4 Introduction

While human epidermal growth factor receptor type 2 (ErbB2, also referred to as HER2/neu) occurs in 25-30% of invasive breast cancer tumors (Berger *et al.* (1988); Slamon *et al.* (1987); Slamon *et al.* (1989)), no mechanism has yet been reported to kill a tumor cell solely based on interfering with its signaling. Nevertheless, since ErbB2 overexpression is found in 50% of ductal carcinomas in situ (DCIS) – noninvasive premalignant lesions of the mammary gland (van de Vijver *et al.* (1988)) – and is present both in the primary tumor and in metastatic lesions (Nahta and Esteva (2006)), the high receptor levels would provide a uniquely tumor-restricted target. The goal of the current work is to investigate how apoptosis induction through ErbB2 can be made possible, without using any toxic agent.

The extracellular domain of ErbB2 adopts a constitutively extended conformation, making ErbB2 the preferred heterodimerization partner for the ligand-activated receptors of the ErbB family. ErbB2 is thus regarded as a non-autonomous amplifier of ErbB signaling that enhances affinity for ligands bound by other family members, attenuates receptor ubiquitination and increases receptor promiscuity by engaging a broader range of signaling adapters (Harari and Yarden (2000); Jones *et al.* (2006)). ErbB2 can potentiate signaling through spontaneous formation of signaling-competent ErbB2 homodimers that assemble at high ErbB2 concentrations as found in breast tumors (Cho *et al.* (2003); Graus-Porta *et al.* (1997)). When overexpressed, ErbB2 becomes a key regulatory element driving cell proliferation, survival, migration and invasiveness of cancer cells.

The activated ErbB receptors trigger multiple signaling pathways (Hynes and MacDonald (2009)). Most activated ErbB receptor complexes utilize growth- and survival-controlling signaling pathways such as MAPK, PI3K/PKB, JAK/STAT and PKC, but since each receptor recruits a specific set of phosphotyrosine-binding effector proteins (Hause *et al.* (2012); Schulze *et al.* (2005)), each ErbB member predominantly activates its own downstream signaling pattern (Alimandi *et al.* (1995); Stern (2008); Wallasch *et al.* (1995)). For instance, within ErbB2–ErbB3 heterodimers, the phosphorylated cytoplasmic tail of ErbB3 strongly activates the PI3K/PKB survival pathway, whereas phosphorylated ErbB2 powerfully signals through the ERK MAPK pathway. This combination of PI3K/PKB and ERK signaling strongly enhances cell proliferation and survival, and for this reason ErbB2/3 forms a potent oncogenic unit (Holbro *et al.* (2003)).
As for many other signaling, genetic or metabolic networks, the ErbB network displays two steady states, i.e. bistability, with ligands transiently switching it from OFF to ON state (Kholodenko *et al.* (2010)). Importantly, pathological ERBB2 amplification maintains signaling by favoring ErbB2-containing receptor dimers and by evading negative feedback regulation, thereby fixing the ON state (Reynolds *et al.* (2003)). Since diseases such as cancer efficiently exploit key regulatory elements of the host networks (Kitano (2003)), these essential hubs could consequently become their 'Achilles heels' (Weinstein (2002)). Such a vulnerability of cancer cells, also referred to as 'oncogene addiction', may thus provide valuable opportunity for targeted therapy (Weinstein and Joe (2008)). In fact, knockdown of ErbB2 triggers apoptosis in ErbB2-addicted breast cancer cells, while barely having an effect on cells that do not overexpress this gene (Colomer *et al.* (1994); Roh *et al.* (2000)). The current work is aimed to achieving the same phenotype on the protein level.

Monoclonal antibodies (mAbs) against ErbB2 with therapeutic efficacy target only few epitopes (Boyer *et al.* (1999); Xu *et al.* (1993); Yip and Ward (2002)). The humanized murine mAb 4D5 (trastuzumab, Herceptin®) is directed against the membrane-proximal domain IV of ErbB2. It specifically inhibits the growth of breast cancer cell lines addicted to the ErbB2 overexpression by attenuation of some of the receptor downstream signaling, resulting in cell

cycle arrest in G1 phase (Lane *et al.* (2000); Neve *et al.* (2000); Pietras *et al.* (1999); Yakes *et al.* (2002)). The anti-proliferative activity of trastuzumab has been proposed to be augmented by antibody-mediated internalization and degradation of ErbB2 receptor (Baselga *et al.* (2001); Sliwkowski *et al.* (1999)) or the suppression of ectodomain cleavage, also referred to as receptor shedding (Anido *et al.* (2006); Scaltriti *et al.* (2007)); however, these phenomena seem to be confined only to a subset of tumors overexpressing ErbB2 (Le *et al.* (2003); Nahta and Esteva (2004); Nahta *et al.* (2004)). Therefore, other conceivable mechanisms, such as dissociation of the ligand-independent ErbB2–ErbB3 heterodimers (Junttila *et al.* (2009)), are a likely component of the enigmatic overall molecular action of trastuzumab.

Another approved ErbB2-binding antibody, 2C4 (pertuzumab, Perjeta®), binds adjacent to the domain II dimerization arm, thereby disturbing the heterodimerization of ErbB2 with the other ligand-bound EGFR-family members (Franklin *et al.* (2004)). Pertuzumab thus abrogates solely the ligand-stimulated growth, independent of ErbB2 overexpression. In fact, pertuzumab failed to show significant effects on the growth of ErbB2-overexpressing breast cancer cells *in vitro* (Nahta *et al.* (2004); Tanner *et al.* (2004)), implying that the *in vivo* effects of pertuzumab are critically potentiated by other cytotoxic mechanisms.

Since none of the known ErbB2-targeting mAbs is sufficient to trigger a robust cell death response in single-agent formats, they cannot fully exploit the addiction to ErbB2 as a fragile point for therapeutic intervention. In addition, the intra-ErbB pathway compensation through feedback loops and other mechanisms rapidly neutralizes the perturbation caused by the approved antibodies, thereby leading to an acquirement of resistance against mAb treatment (Garrett and Arteaga (2011); Hynes and MacDonald (2009)).

This issue has fostered the development of toxin-conjugated ErbB2-binding molecules that might give rise to a response in patients who failed trastuzumab therapy (Burris *et al.* (2011)). Trastuzumab emtansine (T-DM1) (Kadcyla®), a maytansinoid conjugate, is thought to be endocytosed with the slow internalization and recycling rates intrinsic to ErbB2 and thus to release the toxin. In a phase I clinical study thrombocytopenia was found to be a key dose-

limiting toxicity (Krop *et al.* (2010)). In the pivotal phase III study, median progression-free survival was improved from 6.4 to 9.6 months, when comparing T-DM1 to capecitabine (Xeloda®) plus lapatinib (Tykerb®) (Verma *et al.* (2012)), leading to recent FDA approval. These encouraging data stimulate the search for novel mechanisms of action, which may pave the way for agents not requiring a conjugated toxin.

A series of tyrosine kinase inhibitors (TKIs) blocking the ErbB intracellular kinase domains have also been developed, comprising both reversible and irreversible inhibitors with specificity ranging from monospecific EGFR inhibitors (gefitinib, erlotinib), dual-specificity EGFR and ErbB2 inhibitors (lapatinib, neratinib, afatinib), and broad-spectrum inhibitors (canertinib, JNJ-26483327) (Alvarez (2010)). TKIs elicit stronger biological responses *in vitro* than the highly specific yet less potent ErbB2-targeting antibodies (Geyer *et al.* (2006); Gomez *et al.* (2008)). However, the responses tend to be short-lived because of frequent induction of compensatory RTK signaling or activation of feedback loops in downstream signaling (Sergina *et al.* (2007)). Over the duration of the clinical treatment, mutations in the kinase itself or in downstream molecules may occur.

In this study, we aimed at designing and mechanistically dissecting new agents that can completely inhibit the downstream signaling of ErbB2 up to the point of causing cell death in ErbB2-addicted breast cancer cells. High-affinity ErbB2-specific designed ankyrin repeat proteins (DARPins) (Binz *et al.* (2004); Boersma and Plückthun (2011)), recognizing distinct epitopes on extracellular domains I and IV (Steiner *et al.* (2008); Zahnd *et al.* (2007)) as determined by crystallography (Jost *et al.*, 2013, cf. **Chapter 3**), were combined in bispecific constructs, composed of two different DARPins, designed to be in a particular orientation and to be connected by a very short flexible linker. The individual monomeric DARPins do not directly interfere with ErbB2 dimerization, nor do the bispecific constructs induce receptor internalization and downregulation. Instead, crosslinking of ErbB2 monomers by these bispecific DARPins separates the monomers by trapping them in a dimerization-incompetent

state, preventing both homo- and heterodimerization. This inhibition is highly dependent on the geometry of the bispecific constructs.

Based on the X-ray structures of the complexes of the individual DARPins described in detail in an accompanying study, we have formulated models of such inhibited states (Jost *et al.*, 2013, cf. **Chapter 3**). These DARPin constructs, highly cytotoxic only for ErbB2-addicted cells, rely on a simultaneous and sustained inhibition of both the PI3K/PKB and RAS/MAPK signaling pathways, thus enforcing the OFF-state in the oncogene-addicted network. Thus, this strategy constitutes a unique pan-ErbB targeting approach, as it prevents signaling-competent ErbB2 homodimers, as well as ligand-bound and unliganded heterodimers with EGFR or ErbB3, thereby shutting down virtually the whole ErbB signaling network in ErbB2-addicted cancer cells.

5 Results

DARPins are synthetic binding protein derived from ankyrin repeat proteins, developed to expand the range of formats and applications beyond what is possible with immunoglobulin-based proteins (Boersma and Plückthun (2011); Forrer *et al.* (2003)). Various DARPins binding to the ectodomain of ErbB2 and not crossreacting with other members of the EGFR superfamily were selected and affinity-matured by ribosome display and phage display (Steiner *et al.* (2008); Zahnd *et al.* (2006); Zahnd *et al.* (2007)). We tested the collection of monovalent anti-ErbB2 DARPins in cell viability assays, but found no growth-inhibitory activity comparable to trastuzumab or pertuzumab (cf. **Chapter 2**). However, various bivalent and bispecific targeting molecules of varying flexibility, orientation and epitope specificity were constructed and screened, and in particular, binders targeting ErbB2 in a bi-epitopic manner, obtained by fusing two DARPins with distinct specificities, showed significant anti-proliferative and pro-apoptotic activity.

After comprehensive scrutiny and validation in tumor cell culture models, which will be presented elsewhere, the most effective construction scheme proved to be a fusion of two

DARPins recognizing different domains of ErbB2, domain I and domain IV, connected through a very short flexible (Gly_4Ser) linker, with the domain I binder at the N-terminus and the domain IV binder at the C-terminus (Jost *et al.*, 2013, cf. **Chapter 3**) (**Fig. S1A**). The individual (monomeric) DARPins in these constructs do not interfere with ErbB2 signaling. Molecular modeling based on the crystal structures of the DARPins in complex with the recognized ErbB2 domains (Jost *et al.*, 2013, cf. **Chapter 3**) and on the full-length extracellular ErbB2 structures demonstrated that intramolecular binding would not be geometrically possible, not even in a hypothetical highly strained ErbB2 molecule.

5.1 Bispecific DARPins crosslink two HER2 Molecules on the Surface of BT474 Cells

From the markedly lower dissociation rate constants of the bispecific DARPins on BT474 cells (**Fig. S1D**, **S1E**), compared to their respective monovalent DARPin constituents, we conclude that in the bispecific anti-ErbB2 DARPins both DARPin domains are engaged in binding. Almost the same number of bivalent DARPins as monovalent DARPins can be bound (**Fig. S1E**).

To directly confirm intermolecular binding on cells, we performed crosslinking experiments on the surface of BT474 cells (**Fig. 1C**). In the absence of DARPin, a mixture of ErbB2 monomers and dimers is detected. Monomeric DARPins get crosslinked to an ErbB2 molecule, without changing the fraction of ErbB2 dimers. In contrast, after preincubation with bispecific DARPins, we found strong enrichment of the dimer band, indicating two molecules of ErbB2 being linked by the bispecific DARPin. Immunoblots clearly revealed that the high MW bands contain both ErbB2 and DARPins.

5.2 Molecular Models of Bispecific DARPins in Complex With Full-Length ErbB2 Explain their Activity

In the most active bispecific DARPins (**Fig. 1A**), an N-terminal DARPin (either 926 or 929) (Steiner *et al.* (2008)), binding to ErbB2 domain I, is linked to a C-terminal DARPin, binding to domain IV, (either G3 (Zahnd *et al.* (2007)) or H14 (Steiner *et al.* (2008))). The constituent

DARPins are described in the **Supplemental information**. X-ray crystallography (Jost *et al.*, 2013, cf. **Chapter 3**) has shown that the domain I-binding DARPins 929 and 926 recognize the same epitope, while the epitopes of G3 and H14 on domain IV overlap, but are not identical: both DARPins compete with each other , but only H14 competes with trastuzumab (Jost *et al.*, 2013, cf. **Chapter 3**).

While all 4 bispecific combinations of N-terminal domain I and C-terminal domain IV binders lead to highly active molecules, we concentrate here on two of them, 926-Linker-G3 (abbreviated 6-L1-G) and 929-Linker-H14 (abbreviated 9-L1-H), where the linker length (L1) indicates a length of one GGGGS unit.

The main conclusion drawn from the crystal structures and the detailed atomic modeling (Jost *et al.*, 2013, cf. **Chapter 3**) is that the bivalent DARPins cannot bind to both domains within one ErbB2 molecule, nor can they link two ErbB2 molecules in the canonical back-to-conformation in an orientation that would enable signaling-competent homodimers. Instead, two ErbB2 molecules must be bridged in such a manner that domain I of one monomer is brought close to domain IV of the other monomer, thereby preventing the upright orientation of ErbB2 at the cell surface (**Fig. 1B**).

This DARPin-linked arrangement of two ErbB2 molecules has two critical consequences that prevent ErbB2 receptor activation: (i) due to the constraints posed by the membrane anchoring, the transmembrane helices of the two ErbB2 monomers crosslinked by the bispecific DARPin are forced apart (**Fig. 1B**), as the large extracellular domains bend over, and (ii) the formation of signaling-competent homo- or heterodimeric back-to-back complexes (Garrett *et al.* (2003)), mediated by the dimerization loop in domain II, is prevented because proximity of the membrane obstructs access to the dimerization interface of the DARPin-bound bent ErbB2 monomers.

By geometrically separating the TM membrane and thus the juxtamembrane peptide through the bispecific DARPins, the kinases will neither be able to homo- nor heterodimerize. As shown in elegant studies from Kuriyan and coworkers (Arkhipov *et al.* (2013); Endres *et al.*

(2013)), the kinase domains of the EGFR family have only very low affinity for each other, and their mutual interaction and subsequent activation to form a signaling-competent asymmetric dimer is mediated by an interaction of the juxtamembrane regions, located between TM and kinase domain. This interaction, in turn, is only possible if the TM domains dimerize in a conserved GXXXG motif located near the cytoplasmic end, and this is prevented in our approach.

While the literature lacks any structural evidence for the existence of a tethered form of ErbB2, it cannot rigorously be excluded that the described DARPin crosslinking would not induce it. In this case the pivot point would very likely be at the boundary between domain II and III (around residue R317), again described in detail elsewhere (Jost *et al.*, 2013, cf. **Chapter 3**). Nonetheless, the conclusion about the inability of the TM domains to interact via the C-terminal GXXXG dimerization motif, the inability of the juxtamembrane peptides to interact, and consequently, the lack of signaling-competent kinase dimer formation as a function of bispecific DARPin binding holds true just the same.

Mixtures of monovalent or mixtures of homo-bivalent DARPins are inactive (**Fig. S1AB**), and the anti-proliferative activity of bispecific DARPins is highly dependent on the DARPin epitope, their order within the construct and the length of the flexible peptide linker (**Fig. S1C**), thus confirming the concept of a geometric induction of the signaling-incompetent ErbB2 conformation by the active DARPins.

In summary, based on the crystal structures of the DARPin-ErbB2 complexes and the detailed atomic modeling (Jost *et al.*, 2013, cf. **Chapter 3**), we deduce that bispecific DARPins 6-L1-G and 9-L1-H stabilize a form of ErbB2 which is devoid of signaling through its own kinase, can no longer trans-phosphorylate other ErbB2 molecules, nor ErbB3 molecules, nor be trans-phosphorylated from other ErbB receptors.

We now connect these structural conclusions with experimental receptor deactivation and with the induction of apoptosis in ErbB2-addicted cancer cells.

5.3 Anti-proliferative Activity of Bispecific DARPins In Vitro

We have evaluated the anti-proliferative activity of bispecific DARPins by means of XTT cell proliferation assays on a panel of ErbB2-overexpressing breast cancer cell lines that were previously described as trastuzumab-sensitive (BT474, HCC1419, HCC2218, SKBR3, AU565, and ZR75-30). All ErbB2-dependent cell lines without exception showed high sensitivity to the bispecific DARPins 6-L1-G and 9-L1-H (**Fig. 2A**), decreasing the number of viable cells over four days of treatment, while trastuzumab at best maintained it, and pertuzumab showed an even smaller response. The IC_{50} values were in a similar range (200-500 pM) for the DARPins and the antibodies, thereby confirming the high potency of these bivalent ErbB2 binders. The activity is highly specific and could be completely reverted by competition with soluble ErbB2_ECD (**Fig. S1F**).

The modest responses elicited by pertuzumab are expected due to the fact that the cells were grown without adding an external ErbB3 ligand. Notably, the anti-proliferative activity of bispecific DARPins also exceeded the activity of combined trastuzumab and pertuzumab in BT474 cells (**Fig. S1G**). In agreement with our model, the combination of either antibody with a bispecific DARPin leads to a reduction of the DARPins' anti-tumor activity (**Fig. S1H**).

In addition, we used MDA-MB-361 breast cancer cells with an activating mutation in the catalytic subunit alpha of PI3K (PIK3CA) (Kao *et al.* (2009)), which confers resistance to trastuzumab. The response of MDA-MB-361 (**Fig. 2B**) and other ErbB2-overexpressing cell lines with PIK3CA mutations (data not shown) is markedly lower for all treatments in general. Nonetheless, residual activity of DARPins 6-L1-G and 9-L1-H still brought about partial growth inhibition; however, without occurrence of cell death.

To assess the ability to induce reproductive cell death, the anti-proliferative activity of all compounds was further monitored by clonogenic assays in BT474 cells. As shown in **Fig. 2C**, the 4-day treatment with the bispecific DARPins resulted in an almost complete inhibition of the outgrowth of colonies, again markedly exceeding the ability of trastuzumab to reduce the clonogenic ability of this cell line. Moreover, the extent of reproductive cell death was several-

fold higher than the actual death rates as determined by viability measurements, pointing to infliction of irreversible cell damage by the bispecific agents.

5.4 Induction of G1 Arrest and Apoptosis

As shown in **Fig. 3A**, upon treatment with 6-L1-G, 9-L1-H and trastuzumab, but not pertuzumab, the cell cycle profiles of BT474 cells exhibited a G1 phase accumulation with a concomitant reduction of cells passing to S and G2/M phases. This is also found for most other examined ErbB2-dependent cell lines (**Fig. S2A**). A quantitative fitting of the cell cycle histograms by the Dean-Jett-Fox algorithm (**Fig. 3B**) confirmed correlation between the accumulation of cells in G1 phase and the growth inhibition observed by means of XTT proliferation assays (**Fig. 2A**).

Importantly, only for the cytotoxic constructs 6-L1-G and 9-L1-H, but not for trastuzumab, an additional peak with sub-G1 DNA content was observed (**Fig. 3A and 3C**), which is a typical sign of apoptosis. Thus, these findings prompted us to perform analyses aimed at direct characterization of further hallmarks of apoptosis, comprising both early and late apoptotic markers.

First, we analyzed the ErbB2-dependent breast cancer cells in TUNEL assays to quantitatively detect DNA as a result of apoptosis. As shown in **Fig. 3D** and **Fig. S3B**, the treatment with DARPins 6-L1-G and 9-L1-H resulted in an extensive TUNEL staining in the range of 30-50% in BT474, HCC1419, and HCC2218 cells (**Fig. 3 D-E**), while the TUNEL-positive populations were 15-20% in SKBR3, AU565 and ZR75-30 cells (**Fig. S3B**). Because of escape of post-apoptotic cell debris from TUNEL detection, the measurement is prone to some underestimation, especially if apoptosis has progressed far in very sensitive cells. Importantly, in all cell lines the extent of apoptosis induction by the bispecific DARPins surpassed the controls by almost two orders of magnitude; the antibodies trastuzumab and pertuzumab were only slightly above the background values of mock-treated cells.

Second, we probed the cells with Annexin V in conjunction with propidium iodide staining at low concentrations, monitoring early apoptotic flipping of phosphatidylserine and an

augmented permeability of cell membranes at late stages of cell death, respectively. Again, we detected an increase in populations of cells positive for either of these markers or both, proportional to the cytotoxic activity measured in XTT assays of the interrogated constructs (**Fig. 3F**).

Third, we monitored activity of caspases and cleavage of their targets. To distinguish between intrinsic and extrinsic apoptotic pathways, we inspected initiator caspases casp-9 and casp-8 (**Fig. 3G**) (Danial and Korsmeyer (2004)). Both bispecific DARPins 6-L1-G and GDC-0941 strongly activated casp-9, as did the PI3K inhibitor GDC-0941, while only TRAIL (TR10 ligand) was causing activation of casp-8. On the other hand, the effector caspases casp3/7 became activated, as expected, by all apoptotic stimuli irrespective of the source. We thus conclude that bispecific anti-ErbB2 DARPins, despite being *nota bene* extracellular ligands, activate the intrinsic apoptotic pathway.

Forth, we analyzed crucial players involved in the execution phase of apoptosis. As shown in **Fig. 3H**, there was a rapid and intense degradation of the casp-3 target poly-(ADP-ribose)-polymerase (PARP) observed in all cell lines upon treatment with the bispecific DARPins, whereas only a partial response was recorded for trastuzumab in a small subset of the examined cell lines. Furthermore, the upregulated expression of the BH3-only pro-apoptotic Bcl-2-like protein 11 (BIM), also known as master regulator of apoptosis downstream of EGFR-family receptors (Danial (2007); Ewings *et al.* (2007); Faber *et al.* (2011); Marani *et al.* (2004); Tanizaki *et al.* (2011)), reflected again the high potency of bispecific DARPins to unleash apoptosis.

In summary, we conclude that the cytotoxic activity of ErbB2-biepitopic DARPins is mainly attributable to a potent induction of apoptosis in ErbB2-addicted tumor cells.

5.5 Anti-Tumor Activity of Bispecific DARPins In Vivo

To test the constructs *in vivo*, we first extended their *in vivo* half life by PEGylation (Zahnd *et al.* (2010)). To clearly distinguish the DARPin-mediated anti-tumor activity from unrelated effects,

e.g. complement or ADCC responses mediated by an antibody Fc domain, we have on purpose omitted such fusions and chosen PEGylation, even though its half-life extension may not be as powerful as the half-life extension provided by e.g. the fusion to an Fc or to another DARPin binding to serum albumin.

We thus generated and tested a series of bispecific DARPins with a unique cysteine residue at either the N- or C-terminus, which could be subsequently derivatized by a PEG-maleimide of 40 kDa (Tamaskovic *et al.* (2012)). We found that the bispecific DARPins modified with PEG40 right behind the N-terminal his tag did not reduce the maximal anti-proliferative activity on ErbB2-addicted cells *in vitro* (**Fig. S3A**), nor the binding on cells (data not shown). These constructs were termed 6-L1-G_N_PEG and 9-L1-H_N_PEG.

For bioimaging studies, the PEGylated DARPins were additionally decorated with the far red dye Alexa Fluor 680 or the infrared fluorophore IRdye800, which were selectively attached to the N-terminal amino group (Tamaskovic *et al.* (2012)). The *in vivo* half-lives of these constructs were determined as 21.2 h (AUC 15.3 µmol/l·h) for 6-L1-G_N_PEG and 7.0 h (AUC 5.8 µmol/l·h) for 9-L1-H_N_PEG, being at least two orders of magnitude higher than the values of similar underivatized counterparts (Zahnd *et al.* (2010)). As shown in **Fig. 4A**, the PEGylated DARPins became efficiently enriched at the tumor site.

We next examined whether the PEGylated bispecific DARPins show anti-tumor activity *in vivo* on BT474 xenografts. BT474 cells were implanted orthotopically in the mammary fat pad of SCID beige mice. After tumor establishment (about 2-3 weeks), the mice were treated with 20 mg/kg doses three times per week during a three-week period, and the tumor volume was monitored during and after treatment. As shown in **Fig. 4B**, both bispecific PEGylated DARPins caused tumor regression, while the non-targeted PEGylated bivalent DARPin (vehicle control) did not show an effect, similar to the PBS control. Although complete tumor remission could not be achieved and some post-treatment tumor regrowth was evident, likely due to the insufficient half-life of the PEGylated constructs, the obtained data unequivocally confirm the anti-tumor activity of bispecific DARPins *in vivo*.

IHC analysis of sections from the treated tumors demonstrated that the achieved therapeutic effect *in vivo* was due to apoptotic cell death, as manifested by an intense TUNEL staining, formation of apoptotic bodies and detection of a caspase-3 proteolytic fragment in tumor tissue (**Fig. 4C**). Furthermore, treatment with PEGylated bispecific DARPins resulted in substantially smaller tumors with large areas replaced by fibrous myxoid stroma within (**Fig. 4C**). These data confirm that the same mode of action of the bispecific DARPins is operative *in vivo* and *in vitro*. No weight loss or any other adverse symptom was detected in the treated mice, demonstrating that repeated doses of bispecific PEGylated DARPins were well tolerated, and similar data were obtained in naïve animals (data not shown). Further modifications of the molecular targeting format, such as fusions to serum albumin or Fc domains or tightly binding DARPin mediating these interactions, are expected to yield reagents with significantly improved PK/PD profile and higher specific cytotoxicity.

5.6 Active Bispecific DARPins do not Influence ErbB2 Internalization

Receptor internalization coupled to degradation is considered to be a process that robustly attenuates oncogenic signaling by targeting surface receptors for lysosomal degradation, even though for ErbB2, this is not a likely mechanism (see below). We investigated whether bispecific DARPins influence the expression level or the internalization rate of the ErbB2 receptor. As shown in **Fig. 6A,D**, the total expression level of ErbB2 did not change up to 72 hours post-treatment in BT474 or SKBR3 cells, nor did it significantly alter in the other cell lines overexpressing ErbB2 (**Fig. 6G**). Direct probing of ErbB2_ECD on intact cells confirmed that ErbB2 receptor remained expressed on the cell surface during the whole time span of treatment (**Fig. S3B-C**).

Most importantly, an examination of receptor trafficking after incubation with bispecific DARPins or with a mixture of the inactive monovalent counterparts did not uncover any substantial differences. Neither an increased internalization rate nor attenuated endosomal recycling was found for the DARPins with high anti-tumor activity, suggesting that the

cytotoxicity is not caused by such mechanisms (**Fig. S3D-E**). Taken together, these findings imply that the bispecific anti-ErbB2 DARPins achieve their cytotoxic activity by other mechanisms, e.g. through interference with ErbB2 downstream signaling, but not by modulating receptor trafficking. This is in contrast to what we and others recently reported for binders targeting the EGF receptor (Boersma *et al.* (2011); Hackel *et al.* (2012)).

These findings are consistent with studies showing that the ErbB2 expression level remains unaffected by trastuzumab treatment (Junttila *et al.* (2009)), and that trastuzumab does not accelerate the internalization of ErbB2 (Hommelgaard *et al.* (2004)). It is noteworthy that the internalization rate of ErbB2 is inherently low (Hendriks *et al.* (2003)).

5.7 Inhibition of ErbB2 Heterodimerization by Bispecific DARPins in the Presence and Absence of Ligands

Since our bispecific DARPins targeting ErbB2 potentially affect the interaction of ErbB2 with ErbB3, we analyzed receptor dimerization after DARPin treatment. We stimulated ErbB2–ErbB3 heterodimerization with the ErbB3 ligand heregulin-β1 (HRG) (Hynes and Lane (2005); Yarden and Sliwkowski (2001)) and analyzed heterodimerization in the presence or absence of ligand stimulation in BT474 cells by CoIP after crosslinking the cell surface receptors with thiol-cleavable 3,3´-dithiobis[sulfosuccinimidylpropionate] (DTSSP), subsequent reduction and determination of the amount of ErbB2 and ErbB3 by immunoblotting.

Heterodimerization of ErbB2–ErbB3 is strongly stimulated by HRG in BT474 cells (**Fig. 5A**). Trastuzumab did not interfere with ErbB2–ErbB3 heterodimerization upon HRG addition, while pertuzumab did effectively inhibit ErbB2–ErbB3 heterodimerization under these conditions, consistent with previous findings (Junttila *et al.* (2009)). Bispecific DARPins effectively inhibit ErbB2–ErbB3 heterodimerization, both in the presence and absence of HRG stimulation (**Fig. 5A**).

The analysis of ErbB2/EGFR heterodimerization was performed analogously with SKBR3 cells using the EGFR ligand EGF, since SKBR3 cells express significantly more EGFR than BT474

cells, while both are ErbB2 overexpressing cell lines and are highly dependent on ErbB3 expression (Lee-Hoeflich *et al.* (2008)). As expected, we found stimulation of ErbB2/EGFR heterodimerization by EGF addition in SKBR3 cells (**Fig. 5B**). Bispecific DARPins strongly reduced ErbB2/EGFR heterodimerization in the presence or absence of EGF, while the effects of trastuzumab and pertuzumab were not pronounced (**Fig. 5B**).

5.8 Bispecific DARPins Retain Anti-proliferative Activity in the Presence of Heregulin

Addition of HRG stimulated the growth of BT474 control cells by only 20% (**Fig. 5B**). In the presence of HRG, trastuzumab loses its anti-proliferative activity completely, while in the absence of HRG, trastuzumab decreased proliferation by 50-60%. On the other hand, pertuzumab retained 20% anti-proliferative activity in presence and absence of HRG, respectively. The bispecific DARPins reduced cell growth by 50% in the presence of HRG and thus had the strongest effect on BT474 cell viability of all reagents tested under these conditions (**Fig. 5B**).

5.9 Inhibition of Three-Dimensional Spheroid Growth and Morphogenesis

We also investigated the effects of bispecific DARPins and monoclonal antibodies in a three-dimensional culture of BT474 cells on a laminin-rich reconstituted basement membrane. In such an environment the tumor cells become organized into acini-like spheroid structures resembling ductal glandular architecture (Kenny *et al.* (2007)). As shown in **Fig. 5D-E**, both bispecific anti-ErbB2 DARPins and, to a lesser extent, trastuzumab abrogated the 3D growth of BT474 spheroids, while pertuzumab showed only a partial effect in the absence of HRG.

We next investigated the effects of the different ErbB2-targeting agents on the spheroid morphogenesis induced by HRG. As shown in **Fig. 5F-G**, BT474 acini underwent morphogenesis manifested by pronounced budding/branching and invaded the surrounding matrix, which was robustly inhibited by either 6-L1-G, 9-L1-H, or pertuzumab, whereas trastuzumab or the non-

targeted bivalent DARPin control had no effect. Hence, we conclude that the bispecific DARPins prevent the HRG-dependent morphogenesis of breast cancer cells, (**Fig. 5B**).

5.10 Bispecific DARPins Inhibit Cell Migration after Ligand Stimulation

ErbB2 overexpression has been associated with visceral metastasis and micrometastatic bone marrow disease (Pantel *et al.* (1993); Slamon *et al.* (1987)). Correspondingly, enhanced expression of ErbB2 as well as stimulation with EGF or HRG in ErbB2-overexpressing cells have been reported to induce cell migration and invasion in an ErbB2-dependent manner (Le *et al.* (2012); Spencer *et al.* (2000)).

We have therefore examined the effect of bispecific DARPins on cell motility in a wound-healing assay with SKBR3 cells, high in both EGFR and ErbB3. As shown in **Fig. 5H-K**, both EGF and, in particular, HRG induced an extensive resealing of scratches in cell monolayer after a two-day treatment. The EGF-induced cell migration was reversed by DARPins but only slowed down by treatment with both antibodies, correlating with the agents' ability to disrupt the ErbB2/EGFR heterodimers (**Fig. 5B**). DARPins and pertuzumab reduced the potent HRG stimulation of cell migration, while trastuzumab showed no effect, again consistent with their effect on ErbB2/ErbB3 heterodimers.

Consistent data were also found in a cell invasion assay (**Fig. S3H**). The impaired migration after DARPin treatment was correlated to reduction of ErbB2 phosphorylation at phospho-tyrosines pY-1222 and pY-1248 (**Fig. 6A**), i.e. the residues that were postulated to mediate the ErbB2-driven cell migration (Marone *et al.* (2004)).

5.11 Bispecific DARPins but not Trastuzumab Inhibit ErbB2 Phosphorylations

We analyzed multiple ErbB2 tyrosine phosphorylation sites in the C-terminal tail of ErbB2 (Y1139, Y1169 Y1221/1222, Y1248) which serve as docking sites for a specific set of PTB-domain-containing adaptor proteins (Hause *et al.* (2012); Jones *et al.* (2006); Schulze *et al.*

(2005)). Furthermore, we monitored the phosphorylation within the kinase lobe of ErbB2 (Y877).

After 24 h of treatment with bispecific DARPins, we detected a progressive and uniform reduction of ErbB2 Tyr phosphorylation of all sites in BT474 cells (**Fig. 6A**), which followed an exponential decay (**Fig. S4A**). Consistently, bispecific DARPins reduced phospho-ErbB2 levels in all ErbB2-dependent cancer cells (**Fig. 6D,G**). We confirmed the uniform dephosphorylation of all Tyr sites by immunoprecipitation of ErbB2 after treatment and subsequent detection of total phospho-Tyr content (**Fig. 6C**). Consistent with these observations, the adaptor protein GRB2 (**Fig. S4B**) no longer binds.

Importantly, the reduction of phospho-ErbB2 preceded a down-regulation of full-length ErbB2 expression, which was only observed in the population of late apoptotic, detached cells (**Fig. S4C**). This reflects enhanced degradation of ErbB2 during the execution of apoptosis, ErbB2 degradation thus being one of the effects and not the cause of apoptosis. Nonetheless, the appearance of truncated ErbB2 (p95) (shedding) was reduced after treatment with bispecific DARPins in BT474 cells (**Fig. S4D**).

In contrast, we did not detect effects on ErbB2 phosphorylation after trastuzumab treatment, neither at the level of single Tyr phosphorylation sites (**Fig. 6B**) nor at the level of total ErbB2 phosphorylation (**Fig. 6C**). Similarly, ErbB2 phosphorylation remained unaffected by trastuzumab treatment in most of the other ErbB2-dependent cancer cell lines tested (**Fig. 6C,G**). Taken together, bispecific DARPins – but not trastuzumab – can efficiently inhibit the phosphorylation of the ErbB2 receptor.

5.12 Bispecific DARPins Inhibit ErbB3 Phosphorylation by ErbB2

The ErbB2 receptors, when overexpressed on the surface of cancer cells, are known to drive tumor growth in concert with ErbB3, thereby forming a potent oncogenic unit (Holbro *et al.* (2003); Lee-Hoeflich *et al.* (2008)). As shown in **Fig. 6 E-G**, the phosphorylation of the distal ErbB3-Y1289 site was reduced right after treatment with either bispecific DARPins or

trastuzumab and remained dephosphorylated during the entire treatment. Total expression levels of ErbB3 differ among ErbB2 overexpressing cell lines. Nonetheless, treatment with bispecific DARPins or trastuzumab reduced ErbB3 phosphorylation to a similar extent in HCC1419, HCC2218, SKBR3, AU565, and ZR75-30 (**Fig. 6G**). Interestingly, we observed consistent upregulation of ErbB3 expression after treatment with bispecific DARPins and trastuzumab in multiple ErbB2-dependent cell lines (**Fig. 6E-G**).

5.13 Bispecific DARPins also Inhibit ErbB3 Activation after HRG Stimulation

We also analyzed ErbB2 and ErbB3 phosphorylation after treatment with bispecific DARPins in combination with HRG stimulation (**Fig. 6H**). As expected, 1 nM HRG stimulated ErbB3 phosphorylation effectively in SKBR3 cells. Trastuzumab did not inhibit ErbB3 phosphorylation detectably after ligand stimulation, while pertuzumab did so, consistent with previous findings (Sakai *et al.* (2007)). Bispecific DARPins, similar to pertuzumab, strongly impair ErbB3 phosphorylation caused by HRG-stimulated heterodimerization with ErbB2. As detailed above, we also detected a significant ErbB2 dephosphorylation after treatment with bispecific DARPins and HRG.

In summary, the inhibition of ErbB2–ErbB3 heterodimerization by bispecific DARPins – in the absence and presence of HRG – was observed both in experiments directly detecting the heterodimers on cells by co-immunoprecipitation (**Fig. 5A**) and in assays detecting the level of ErbB2 and ErbB3 phosphorylation (see **Fig. 6H**).

5.14 Bispecific DARPins Efficiently Inhibit the PI3K/PKB Pathway

Dephosphorylation of ErbB3 by trastuzumab treatment results in the loss of SH2 docking sites for the negative regulatory subunit p85 of phosphatidyl-inositol-3-kinase (PI3K), which consequently inhibits the catalytic subunit p110 (Junttila *et al.* (2009)). As shown in **Fig. 7A,D,K**, the phosphorylation of PKB (AKT), an important player downstream of p110, was diminished upon treatment by both trastuzumab and bispecific DARPins. However, the bispecific DARPins

caused stronger and, importantly, sustained dephosphorylation of PKB in all ErbB2-dependent cell lines. In contrast, trastuzumab induced a strong transient PKB dephosphorylation for up to 6 h in BT474 and SKBR3 cells equivalently, but from this time point on, PKB became progressively re-phosphorylated (see also **Fig. S4E**).

5.15 Bispecific DARPins Efficiently Inhibit the MAPK Pathway

ErbB2 and EGFR receptor signaling, and especially signaling by homodimers, is closely associated to activation of the RAS/MAPK pathways (reviewed in (Yarden and Sliwkowski (2001))). We measured the output of the mitogenic signaling at the level of ERK. An initial strong and transient pulse of ERK phosphorylation was observed, ranging from 3- to 8-fold in BT474 or SKBR3 cells over the steady-state ERK phosphorylation levels, immediately after treating with either bispecific DARPins or trastuzumab (**Fig. 7B,E**). Stimulation of ERK phosphorylation by trastuzumab has been observed before (Gijsen *et al.* (2010)). It takes place already very early and at very low concentrations of all anti-ErbB2 agents (**Fig. S4F**), in a range where both trastuzumab and bispecific DARPins exhibit strong cytostatic or cytotoxic activity, respectively (cf. **Fig. 2A** and **Fig. 3D,E**).

Importantly, only treatment with bispecific DARPins reduced ERK phosphorylation rapidly down to 20% of the initial steady state level in BT474, and phospho-ERK levels remained consistently low in all other cell lines (**Fig. 7K**) in a sustained manner (see also **Fig. S4G**). In contrast, trastuzumab induced only a transient stimulation of ERK-phosphorylation, which returns to the steady state phosphorylation level without ever going below, in the ErbB2-dependent cell lines investigated, except in ZR75-30 cells.

We did not observe a direct correlation of the pulsed ERK phosphorylation and the phospho-status of ErbB2 (**Fig. 6A-D**), and thus the phospho-ERK stimulus seems to be not directly caused by increased ErbB2 phosphorylation.

5.16 Downstream Effects of Bispecific DARPins on the Cell Cycle

The examination of cell cycle regulators p27Kip1 (cyclin-dependent kinase inhibitor) and cyclinD1 (CDK4/6 activator), which governs G1/S-phase transition, revealed that their expression levels are affected by trastuzumab as reported (Lane *et al.* (2000)) and consistent with the recorded cell cycle profiles (**Fig. 3A**, **Fig. S2A**). With bispecific DARPins, on the other hand, we observed stronger p27Kip1 upregulation in BT474 and SKBR3 cells (**Fig. 7G,H**) and stronger reduction of cyclinD1 expression in BT474 cells (**Fig. 7I**), starting after 12-24 hours of treatment. Other ErbB2-overexpressing cell lines showed similar effects for upregulation of p27Kip1, however down-regulation of cyclinD1 was not as pronounced in these cells compared to BT474 cells (**Fig. 7K**).

5.17 Downstream Effects of Bispecific DARPins on Apoptosis

The up-regulation of BIM expression (**Fig. 3H** and **Fig. 7C,F**) and cleavage of PARP (monitored by increased amounts of PARP p89) (**Fig. 3H**) was observed only after bispecific DARPin treatment in all ErbB2-dependent cell lines, but not after trastuzumab treatment. The one exception are ZR75-30 cells, which show some BIM upregulation and detectable phenotypic signs of apoptosis also upon treatment with trastuzumab.

5.18 Plasticity of ErbB2 Signaling Network and Resistance against Anti-ErbB2 Treatments

We have summarized most significant findings on the ErbB2-driven signaling network by bispecific DARPins in a scheme (**Fig. 7L**). Since bispecific DARPins show strong impact on both the PI3K/PKB and the RAS/MAPK pathway, we assessed the plasticity of these pathways in BT474 cells after selective stimulation of each pathway individually. To stimulate PI3K activity (indirectly), we antagonized its back-reaction by inhibiting the tumor suppressor phosphatase and tensin homolog (PTEN) (Xiao *et al.* (2007)) by bis-peroxo(pyridine-2-carboxyl)oxovanadate (bpV(pic)) (Schmid *et al.* (2004)). Indeed, PTEN inhibition resulted in stimulation of PKB

phosphorylation independent of treatment (**Fig. S4H**). We observed that PTEN inhibition translated to a reduced activity of trastuzumab and bispecific DARPins in viability assays (**Fig. S4I**), but we still detected a cytotoxic effect of DARPins, indicating that they can overcome even stimulated PI3K action.

To assess the MAPK pathway contribution, we directly stimulated protein kinase C (PKC) by 12-O-tetradecanoylphorbol-13-acetate (TPA). TPA induced specific ERK phosphorylation after 2 h (**Fig. S4K**), which in turn translated to a reduced effect of trastuzumab and bispecific-DARPins on cell viability. Note, however, that the anti-proliferative activity of trastuzumab treatment was reduced to a much higher extent than that of bispecific DARPins.

6 Discussion

By targeting two distinct epitopes of ErbB2 with appropriately designed bispecific binding proteins that completely disengage ErbB2 from the signaling network, we developed powerful agents with apoptotic activity against ErbB2-addicted breast cancer cells.

We examined a broad panel of ErbB2-dependent tumor cell lines, all showing 20-50% apoptosis after a 3-day treatment with the bispecific DARPins. To our knowledge, this bi-epitopic targeting is the only strategy described so far for ErbB2-targeting proteins inducing a potent apoptotic response. In contrast, the action of trastuzumab is limited to causing an arrest of proliferation in the G1 phase of the cell cycle.

Importantly, this ability is retained in cells with p53 deficiency and low PTEN activity, which represents a common feature of cancer cells leading to emergence of resistance during trastuzumab treatment. Even under circumstances of a constitutively active PI3K-PKB-mTOR pathway, as a consequence of activating PIK3CA mutations, DARPins still displayed significant anti-proliferative activity. Finally, studies on orthotopically xenografted tumors confirmed that the bispecific DARPins retained the ability to induce apoptosis *in vivo*, and thus, the achieved apoptotic effect could be translated to the *in vivo* situation and was attributable to the same mode of action as in the cell culture tumor models.

6.1 The Pathway of Apoptosis Induction by bispecific DARPins

As previously reported, the induction of apoptosis in ErbB2-amplified breast cancer tumors is dependent on the expression level of the BH3-only proapoptotic protein BIM (Tanizaki *et al.* (2011)). Ablation of BIM by RNAi leads to abolition of lapatinib-induced apoptosis, implying that BIM is controlled by survival signals emanating from ErbB receptors and itself critically controlling apoptosis (Faber *et al.* (2011)). BIM levels are mainly regulated by controlling its ubiquitination (Ewings *et al.* (2007)) via ERK phosphorylation (Marani *et al.* (2004)) and to a lesser extent by controlling FoxO3-mediated transcription, which stands under negative control of PKB. Through neutralization of anti-apoptotic proteins from the Bcl-2 family, the upregulation of BIM triggers activation of casp-9 (reviewed in (Danial (2007)), an apoptosome caspase that, in turn, is kept in check by PKB phosphorylation (Cardone *et al.* (1998)).

Our results show that the upregulation of BIM is only detectable after sustained inhibition of both the ERK and PKB pathway, which is achieved after the treatment with bispecific DARPins. In contrast, the inhibition of PKB by trastuzumab, in the presence of an active ERK pathway, fails to augment expression of this pro-apoptotic protein.

We thus conclude that the activation of the apoptotic program is enabled only in a background of simultaneous inhibition of both PKB and ERK signaling pathways (see scheme in **Fig. 7L**).

6.2 Non-liganded ErbB2–ErbB3 Heterodimers

Heterodimerization of overexpressed ErbB2 with ErbB3 is known to be essential to promote the growth of cancer cells (Holbro *et al.* (2003); Lee-Hoeflich *et al.* (2008)), and a hallmark of ErbB2-overexpressing tumor cells is that non-liganded ErbB2–ErbB3 complexes form also in the absence of ErbB3 ligand (Junttila *et al.* (2009)). Such non-liganded ErbB2–ErbB3 heterodimers are thought to form different association complexes than the canonical back-to-back dimers, e.g. without depending on contacts between domains II, but still to be signaling-competent and

thereby driving the proliferation of ErbB2 overexpressing cells. The bispecific DARPins clearly prevent the formation of these complexes.

Notably, a negative feedback loop linking inhibition of phospho-PKB to transcriptional upregulation of ErbB3 expression via the transcription factor FoxO3 has been recently described as a mechanism of resistance against tyrosine kinase inhibitors (TKI) (Garrett *et al.* (2011)), and it appears to be a general mechanism under the control of PKB (Chandarlapaty *et al.* (2011)). This feedback loop maintains oncogenic ErbB2/3 signaling, illustrating the robustness of the ErbB network against perturbations.

We observed a rapid collapse of ErbB3 and PKB phosphorylation accompanied by a marked upregulation of ErbB3 expression after treatment with both bispecific DARPins and trastuzumab, indicating that the PKB/ErbB3 feedback loop also operates when targeting ErbB2 via binding proteins. Despite of the high expression level, however, the ErbB3 receptor remained in an unphosphorylated state. Hence, the observed rapid decay of ErbB2–ErbB3 complexes in the absence of ErbB3 ligand, disengaging the active ErbB2 receptor kinase from its substrate, the ErbB3 tail, most likely accounts for the attenuation of PKB signaling. This entails a blockade of cell survival signals, caused by the ErbB2-trapping DARPins.

6.3 Ligand-induced Heterodimers

After ligand binding, ErbB3 adopts the extended conformation (Dawson *et al.* (2007)) and forms contacts via domain II and IV with its partner ErbB2 (Franco-Gonzalez *et al.* (2013); Franklin *et al.* (2004); Zhang *et al.* (2012)). It is believed that the heterodimerization between ErbB2 and EGF-activated EGFR is fairly similar, yet not identical (Cai *et al.* (2008); Macdonald-Obermann *et al.* (2012)). Bispecific DARPins are active against both ligand-stimulated ErbB2–ErbB3 and ErbB2–EGFR complexes to an equal or higher extent than the antibody pertuzumab, as shown in ligand-induced cell growth assays for three-dimensional spheroid morphogenesis, ligand-dependent cell proliferation and the wound-healing migration or invasion and, in particular, by the co-immunoprecipitation studies.

In contrast, trastuzumab inhibited receptor heterodimerization after incubation with EGF only to a minor extent, and was inactive after stimulation with HRG. Hence, the bispecific DARPins combine properties of the two monoclonal antibodies in a single targeting molecule, with even greater activity.

Inhibition of ErbB3 signaling has been proposed to up-regulate the protease ADAM17 (TACE), which then becomes part of another reported feedback loop leading to an increased conversion of endogenous ligand precursors to active ligands (e.g. betacellulin and heregulin), thereby reactivating the ErbB2/3 signaling (Gijsen *et al.* (2010)). However, we did not observe increased amounts of phospho-ErbB3 after treatment of non-stimulated cells with any targeting agent, suggesting that this feedback loop is not operational in our model.

While the reduction of PKB phosphorylation persisted for the whole period of DARPin treatment, the effect of trastuzumab on PKB phosphorylation was only transient, despite sustained dephosphorylation of ErbB3. This implies the existence of a crucial signaling bypass of ErbB3 in trastuzumab-treated cells (see below).

6.4 ErbB2 Homodimers

ErbB2 can form signaling-competent homodimers that stimulate the ERK pathway through activation of the small GTPase RAS (Ghosh *et al.* (2011)). We observed that all phospho-Tyr sites exhibited a slow exponential decay of phosphorylation, with half-lives of individual phospho-sites varying between 12 to 20 h after treatment with bispecific DARPins, but not trastuzumab, leading to silencing of this pathway (Kawano *et al.* (2009)).

Consistent with the observation that only bispecific DARPins lead to a dephosphorylation of ErbB2, only they inhibited ERK phosphorylation up to 90% in BT474 cells (after an initial pulse shown by both agents), while trastuzumab failed to overcome ErbB2 phosphorylation and, consequently, ERK returned to steady-state phosphorylation levels after the phospho-ERK pulse. Because of this parallel behavior of phosho-ErbB2 and phospho-ERK,

we conclude, similar to previous reports (Ghosh *et al.* (2011)), that ERK activation is maintained mainly by the active ErbB2 homodimers.

6.5 3D Model and Mechanism

The model recently described (Jost *et al.*, 2013, cf. **Chapter 3**) (**Fig. 1B**) accounts for the observed absence of (i) ErbB2–ErbB2 signaling complexes, (ii) ErbB2–ErbB3 signaling complexes in the absence of ligand (even though their geometry is not yet known), and finally (iii) the absence of complexes of ErbB2 with ligand-activated ErbB3 and/or EGFR. This prevention of productive ErbB2 complexes thus explains how the ErbB2-driven ErbB network is inhibited at multiple levels. Thus, this mode of action resembles the phenotypic effects of an ErbB2 knock-out (Cho *et al.* (2003); Graus-Porta *et al.* (1997)) and a pan-ErbB2 inhibition, which switches the ErbB network into the OFF state.

The model builds on recent structural work on the mechanisms of kinase activation within the EGFR homodimer (Arkhipov *et al.* (2013); Endres *et al.* (2013)). Importantly, the interaction between the kinase domains themselves is very weak, and needs to be mediated by the juxtamembrane region, a peptide assuming different conformations, located between TM region and the kinase domain. Their dimerization requires in turn, that the TM domains of two ErbB receptors come together such that they can associate at the GXXXG motif close to the cytoplasmic side. As a consequence, this particular TM association mode may constitute a decisive switch.

Our structural model, which is based on the structures of the DARPins with the HER2 domains described in detail in an accompanying paper (Jost *et al.*, 2013, cf. **Chapter 3**), shows that this particular TM association is prevented (**Fig. 1B**) by enforced separation of the extracellular domains by the bispecific DARPins, combined with a dimerization-incompetent orientation of the extracellular domain relative to the membrane. Coverage of the ErbB2 surface by the DARPins, combined with the constrained orientation of the ErbB2 monomers relative to

the membrane, can also be expected to interfere with alternative associations, such as the formation of tetramers and oligomers.

6.6 Interconnection of ERK and PKB Pathway

By using selective stimulators of either ERK or PKB pathway, we observed that the anti-tumor activity of bispecific DARPins was diminished. Hence, both the ERK and the PKB pathway mediate protection from apoptosis and stimulate growth, which illustrates the functional flexibility of both pathways and, thus, the potential to compensate for pathway specific perturbations (Yarden and Pines (2012)).

While the ErbB network is more robust against ERK perturbation than against PI3K/PKB pathway perturbations, inhibition of PI3K/PKB eventually results in pathway switching and, consequently, in an increased dependency on ERK (Birtwistle *et al.* (2007)). By these means, a new steady-state signaling is established with nearly identical phenotypic outcome, probably requiring expression of additional components in the network (Amit *et al.* (2007)).

Furthermore, a direct connection between activated RAS and the PI3K/PKB pathway creates an inter-pathway crosstalk (reviewed in (Castellano and Downward (2011))) that relieves the dependency on ErbB3, since the abundant active ErbB2 homodimers can stimulate PKB pathway via this alternative route. In context of ErbB2 targeting, the failure to achieve ErbB2 dephosphorylation as seen for trastuzumab treatment may thus result in reactivation of PKB despite persisting ErbB3 dephosphorylation. Consequently, this bypass of ErbB3 switches the ErbB network again into the ON state. In fact, the pharmacological interference with RAS function substantially potentiated the anti-tumor activity of trastuzumab and, as expected, the observed gain of cytotoxicity was accompanied both by inhibition of the ERK pathway as well as by prevention of the re-phosphorylation of PKB. In agreement with our findings, this observation again underlines the importance of simultaneous and sustained inhibition of both pathways for induction of apoptosis in the ErbB2-dependent cancer cells.

6.7 Overcoming Clinical Resistance

The persisting problem in therapy of ErbB2-overexpressing tumors is that the majority of patients who achieve an initial response to trastuzumab or TKI treatment usually acquire resistance within several months (Blackwell *et al.* (2010); Esteva *et al.* (2002); Johnston *et al.* (2008); Slamon and Pegram (2001)). The resistance often arises due to the intra-ErbB family signal compensation, e.g. by ligand or receptor upregulation as well as by receptor shedding, or inter-pathway crosstalk with associated receptors such as IGF1R and cMET (Nahta *et al.* (2005); Ritter *et al.* (2007); Shattuck *et al.* (2008)). Hence, an efficient treatment regimen would ideally involve agents that (i) delay onset of resistance by interfering with the compensatory mechanisms and (ii) induce potent and rapid tumor cell death, thereby precluding adaptation of tumor cells to the treatment challenge. Since the ErbB2 trapping by bispecific DARPins is not constrained solely to ErbB2 homodimers, but it also extends to the other EGFR-family members forming the signaling-competent heterodimers with ErbB2, we believe that such a pan-ErbB targeting may be of particular importance to disable the compensatory mechanisms that frequently lead to the acquired resistance.

Apoptosis is deregulated in many cancers, including the ErbB2-overexpressing breast tumors, thus conferring resistance to chemotherapy that primarily works by inducing apoptosis. A plethora of agents are currently being developed for lowering the apoptotic threshold mainly by modulating homeostasis of Bcl-2 proteins or by priming the extrinsic apoptotic pathway through targeting the tumor-necrosis factor (TNF)-related apoptosis-inducing ligand (TRAIL) receptors (reviewed in (Fesik (2005))). However, these substances lack tumor targeting capability, thus making healthy tissues also vulnerable. Therefore, there is a need for targeting agents potentiating the action of chemotherapeutics at the site of tumor, thereby increasing the specific tumor cytotoxicity. Drugs such as bispecific DARPins, designed to restore sensitivity to apoptosis exclusively in the targeted tumor cells, might thus be effective in tumor therapy also as sensitizer for increasing cell susceptibility to other cytotoxic compounds.

7 Conclusions

In conclusion, our study has untangled the mechanism underlying a cancer cell-specific apoptotic response in ErbB2-addicted cells obtained via treatment with engineered receptor-binding molecules, and we could demonstrate that this approach is effective. Nonetheless, it will have to be tested in future preclinical and clinical experiments whether the induction of apoptosis in tumors is rapid and potent enough in order to eliminate cells that otherwise would acquire resistance, bearing e.g. constitutively active PI3K, and to what degree cells with preexisting mutations would have a selective growth advantage. We believe, however, that the structure- and mechanism-based engineering of ErbB2 ligands, which induce cell-specific apoptosis, will be an important component of future therapies. The new insights arising from this study can thus aid in rational design of a novel class of extracellular receptor-targeting therapeutics.

8 Experimental Procedures

8.1 Cell Culture

Breast cancer cell lines BT474, SKBR3, AU565, HCC1419, HCC2218, MDA-MB-361, ZR75-30 were obtained from American Type Culture Collection (ATCC; LGC Promochem). MDA-MB-361 were cultured in DMEM:Hams F12 (Sigma) supplemented with 20% heat-inactivated FCS (Amimed) and 100 U/ml penicillin/streptomycin (Sigma). All other cells were maintained in RPMI 1640 medium (Life Technologies) containing 10% FCS and grown at 37°C in a humidified incubator with 5% CO_2 atmosphere.

8.2 XTT Cell Proliferation Assay

Cells were seeded in 96-well plates at a density of 2,000 - 10,000 cells/cm^2 predetermined for each breast cancer cell line. After 24 h, DARPins or MAbs were added in triplicates, and cells were incubated for another 96 h. XTT assay was developed according to manufacturer's

instructions (Cell proliferation kit II; Roche). Absorbance was measured at 450 nm and expressed as percentage of the untreated control.

8.3 Clonogenic Assay

BT474 cells were treated for 4 days with 100 nM of anti-ErbB2 agents. Cells were then collected by trypsinization, washed three times with complete culture medium, serially diluted and seeded in fresh 6-well plates. Colonies were grown for 5 weeks, and the cell culture medium was refreshed twice per week. Colonies were fixed with glutaraldehyde, stained with crystal violet and the colony number was estimated in triplicate determination for a single dilution.

8.4 Cell Migration Assay

SKBR3 cell motility was assessed using a wound healing assay. The cells were seeded in 35 mm dishes at 2×10^5 cells/cm^2 and allowed to adhere for 8 h. The confluent cell monolayers were wounded using sterile pipette tips to create an open "scratch" of 500 µm. The dislodged cells were removed by three washes with complete culture medium, and cells were incubated for 2 h with 100 nM targeting agents prior to addition of 1 nM HRG or 4 nM EGF. Migration into the open area was documented at 48 h post-scratching. The open scratched area of eight wound fields per treatment was quantified with TScratch software (Gebäck *et al.* (2009)) .

8.5 Three-dimensional Growth Assay

BT474 cells were seeded overnight at 1×10^4 cells/cm^2 on top of commercially available laminin-rich extracellular matrix (Matrigel, BD Biosciences) following the manufacturer's protocol. Cells were treated with 100 nM targeting agents in the absence or presence of 1 nM HRG, and the culture medium was refreshed every 3 days. Growth and morphogenesis of acini were analyzed after twelve days by a modified XTT assay or by counting budding sites for three times 100 acini per treatment, respectively.

8.6 Flow cytometery: Cell Cycle, TUNEL and Annexin V

Cells were seeded at 5,000 to 10,000 cells/cm^2 under standard conditions 24 h prior to treatment with 100 nM of anti-ErbB2 agents. After three days, cells were collected by trypsinization and fixed in 70% EtOH or in 4% paraformaldehyde for propidium iodide (20 µg/ml; 2 Kunitz units/ml of RNAse) or TUNEL labeling (In-situ cell death detection kit, Roche), respectively. The AnnexinV/PI assay was performed with non-fixed cells treated for two days (ApoDETECT Kit; Life Technologies). The cell cycle distribution and apoptosis rate were quantified with FlowJo software.

8.7 Mouse Xenograft Studies

8-week-old female SCID beige mice were obtained from Charles River Laboratories and implanted with 0.025-mg, 90-day release, 17β-estradiol pellets (Innovative Research of America). After two days, 2 × 10^6 BT474 cells were resuspended in 100 µl of PBS and 1:1 mixture with BD Matrigel was inoculated orthotopically into the mammary gland fat pad of mice. Once tumors reached a volume of 200 mm^3, six to eight animals were selected and randomly assigned into four treatment cohorts with equal average tumor volumes. The DARPins were administered by i.v. injection three times per week in a total of nine doses of 20 mg/kg. Tumor diameters were serially measured every 2 days, and tumor volumes were calculated using the following formula: V = (L × W2)/2, where V = volume (cubic millimeters), L = length (millimeters), and W = width (millimeters). For immunohistochemistry analyses, the animals were perfused and tumors were resected on day 14 after initiation of treatment (**Supplemental Experimental Procedures**). Bioimaging studies were performed after single i.p. injection of 1 mg/kg DARPin on IVIS 100 instrument (Caliper Life Sciences), and biodistribution was quantified with Living Image software All mice were maintained and handled under aseptic conditions. The studies were approved by the Cantonal Veterinary Office (Zurich, Switzerland). Housing and experimental procedures were in accordance with the Swiss animal protection law (see **extended Materials and Methods**).

9 Acknowledgements

We thank Dr. Birgit Dreier for support with planning animal experiments and the anti-DARPin serum, Dr. Johannes vom Berg for assistance with IVIS bio imaging and Prof. Uwe Zangenmeister-Wittke for helpful discussions.

This work was supported by consecutive grants to AP from the Swiss Anti-Cancer League (Krebsliga Schweiz; KLS-01686-02-2005, OCS 02128-08-2007, KFS 02448-08-2009, KLS-2841-08-2011), the Swiss National Science Foundation (3100A0B-12867) and the University of Zurich.

10 References

1. Alimandi M*, et al.* (1995) Cooperative signaling of ErbB3 and ErbB2 in neoplastic transformation and human mammary carcinomas. (Translated from eng) *Oncogene* 10:1813-1821 (in eng).
2. Alvarez RH (2010) Present and future evolution of advanced breast cancer therapy. (Translated from eng) *Breast Cancer Res* 12 Suppl 2:S1 (in eng).
3. Amit I, Wides R, & Yarden Y (2007) Evolvable signaling networks of receptor tyrosine kinases: relevance of robustness to malignancy and to cancer therapy. (Translated from eng) *Mol Syst Biol* 3:151 (in eng).
4. Anido J*, et al.* (2006) Biosynthesis of tumorigenic HER2 C-terminal fragments by alternative initiation of translation. (Translated from eng) *Embo J* 25:3234-3244 (in eng).
5. Arkhipov A*, et al.* (2013) Architecture and membrane interactions of the EGF receptor. *Cell* 152:557-569.
6. Baselga J, Albanell J, Molina MA, & Arribas J (2001) Mechanism of action of trastuzumab and scientific update. (Translated from eng) *Semin Oncol* 28:4-11 (in eng).
7. Berger MS*, et al.* (1988) Correlation of c-erbB-2 gene amplification and protein expression in human breast carcinoma with nodal status and nuclear grading. (Translated from eng) *Cancer Res* 48:1238-1243 (in eng).
8. Binz HK*, et al.* (2004) High-affinity binders selected from designed ankyrin repeat protein libraries. *Nat. Biotechnol.* 22:575-582.
9. Birtwistle MR*, et al.* (2007) Ligand-dependent responses of the ErbB signaling network: experimental and modeling analyses. (Translated from eng) *Mol Syst Biol* 3:144 (in eng).
10. Blackwell KL*, et al.* (2010) Randomized study of Lapatinib alone or in combination with trastuzumab in women with ErbB2-positive, trastuzumab-refractory metastatic breast cancer. (Translated from eng) *J Clin Oncol* 28:1124-1130 (in eng).
11. Boersma YL, Chao G, Steiner D, Wittrup KD, & Plückthun A (2011) Bispecific designed ankyrin repeat proteins (DARPins) targeting epidermal growth factor receptor inhibit A431 cell proliferation and receptor recycling. *J. Biol. Chem.* 286:41273-41285.
12. Boersma YL & Plückthun A (2011) DARPins and other repeat protein scaffolds: advances in engineering and applications. *Curr. Opin. Biotechnol.* 22:849-857.
13. Boyer CM*, et al.* (1999) Relative cytotoxic activity of immunotoxins reactive with different epitopes on the extracellular domain of the c-erbB-2 (HER-2/neu) gene product p185. (Translated from eng) *Int J Cancer* 82:525-531 (in eng).
14. Burris HA, 3rd, Tibbitts J, Holden SN, Sliwkowski MX, & Lewis Phillips GD (2011) Trastuzumab emtansine (T-DM1): a novel agent for targeting HER2+ breast cancer. *Clin Breast Cancer* 11:275-282.
15. Cai Z*, et al.* (2008) Differential binding patterns of monoclonal antibody 2C4 to the ErbB3-p185her2/neu and the EGFR-p185her2/neu complexes. (Translated from eng) *Oncogene* 27:3870-3874 (in eng).
16. Cardone MH*, et al.* (1998) Regulation of cell death protease caspase-9 by phosphorylation. (Translated from eng) *Science* 282:1318-1321 (in eng).
17. Castellano E & Downward J (2011) RAS Interaction with PI3K: More Than Just Another Effector Pathway. (Translated from eng) *Genes Cancer* 2:261-274 (in eng).
18. Chandarlapaty S*, et al.* (2011) AKT inhibition relieves feedback suppression of receptor tyrosine kinase expression and activity. (Translated from eng) *Cancer Cell* 19:58-71 (in eng).
19. Cho HS*, et al.* (2003) Structure of the extracellular region of HER2 alone and in complex with the Herceptin Fab. *Nature* 421:756-760.
20. Colomer R, Lupu R, Bacus SS, & Gelmann EP (1994) erbB-2 antisense oligonucleotides inhibit the proliferation of breast carcinoma cells with erbB-2 oncogene amplification. (Translated from eng) *Br J Cancer* 70:819-825 (in eng).

21. Danial NN (2007) BCL-2 family proteins: critical checkpoints of apoptotic cell death. (Translated from eng) *Clin Cancer Res* 13:7254-7263 (in eng).
22. Danial NN & Korsmeyer SJ (2004) Cell death: critical control points. (Translated from eng) *Cell* 116:205-219 (in eng).
23. Dawson JP, Bu Z, & Lemmon MA (2007) Ligand-induced structural transitions in ErbB receptor extracellular domains. *Structure* 15:942-954.
24. Endres NF*, et al.* (2013) Conformational coupling across the plasma membrane in activation of the EGF receptor. *Cell* 152:543-556.
25. Esteva FJ*, et al.* (2002) Phase II study of weekly docetaxel and trastuzumab for patients with HER-2-overexpressing metastatic breast cancer. (Translated from eng) *J Clin Oncol* 20:1800-1808 (in eng).
26. Ewings KE*, et al.* (2007) ERK1/2-dependent phosphorylation of BimEL promotes its rapid dissociation from Mcl-1 and Bcl-xL. (Translated from eng) *Embo J* 26:2856-2867 (in eng).
27. Faber AC*, et al.* (2011) BIM expression in treatment-naive cancers predicts responsiveness to kinase inhibitors. (Translated from eng) *Cancer Discov* 1:352-365 (in eng).
28. Fesik SW (2005) Promoting apoptosis as a strategy for cancer drug discovery. (Translated from eng) *Nat Rev Cancer* 5:876-885 (in eng).
29. Forrer P, Stumpp MT, Binz HK, & Pluckthun A (2003) A novel strategy to design binding molecules harnessing the modular nature of repeat proteins. (Translated from eng) *FEBS Lett* 539:2-6 (in eng).
30. Franco-Gonzalez JF, Ramos J, Cruz VL, & Martinez-Salazar J (2013) Simulation of homology models for the extracellular domains (ECD) of ErbB3, ErbB4 and the ErbB2-ErbB3 complex in their active conformations. (Translated from eng) *J Mol Model* 19:931-941 (in eng).
31. Franklin MC*, et al.* (2004) Insights into ErbB signaling from the structure of the ErbB2-pertuzumab complex. *Cancer Cell* 5:317-328.
32. Garrett JT & Arteaga CL (2011) Resistance to HER2-directed antibodies and tyrosine kinase inhibitors: mechanisms and clinical implications. (Translated from eng) *Cancer Biol Ther* 11:793-800 (in eng).
33. Garrett JT*, et al.* (2011) Transcriptional and posttranslational up-regulation of HER3 (ErbB3) compensates for inhibition of the HER2 tyrosine kinase. (Translated from eng) *Proc Natl Acad Sci U S A* 108:5021-5026 (in eng).
34. Garrett TP*, et al.* (2003) The crystal structure of a truncated ErbB2 ectodomain reveals an active conformation, poised to interact with other ErbB receptors. *Mol. Cell* 11:495-505.
35. Gebäck T, Schulz MM, Koumoutsakos P, & Detmar M (2009) TScratch: a novel and simple software tool for automated analysis of monolayer wound healing assays. (Translated from eng) *Biotechniques* 46:265-274 (in eng).
36. Geyer CE*, et al.* (2006) Lapatinib plus capecitabine for HER2-positive advanced breast cancer. (Translated from eng) *N Engl J Med* 355:2733-2743 (in eng).
37. Ghosh R*, et al.* (2011) Trastuzumab has preferential activity against breast cancers driven by HER2 homodimers. *Cancer Res.* 71:1871-1882.
38. Gijsen M*, et al.* (2010) HER2 phosphorylation is maintained by a PKB negative feedback loop in response to anti-HER2 herceptin in breast cancer. (Translated from eng) *PLoS Biol* 8:e1000563 (in eng).
39. Gomez HL*, et al.* (2008) Efficacy and safety of lapatinib as first-line therapy for ErbB2-amplified locally advanced or metastatic breast cancer. (Translated from eng) *J Clin Oncol* 26:2999-3005 (in eng).
40. Graus-Porta D, Beerli RR, Daly JM, & Hynes NE (1997) ErbB-2, the preferred heterodimerization partner of all ErbB receptors, is a mediator of lateral signaling. *EMBO J.* 16:1647-1655.
41. Hackel BJ, Neil JR, White FM, & Wittrup KD (2012) Epidermal growth factor receptor downregulation by small heterodimeric binding proteins. *Protein Eng. Des. Sel.* 25:47-57.

42. Harari D & Yarden Y (2000) Molecular mechanisms underlying ErbB2/HER2 action in breast cancer. (Translated from eng) *Oncogene* 19:6102-6114 (in eng).
43. Hause RJ, Jr.*, et al.* (2012) Comprehensive binary interaction mapping of SH2 domains via fluorescence polarization reveals novel functional diversification of ErbB receptors. (Translated from eng) *PLoS One* 7:e44471 (in eng).
44. Hendriks BS, Wiley HS, & Lauffenburger D (2003) HER2-mediated effects on EGFR endosomal sorting: analysis of biophysical mechanisms. (Translated from eng) *Biophys J* 85:2732-2745 (in eng).
45. Holbro T*, et al.* (2003) The ErbB2/ErbB3 heterodimer functions as an oncogenic unit: ErbB2 requires ErbB3 to drive breast tumor cell proliferation. (Translated from eng) *Proc Natl Acad Sci U S A* 100:8933-8938 (in eng).
46. Hommelgaard AM, Lerdrup M, & van Deurs B (2004) Association with membrane protrusions makes ErbB2 an internalization-resistant receptor. *Mol. Biol. Cell* 15:1557-1567.
47. Hynes NE & Lane HA (2005) ERBB receptors and cancer: the complexity of targeted inhibitors. *Nat. Rev. Cancer* 5:341-354.
48. Hynes NE & MacDonald G (2009) ErbB receptors and signaling pathways in cancer. (Translated from eng) *Curr Opin Cell Biol* 21:177-184 (in eng).
49. Johnston S*, et al.* (2008) Phase II study of predictive biomarker profiles for response targeting human epidermal growth factor receptor 2 (HER-2) in advanced inflammatory breast cancer with lapatinib monotherapy. (Translated from eng) *J Clin Oncol* 26:1066-1072 (in eng).
50. Jones RB, Gordus A, Krall JA, & MacBeath G (2006) A quantitative protein interaction network for the ErbB receptors using protein microarrays. (Translated from eng) *Nature* 439:168-174 (in eng).
51. Junttila TT*, et al.* (2009) Ligand-independent HER2/HER3/PI3K complex is disrupted by trastuzumab and is effectively inhibited by the PI3K inhibitor GDC-0941. *Cancer Cell* 15:429-440.
52. Kao J*, et al.* (2009) Molecular profiling of breast cancer cell lines defines relevant tumor models and provides a resource for cancer gene discovery. (Translated from eng) *PLoS One* 4:e6146 (in eng).
53. Kawano S, Ikeda W, Kishimoto M, Ogita H, & Takai Y (2009) Silencing of ErbB3/ErbB2 signaling by immunoglobulin-like Necl-2. *J. Biol. Chem.* 284:23793-23805.
54. Kenny PA*, et al.* (2007) The morphologies of breast cancer cell lines in three-dimensional assays correlate with their profiles of gene expression. (Translated from eng) *Mol Oncol* 1:84-96 (in eng).
55. Kholodenko BN, Hancock JF, & Kolch W (2010) Signalling ballet in space and time. (Translated from eng) *Nat Rev Mol Cell Biol* 11:414-426 (in eng).
56. Kitano H (2003) Cancer robustness: tumour tactics. (Translated from eng) *Nature* 426:125 (in eng).
57. Krop IE*, et al.* (2010) Phase I study of trastuzumab-DM1, an HER2 antibody-drug conjugate, given every 3 weeks to patients with HER2-positive metastatic breast cancer. *J. Clin. Oncol.* 28:2698-2704.
58. Lane HA*, et al.* (2000) ErbB2 potentiates breast tumor proliferation through modulation of p27(Kip1)-Cdk2 complex formation: receptor overexpression does not determine growth dependency. (Translated from eng) *Mol Cell Biol* 20:3210-3223 (in eng).
59. Le XF*, et al.* (2012) Modulation of MicroRNA-194 and cell migration by HER2-targeting trastuzumab in breast cancer. (Translated from eng) *PLoS One* 7:e41170 (in eng).
60. Le XF*, et al.* (2003) The role of cyclin-dependent kinase inhibitor p27Kip1 in anti-HER2 antibody-induced G1 cell cycle arrest and tumor growth inhibition. (Translated from eng) *J Biol Chem* 278:23441-23450 (in eng).
61. Lee-Hoeflich ST*, et al.* (2008) A central role for HER3 in HER2-amplified breast cancer: implications for targeted therapy. *Cancer Res.* 68:5878-5887.

62. Macdonald-Obermann JL, Piwnica-Worms D, & Pike LJ (2012) Mechanics of EGF receptor/ErbB2 kinase activation revealed by luciferase fragment complementation imaging. (Translated from eng) *Proc Natl Acad Sci U S A* 109:137-142 (in eng).
63. Marani M*, et al.* (2004) Role of Bim in the survival pathway induced by Raf in epithelial cells. (Translated from eng) *Oncogene* 23:2431-2441 (in eng).
64. Marone R*, et al.* (2004) Memo mediates ErbB2-driven cell motility. *Nat Cell Biol* 6:515-522.
65. Nahta R & Esteva FJ (2004) In vitro effects of trastuzumab and vinorelbine in trastuzumab-resistant breast cancer cells. (Translated from eng) *Cancer Chemother Pharmacol* 53:186-190 (in eng).
66. Nahta R & Esteva FJ (2006) Herceptin: mechanisms of action and resistance. (Translated from eng) *Cancer Lett* 232:123-138 (in eng).
67. Nahta R, Hung MC, & Esteva FJ (2004) The HER-2-targeting antibodies trastuzumab and pertuzumab synergistically inhibit the survival of breast cancer cells. (Translated from eng) *Cancer Res* 64:2343-2346 (in eng).
68. Nahta R, Takahashi T, Ueno NT, Hung MC, & Esteva FJ (2004) P27(kip1) down-regulation is associated with trastuzumab resistance in breast cancer cells. (Translated from eng) *Cancer Res* 64:3981-3986 (in eng).
69. Nahta R, Yuan LX, Zhang B, Kobayashi R, & Esteva FJ (2005) Insulin-like growth factor-I receptor/human epidermal growth factor receptor 2 heterodimerization contributes to trastuzumab resistance of breast cancer cells. (Translated from eng) *Cancer Res* 65:11118-11128 (in eng).
70. Neve RM*, et al.* (2000) Effects of oncogenic ErbB2 on G1 cell cycle regulators in breast tumour cells. (Translated from eng) *Oncogene* 19:1647-1656 (in eng).
71. Pantel K*, et al.* (1993) Differential expression of proliferation-associated molecules in individual micrometastatic carcinoma cells. (Translated from eng) *J Natl Cancer Inst* 85:1419-1424 (in eng).
72. Pietras RJ*, et al.* (1999) Monoclonal antibody to HER-2/neureceptor modulates repair of radiation-induced DNA damage and enhances radiosensitivity of human breast cancer cells overexpressing this oncogene. (Translated from eng) *Cancer Res* 59:1347-1355 (in eng).
73. Reynolds AR, Tischer C, Verveer PJ, Rocks O, & Bastiaens PIH (2003) EGFR activation coupled to inhibition of tyrosine phosphatases causes lateral signal propagation. (Translated from English) *Nat Cell Biol* 5:447-453 (in English).
74. Ritter CA*, et al.* (2007) Human breast cancer cells selected for resistance to trastuzumab in vivo overexpress epidermal growth factor receptor and ErbB ligands and remain dependent on the ErbB receptor network. (Translated from eng) *Clin Cancer Res* 13:4909-4919 (in eng).
75. Roh H, Pippin J, & Drebin JA (2000) Down-regulation of HER2/neu expression induces apoptosis in human cancer cells that overexpress HER2/neu. (Translated from eng) *Cancer Res* 60:560-565 (in eng).
76. Sakai K*, et al.* (2007) Pertuzumab, a novel HER dimerization inhibitor, inhibits the growth of human lung cancer cells mediated by the HER3 signaling pathway. (Translated from eng) *Cancer Sci* 98:1498-1503 (in eng).
77. Scaltriti M*, et al.* (2007) Expression of p95HER2, a truncated form of the HER2 receptor, and response to anti-HER2 therapies in breast cancer. (Translated from eng) *J Natl Cancer Inst* 99:628-638 (in eng).
78. Schmid AC, Byrne RD, Vilar R, & Woscholski R (2004) Bisperoxovanadium compounds are potent PTEN inhibitors. (Translated from eng) *FEBS Lett* 566:35-38 (in eng).
79. Schulze WX, Deng L, & Mann M (2005) Phosphotyrosine interactome of the ErbB-receptor kinase family. (Translated from eng) *Mol Syst Biol* 1:2005 0008 (in eng).
80. Sergina NV*, et al.* (2007) Escape from HER-family tyrosine kinase inhibitor therapy by the kinase-inactive HER3. *Nature* 445:437-441.

81. Shattuck DL, Miller JK, Carraway KL, 3rd, & Sweeney C (2008) Met receptor contributes to trastuzumab resistance of Her2-overexpressing breast cancer cells. (Translated from eng) *Cancer Res* 68:1471-1477 (in eng).
82. Slamon D & Pegram M (2001) Rationale for trastuzumab (Herceptin) in adjuvant breast cancer trials. (Translated from eng) *Semin Oncol* 28:13-19 (in eng).
83. Slamon DJ*, et al.* (1987) Human breast cancer: correlation of relapse and survival with amplification of the HER-2/neu oncogene. (Translated from eng) *Science* 235:177-182 (in eng).
84. Slamon DJ*, et al.* (1989) Studies of the HER-2/neu proto-oncogene in human breast and ovarian cancer. (Translated from eng) *Science* 244:707-712 (in eng).
85. Sliwkowski MX*, et al.* (1999) Nonclinical studies addressing the mechanism of action of trastuzumab (Herceptin). *Semin. Oncol.* 26:60-70.
86. Spencer KS, Graus-Porta D, Leng J, Hynes NE, & Klemke RL (2000) ErbB2 is necessary for induction of carcinoma cell invasion by ErbB family receptor tyrosine kinases. (Translated from eng) *J Cell Biol* 148:385-397 (in eng).
87. Steiner D, Forrer P, & Plückthun A (2008) Efficient selection of DARPins with sub-nanomolar affinities using SRP phage display. *J. Mol. Biol.* 382:1211-1227.
88. Stern DF (2008) ERBB3/HER3 and ERBB2/HER2 duet in mammary development and breast cancer. (Translated from eng) *J Mammary Gland Biol Neoplasia* 13:215-223 (in eng).
89. Tamaskovic R, Simon M, Stefan N, Schwill M, & Plückthun A (2012) Designed ankyrin repeat proteins (DARPins) from research to therapy. *Methods Enzymol.* 503:101-134.
90. Tanizaki J*, et al.* (2011) Roles of BIM induction and survivin downregulation in lapatinib-induced apoptosis in breast cancer cells with HER2 amplification. *Oncogene* 30:4097-4106.
91. Tanner M*, et al.* (2004) Characterization of a novel cell line established from a patient with Herceptin-resistant breast cancer. (Translated from eng) *Mol Cancer Ther* 3:1585-1592 (in eng).
92. van de Vijver MJ, Mooi WJ, Peterse JL, & Nusse R (1988) Amplification and over-expression of the neu oncogene in human breast carcinomas. (Translated from eng) *Eur J Surg Oncol* 14:111-114 (in eng).
93. Verma S*, et al.* (2012) Trastuzumab emtansine for HER2-positive advanced breast cancer. *N. Engl. J. Med.* 367:1783-1791.
94. Wallasch C*, et al.* (1995) Heregulin-dependent regulation of HER2/neu oncogenic signaling by heterodimerization with HER3. (Translated from eng) *Embo J* 14:4267-4275 (in eng).
95. Weinstein IB (2002) Cancer. Addiction to oncogenes--the Achilles heal of cancer. (Translated from eng) *Science* 297:63-64 (in eng).
96. Weinstein IB & Joe A (2008) Oncogene addiction. (Translated from eng) *Cancer Res* 68:3077-3080; discussion 3080 (in eng).
97. Xiao Y*, et al.* (2007) PTEN catalysis of phospholipid dephosphorylation reaction follows a two-step mechanism in which the conserved aspartate-92 does not function as the general acid--mechanistic analysis of a familial Cowden disease-associated PTEN mutation. (Translated from eng) *Cell Signal* 19:1434-1445 (in eng).
98. Xu F*, et al.* (1993) Antibody-induced growth inhibition is mediated through immunochemically and functionally distinct epitopes on the extracellular domain of the c-erbB-2 (HER-2/neu) gene product p185. (Translated from eng) *Int J Cancer* 53:401-408 (in eng).
99. Yakes FM*, et al.* (2002) Herceptin-induced inhibition of phosphatidylinositol-3 kinase and Akt Is required for antibody-mediated effects on p27, cyclin D1, and antitumor action. (Translated from eng) *Cancer Res* 62:4132-4141 (in eng).
100. Yarden Y & Pines G (2012) The ERBB network: at last, cancer therapy meets systems biology. (Translated from eng) *Nat Rev Cancer* 12:553-563 (in eng).
101. Yarden Y & Sliwkowski MX (2001) Untangling the ErbB signalling network. *Nat. Rev. Mol. Cell Biol.* 2:127-137.

102. Yip YL & Ward RL (2002) Anti-ErbB-2 monoclonal antibodies and ErbB-2-directed vaccines. (Translated from eng) *Cancer Immunol Immunother* 50:569-587 (in eng).
103. Zahnd C*, et al.* (2010) Efficient tumor targeting with high-affinity designed ankyrin repeat proteins: effects of affinity and molecular size. *Cancer Res.* 70:1595-1605.
104. Zahnd C, Pecorari F, Straumann N, Wyler E, & Plückthun A (2006) Selection and characterization of Her2 binding-designed ankyrin repeat proteins. *J. Biol. Chem.* 281:35167-35175.
105. Zahnd C*, et al.* (2007) A designed ankyrin repeat protein evolved to picomolar affinity to HER2. *J. Mol. Biol.* 369:1015-1028.
106. Zhang Q, Park E, Kani K, & Landgraf R (2012) Functional isolation of activated and unilaterally phosphorylated heterodimers of ERBB2 and ERBB3 as scaffolds in ligand-dependent signaling. *Proc. Natl. Acad. Sci. U. S. A.* 109:13237-13242.

(subsequent page) Figure 1. Mechanism of Action of Bispecific DARPins: **(A)** Model of bispecific DARPin 926-(GGGGS)-G3 (abbreviated 6-L1-G) with strong anti-tumor activity.
(B) Model of the ErbB2 back-to-back homodimer (blue, shaded by domain) in complex with the monovalent DARPins 929 (red) and G3 (yellow), based on structures and models described in detail in Jost *et al.* (2013), cf. **Chapter 3**. The structures show that the individual DARPin epitopes do not directly overlap with canonical ErbB2 dimerization interfaces for homo- or heterodimerization (left) and indeed both monovalent DARPins as well as their mixtures lack anti-tumor activity. The short 17-Å GGGGS peptide linker is too short to even span the minimal distance (50 Å) between the C-terminus of DARPin 929 bound to one HER2 monomer and N-terminus of G3 bound to a second monomer. Therefore the ErbB2 monomers have to bend over (right) from the upright position (ECD in white, hazy) to allow binding of both DARPins (ECD in shades of blue). The steric constraints imposed by the membrane force the transmembrane helices apart, as well as the attached kinases, and obstruct the dimerization interface of ErbB2.
(C) Western blot of ErbB2 receptors crosslinked on the surface of BT474 cells in the absence and presence of monovalent, bivalent and bispecific DARPins (symbols at the bottom), with bis[sulfosuccinimidyl] suberate (BS3). The panel shows the anti-ErbB2 blot (top) with the corresponding anti-DARPin blot (middle) and the loading control anti-GAPDH (bottom). ErbB2–bisp. DARPin–ErbB2, two ErbB2 molecules bridged by a bispecific DARPin.

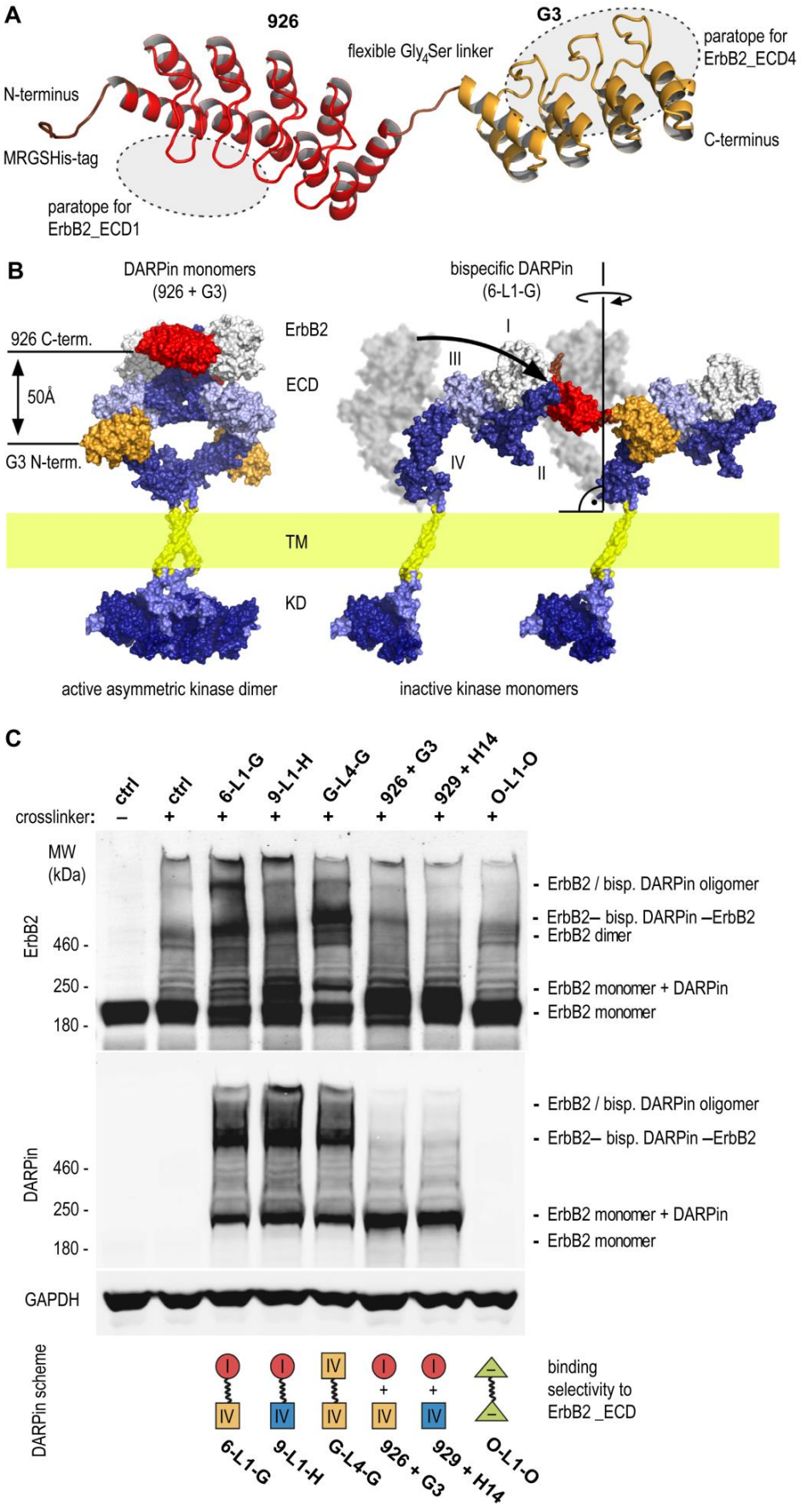
A
926
G3
flexible Gly4Ser linker
paratope for ErbB2_ECD4
N-terminus
C-terminus
MRGSHis-tag
paratope for ErbB2_ECD1
B
DARPin monomers (926 + G3)
bispecific DARPin (6-L1-G)
926 C-term.
50Å
G3 N-term.
ErbB2
ECD
TM
KD
I
II
III
IV
active asymmetric kinase dimer
inactive kinase monomers
C
crosslinker:
ctrl
ctrl
6-L1-G
9-L1-H
G-L4-G
926 + G3
929 + H14
O-L1-O
MW (kDa)
ErbB2
460 -
250 -
180 -
ErbB2 / bisp. DARPin oligomer
ErbB2– bisp. DARPin –ErbB2
ErbB2 dimer
ErbB2 monomer + DARPin
ErbB2 monomer
DARPin
GAPDH
DARPin scheme
binding selectivity to ErbB2 _ECD

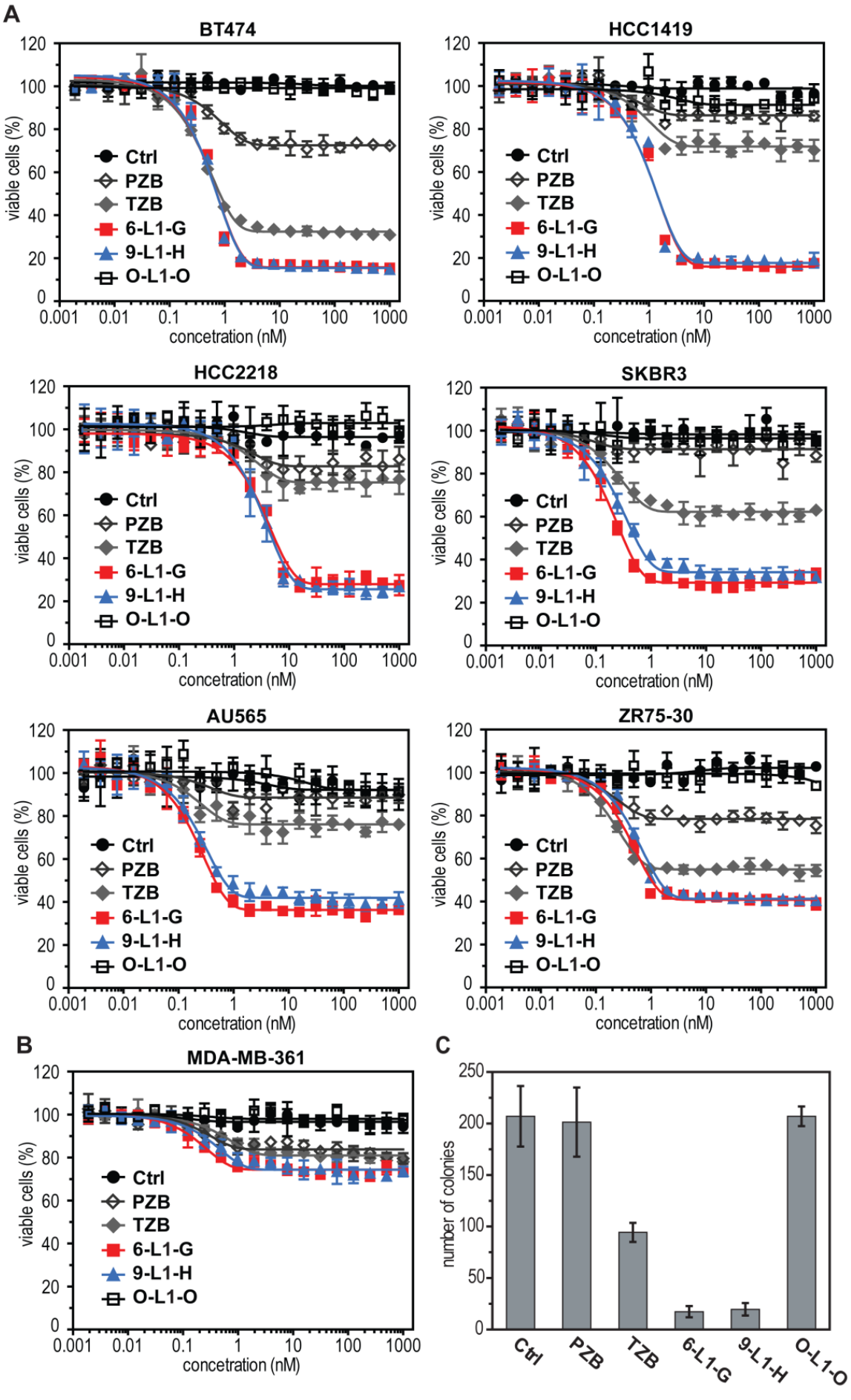
A
BT474
HCC1419
HCC2218
SKBR3
AU565
ZR75-30
B
MDA-MB-361
C
viable cells (%)
concetration (nM)
Ctrl
PZB
TZB
6-L1-G
9-L1-H
O-L1-O
number of colonies

(preceding page) Figure 2. Anti-Proliferative Activity Bispecific DARPins: **(A-B)** Inhibition of cell proliferation in 2D cultured ErbB2-overexpressing breast cancer cell lines derived from mammary gland adenocarcinomas, comprising BT474, HCC1419, HCC2218, SKBR3, AU565, ZR75-30 with intact PI3K pathway signaling pathway in **(A)**, and MDA-MB-361 with PI3K activating mutations in **(B)**. Cells were treated for four days with increasing concentrations of bispecific DARPins 6-L1-G and 9-L1-H, non-binding DARPin control O-L1-O (Off7-Gly4Ser-Off7), both monoclonal antibodies (trastuzumab; TZB or pertuzumab; PZB), or PBS alone (Ctrl).
(C) Clonogenic assays of BT474 cells, treated for 4 days with 100 nM of indicated agent, and afterwards equal number of treated cancer cells were re-seeded, grown in absence of agents, while capacity of single cells to initiate colony outgrowth was measured after 5 weeks culturing.

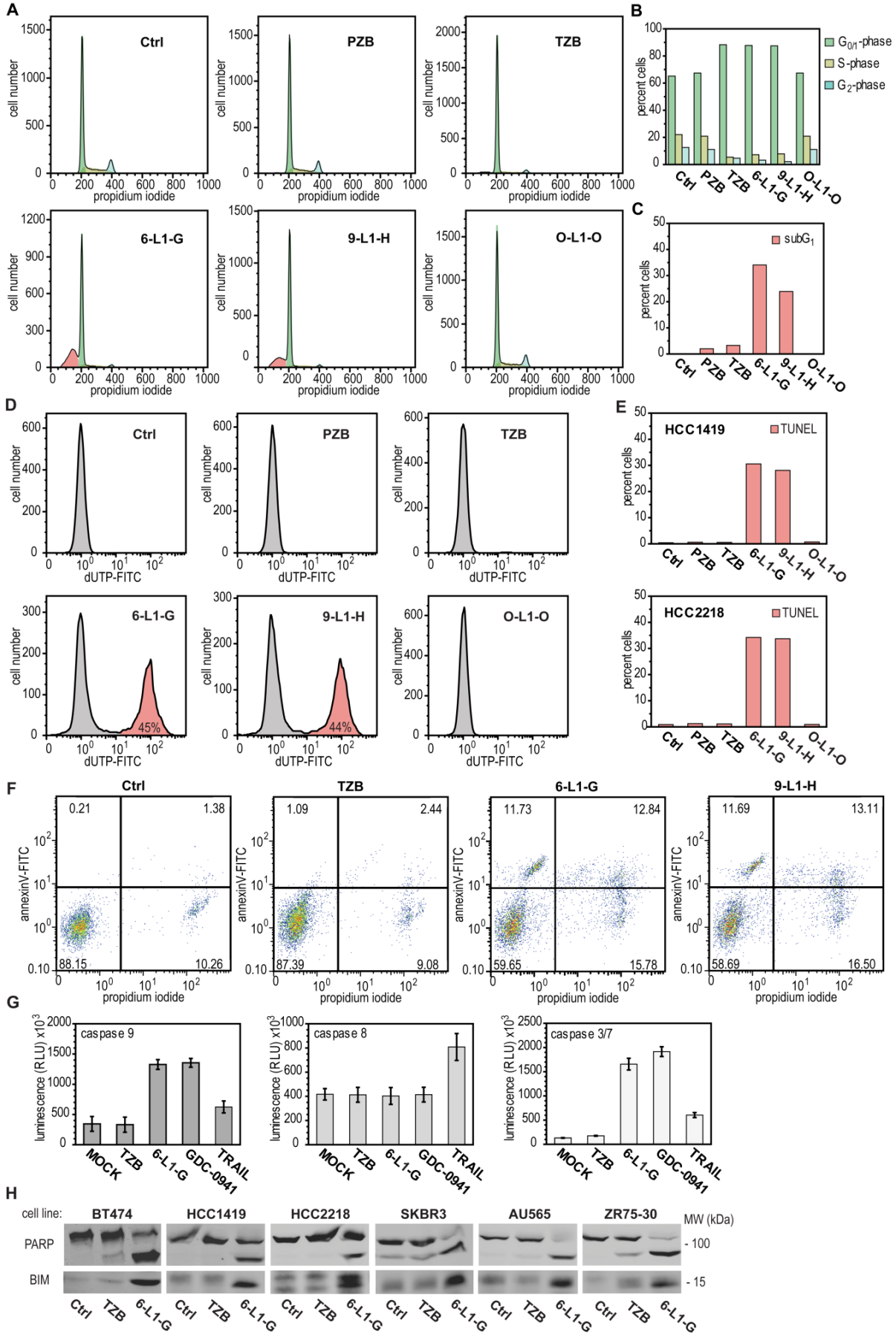
A
Ctrl
PZB
TZB
6-L1-G
9-L1-H
O-L1-O
cell number
propidium iodide
B
percent cells
G0/1-phase
S-phase
G2-phase
C
subG1
D
dUTP-FITC
45%
44%
E
HCC1419
HCC2218
TUNEL
F
annexinV-FITC
propidium iodide
0.21
1.38
88.15
10.26
1.09
2.44
87.39
9.08
11.73
12.84
59.65
15.78
11.69
13.11
58.69
16.50
G
caspase 9
caspase 8
caspase 3/7
luminescence (RLU) x10^3
MOCK
TZB
6-L1-G
GDC-0941
TRAIL
H
cell line:
BT474
HCC1419
HCC2218
SKBR3
AU565
ZR75-30
MW (kDa)
PARP
BIM
- 100
- 15

(preceding page) Figure 3. Induction of Apoptosis by Bispecific DARPins:
(A-C) Cell cycle distribution analysis of BT474 cells after 3 d treatment with indicated agents each at 100 nM concentration. Ethanol-fixed cells were stained with propidium iodide (PI, 20 μg/ml) and analyzed by FACS. Depicted PI-staining histograms show cell cycle profiles of gated single cells and quantification with Dean-Jett-Fox algorithm **(B)**. Cells with subG1 DNA content (red) represent post apoptotic cell population with marked degradation of genomic DNA that have been quantified separately **(C)**.
(D-E) TUNEL assays of treated BT474 cells in histograms **(D)** or quantification of HCC1419 and HCC2218 cells **(E)** showing apoptotic cell populations. Cells were treated with 100 nM of indicated agents for 3 d, PFA-fixed and triton-permeabilized, stained with terminal deoxynucleotidyl transferase (TdT) using dUTP-fluoresceine substrate and subsequently analyzed by FACS. Presented histograms depict the recorded TUNEL profiles of non-apoptotic (left peak, centered around 100) and apoptotic cells (right peak, centered around 102).
(F) Annexin-V and propidium iodide (PI) assay of BT474 cells after 2 days treatment with 100 nM of indicated agents. Population of early apoptotic cells was monitored by Annexin-V_FITC detection (upper left and right quadrants) and staining for membrane permeability (PI at 1 μg/ml) indicates late stages of cell death (upper and lower right quadrants).
(G) Caspase activity assay for initiator caspases-8 and -9 as well as effector caspases-3/7 by specific chemiluminiscent substrates in cell extracts of treated BT474 cells. Cells were treated with bispecific DARPin and trastuzumab for 3 days or GDC-0941 and TRAIL for 12h.
(H) Expression analysis of the apoptotic markers cleaved PARP (p89) and BIM by western blot in panel of ErbB2-dependent breast cancer cell lines after treatment with 6-L1-G, TZB or PBS control for 3 days.

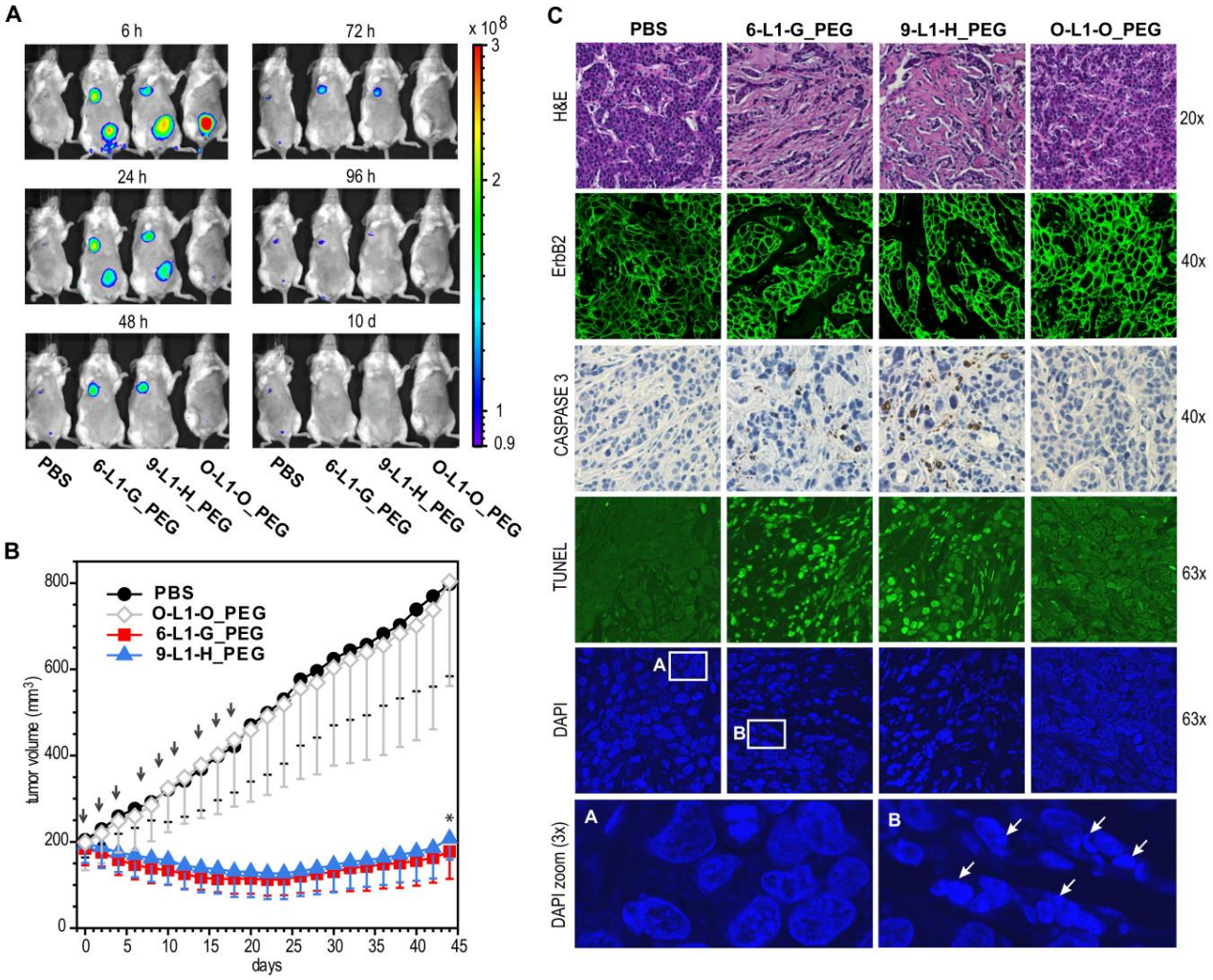

Figure 4. Bispecific DARPins accumulate at the site of tumor and induce tumor regression in vivo: **(A)** Biodistribution analysis in BT474 xenografted mice, injected once (intravenously; 1 mg/kg) with the Alexa680-conjugated and PEGylated DARPins or PBS. Mouse were imaged on an IVIS device for a period of ten days, while accumulation of 6-L1-G_PEG and 9-L1-H_PEG, but not the negative control DARPin (O-L1-O_PEG) can be observed at the site of implant in the right mammary fat pad. The urinal excretion of the injected agents is visualized as bladder staining.
(B) Tumor growth inhibition by PEGylated bispecific DARPins in SCID beige mice with pre-established BT474 xenografts. Treatment schedule was started as soon as tumors size reached 200 mm3 Agents were injected three times per week intravenously (20 mg/kg) as indicated by the arrows. The statistical significance between the treated (6-L1-G_PEG and 9-L1-H_PEG) and control (PBS, O-L1-O_PEG) cohorts was determined by student's t-test (* $p<0.001$).
(C) In situ immunohistochemical staining of apoptotic markers in treated BT474 xenografts. Representative tumor sections from PFA-fixed, paraffin-embedded tumors were analyzed by H&E, anti-ErbB2 antibody fluorescence, anti-cleaved caspase-3 peroxide, TUNEL fluorescence, and DAPI fluorescence staining. Enlargement of DAPI stained picture (bottom), shows apoptotic bodies after bispecific DARPin treatment.

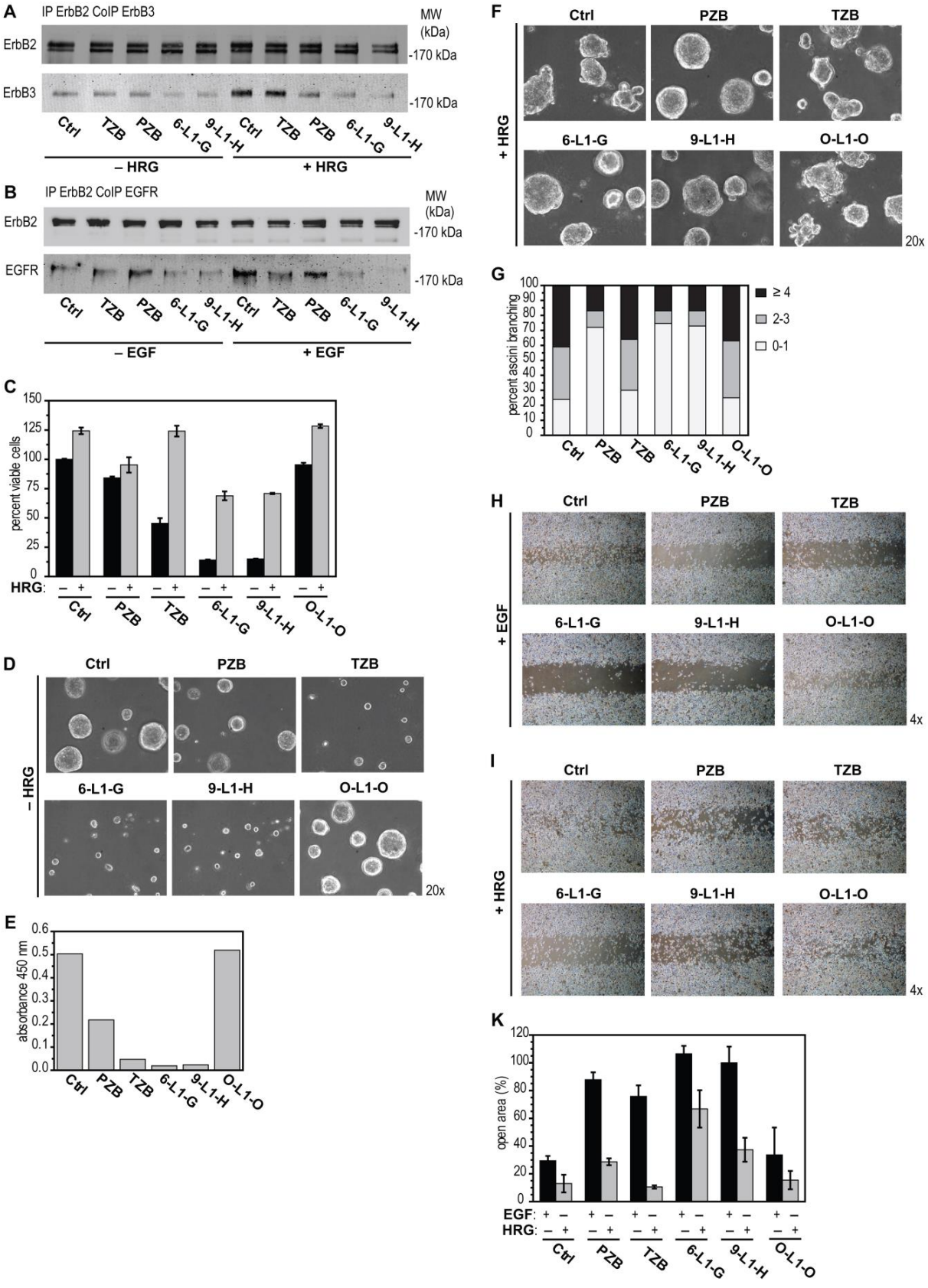
A
IP ErbB2 CoIP ErbB3
MW (kDa)
ErbB2
-170 kDa
ErbB3
-170 kDa
Ctrl TZB PZB 6-L1-G 9-L1-H Ctrl TZB PZB 6-L1-G 9-L1-H
– HRG
+ HRG
B
IP ErbB2 CoIP EGFR
MW (kDa)
ErbB2
-170 kDa
EGFR
-170 kDa
Ctrl TZB PZB 6-L1-G 9-L1-H Ctrl TZB PZB 6-L1-G 9-L1-H
– EGF
+ EGF
C
percent viable cells
150
125
100
75
50
25
0
HRG: – + – + – + – + – + – +
Ctrl PZB TZB 6-L1-G 9-L1-H O-L1-O
D
Ctrl PZB TZB
– HRG
6-L1-G 9-L1-H O-L1-O
20x
E
absorbance 450 nm
0.6
0.5
0.4
0.3
0.2
0.1
0.0
Ctrl PZB TZB 6-L1-G 9-L1-H O-L1-O
F
Ctrl PZB TZB
+ HRG
6-L1-G 9-L1-H O-L1-O
20x
G
percent ascini branching
100
90
80
70
60
50
40
30
20
10
0
≥ 4
2-3
0-1
Ctrl PZB TZB 6-L1-G 9-L1-H O-L1-O
H
Ctrl PZB TZB
+ EGF
6-L1-G 9-L1-H O-L1-O
4x
I
Ctrl PZB TZB
+ HRG
6-L1-G 9-L1-H O-L1-O
4x
K
open area (%)
120
100
80
60
40
20
0
EGF: + – + – + – + – + – + –
HRG: – + – + – + – + – + – +
Ctrl PZB TZB 6-L1-G 9-L1-H O-L1-O

(preceding page) Figure 5. Inhibition of ErbB2 Heterodimerization by Bispecific DARPins:
(A-B) Formation of ErbB2 scaffolding heterodimers with and without ligand stimulation. ErbB2–ErbB3 dimerization was triggered by addition of 1 nM heregulin-β1 (HRG) in BT474 cells **(A)** and ErbB2–EGFR dimerization was triggered by 1 nM epidermal growth factor (EGF) in SKBR3 cells **(B)** after preincubation with 100 nM of indicated agents, respectively. Afterwards, surface receptors were crosslinked with the reducible crosslinker DTSSP, ErbB2 was immunoprecipitated by an anti-ErbB2-C-terminal antibody, samples were reduced and amount of co-immunoprecipitated receptor was analyzed by western blot.
(C) XTT of cell proliferation assay of 2D cultured BT474 cells in presence of 1 nM ErbB3 ligand heregulin-β1 (HRG) and 100 nM of indicated treatment agents after 4 d of coincubation.
(D-E) Three-dimensional cultures of mammary carcinoma BT474 cells were established using reconstituted basement membrane (Matrigel BD). Micrographs shown of BT474 spheroids after 12 d treatment with indicated agents **(D)**. The proliferation of treated spheroids was analyzed by XTT assay **(E)**.
(F-G) Induction of morphogenesis in 3D cultured BT474 cells. Acini branching was induced by addition of 1 nM heregulin-β1 (HRG) shortly after preincubation with 100 nM of indicated agents. The effect of the bispecific DARPins or MAbs was monitored after 12 d incubation **(F)**. The extent of spheroid branching was quantified by scoring three times 100 acini that were classified into three populations, depending on the number of buds per acinus **(G)**.
(H-K) Effect of the ErbB2-targeting agents on cell migration in a wound-healing assay. SKBR3 cells were seeded to confluence, and scratch a wound of 500 μm was made in the monolayer. Cells were treated with the indicated agents at 100 nM concentrations and co-stimulated with 4 nM epidermal growth factor (EGF) **(H)** or with 1 nM heregulin-β1 (HRG) **(I)**. Representative micrographs of four parallel scratches were taken after two days at 4x magnification. The cell motility was assessed after two days. Quantification of wound-healing assays. The open area (scratch) was analyzed with the TScratch software, and the migration was expressed as the percentage of open area and compared to mock-treated SKBR3 cells **(K)**.

(subsequent page) Figure 6. Inhibition of ErbB2 and ErbB3 Phosphorylation by Bispecific DARPins: **(A-F)** Quantitative infra red fluorescence western blot; integrated intensity signals are plotted as percent signals of internal control phosphorylation of untreated cells 24 h post seeding (0 min). Note that detached late apoptotic cells are excluded from analysis. Cells were treated in excess of medium with a single dose of 100 nM of either bispecific DARPin (6-L1-G) or trastuzumab (TZB) for the indicated times, and cell extracts were normalized for protein concentration by BCA assays. A collection of individual ErbB2 tyrosine phosphorylation sites of p185 in BT474 cells after treatment with DARPin **(A)** or trastuzumab **(B)** are shown.
(C) Immunoprecipitation of ErbB2 and non specific anti-phospho Tyr blot quantification of p185 from BT474 cells after treatment with both agents. **(D)** ErbB2 expression of p185 and phosphorylation of Y1248 in SKBR3 cells after treatment with both agents.
(E-F) ErbB3 expression and phospho-status of Y1289 of p180 in BT474 (E) or SKBR3 (F) cells after treatment with both agents. **(G)** Expression and phosphorylation of p185 ErbB2 and Y1248 or p180 ErbB3 and Y1289 in ErbB2 depended cell lines after 72h of treatment with single dose of 100 nM of both agents. **(H)** Heregulin-stimulated transphosphorylation in SKBR3 cells. Preincubated cells with indicated agents were stimulated with 1 nM HRG. The phosphorylation of ErbB2 Y1248 and ErbB3 Y1289 was determined by western blot.

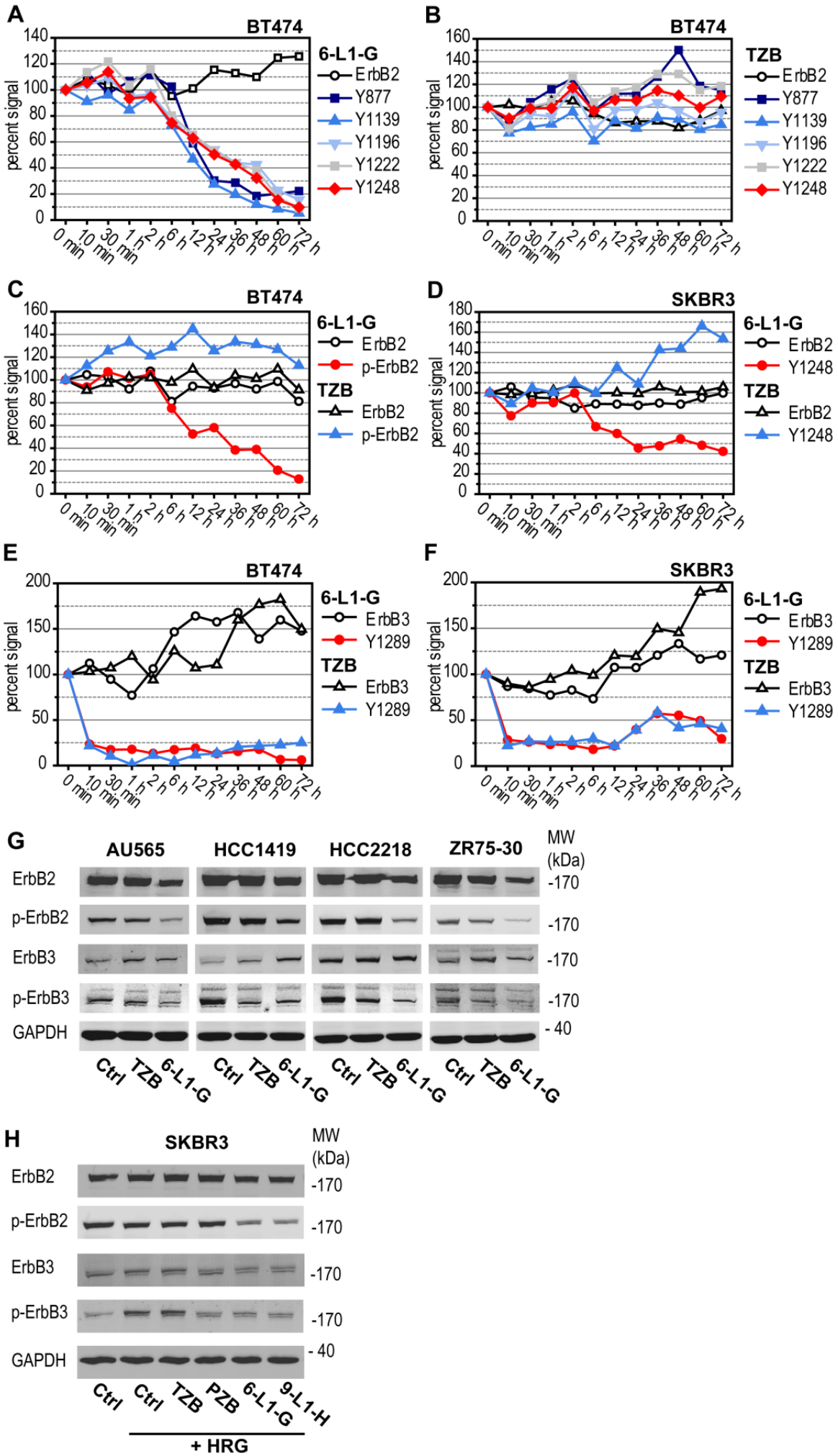
A
BT474
6-L1-G
ErbB2
Y877
Y1139
Y1196
Y1222
Y1248
percent signal
B
BT474
TZB
C
BT474
6-L1-G
ErbB2
p-ErbB2
TZB
D
SKBR3
E
BT474
6-L1-G
ErbB3
Y1289
TZB
F
SKBR3
G
AU565
HCC1419
HCC2218
ZR75-30
MW (kDa)
ErbB2
p-ErbB2
ErbB3
p-ErbB3
GAPDH
-170
- 40
Ctrl
TZB
6-L1-G
H
SKBR3
PZB
9-L1-H
+ HRG

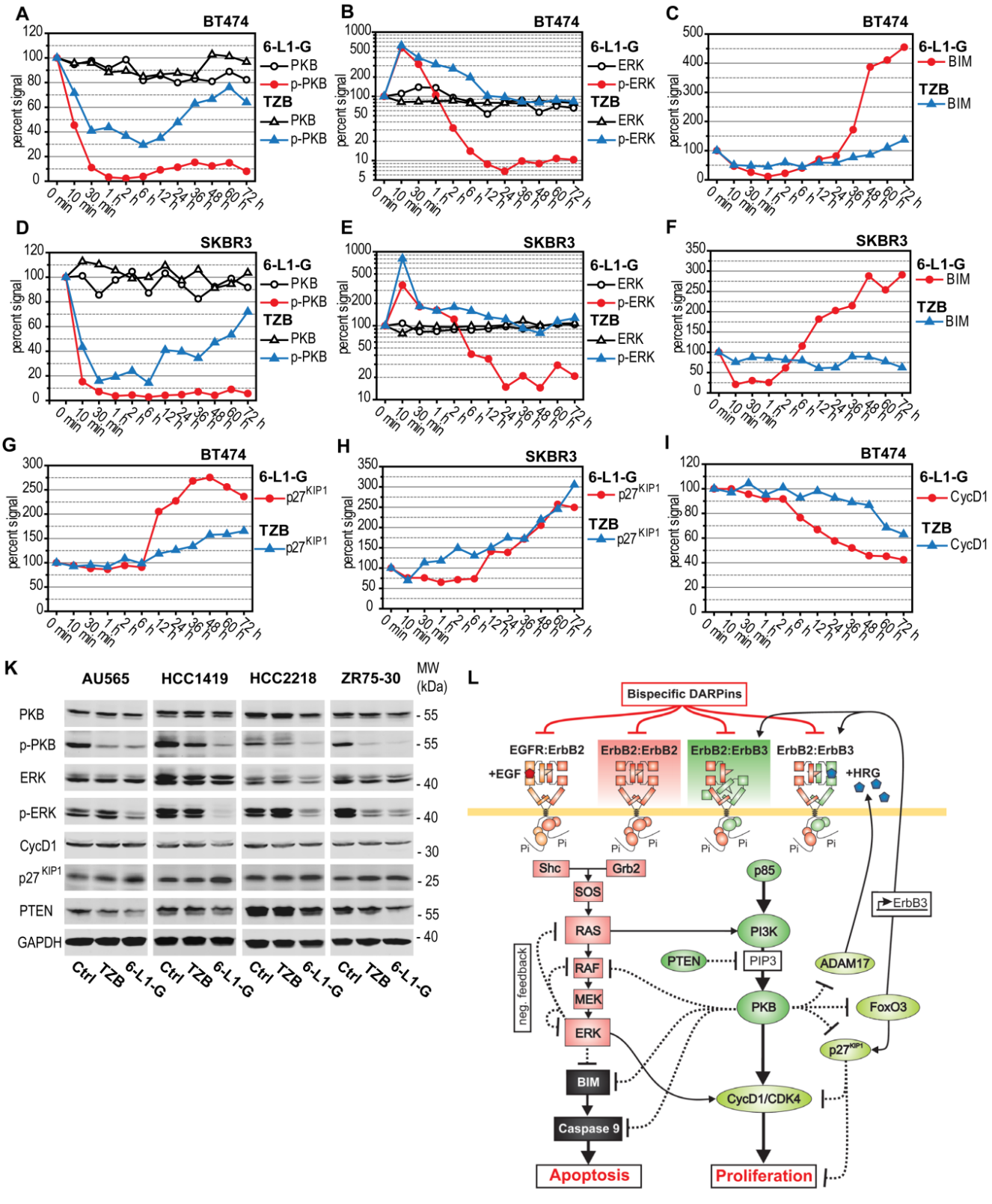
A
BT474
6-L1-G
PKB
p-PKB
TZB
PKB
p-PKB
percent signal
B
BT474
6-L1-G
ERK
p-ERK
TZB
ERK
p-ERK
C
BT474
6-L1-G
BIM
TZB
BIM
D
SKBR3
6-L1-G
PKB
p-PKB
TZB
PKB
p-PKB
E
SKBR3
6-L1-G
ERK
p-ERK
TZB
ERK
p-ERK
F
SKBR3
6-L1-G
BIM
TZB
BIM
G
BT474
6-L1-G
p27KIP1
TZB
p27KIP1
H
SKBR3
6-L1-G
p27KIP1
TZB
p27KIP1
I
BT474
6-L1-G
CycD1
TZB
CycD1
0 min 10 min 30 min 1 h 2 h 6 h 12 h 24 h 36 h 48 h 60 h 72 h
K
AU565
HCC1419
HCC2218
ZR75-30
MW (kDa)
PKB
p-PKB
ERK
p-ERK
CycD1
p27KIP1
PTEN
GAPDH
- 55
- 55
- 40
- 40
- 30
- 25
- 55
- 40
Ctrl
TZB
6-L1-G
L
Bispecific DARPins
EGFR:ErbB2
ErbB2:ErbB2
ErbB2:ErbB3
ErbB2:ErbB3
+EGF
+HRG
Pi
Shc
Grb2
SOS
RAS
RAF
MEK
ERK
p85
PI3K
PTEN
PIP3
ADAM17
ErbB3
neg. feedback
PKB
FoxO3
p27KIP1
BIM
CycD1/CDK4
Caspase 9
Apoptosis
Proliferation

(preceding page) Figure 7. Inhibition of ErbB2–ErbB2 and ErbB2–ErbB3 Mediated Downstream Signaling by Bispecific DARPins: **(A-I)** Analog to proceeding in **Fig. 6** (see above). Phosphorylation of protein kinase B (AKT/PKB) at S473 was monitored in BT474 **(A)** or SKBR3 cells **(D)**. Phosphorylation of Erk1/2 at Tyr204/Thr202 was monitored in BT474 **(B)** or SKBR3 cells **(E)**. The expression of the pro-apoptotic protein Bcl-2 interacting mediator of cell death (BIM) was measured in BT474 **(C)** or SKBR3 cells **(F)** (see **Fig. 3**). Expression of the cyclin depended kinase inhibitor p27KIP1 was monitored in BT474 **(G)** or SKBR3 **(H)** cells. Expression of cyclinD1 (CycD1) was monitored in BT474 cells **(I)**.
(K) ErbB2-dependent cancer cell lines (AU565, HCC1419, HCC2218 and ZR75-30) were treated for 72 h with single dose of 100 nM of both agents. Phosphorylation of PKB and ERK as well as well as expression of cyclinD1, p27KIP1 (see above) and phosphatase and tensin homolog (PTEN) was monitored. **(L)** Signaling diagram connecting the ErbB2–ErbB3, ErbB2–ErbB2 and ErbB2–EGFR signaling output with PI3K/PKB or MAPK pathway activation. Reported positive (unbroken) and negative (dotted) interactions are indicated as lines, and the predominant origin of the signal is drawn as well: from ErbB2–ErbB3 oncogenic unit as green ovals, for the PI3K/PKB pathway; originating from ErbB2–ErbB2: for the MAPK pathway as red squares. The model illustrates how the pathways are interconnected at several points, how inhibition of a single pathway releases negative feedbacks und thus why both have to be turned off simultaneously to achieve induction of apoptosis in ErbB2 dependent cancer cells. Since the bispecific DARPins obstruct ErbB2 from all drawn complexes, they act as a pan-ErbB inhibition response and induce apoptosis in a broad panel of ErbB2 dependent cancer cells.

Extended Materials and Methods

Protease and Phosphatase Inhibitors

The following protease inhibitors were used at the indicated final concentrations: 1 mM pefabloc/AEBSF (Meck), 0.02 mM leupeptin (Serva), 0.01 mM pepstatin (Serva) and 0.02 mM marimastat (Calbiochem). The following phosphatase inhibitors were obtained from Sigma Aldrich and used at the indicated final concentrations: 1 mM sodium orthovanadate, 1 mM sodium metavanadate, 10 mM sodium molybdate, 50 mM sodium β-glycerol phosphate, 50 mM sodium fluoride.

Reagents

Antibodies against the following targets were used, and their manufacturers are listed: Bim, EGFR, Phospho-ErbB3 (Y1289), Phospho-ErbB2 (Y877), Phospho-ErbB2 (Y1196), Phospho-ErbB2 (Y1222), Phospho-ERK (T202/Y204), ERK, Phospho-PKB (S473), pan-PKB, PARP, PTEN from Cell Signaling; c-erbB-2 (L87 + 2ERB19) from Thermo Scientific; Phospho-ErbB2 (Y1139) from Abcam; ErbB2 mouse, Phospho-ErbB2 (1248) from Millipore; Phospho-ErbB3 (Y1262) from R&D Systems; GAPDH, CyclinD1, ErbB3 mouse mAb (5A12), ErbB3 rabbit mAb (C-17), ErbB2 rabbit mAb (C-18) from Santa Cruz; ErbB2 (4B5) from Ventana; Anti-Mouse IgG IRDye800 conjugate from Rockland; Anti-$Alexa_{488}$ quenching antibody, Anti-Rabbit IgG Alexa680 from Invitrogen; Anti-Phospho-Tyr (pY20) from Sigma; p27KIP1 from BD Transduction Laboratories. The anti-DARPin polyclonal rabbit serum was obtained from Eurogentech. Trastuzumab (Herceptin®) was obtained from Kantonsapotheke Zürich. Pertuzumab (Omnitarg, Perjeta®) was a kind gift from Genentech Roche. The affibody zHER2 was cloned into the vector pQE30 vector and expressed in *E. coli* XL1 and purified as described below for DARPins.

The following signaling modulating agents were used: 12-O-tetradecanoylphorbol-13-acetate (TPA) from Cell Signaling; GDC0941 bismesylate from Axon Medchem. TNF-related apoptosis-inducing ligand (TRAIL) was obtained from Dr. Robbert H. Cool, University of

Groningen, Netherlands. ErbB2_ECD was obtained from EMP Genetech (Ingolstadt, Germany) from expression in HEK cells.

Cloning of Bispecific DARPins

DARPin 926 was originally termed 9_26, and DARPin 929 was termed 9_29 (Steiner et al., 2008). DARPin G3 was originally termed H10-2-G3 (Zahnd et al., 2007) and DARPin H14 is derived from H_14 (Steiner et al., 2008) with a C31R Mutation.

To make bispecific constructs, the DARPin ORFs were digested with BamHI and HindIII (New England Biolabs, Ipswich, Massachusetts) and ligated into compatible expression vectors based on pQiB containing $(Gly_4Ser)_{1-4}$ linkers (abbreviated as L1, L2, L3 and L4), indicating the number of Gly_4Ser units.

Expression and Purification

DARPin expression and purification has been described in detail previously (Zahnd et al., 2010). Briefly, DARPins were expressed in pQE30-derived vectors in *E. coli* strains XL1 blue or BL21. DARPins were purified via their $MRGS(H)_6$ tag on NiNTA (Qiagen) bench-top columns and endotoxin was removed by excessive washing with an additional 80 column volumes of PBS containing 0.1 % Triton-X115. DARPins were further purified by ion exchange chromatography on MonoQ columns (GE Healthcare) and finally size-exclusion chromatography on a Superdex 200 column (GE Healthcare) on an Aekta Explorer FPLC system (GE Healthcare). Endotoxin levels were determined by a LAL chromogenic endotoxin quantification kit (CRL) according to manufacturer's protocol and protein samples displayed a maximum of 10 EU/ml.

Caspase Activity

BT474 cells were seeded at 10,000 cells/cm^2 16 h before treatment in RPMI1640 medium containing 10 % FCS. Cells were treated with anti-ErbB2 agents for the indicated times and washed 2 times with ice-cold PBS. Cells were scraped in PBS, centrifuged at 300 rpm and

lysed in PBS containing 1% Triton X-100 for 10 min at 4 °C. Afterwards, lysates were centrifuged at 20,000 *g* at 4 °C for 10 min and subsequently frozen in liquid nitrogen. Protein concentrations were determined by BCA assays (Pierce). Caspase 3/7, 8 and 9 luminescence substrates (Promega) were prepared according to the manufacturer's protocol. 50 µl of luminescence substrates and the supplied inhibitors were mixed with 50 µl of 0.1 mg/ml lysates in a chilled white 96-well plate (Nunc) and fluorescence was detected on an ELISA plate reader (Tecan, Infinite M1000).

Western Blots

Cells were seeded at a density of 5,000 to 10,000 cells/cm^2 24 h prior to treatment in RPMI1640 medium containing 10 % FCS. Cells were treated with 100 nM of anti-ErbB2 agents for the indicated times. Afterwards, cells were washed with cold PBS and scraped in PBS containing all inhibitors (see above). Cells were centrifuged at 300 rpm and washed once in cold PBS-containing inhibitors. Cells were lysed for 30 min at 4 °C in cold PBS containing 1 % Triton X-100 and inhibitors. Lysates were cleared by centrifugation at 20,000 *g* for 10 min and protein concentrations were determined by BCA assays (Pierce). Samples were adjusted to 2 mg/ml in reducing LDS sample buffer (Invitrogen) containing 0.05 % β-mercaptoethanol and boiled for 3 min. Samples were subjected to 10 % SDS-PAGE and blotted onto a PVDF-FL membrane (Millipore) using wet blot protocol from Biorad. The membrane was blocked with PBS containing 1x casein blocking buffer (Sigma) and primary antibodies (see above) were incubated in PBS casein buffer containing 0.1 % Tween-20 overnight at 4°C. Membranes were washed three times in PBS containing 0.1% Tween-20 and fluorescence-labeled secondary antibodies (see above) were incubated for 2 h at room temperature. Membranes were washed 3 times in PBS 0.1% Tween-20 and fluorescence was detected on an Odyssey imaging system (LI-COR).

Immunoprecipitation ErbB2 for Total Phosphorylation Analysis by Western Blot

BT474 cells were treated and cell lysates were obtained as described above. The affibody molecule zHER2 binding to the extracellular domain III of ErbB2 has been described recently (Eigenbrot et al., 2010). The ErbB2 receptor was immunoprecipitated using a fusion

construct of the DARPin 901 (previously termed 9_01) with the zHER2 affibody, to construct 901-L4-zHER2, a bispecific binder that does not compete with any of the anti-ErbB2 agents used here. 901-L4-zHER2 was coupled to Biosupport Ultra Link beads (Pierce) overnight in 25 mM HEPES pH 8. ErbB2 receptor was immunoprecipitated from 1 mg/ml BT474 cell extracts overnight at 4°C. Beads were washed three times with cold PBS containing 1 % Triton X-100 and inhibitors. ErbB2 receptor was eluted from beads by heating up to 80 °C for 5 min in reducing SDS sample buffer. Western blots were performed as described above.

Fluorescence Labeling and PEGylation of DARPins for In Vivo Experiments

$Alexa_{488}$ C_5 maleimide, $Alexa_{488}$ NHS ester, $Alexa_{680}$ NHS ester (Invitrogen) and IR_{800} NHS ester (LICOR) were coupled to proteins as described in Tamaskovic et al. (2012). Branched PEG-40 maleimide (NOF Sunbright) was coupled to DARPins as described in Tamaskovic et al. (2012). The PEGylated proteins were purified as described in Zahnd et al. (2010). For following receptor internalization and/or recycling, the affibody zHER2 and the DARPin 901 were conjugated with $Alexa_{488}$ NHS ester as described (Tamaskovic et al., 2012). The following DARPins, 926, 929, H14, G3, 6-L1-G, 9-L1-H, 9-L4-H were conjugated with $Alexa_{488}$ C_5 maleimide at a cysteine reside located between the $MRGSHis_6$-tag and the DARPin (Tamaskovic et al., 2012).

Crosslinking ErbB2-ErbB3 and ErbB2-EGFR Heterodimers with DTSSP and Co-immunoprecipitation

Cells were seeded at a density of 2.5 x 10^4 (BT474) or 5 x 10^4 (SKBR3) cells/cm^2 16 h before treatment in RPMI1640 medium containing 10 % FCS. Cells were treated for 2 h with 100 nM of anti-ErbB2 agents. Afterwards, cells were stimulated by adding 1 nM of heregulin β-1 (HRG, 26 kDa, R&D Systems) or 2 nM of epidermal growth factor (EGF, 6 kDa, Sigma) for 15 min. Subsequently, cells were placed on ice and washed 2 times with cold 25 mM HEPES buffer, pH 7.5, 150 mM sodium chloride and scraped gently in HEPES buffer. Cells were incubated with in HEPES buffer containing 1 mM 3,3'-dithiobis[sulfosuccinimidylpropionate] (DTSSP) for 1 h at 4 °C on a rocker. Afterwards, cells were washed twice with 50 mM Tris buffer pH 7.5, gently centrifuged at 300 *g* for 2 min in between washes. Cells were lysed

using PBS buffer containing 1 % Triton X-100 and inhibitors at 4°C for 30 min and lysates were cleared by centrifugation at 20,000 *g* for 10 min at 4°C. Extracts (500 µl) containing 1 mg/ml protein, as determined by BCA assay (Pierce), were used for immunoprecipitation of ErbB2. Ultralink Biosupport beads (Pierce) were used that had been previously coupled with antibody recognizing the C-terminus of ErbB2 (C-18/sc-284, Santa Cruz) and immunoprecipitation was performed overnight at 4°C. Beads were washed 3 times with PBS containing all inhibitors and eluted by boiling in reducing SDS loading buffer for 5 min at 80 °C. Samples were subjected to 10 % SDS PAGE and western blot (see above).

Crosslinking of ErbB2 Homodimers with BS3 on the Surface of BT474 Cells

Semi-confluent BT474 cells were detached by Accutase treatment (PAA) for 5 min at 37°C, washed with RPMI1640 medium containing 10 % FCS, and afterwards washed three times with 25 mM HEPES, pH 7.5, 150 mM NaCl. Note that Accutase was chosen instead of trypsin, because of an additional band in western blots at 130 kDa caused by trypsin digest. Cells were counted on a CASY Counter, and 2 x 10^6 cells per sample were transferred in 200 µl HEPES buffer containing 10 nM of each DARPin. Cells were incubated for 1 h at 37°C. Afterwards, cells were placed on ice, washed two times with 1 ml HEPES buffer and resuspended in 200 µl HEPES containing 2.5 mM bis[sulfosuccinimidyl]suberate (BS3) (Pierce). Crosslinking was performed for 1 h at room temperature; afterwards the reaction was quenched by washing twice with 1 ml of 50 mM Tris buffer, pH 7.5, 150 mM NaCl. Cells were lysed for 15 min in 50 mM Tris buffer containing 1 % Triton X-100 and all inhibitors (see section on western blots) at 4 °C. Lysates were kept on ice, cleared by centrifugation for 10 min at 20,000 *g* and 4°C and supernatants were prepared for SDS-PAGE in reducing SDS sample buffer and boiled for 3 min. Samples were loaded on NuPAGE 4-12 % gradient gels (Invitrogen) and afterwards blotted with 100 V for 75 min onto activated PVDF-FL membrane using NuPAGE transfer buffer (Invitrogen) containing 10 % MeOH.

Mouse Housing

8-week-old female SCID beige mice were obtained from Charles River Laboratories. The mice were free of all viral, bacterial and parasitic pathogens listed in the Federation of European

Laboratory Animal Associations (FELASA) recommendations. Animals were kept in type III plastic cages (425 x 266 x 150 mm, floor area 820 cm^2) with autoclaved dust-free wooden bedding (80-90 g/cage) (Schill AG, Muttenz, Switzerland) and autoclaved paper tissues (2/cage) and a paper house as nesting material. They were fed a pelleted mouse diet (Kliba No. 3431, Provimi Kliba, Kaiseraugst, Switzerland) *ad libitum* and had unrestricted access to sterilized drinking water. The light/dark cycle in the room consisted of 12/12 h with artificial light (40 Lux in the cage) from 07:00 to 19:00h. The temperature was 21 ± 1°C, with a relative humidity of 50 ± 5% and with 15 complete changes of filtered air per hour (HEPA H 14 filter, Vokes-Air, Uster, Switzerland); the air pressure was controlled at 50 Pa. The studies were approved by the Cantonal Veterinary Office (Zurich, Switzerland). Housing and experimental procedures were in accordance with the Swiss animal protection law and conformed to the European Convention for the protection of vertebrate animals used for experimental and other scientific purposes (Council of Europe no. 123 Strasbourg 1985). The animals had a two weeks adaptation time after the arrival at the animal facility.

Mouse Perfusion

After anesthesia by intraperitoneal injection of Ketasol (100 mg/kg body weight) / Xylasol (10 mg/kg body weight) mice were perfused with paraformaldehyde. The abdominal and thoracal cavity was opened, followed by incision of the left ventricle. 0.9 % NaCl was perfused (gravity flow – height 70 cm), by simultaneously opening of the right atrium, perfusion was performed until blood became colorless (approx. 1-3 min.). Perfusion was continued with 4 % paraformaldehyde solution for 5 min. Tumors were dissected and additionally fixed for 2-3 h at RT with 4% PFA.

Histology and Immunohistochemistry

Five-µm sections from paraformaldehyde-fixed and paraffin embedded (using the facility of the Institute of Anatomy, University of Zurich, with standard histology protocols) BT474 tumors were performed and stained with a Hematoxylin solution according to Gill II and Eosin Y solution (0.5 %) in water (Carl Roth GmbH, Germany) using routine methods. To stain with antibodies specific for HER2 (HER2 monoclonal mouse antibody, Millipore, Switzerland),

cleaved Caspase-3 (polyclonal rabbit antibody, Cell Signaling Technology Inc., USA) and TUNEL reagent (*In Situ* Cell Death Detection Kit, Fluorescein, Roche Applied Science, Switzerland) slides were dried overnight at 37°C and baked in an oven at 60 °C for 1 h. After deparaffinization and rehydration (xylene and alcohol bath solutions) the tissue sections were exposed to heat-induced antigen retrieval by incubating slides in a microwave oven (5 min 350 W, 5 min 800 W).

The DAKO EnVision TM+ System Peroxidase (DAB) Kit (K4011) was used for cleaved caspase-3 staining. Primary antibody was diluted 1:100 in Tris-buffered saline (TBS), 50 mM, pH 7.5 with 1% bovine serum albumin and the tissue sections were incubated with antibody for 1 hour at room temperature. TBS with 0.1 % Tween-20 was used for the washing steps. The subsequent steps of the staining procedure followed the standard protocol of the kit. After specific staining, all slides were counterstained with Hematoxylin (according to Gill II), mounted and cover-slipped with Histomount mounting medium (Invitrogen Life Technologies)

The In Situ Cell Death Detection Kit was used according to the protocol provided by the manufacturer. For HER2 staining, the primary antibody was detected with Alexa488-conjugated goat anti-mouse antibody (Invitrogen) and nuclei were stained with 4‘,6-diamidino-2-phenylindole (DAPI) using standard IHC protocols.

Association and Dissociation Binding Analysis of Monovalent and Bivalent DARPins by FACS

The association and dissociation binding analysis to the surface cancer cells was measured as described previously in detail (Tamaskovic et al., 2012). Internalization was inhibited by incubation of cancer cells with sodium azide prior to binding analysis.

ErbB2 Receptor Cell Surface Expression Analysis by FACS

BT474 cells were seeded 24 h before treatment. Cells were incubated with $Alexa_{488}$-conjugated DARPin constructs for the indicated times. Cells were washed twice with PBS, collected by Accutase (PAA) treatment, washed once with culture medium and afterwards 2

times with cold PBS. Cells were incubated with 100 nM of either zHER2- $Alexa_{488}$ or 901-$Alexa_{488}$ for 1 h at 4°C. Afterwards, cells were washed 3 times with cold PBS and mean fluorescence intensities were recorded on flow cytometer.

ErbB2 Receptor Internalization and Recycling Analysis by FACS

The internalization and recycling assay was described for EGFR previously (Boersma et al., 2012; Spangler et al., 2010)) and carried out accordingly. The anti-ErbB2 bispecific DARPins presented here show full anti-proliferative activity and induction of apoptosis under medium conditions with 10 % serum. Consequently, we did not perform serum starvation to be able to analyze the mode of action under standard treatment conditions. BT474 cells were seeded 24 h prior to treatment. Cells were treated for 2 h with 100 nM of the indicated $Alexa_{488}$-conjgated DARPins at 37 °C to allow for internalization. Afterwards, cells were washed with PBS and harvested by Accutase treatment, washed with medium and washed 2 times with PBS. Afterwards, 25 µg/ml anti-$Alexa_{488}$ quenching antibody was added to the cells and samples were incubated for 30 min at 4°C. Thereafter, the amount of internalized DARPins was measured by FACS. Additionally, to perform the ErbB2 receptor pulse chasing assay, cells were resuspended in warm medium containing 25 µg/ml anti-$Alexa_{488}$ quenching antibody and incubated at 37°C for the indicated times. Afterwards, cells were returned to ice and washed 2 times with cold PBS and the remaining fluorescence signals (internalized DARPins) were detected by FACS.

In-Cell ELISA

In-cell ELISA, also termed in-cell western blot, was performed according to the manufacturer's protocol (LI-COR). Briefly, BT474 cells were seeded 24 h before treatment at a high density of 20,000 cells/cm^2 in black-clear-well plates (Corning). Cells were treated with the indicated concentrations of indicated agent for 1 h in the experiments shown in Fig. S4F, or cells were treated for 2 h with 100 nM of the indicated agents and additionally for 15 min with the indicated pathway stimulator for the experiments shown in Fig. S4H,K. Both pathway stimulating agents were titrated, while the PTEN inhibitor bisperoxo(pyridine-2-carboxyl)oxovanadate (bpV(pic)) was used finally at 5 µM and the PKC-ERK stimulator 12-O-

tetradecanoylphorbol-13-acetate (TPA) at 500 nM. Afterwards, cells were fixed by formaldehyde, blocked with casein blocking buffer (Sigma) and incubated overnight at 4°C with specific antibodies. Secondary antibody was incubated for 2 h at room temperature and finally plates were measured dry. Shown are the average values of triplicate measurements.

Invasion Assay

Invasion assays were performed using BD Biocoat 24-well invasion chambers containing 8 µm pore PET membranes coated with basement membrane matrix (BD Matrigel), following the manufacturer's instructions. Briefly, 1 x 10^5 SKBR3 cells in serum-free medium were introduced into the upper compartment and co-incubated with mixtures of ErbB2-targeting agents and HRG. The lower compartment was filled with medium supplemented with 20% FCS, serving as chemoattractant. After 72 hrs of incubation, the non-invading cells were wiped off with a cotton swab from the upper membrane surface. The invading cells attached to the lower surface were fixed with 4% paraformaldehyde, stained with 0.5% crystal violet, and counted in ten randomly selected microscopic fields.

Supplemental Reference List

Boersma, Y.L., Chao, G., Steiner, D., Wittrup, K.D., and Plückthun, A. (2011). Bispecific designed ankyrin repeat proteins (DARPins) targeting epidermal growth factor receptor inhibit A431 cell proliferation and receptor recycling. J Biol Chem 286, 41273-41285.

Eigenbrot, C., Ultsch, M., Dubnovitsky, A., Abrahmsen, L., and Hard, T. (2010). Structural basis for high-affinity HER2 receptor binding by an engineered protein. Proc Natl Acad Sci U S A 107, 15039-15044.

Spangler, J.B., Neil, J.R., Abramovitch, S., Yarden, Y., White, F.M., Lauffenburger, D.A., and Wittrup, K.D. (2010). Combination antibody treatment down-regulates epidermal growth factor receptor by inhibiting endosomal recycling. Proc Natl Acad Sci U S A 107, 13252-13257.

Tamaskovic, R., Simon, M., Stefan, N., Schwill, M., and Plückthun, A. (2012). Designed ankyrin repeat proteins (DARPins) from research to therapy. Methods Enzymol 503, 101-134.

Zahnd, C., Kawe, M., Stumpp, M.T., de Pasquale, C., Tamaskovic, R., Nagy-Davidescu, G., Dreier, B., Schibli, R., Binz, H.K., Waibel, R., et al. (2010). Efficient tumor targeting with high-affinity designed ankyrin repeat proteins: effects of affinity and molecular size. Cancer Res 70, 1595-1605.

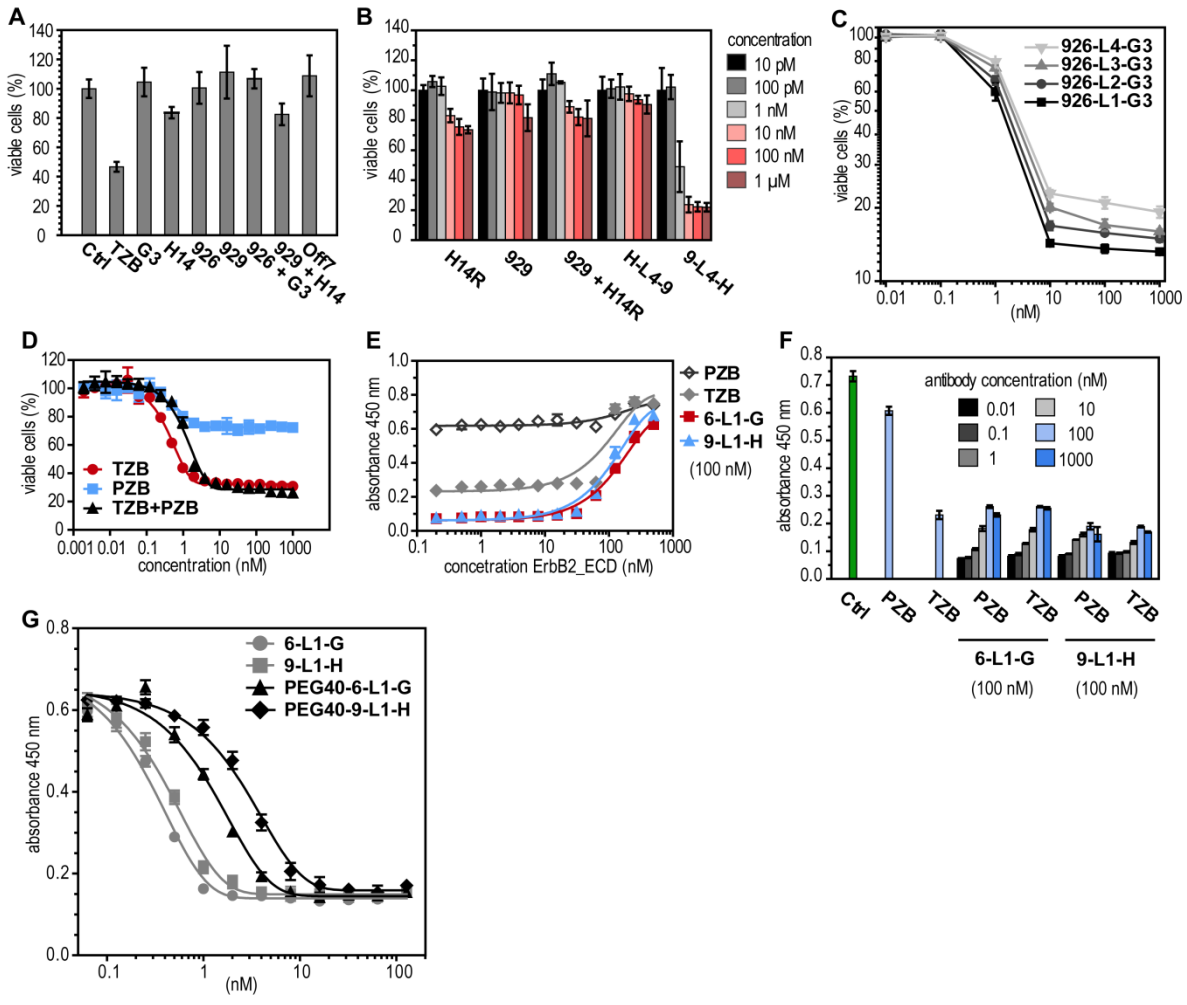
A
viable cells (%)
Ctrl
TZB
G3
H14
926
929
926 + G3
929 + H14
Off7
B
viable cells (%)
concentration
10 pM
100 pM
1 nM
10 nM
100 nM
1 µM
H14R
929
929 + H14R
H-L4-9
9-L4-H
C
viable cells (%)
926-L4-G3
926-L3-G3
926-L2-G3
926-L1-G3
(nM)
D
viable cells (%)
TZB
PZB
TZB+PZB
concentration (nM)
E
absorbance 450 nm
PZB
TZB
6-L1-G
9-L1-H
(100 nM)
concetration ErbB2_ECD (nM)
F
absorbance 450 nm
antibody concentration (nM)
0.01
0.1
1
10
100
1000
Ctrl
PZB
TZB
PZB
TZB
PZB
TZB
6-L1-G
(100 nM)
9-L1-H
(100 nM)
G
absorbance 450 nm
6-L1-G
9-L1-H
PEG40-6-L1-G
PEG40-9-L1-H
(nM)

(preceding page) Figure S1: Anti-Proliferative Activity of Monovalent and Bivalent DARPins, Binding to Cell Surface, Specificity of Anti-Proliferative Activity, Combination of Trastuzumab with Pertuzumab and Combination of Both Antibodies with Bispecific DARPins, measured on BT474 Cells

(A) XTT cell proliferation assay detecting anti-proliferative activity on BT474 cells of monovalent DARPins (100 nM) and their combination (each 100 nM) after 4 d treatment. TZB, trastuzumab. All DARPins bind to ErbB2, except Off7.

(B) XTT cell proliferation demonstrating the necessity to link the DARPins to a particular bispecific format. BT474 cells were measured after 4 d of treatment. The ErbB2 ECD_IV binding DARPin H14 displays a reduction of 20% viability, the ErbB2_I binding DARPin 929 shows no anti-proliferative activity and their combination shows anti-proliferative activity similar to H14 treatment alone. The anti-proliferative activity of the bispecific DARPins is determined by the orientation of the monovalent DARPins within the bispecific constructs. The bispecific DARPins exist in an inactive orientation (H-L4-9) and active orientation (9-L4-H). The active orientation shows strong anti-proliferative activity that exceeds by far simple additive effects.

(C) XTT cell proliferation assay measuring the effect of the flexible linker length within the active bispecific DARPin on anti-proliferative activity in BT474 cells after 4 d of treatment. Reducing the linker length from L4 $(GGGGS)_4$ to L1 (GGGGS) increases the maximal anti-proliferative activity.

(D) Association rates of mono- and bivalent DARPins to ErbB2 receptor on the surface of BT474 cells. Internalization was inhibited with azide prior to incubation. $Alexa_{488}$-conjugated DARPins (indicated by an asterisk) were incubated for the indicated times at the indicated concentrations and mean fluorescence intensity (MFI) was recorded by FACS measurements. Association rate constants of 2.0×10^5 M^{-1} s^{-1} for H14, 0.7×10^5 M^{-1} s^{-1} for DARPin929, and 0.8×10^5 M^{-1} s^{-1} for 9-L4-H were obtained.

(E) Dissociation rate of mono- and bivalent DARPins from ErbB2 receptor on the surface of BT474 cells. Internalization was inhibited with azide prior to incubation. $Alexa_{488}$-conjugated DARPins were bound to saturation, subsequently DARPins were competed for the indicated times with an excess of their respective non-labeled DARPin counterparts and MFI values were recorded by FACS measurements. Dissociation rate constants of 1.8×10^{-4} s^{-1} for H14, 2.2×10^{-3} s^{-1} for DARPin 929, and 4.0×10^{-5} s^{-1} for DARPin 9-L1-H were obtained. From **(D)** and **(E)**, functional affinities of K_D = 1 nM can be calculated for DARPin H14, 33.5 nM for 929, and 0.5 nM for 9-L1-H on the surface of BT474 cells.

(F) XTT cell proliferation assay showing the specificity of the anti-proliferative activity of bispecific DARPins (6-L1-G and 9-L1-H) and the antibodies trastuzumab (TZB) and pertuzumab (PZB) by competition with soluble full-length ErbB2_ECD on BT474 cells after 4 days of treatment. Anti-ErbB2 agents (each 100 nM) were preincubated with increasing concentrations of ErbB2_ECD and given to the cancer cells. Increasing concentrations of ErbB2_ECD reduced the anti-proliferative activity of each anti-ErbB2 agent to completion in a concentration-dependent manner.

(G) XTT cell proliferation assay detecting the anti-proliferative activity of the equimolar combination of trastuzumab (TZB) with pertuzumab (PZB) on BT474 cells after 4 days of treatment.

(F) XTT cell proliferation assay showing the effect of combination of bispecific DARPins at a constant concentration of 100 nM with increasing concentration of either trastuzumab (TZB) or pertuzumab (PZB) on the activity to BT474 cells after 4 days of treatment. With increasing concentration of either antibody, the strong anti-proliferative activity of bispecific DARPins is markedly reduced. Note that H14 competes with TZB for binding to ErbB2_IV, while G3 does not (data not shown). None of the monovalent DARPins (926, 929, H14, G3) competes with PZB for binding to ErbB2_ECD (data not shown). However, anti-proliferative activity of both bispecific DARPins is reduced by both antibodies, respectively.

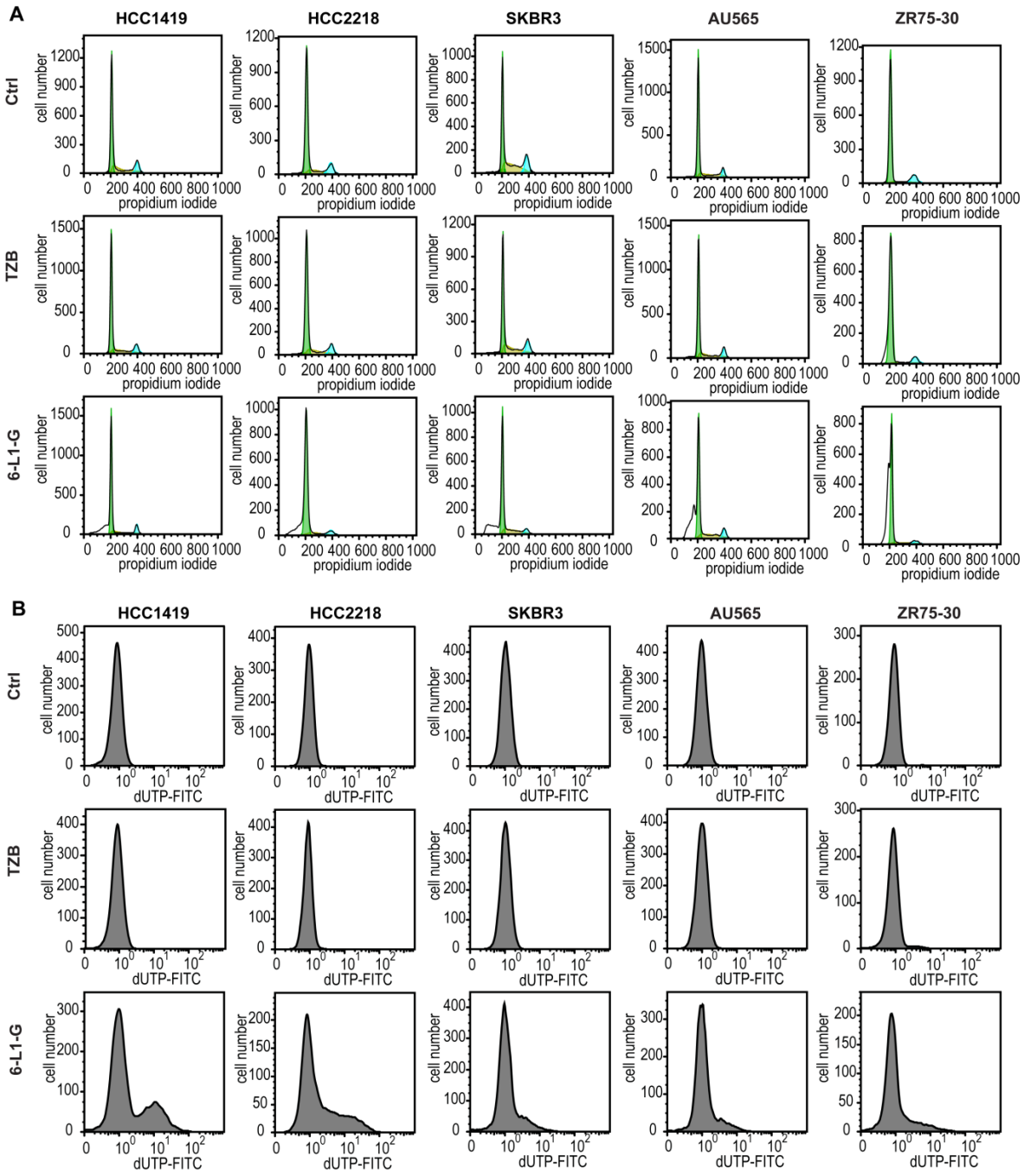

Figure S2:
Analysis of Cell Cycle Distribution and TUNEL Assay after Treatment with 6-L1-G and Trastuzumab on a Panel of ErbB2 Dependent Breast Cancer Cell Lines
(A) Cell cylce distribution analysis of ErbB2-overexpressing cancer cells after 3 days of treatment with the indicated agents, each at 100 nM concentration. Ethanol-fixed cells were stained with propidium iodide (PI, 20 µg/ml) and analyzed by FACS. Depicted PI-stained histograms show cell cycle profiles of gated single cells and are quantified with the Dean-Jett-Fox algorithm (indicated by the colors). **(B)** TUNEL assays of treated ErbB2-overexpressing cancer cells in histograms showing apoptotic cell populations. Cells were treated with 100 nM of indicated agents for 3 days, PFA-fixed and Triton-permeabilized, stained with terminal deoxynucleotidyl transferase (TdT) using dUTP-fluoresceine substrate and subsequently analyzed by FACS. Presented histograms depict the recorded TUNEL profiles of non-apoptotic (left peak, centered around 10^0) and apoptotic cells (right peak, centered up to 10^2).

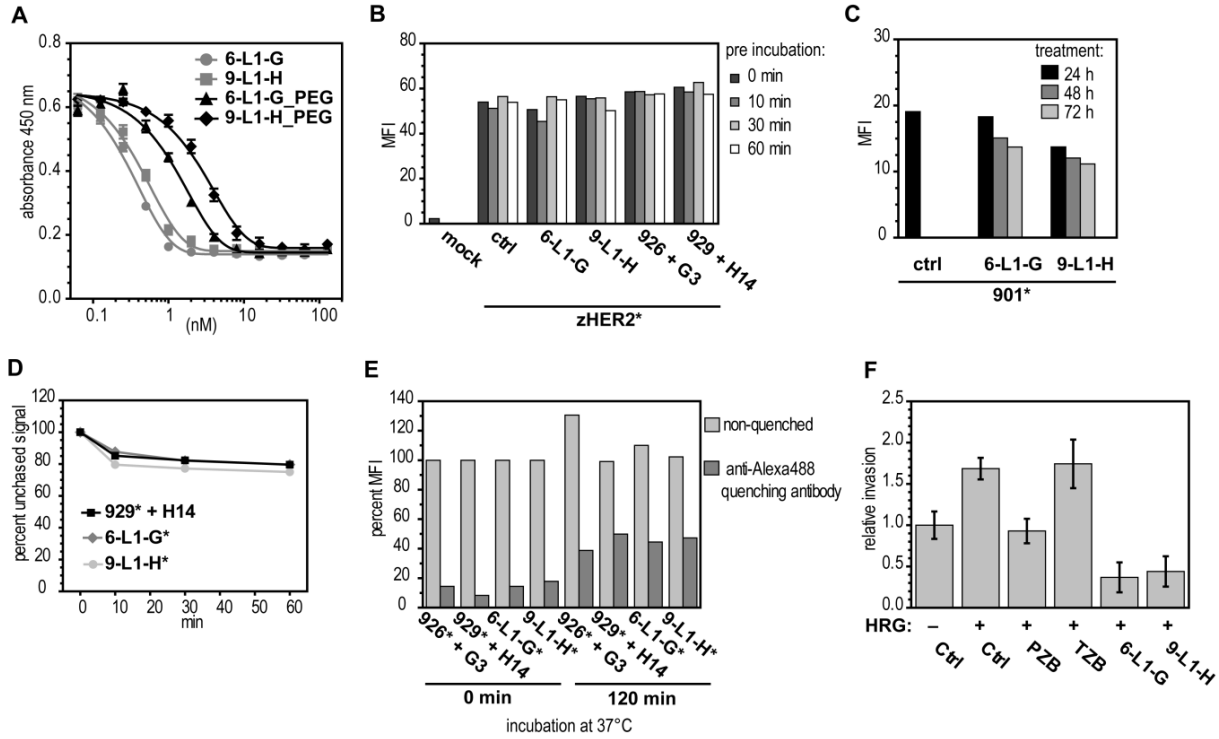

Figure S3. Anti-proliferative Activity after PEGylation of Bispecific DARPins and Effect of Treatment with Bispecific DARPins on ErbB2 Receptor Surface Expression, Internalization and Recycling on BT474 Cells:

(A) XTT cell proliferation assay showing the effect of PEGylation on both bispecific DARPins (6-L1-G and 9-L1-H). Anti-proliferative activity was measured on BT474 cells after 4 days of treatment. The maximal anti-proliferative activity was not affected by PEGylation, while dose effectiveness was reduced. IC_{50} values of bispecific non-PEGylated DARPins increased from the picomolar range to the low nanomolar concentrations for PEGylated constructs. **(B)** ErbB2 expression levels measured by FACS. $Alexa_{488}$-conjugated anti-ErbB2 affibody (zHER2* (Eigenbrot *et al.*, 2010), the asterisk indicating the label) was bound to ErbB2 on the surface of BT474 cells, which were treated with the indicated DARPins for up to 1 h. Note that zHER2* binds to ErbB2_III and does not compete with monovalent DARPins (926, 929, G3, H14) for binding to ErbB2 receptor (data not shown). **(C)** ErbB2 expression levels measured by FACS. $Alexa_{488}$-conjugated monovalent DARPin (901*, the asterisk indicating the label) were bound to the surface of BT474 cells after preincubation with indicated DARPins for indicated times. ErbB2 surface expression levels remained constant after treatment with bispecific DARPins. **(D)** Pulse-Chase-Assay performed by FACS measurement, detecting the quenching of mono- and bivalent $Alexa_{488}$-conjugated DARPins (indicated by an asterisk) that are recycled back to the surface on BT474 cells, remaining bound to ErbB2. Indicated agents were preincubated for 2 h at 37°C to allow for internalization, fluorescence of $Alexa_{488}$-conjugated DARPins bound to the cell surface were quenched by an anti-$Alexa_{488}$ antibody at 4°C, and afterwards cells were incubated for the indicated times in the presence of the quenching antibody at 37°C and remaining fluorescence was measured by FACS. Active and inactive constructs recycled with the same rate.

(E) Internalization assay performed by FACS measurement. BT474 cells were treated for 2 h with 100 nM concentration of mono- and bivalent $Alexa_{488}$-conjugated DARPins (indicated by an asterisk). Afterwards, surface fluorescence was quenched by incubation with anti-$Alexa_{488}$ antibody at 4°C and residual fluorescence was measured by FACS. Active and inactive constructs internalize with the same rate. **(F)** Effect of the ErbB2-targeting agents on cell invasion. SKBR3 cells pre-seeded on a basement membrane matrix were treated with the indicated agents at 100 nM concentrations and co-stimulated for 72 h with 1 nM heregulin-β1 (HRG). Cell invasion was expressed as relative invasion to the invasion of control-treated cells.

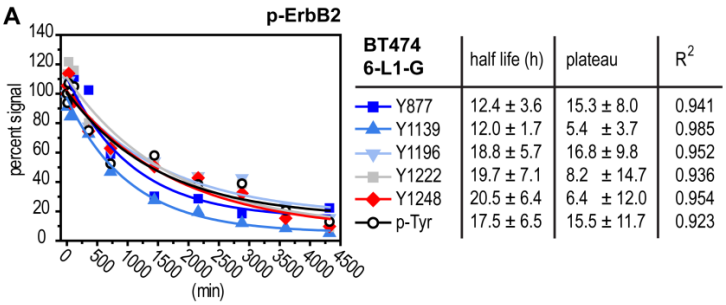

BT474 6-L1-G	half life (h)	plateau	R^2
Y877	12.4 ± 3.6	15.3 ± 8.0	0.941
Y1139	12.0 ± 1.7	5.4 ± 3.7	0.985
Y1196	18.8 ± 5.7	16.8 ± 9.8	0.952
Y1222	19.7 ± 7.1	8.2 ± 14.7	0.936
Y1248	20.5 ± 6.4	6.4 ± 12.0	0.954
p-Tyr	17.5 ± 6.5	15.5 ± 11.7	0.923

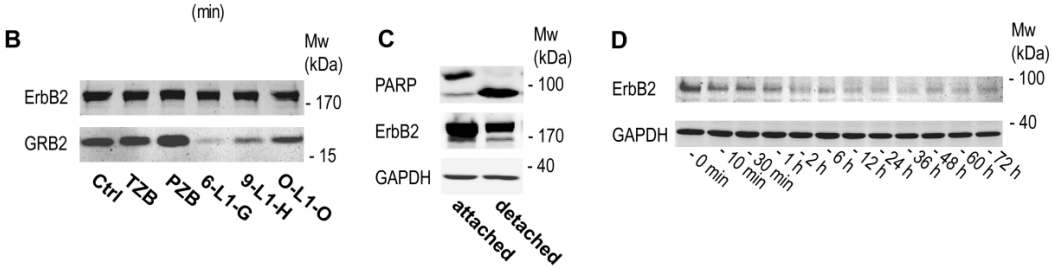

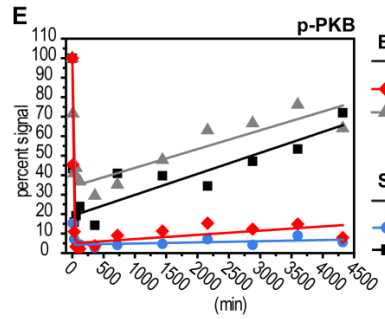

BT474	half life (min)	minimum	Re- phosphorylation rate (min^{-1})	R^2
6-L1-G	3.2 ± 0.1	5.0 ± 2	0.00216 ± 0.0008	0.996
TZB	11.3 ± 0.3	34.1 ± 4	0.00963 ± 0.0017	0.869

SKBR3	half life (min)	minimum	Re- phosphorylation rate (min^{-1})	R^2
6-L1-G	7.9 ± 0.11	4.3 ± 1	0.00058 ± 0.0003	0.981
TZB	5.48 ± 0.3	19.1 ± 3.7	0.01078 ± 0.0017	0.904

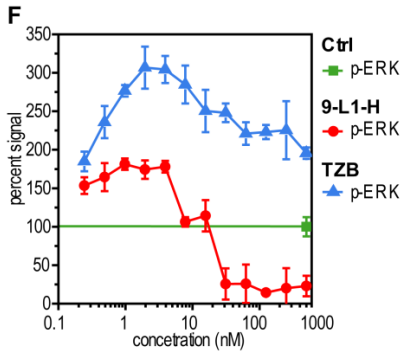

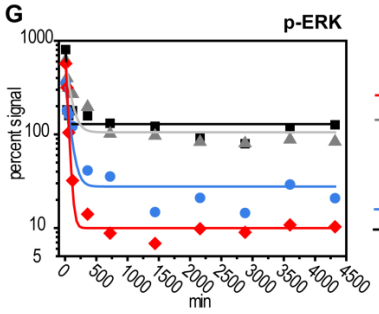

BT474	half life (min)	plateau	R^2
6-L1-G	21.2 ± 0.7	10 ± 3	0.998
TZB	53.2 ± 14	105 ± 19	0.919

SKBR3	half life (min)	plateau	R^2
6-L1-G	44.8 ± 11	28 ± 11	0.921
TZB	5.56 ± 1.4	139 ± 19	0.976

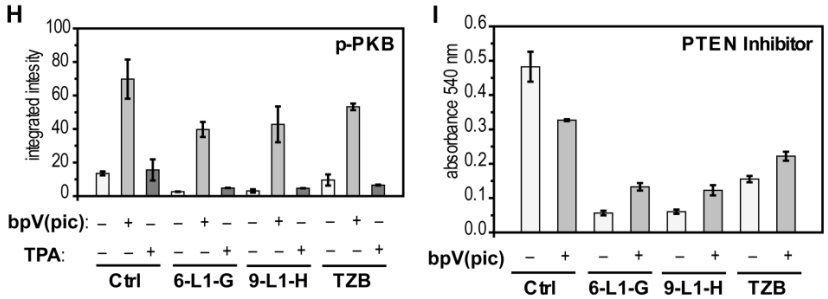

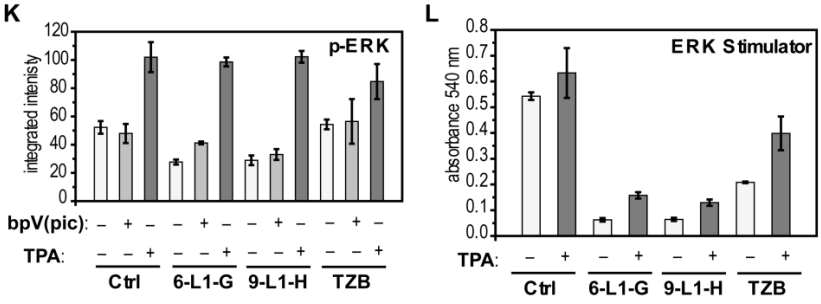

(preceding page) Figure S4. Bispecific DARPins induce ErbB2 Dephosphorylation and Consequently Inhibit Downstream Signaling of PKB and ERK Simultaneously and thereby Overcome Pathway Plasticity:
(A) Quantitative western blot analysis of single Tyr phosphorylation sites and total Tyr phosphorylation of ErbB2 receptor in BT474 cells after treatment with bispecific DARPin (6-L1-G). A single exponential decay function was fitted to integrated signal intensity signals.
(B) Analysis of GRB2 dissociation from ErbB2 receptor after treatment of BT474 cells with indicated agents for 3 days. ErbB2 receptor was immunoprecipitated using 901-L4_zHER2 coupled to beads. Reduced GRB2 CoIP-levels were detected after treatment with bispecific DARPins (6-L1-G and 9-L1-H), but not after trastuzumab (TZB) or pertuzumab (PTZ) treatment.
(C) Detection of ErbB2 expression levels in late apoptotic SKBR3 cells after 3 days of treatment with bispecific DARPins. Adherent and detached cells were separately collected and subjected to western blot. Adherent cells show less PARP cleavage in comparison to detached cells (less PARP p89 visible). Constant expression levels of ErbB2 have been observed in adherent cells, while detached late apoptotic cells show reduced ErbB2 receptor expression level. The population of adherent cells greatly reduces over time and accumulates in the supernatant. Nonetheless, signaling analysis of adhering cells could be performed for up to 3 days, since the experiments could be scaled up, but examination after 3 days becomes increasingly difficult.
(D) Western blot analysis of ErbB2_p95 expression in BT474 cells after treatment with bispecific DARPin 6-L1-G.
(E) Quantitative western blot analysis of PKB phosphorylation in BT474 or SKBR3 cells after treatment with bispecific DARPin (6-L1-G) or trastuzumab (TZB). An exponential decay, coupled to a linear function was fitted to integrated signal intensities.
(F) In-cell ELISA detecting ERK phosphorylation in BT474 cells after 1 h of treatment with indicated concentrations of bispecific DARPins or trastuzumab.
(G) Quantitative western blot analysis of ERK phosphorylation in BT474 or SKBR3 cells after treatment with bispecific DARPin (6-L1-G) or trastuzumab (TZB). A single exponential decay function was fitted to integrated signal intensity signals.
(H-L) Effect of selective stimulation of PI3K/PKB pathway by inhibition of PTEN with bisperoxo(pyridine-2-carboxyl)oxovanadate (TPA). In-cell ELISA detecting phospho-PKB **(H)** or phospho-ERK **(K)** levels in BT474 cells after 2 h of treatment with bispecific DARPins or trastuzumab and subsequent stimulation of PKB with bpV(pic), or ERK with TPA, for 15 min. Cell viability assay measuring the effect of combination of bispecific DARPins or trastuzumab with the agonistic PTEN inhibitor **(I)** or ERK stimulator **(L)**. Note that the PTEN inhibitor had to be used at concentrations that showed anti-proliferative activity in control cells; however, the PTEN inhibitor induces growth stimulation in cancer cells treated with bispecific DARPins or trastuzumab.

Chapter 5
Further Methods and Results

Contents

1 Introduction 156

2 Construction of bivalent DARPins 157

2.1 Construction of vectors coding for flexible linkers with various lengths 157

2.2 Construction of vectors coding for various rigid DARPin linkers 158

2.3 Construction of pQi_scZIP and pQi_scdHLX 162

3 Approaches to gain insight into the DARPins' epitopes 163

3.1 Refolding of HER2_IV 164

3.2 Refolding of further extracellular HER2-subdomains 171

3.3 Chemical Linkage of Peptides onto Scaffolds (CLiPS) 173

4 Xtal- conditions screened 175

5 Preliminary work and cloning for Sf9-expression 192

6 Immunoprecipitation with DARPins 194

7 Cell proliferation assays with further interesting constructs 197

8 References 201

1 Introduction

Chapter five contains a collection of further methods and results conducted in the course of my PhD-project, that did not necessarily yield data for publications, but should still be mentioned for several reasons.

First, there is a category of methods that have been used within the whole project and that certainly have expanded into the earlier chapters of this work. Still, such methods, like for instance the construction of the different flexible or inflexible linkers, deserve to be explained in more detail.

Another less glorious category of methods are those that have been tried out without real success but with the final outcome that this was not the way to succeed (best examplified by the manifold experimental attempts within the struggle to obtain information on the epitopes of the HER2-binders). These methods and results are summarized in order to give an inspiration on what – at least theoretically – could work and on what all has been tried out.

Last, not least, this Chapter summarizes methods and results that are part of side-projects which are still ongoing and not completed, but that might yield interesting data in the near future and that therefore should not stay unmentioned.

All methods and results are thematically grouped in subchapters. Basic techniques (like cloning or ELISA) were performed in analogy to the protocols given in the Material and Methods section of **Chapters 2** to **4**. All further techniques (like e.g. *in vitro* refolding) are explained within the respective subchapter.

2 Construction of bivalent DARPins

All plasmids used in this work for the construction of bivalent DARPin-constructs were derivatives of vector pQiBi_22 (**Figure 5.1**:), which in turn is a lacIq-containing derivative of vector pQE30 from Qiagen. All pQiBi-vectors carry two cloning cassettes, one *Bam*HI/*Hin*dIII cassette upstream and one *Bgl*II/*Bsa*I cassette downstream of a sequence coding for the respective linker. Vectors coding for bivalent constructs (or e.g. SNAP-tag constructs used in **Appendix 2**) were obtained by sequentially cloning *Bam*HI/*Hin*dIII-digested inserts into the two cassettes. *Hin*dIII/*Bgl*II cloning allowed the exchange of the linker sequence, varying either the length (e.g. $(G_4S)_2$ vs. (G4S), cf **Chapter 3**) or the rigidity (e.g. $(G_4S)_2$ vs. N6C, cf. **Chapter 2**) of the linker.

Besides the flexible and rigid linkers described in **Chapters 2** and **3**, further linkers composed of a leucine zipper (scZIP (Pack and Plückthun (1992))) or a double helix motif (scdHLX (Pack *et al.* (1993))) were tested as well. These constructs, however, did not prove to show significant effects on the cell proliferation of BT474 cells.

2.1 Construction of vectors coding for flexible linkers with various lengths

pQiBi-vectors with flexible $(G_4S)_n$ peptide linkers (with n = 1, 2, 4, 6 or 8) were prepared starting from vector "pQiBi_22" encoding an $(G_4S)_4$-linker.

The coding sequence (cds) for the shortest flexible linker (G_4S) was ordered as complementary oligonucleotides "G4S_for" and "G4S_rev" (from Microsynth), that were phosphorylated (using polynucleotide kinase (PNK)), annealed, and ligated into *Hin*dIII/*Bgl*II-cut vector pQiBi.

The coding sequences for the longer flexible linkers were created by ligating "building blocks" of linker sequences obtained via PCR on e.g. pQiBi_22 and pQiBi_11 (to generate $(G_4S)_4$ and $(G_4S)_2$ building blocks for creation of $(G_4S)_6$) using primer-pairs "33_for2" × "QE_rev" and "QE_for" × "33_rev1". Before ligation into *Hin*dIII/*Bgl*II-cut vector pQiBi, these „flexible linker building blocks" were digested with *Hin*dIII x *Bpi*I or *Bpi*I x *Bgl*II, respectively.

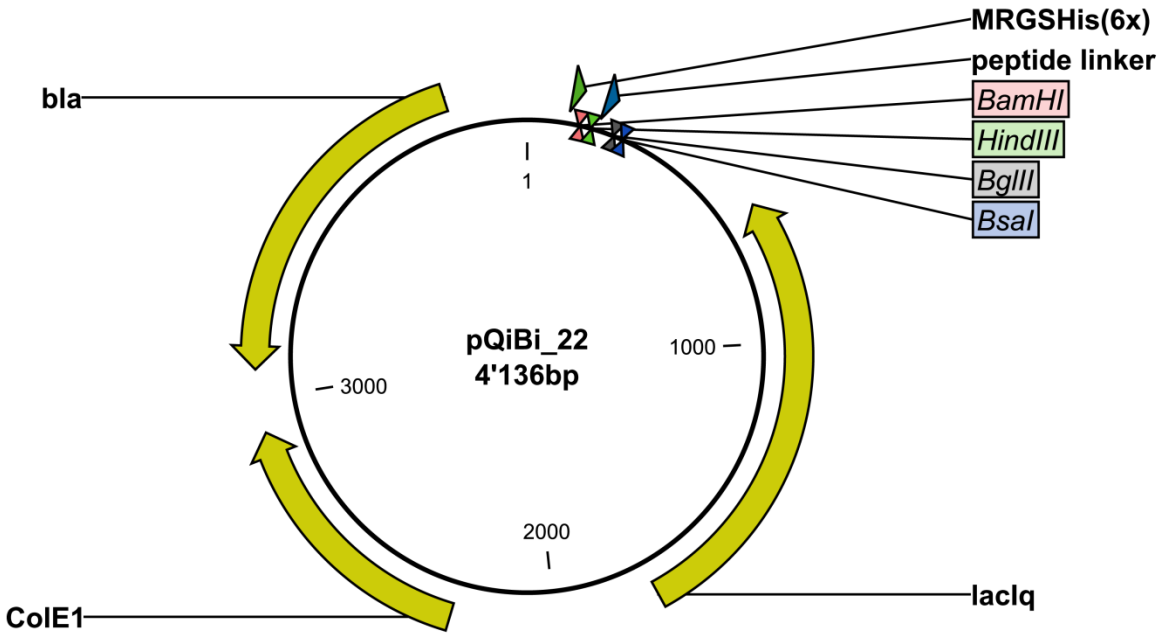

Figure 5.1: Vector map of pQiBi_22_. This vector was the starting point for the cloning of all bispecific DARPins. All pQiBi-vectors carry two cloning cassettes, one *Bam*HI/*Hin*dIII cassette upstream and one *Bgl*II/*Bsa*I cassette downstream of a sequence coding for the respective linker.

Table 5.1: Oligonucleotides used for the construction of flexible linkers by means of PCR. Nucleotides that introduce point mutations (in order to create a *Bpi*I-recognition-site (5'-GAAGAC-3')) are highlighted in red. PTO-linkages, introduced instead of standard phosphodiester bonds close to the 3'-end of the primers, are indicated by asterisks (*). The PTO-linkages were introduced in order to abolish the 3'→5'-proofreading-activity of the DNA-polymerase, which would otherwise correct the point mutations introduced by the oligonucleotides (de Noronha and Mullins (1992)).

Name	Sequence (5'-3')	Comment
G4S_for	AGCTTGGCGGCGGTAGCT	for annealing with G4S_rev
G4S_rev	CTAGAGCTACCGCCGCCA	for annealing with G4S_for
QE_for	CGGATAACAATTTCACACAG	
QE_rev	GTTCTGAGGTCATTACTGG	
33_for2	GTCGACCTGCAGGAAGACTTGG*C*G	for use with QE_rev
33_rev1	TGTCGAAGACAGCGCCAGAACCGCCACCGCCAGA	for use with QE_for

2.2 Construction of vectors coding for various rigid DARPin linkers

Consensus DARPins with more than 6 internal modules used as rigid linkers for the bivalent DARPins described in **Chapter 2** were prepared following a "building block strategy" resembling the assembly strategy described in **Section 2.1**, where the upstream building block codes for a DARPin-N-cap and a defined number of internal consensus repeats, and the downstream building block codes for further internal consensus repeats and a DARPin-C-cap.

The building blocks for the ligation of the chimeric DARPins cds were obtained via PCR on e.g. pQE30_N4C_ss using primer-pairs "NPR_f" × "bbN_rev" and "bbC_for" × "bbc_rev" (to generate "N4" and "4C" building blocks, i.e. constructs of the N-cap and 4 internal repeats or 4 internal repeats and the C-cap, for the creation of the consensus N8C sequence). The building blocks were then *Bsa*I-digested and ligated, before *Bam*HI × *Hin*dIII -cloning into the expression-vector pQE30_ss (pDST67). As nucleotide sequencing of long consensus DARPins (of a length where forward- and reverse- Sanger sequencing are required to determine the whole DARPin-sequence) is not trivial due to the repetitive nature of the sequence, the primers bbN_rev and bbC_for at the building block boundaries were designed to introduce a silent mutation in the D of the GADVNA motif (GAC→GAT), allowing identification of this "ligation scar" within the consensus-DARPin-cds.

The assembled NxC-consensus DARPins, which were meant to serve as linkers in the pQiBi-format, were finally extended via PCR for *Hind*III- and *Bgl*II-sites and linker glycines prior to cloning into pQiBi.

Chimeric DARPins built up from both consensus and target-specific internal modules were constructed using the same assembly protocol (with e.g. consensus N2C and HER2-binding DARPin H14 as templates). These DARPins could be used for epitope characterization studies depicted in **Figure 5.3**:.

Table 5.2: Oligonucleotides used for the construction of chimeric DARPins (see Figure 5.2: for the construction scheme used). Nucleotides that introduce point mutations (in order to create a *Bsa*I-recognition-site (5'-GGTCTC-3')) are highlighted in red. Nucleotides that introduce a silent mutation (allowing the identification of this "ligation scar" within the assembled consensus-DARPin-cds) are highlighted in blue. PTO-linkages, introduced instead of standard phosphodiester bonds close to the 3'-end of the primers, are indicated by asterisks (*). The PTO-linkages were introduced in order to abolish the 3'→5'-proofreading-activity of the DNA-polymerase, which would otherwise correct the point mutations introduced by the oligonucleotides (de Noronha and Mullins (1992)).

Name	Sequence (5'-3')	Comment
NPR_f	GGGAAAGGATCCGACCTGGGTAAGAAACTGCTGG	
bbN_rev	CTTACCGAATTTGTCCTGGGTCTCAACATC*A*G	introduces silent mutation
bbC_for	CCTGATGGCTAACGGTCTCGATGTTAACGC	introduces silent mutation
bbC_rev	ATTAAGCTTTTGCAGGATTTCAGCCAGG	
2G_Hind	CCCAAGCTTGGTGGCTCTGACCTGGGTAAGAAACTGC	introduces 2G-linker
2G_Bgl	GAAGATCTGCCACCTTGCAGGATTTCAGCCAGG	introduces 2G-linker

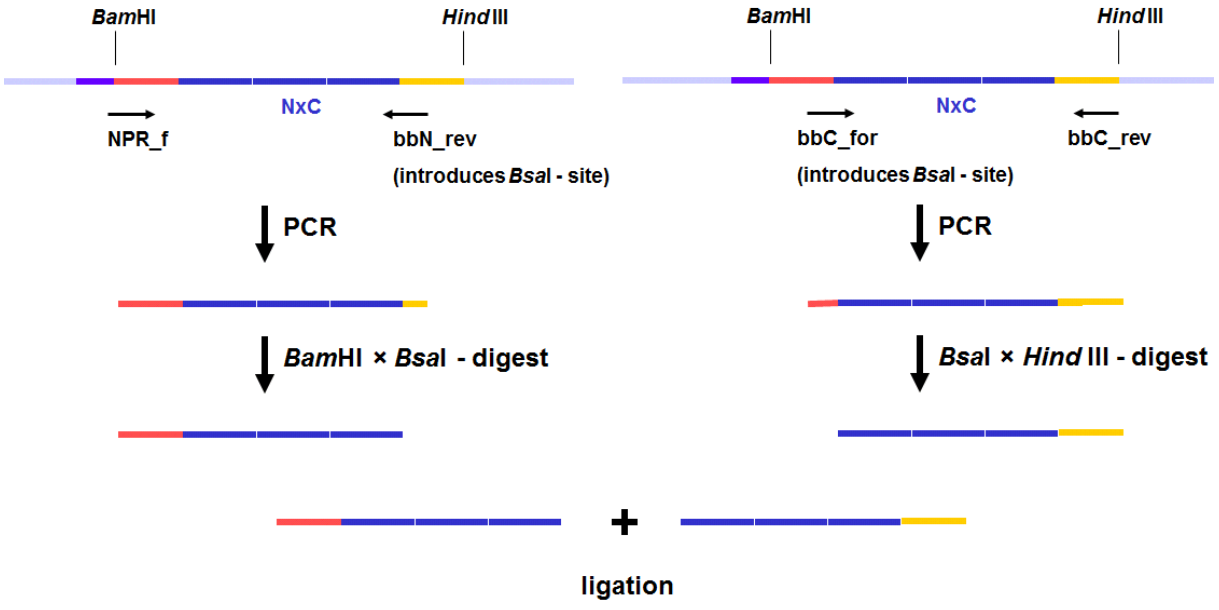

Figure 5.2: Construction scheme for the creation of chimeric DARPins-cds. The "building blocks" were obtained via PCR on DARPin-cds, introducing *Bsa*I-sites. Digestion with *Bam*HI × *Bsa*I for the N-terminal building block and *Hind*III × *Bsa*I for the C-terminal building block allowed ligation of the building blocks into, e.g., vector pDST67 to obtain the chimeric DARPin cds for the expression of the chimeric DARPin.

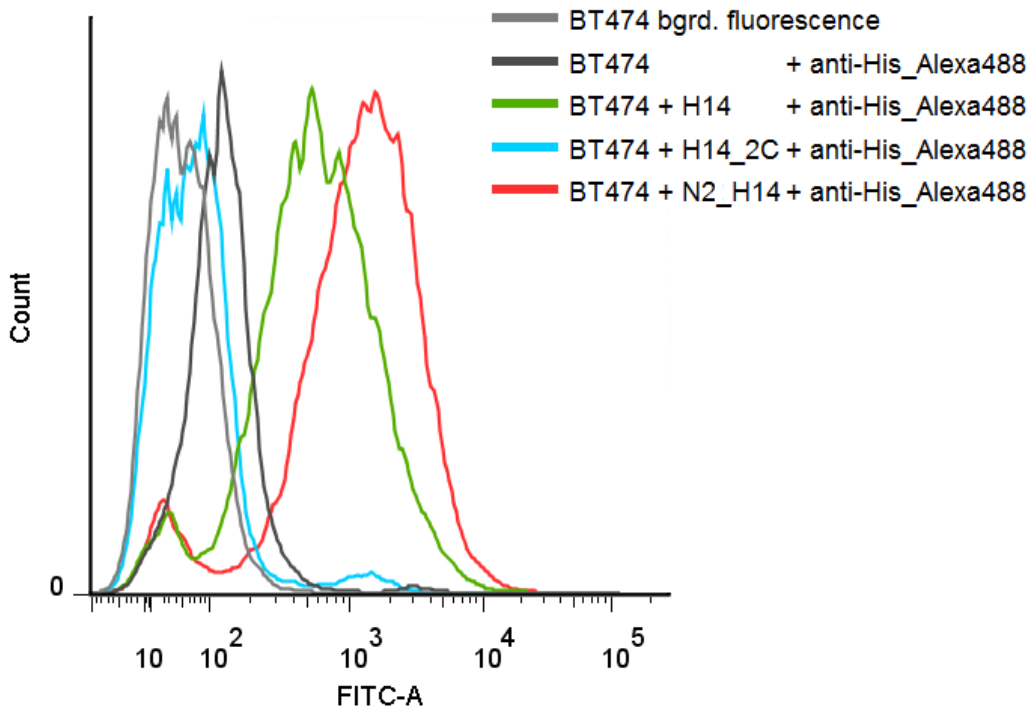

Figure 5.3: Flow cytometry with DARPin H14 and chimeric H14-DARPins binding to BT474 cells. DARPins H14_2C and N2_H14 are chimeric DARPins in which DARPin H14 has been elongated C- or N-terminally by introduction of 2 consensus repeat modules next to the respective capping repeat. DARPin binding at 100 nM to 0.5 × 10^6 cells in 1 ml PBS_BA was allowed for 1.5 h on ice. After two washings with ice-cold buffer, cells were incubated with an AlexaFluor488-conjugated α-His_5-antibody (Qiagen) for another hour. Cells incubated without any binder or with antibody only served as controls.

2.3 Construction of pQi_scZIP and pQi_scdHLX

Further bivalent DARPin-constructs were designed by replacing linker and downstream cloning cassette in pQiBi by a short PSTPPGSS linker sequence and sequences coding for either a leucine zipper (scZIP (Pack and Plückthun (1992))) or a four-helix bundle (scdHLX (Pack *et al.* (1993))). The resulting vectors pQi_scZIP and pQi_scdHLX still carry the *Bam*HI/*Hin*dIII cassette in order to construct DARPins with the respective dimerization module at the C-terminus.

Vector pQi_scZIP was later used as starting point by N. Stefan for the creation of pQiBi_LZ_, a vector that allows for the insertion of DARPin-cds N- and C-terminally oft he leucine zipper, creating tetravalent DARPin-constructs (Stefan *et al.* (2011)).

3 Approaches to gain insight into the DARPins' epitopes

Every biochemical research that involves binding proteins, no matter of which nature, will necessarily improve with increasing knowledge concerning the mode of binding. From the very beginning of the project the question of place and orientation of binding of the originally characterized DARPins was one of the central ones. No matter if thinking about the biological activity of monomeric DARPin H14 in comparison to its competitors for binding – DARPin G3 and scFv 4D5 (**Chapter 2**), the question which binders to use for the construction and screening of bispecific DARPin constructs (**Chapter 3**), or the final and still ongoing interpretation and explanation of the strong cytotoxic effects caused by these bispecific DARPins – to name only a few examples; The question of the particular epitope and the DARPin's orientation of binding was always obvious to ask.

For that reason, efforts to characterize the DARPin epitopes on HER2 have been undertaken continuously in the course of the whole PhD-project. These trials were highly complicated by the nature of the DARPins' target: The extracellular part of HER2 contains 50 cysteines that are required to form 25 disulfides, very precisely matched, in order to allow the protein to fold correctly. This does, for instance, preclude HER2_ECD from simply being functionally expressed in the *E. coli* cytoplasm. The task to identify the correct epitopes is further hampered by the fact, that DARPins usually recognize conformational epitopes. The correct folding of the epitope can therefore be regarded as a prerequisite for successful epitope characterization experiments.

The following smaller sections are meant to outline the different approaches in epitope characterization, that have been undertaken, besides the initial competition assays already described in **Chapter 2** and in **Chapter 3** and the final successful crystallization experiments described in **Chapter 3**.

.

3.1 Refolding of HER2_IV

The chronologically first anti-HER2 DARPin within the project, for which great interest in the epitope and the orientation of binding arose, was DARPin H14. Its special characteristic to have anti-proliferative effects on HER2 overexpressing cancer cells and its similarity to scFv 4D5 and yet difference to DARPin G3 (detailed in

Chapter 2) made it very desirable to increase the structural knowledge on binding of H14. One side project arising quite early was therefore to produce HER2_IV – the subdomain recognized by H14 – in the correctly folded state.

The first technique, which was tried out in order to produce correctly folded recombinant HER2_IV, was *in vitro* protein refolding. Starting with the cloning of the HER2_IV cds (A488-L629) into vector pAT222 for cytosolic expression of HER2_IV_A488-L629 with an N-terminal Avi-tag and a C-terminal His_6-tag, the subdomain was expressed in *E. coli* XL1-blue and found to form insoluble inclusion bodies. Following the review by Lange and Rudolph (2008) and protocols 1-3 given therein, the inclusion bodies were used as starting point to screen various refolding conditions, varying pH (in 0.1 M Tris/HCl buffered refolding buffer) and concentrations of L-Arg (as additive) and GSH/GSSG (as redox-shuffling system).

The success of every refolding project strongly depends on being able to monitor the degree of correctly formed protein structure in order to discriminate the potential of the different refolding conditions. The fidelity of the chosen refolding efficacy test and its ability to monitor as many characteristics as possible, will decide on whether the refolding project is likely to succeed or not.

For the refolding of HER2_IV it was crucial to find a condition in which all 20 cysteines formed the correct pattern of 10 disulfides. A correctly refolded HER2_IV would contain no free thiol group and would allow binding of trastuzumab and DARPin H14 and G3. Furthermore the POI should in the best case show monomeric running behaviour in size-exclusion chromatography (SEC), indicating that it does not form soluble aggregates.

The refolding condition yielding HER2_IV with most favourable characteristics was the refolding of solubilized inclusion bodies by rapid dilution into refolding buffer with 25 mM Tris/HCl, pH 9.0; 100 mM NaCl; 10% glycerol; 0.5 M L-Arg; 1.25 mM GSH and 0.25 mM GSSG. Inclusion bodies were previously solubilized in Tris buffered saline (TBS: 20 mM TRIS/HCl, pH 8.0, 500 mM NaCl) containing 5 mM DTT.

Immunoblots (IB) using trastuzumab as primary antibody for the detection of the correctly folded epitope on HER2_IV are shown in **Figure 5.4**: and **Figure 5.5**:. Detection of its correctly folded epitope by trastuzumab was performed by ELISA as well (**Figure 5.5**:). The experiment described in **Figure 5.5**: highlights the importance of the GSH:GSSG redox-shuffling system for proper refolding of the cysteine-rich HER2_IV_A488-L629.

Besides trastuzumab-based refolding efficiency assays, the DPS-assay (Hansen *et al.* (2007)) and analytical SEC were performed to rank different refolding conditions. The results of these tests with HER2_IV_A488-L629 from the most promising refolding condition (detailed above) are depicted in **Figure 5.7**: and **Figure 5.8**:.

It has to be mentioned, that in the course of the refolding trials the initial construct HER2_IV_A488-L629 (described above) was exchanged by the construct pD_HER2_IV_A488-L629, carrying an N-terminal protein D fusion. Protein D (pD) – a protein from bacteriophage lambda – has previously been shown to assist folding and help keeping its fusion partner soluble (Forrer and Jaussi (1998)). As refolded HER2_IV_A488-L629, after being dialyzed against PBS, had shown an early running peak in analytical SEC, the pD-fusion was introduced to counteract oligomerization.

However, even though the pD-equipped POI refolded via the favored refolding condition looked rather good in all described tests, indicating the presence of the properly folded trastuzumab epitope in a soluble monomeric protein without any free thiols, the 1D proton spectrum recorded in ^{1}H NMR indicated that the refolded protein was still rather inhomogeneously folded (

Figure 5.9:).

As structural studies like protein X-ray crystallography require highly homogeneous protein material, the efforts to *in vitro* refold HER2_IV as starting material for crystallization screens with DARPin H14 were shelved at that time.

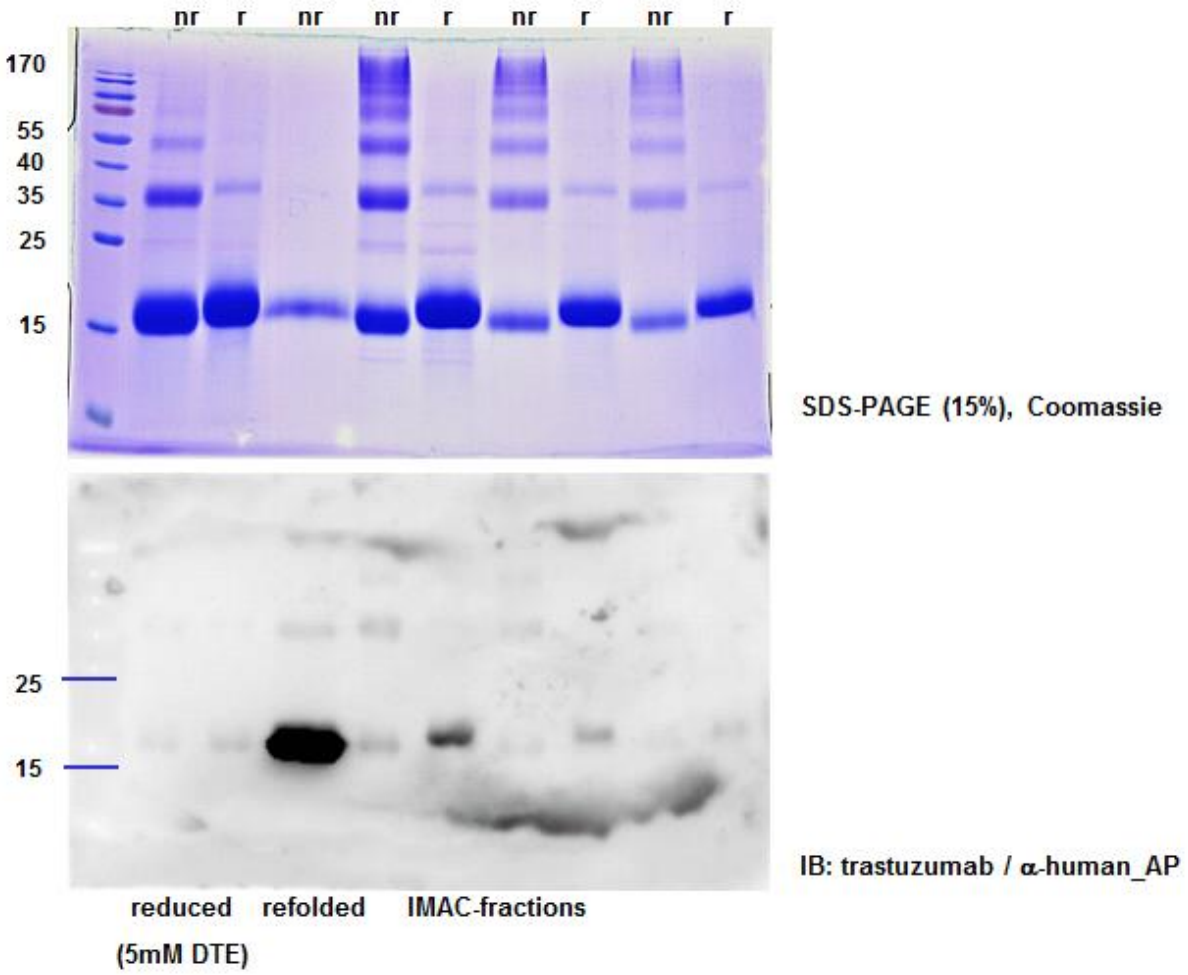

Figure 5.4: HER2_IV from inclusion bodies in SDS-PAGE and trastuzumab-IB. HER2_IV_A488-L629 expressed in *E. coli* XL1 blue was IMAC-purified from inclusion bodies and subjected to *in vitro* refolding by rapid dilution. For analysis, reduced (r) or non-reduced (nr) samples were loaded on 15% SDS-PAGE gels before ("IMAC-fractions") or after in vitro refolding. Gels were either Coomassie-stained or subjected to immunoblotting using trastuzumab as primary antibody and anti-human_AP as secondary antibody.

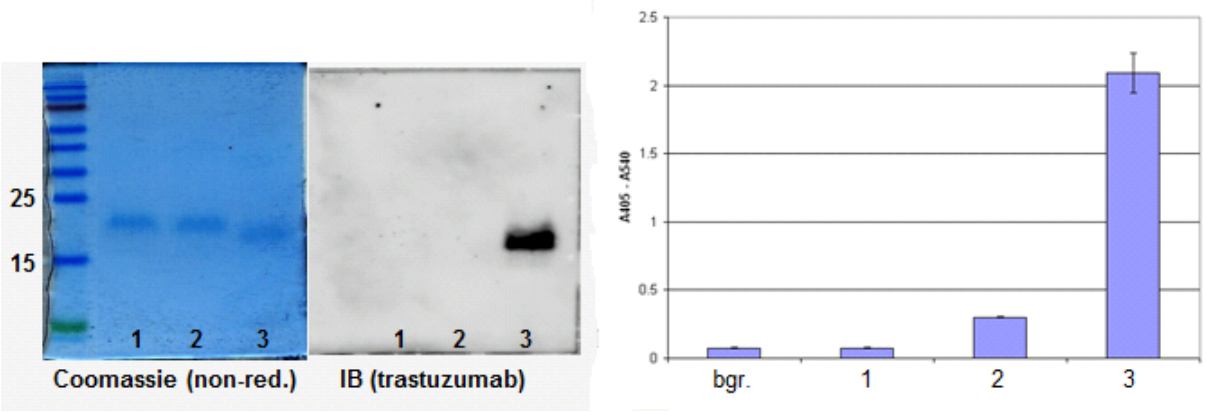

Figure 5.5: Effect of the redox-shuffling system on refolding of the trastuzumab epitope. HER2_IV_A488-L629 was refolded in refolding buffer (25 mM Tris/HCl, pH 8.6; 100 mM NaCl; 10% glycerol; 0.5 M L-Arg) without GSH/GSSH (1), or in the presence of 1.25 mM GSH : 0.25 mM GSSG (2) or 0.25 mM GSH : 1.25 mM GSSG (3). Refolded protein from different refolding conditions was then analysed by SDS-PAGE (left), trastuzumab IB (middle) and ELISA (with trastuzumab as primary antibody) (right).

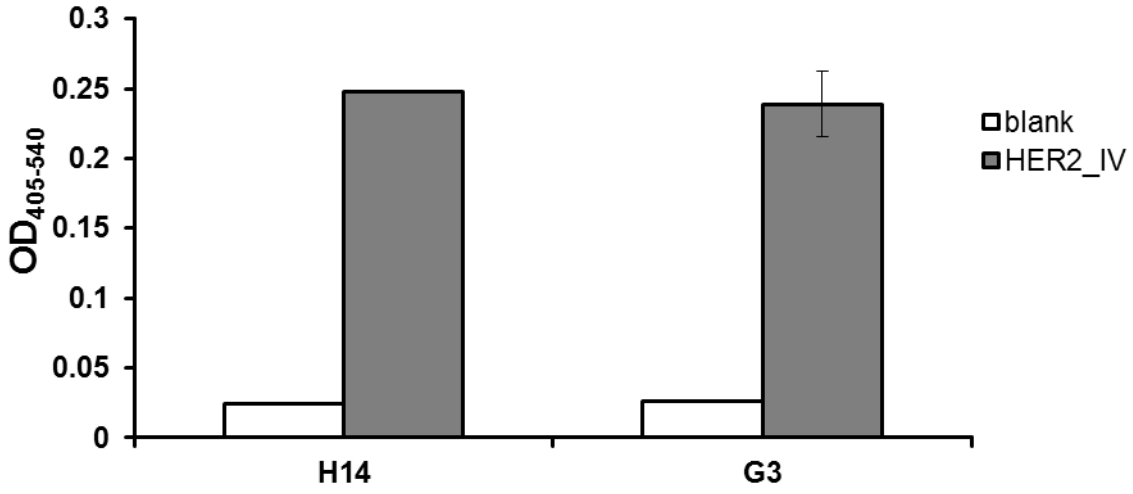

Figure 5.6: ELISA with DARPins H14 and G3 binding to refolded HER2_IV_A488-L629. HER2_IV_A488-L629 was refolded in refolding buffer (25 mM Tris/HCl, pH 8.6; 100 mM NaCl; 10% glycerol; 0.5 M L-Arg; 0.25 mM GSH; 1.25 mM GSSG).

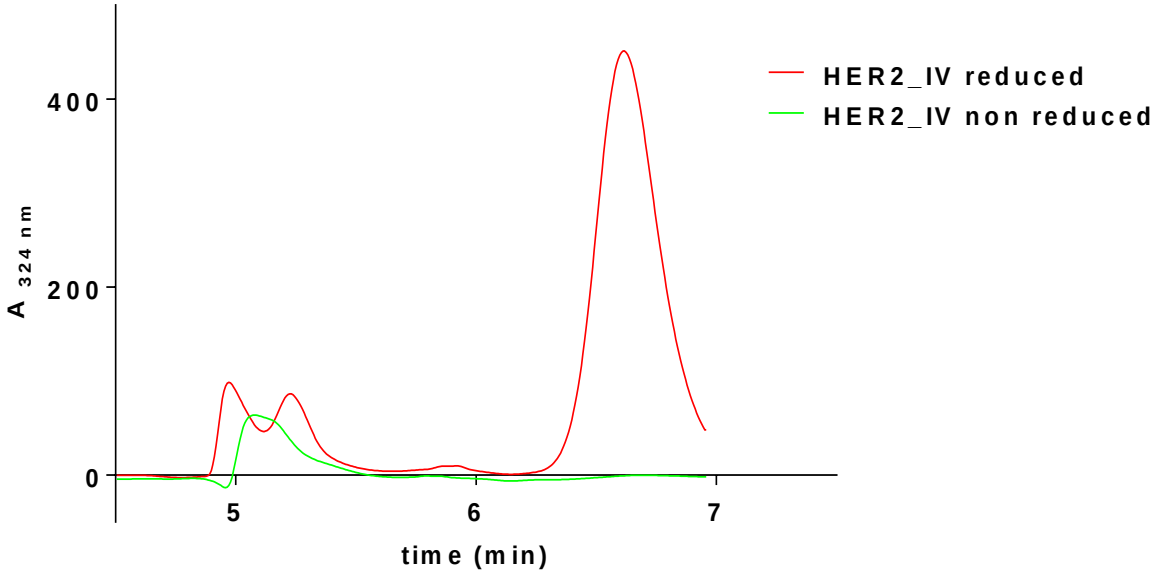

Figure 5.7: HPLC run from a DPS-assay for quantification of free thiols in refolded HER2_IV_A488-L629. In orer to quantify the free thiol, 280 pmol of refolded and dialyzed HER2_IV was incubated with 0.36 mM 4-DPS (4.4'-dithiodipyridine), 6 M urea, 0.2 mM EDTA, and 0.1 M citrate at pH 4.5 for 30 min before HPLC analysis. For quantification of the total amount of thiol, an equal amount of HER2_IV was treated with 30% (w/v) alkaline sodium borohydride (BH) and incubated at 50°C for 30 min to reduce all disulfide bonds. Prior to quantification with DPS, all BH was destroyed by the addition of 1.8 M HCl. The peak eluting after 6' 30'' in the reduced sample ("HER2_IV reduced") corresponds to 4-thiopyridone stoichiometrically released in the reaction of 4-DPS with the thiols reduced on purpose. According to the DPS-assay, the original refolded HER2_IV ("HER2_IV non reduced") does not contain any free thiols. The peaks eluting early at 5 min are irrelevant solvent peaks (reported by Hansen et al. (2007), as well).

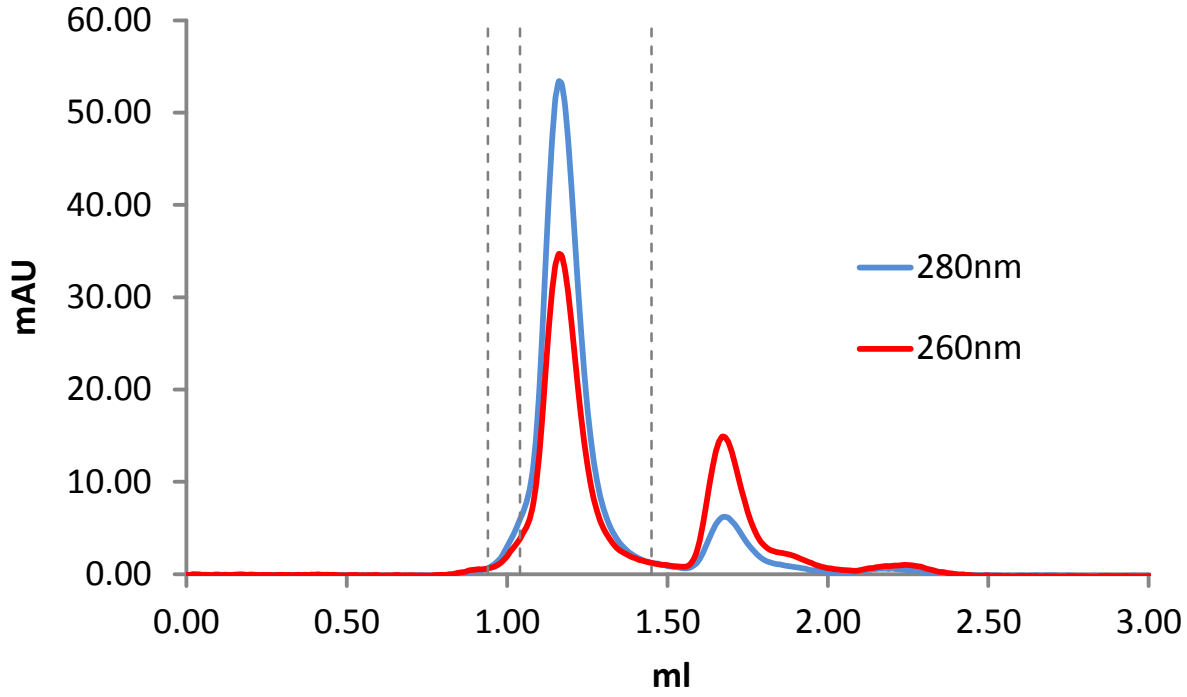

Figure 5.8: Analytical Size Exclusion Chromatography (SEC) with pD_HER2_IV_A488-L629, refolded by rapid dilution. Absorbance at 280 nm (blue line) and 260 mm (red line) is shown. Elution volumes of the molecular weight standard consisting of BSA (66 kDa), SHP (50 kDa) and cytochrome c (12.4 kDa) are indicated in gray dotted lines. The peak eluting at about 1.75 ml is most probably composed of remains from the refolding buffer.

Table 5.3: Summary of apparent and expected molecular weights of pD_HER2_IV_A488-L629 calculated from the SEC-run shown in Figure 5.8:.

sample	retention volume (ml)	MW_{app} (kDa)	MW_{seq} (kDa)
pD_HER2_IV_A488-L629	1.18	31.4	27.8

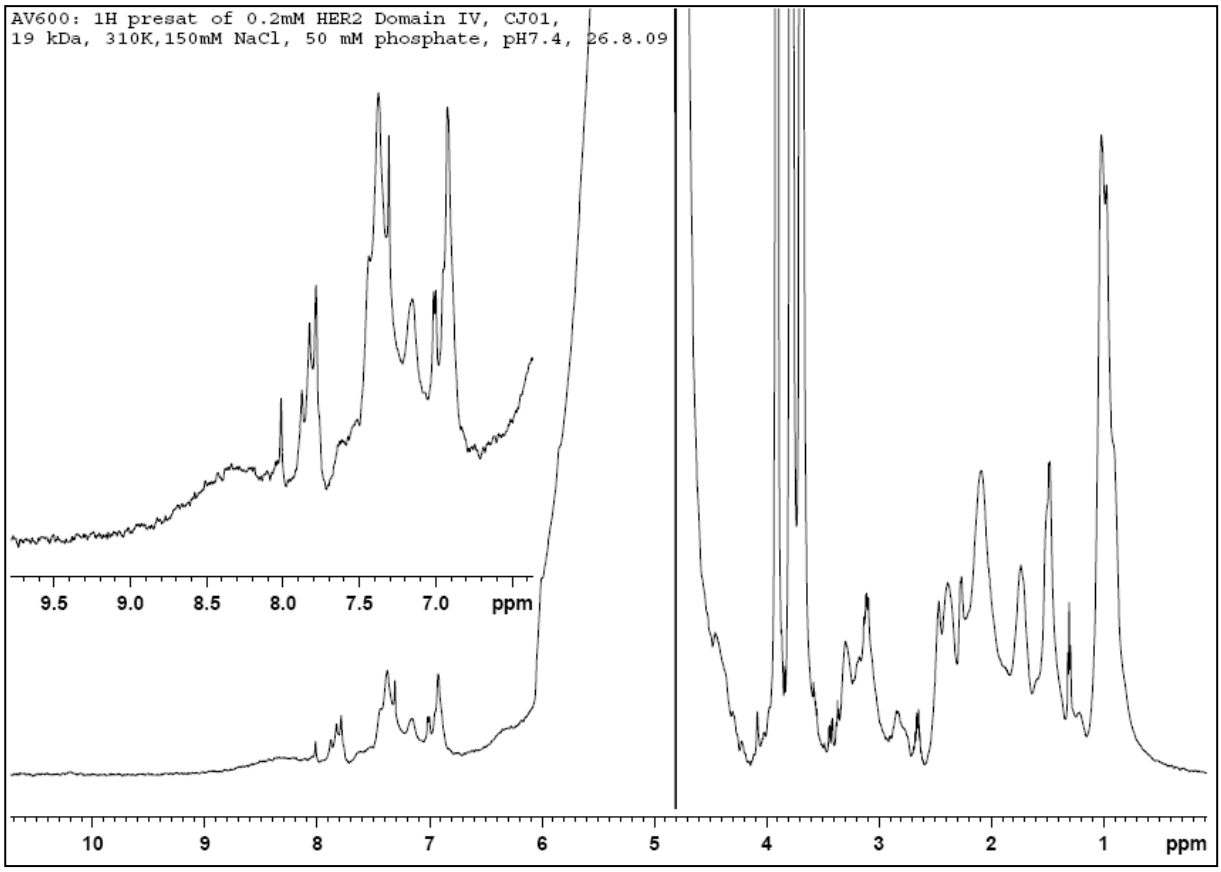

Figure 5.9: ^{1}H-NMR spectrum of refolded HER2_IV_A488-L629 (recorded by C. Ewald). 500 µl of a 200 µM protein solution in PBS_{150} were mixed with 10% D2O and measured using a Baker AV-700 MHz spectrometer. The recorded spectrum shows no peaks beyond 8.5 ppm, indicating that the protein is rather inhomogeneously folded. The 1D proton spectrum of a homogeneously folded protein should contain a cluster of peaks (derived from methylprotons) around 1 ppm and another cluster of peaks above 8.5 ppm (derived from amide protons).

3.2 Refolding of further extracellular HER2-subdomains

Besides the efforts to obtain properly folded HER2_IV for structural studies with DARPins H14 and G3, known to bind HER2_IV, the need for an at least rough epitope mapping of the anti-HER2 DARPins known to bind within HER2 domains I-III became apparent as soon as those DARPins were found to build powerful bispecific constructs (detailed in and **Chapter 4**). In order to allow an epitope mapping – at least on the domain level, the coding sequences for the three extracellular subdomains I, II and III of HER2 were subcloned via ligation-independent cloning (LIC) into the vector pEa_HP-lacIq-T5-avi-gpD-his6 (ID eLIC_043, kindly provided by Yvonne Neldner) yielding POIs with N-terminal Avi-, pD- and His_6-tag for cytoplasmatic expression in *E. coli*. Proteins were purified from inclusion bodies and refolded via dialysis in refolding buffer containing 25 mM Tris/HCl, pH 8.5; 100 mM NaCl; 10% glycerol; 0.5 M L-Arg; 0.25 mM GSH and 1.25 mM GSSG.

Refolded HER2 domains were used for epitope estimation studies of HER2-binding DARPins from phage display selections on HER2_I-III. For this, a competition ELISA set-up was chosen with DARPin-binding to immobilized HER2_ECD ("$HER2\_623_{biot}$" used for initial selection) being competed with the refolded HER2 domains. **Figure 5.10**: shows the result of a competition ELISA performed with 25 nM DARPin competed with 1 µM refolded domain for binding to $HER2\_623_{biot}$, immobilized on neutravidin coated wells. Comparison of the signals from competition mixtures with the signals obtained from non-competed binding suggests that all binders except DARPin H14 might bind HER2_I.

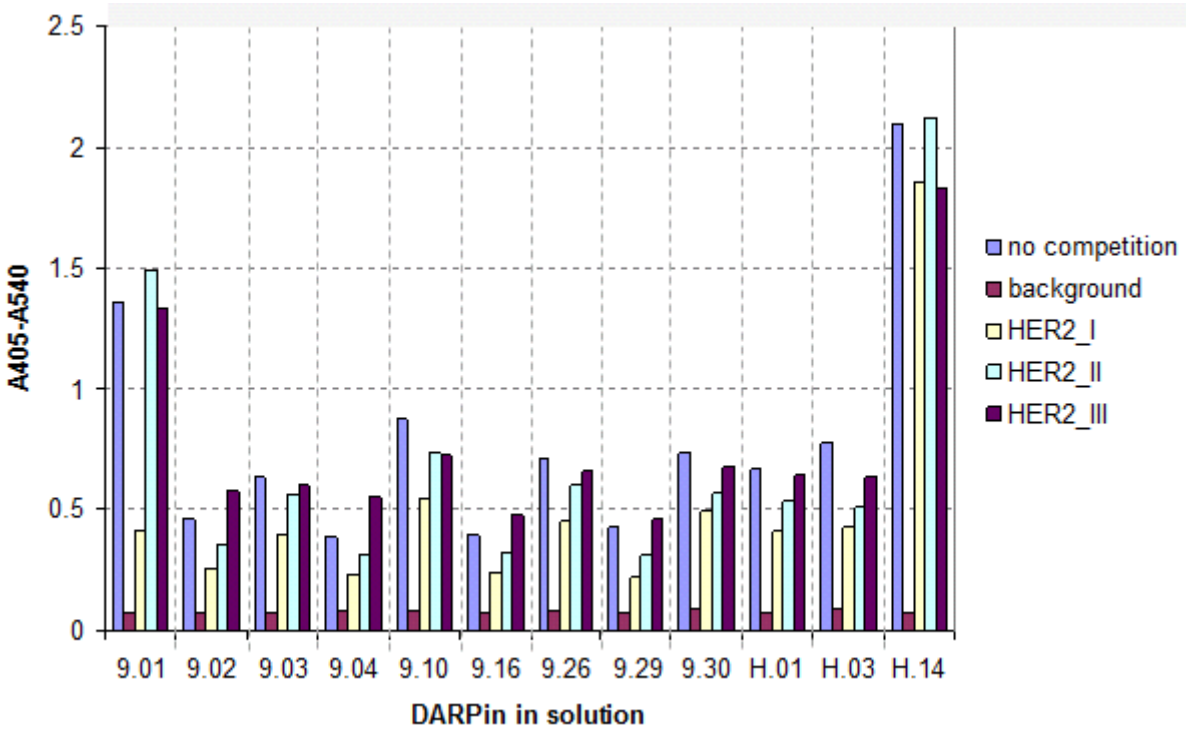

Figure 5.10: Competition ELISA with HER2-binding DARPins competed by different refolded HER2 domains. 25 nM solutions of HER2 binders were preincubated for 1 h at RT either without ("no competition") or with 1 µM of the respective refolded HER2 domains. Precincubated volumes were than applied to an ELISA with immobilized HER2_ECD (coated with 100 µl of a 15 nM solution per well on neutravidin-precoated plates).

3.3 Chemical Linkage of Peptides onto Scaffolds (CLiPS)

Besides the above-mentioned refolding trials of the extracellular HER2-subdomains, one further technique of conformational epitope-mapping, namely CLiPS (Chemical Linkage of Peptides onto Scaffolds) (Timmerman *et al.* (2005)), was tested in a collaboration with Pepscan Presto BV, Inc.

The CLiPS-methodology (CLIPScan™) involves cyclization of small linear peptides (20-30 aa) with two or three cysteines via reaction with a small synthetic entity carrying reactive benzyl bromides.

In our case, 5000 different HER2-CLIPS peptides, covering the whole HER2_ECD, were synthesized and immobilized onto chips. DARPin binding was tested at 1 µg/ml (~ 55 nM) in PBS containing 1% Tween, followed by detection of the DARPins' His-tag via primary and secondary antibodies.

Unfortunately, the CLIPScan-method did not provide useful data for any of the tested HER2-binding DARPins. Even though the positive control (trastuzumab) had worked nicely on the generated HER2-CLIPS-library, the epitope mapping for the DARPins was inconsistent with data from ELISA-measurements, that had e.g. shown binding of the 9.xx-DARPins to HER2_I but not to HER2_III (data, that was later confirmed by X-ray crystallography). One possible explanation for this inconsistency might lie in the high stability of the DARPins: Within the screening procedure, the chips containing the HER2-peptide-library are usually reused for several binders after a thorough stripping-step. It is likely that some of the bound DARPins resisted that stripping and remained bound to the chip. However, this would not explain another inconsistency, which is the CLIPScan-mapping of e.g. the DARPin 9_26 epitope to a region on HER2 subdomain III. Since accoding to today's knowledge, based on data from ELISA, SEC and X-ray crystallography, none of the known HER2-binding DARPins has its epitope on HER2_III, this CLIPScan-output is cleary wrong. It remains to be seen, if the CLIPScan-technology might be used for epitope mapping of DARPins with other targets.

In the case of the HER2-binding DARPins the approach yielding cleary the most reliable epitope data has proven to be the expression of single HER2_ECD subdomains, followed by ELISA (cf. **Chapter 2** and **Appendix 3**) and crystallization (cf. **Chapter 2**).

3.4 Xtal- conditions screened

The most interesting HER2-binding DARPins proved to be DARPins 9_26 and 9_29, binding to HER2_I, and DARPins G3 and H_14, binding to HER2_IV, as described above. As **Chapter 3** only lists the crystallization conditions which finally yielded the well diffracting crystals, but by far not all conditions screened, the following section is supposed to supplement this information.

Besides screening different putative crystallization conditions (listed in **Table 5.4**: to **Table 5.11**:), different formats both of the respective DARPin (e.g. old C-cap, new C-cap, chimeric versions) or its domain (e.g. glycosylated, non-glycosylated, single or fused domains) were tested.

In general, all different SEC-purified DARPin:target complexes to be tested in the crystallization screens were brought to concentrations of 8 to 12 g/l in TBS_{150} and then screened in sitting drops with three drops per condition (usually 100+100, 200+100 and 100+200 [nl protein solution + nl mother liquor]).

Table 5.4: Grid screen "GS001" used for primary screening of crystallization conditions.

		Salt			Buffer			Precipitant		
Well	**pH**	**Value**	**Units**	**Name**	**Value**	**Units**	**Name**	**Value**	**Units**	**Name**
A01	3	0.2	M	Li_2SO_4	0.1	M	malonic acid	5	% w/v	PEG 4000
A02	3	0.2	M	Li_2SO_4	0.1	M	malonic acid	10	% w/v	PEG 4000
A03	3	0.2	M	Li_2SO_4	0.1	M	malonic acid	15	% w/v	PEG 4000
A04	3	0.2	M	Li_2SO_4	0.1	M	malonic acid	20	% w/v	PEG 4000
A05	3	0.2	M	Li_2SO_4	0.1	M	malonic acid	25	% w/v	PEG 4000
A06	3	0.2	M	Li_2SO_4	0.1	M	malonic acid	30	% w/v	PEG 4000
A07	3				0.1	M	malonic acid	5	% w/v	PEG 8000
A08	3				0.1	M	malonic acid	10	% w/v	PEG 8000
A09	3				0.1	M	malonic acid	15	% w/v	PEG 8000
A10	3				0.1	M	malonic acid	20	% w/v	PEG 8000
A11	3				0.1	M	malonic acid	25	% w/v	PEG 8000
A12	3				0.1	M	malonic acid	30	% w/v	PEG 8000
B01	4	0.2	M	Li_2SO_4	0.05	M	succinic acid	5	% w/v	PEG 4000
B02	4	0.2	M	Li_2SO_4	0.05	M	succinic acid	10	% w/v	PEG 4000
B03	4	0.2	M	Li_2SO_4	0.05	M	succinic acid	15	% w/v	PEG 4000
B04	4	0.2	M	Li_2SO_4	0.05	M	succinic acid	20	% w/v	PEG 4000
B05	4	0.2	M	Li_2SO_4	0.05	M	succinic acid	25	% w/v	PEG 4000
B06	4	0.2	M	Li_2SO_4	0.05	M	succinic acid	30	% w/v	PEG 4000
B07	4				0.05	M	succinic acid	5	% w/v	PEG 8000
B08	4				0.05	M	succinic acid	10	% w/v	PEG 8000
B09	4				0.05	M	succinic acid	15	% w/v	PEG 8000
B10	4				0.05	M	succinic acid	20	% w/v	PEG 8000
B11	4				0.05	M	succinic acid	25	% w/v	PEG 8000
B12	4				0.05	M	succinic acid	30	% w/v	PEG 8000
C01	5	0.2	M	Li_2SO_4	0.1	M	citric acid	5	% w/v	PEG 4000
C02	5	0.2	M	Li_2SO_4	0.1	M	citric acid	10	% w/v	PEG 4000
C03	5	0.2	M	Li_2SO_4	0.1	M	citric acid	15	% w/v	PEG 4000
C04	5	0.2	M	Li_2SO_4	0.1	M	citric acid	20	% w/v	PEG 4000
C05	5	0.2	M	Li_2SO_4	0.1	M	citric acid	25	% w/v	PEG 4000
C06	5	0.2	M	Li_2SO_4	0.1	M	citric acid	30	% w/v	PEG 4000
C07	5				0.1	M	citric acid	5	% w/v	PEG 8000
C08	5				0.1	M	citric acid	10	% w/v	PEG 8000
C09	5				0.1	M	citric acid	15	% w/v	PEG 8000
C10	5				0.1	M	citric acid	20	% w/v	PEG 8000
C11	5				0.1	M	citric acid	25	% w/v	PEG 8000
C12	5				0.1	M	citric acid	30	% w/v	PEG 8000
D01	6	0.2	M	Li_2SO_4	0.1	M	MES	5	% w/v	PEG 4000
D02	6	0.2	M	Li_2SO_4	0.1	M	MES	10	% w/v	PEG 4000
D03	6	0.2	M	Li_2SO_4	0.1	M	MES	15	% w/v	PEG 4000
D04	6	0.2	M	Li_2SO_4	0.1	M	MES	20	% w/v	PEG 4000
D05	6	0.2	M	Li_2SO_4	0.1	M	MES	25	% w/v	PEG 4000
D06	6	0.2	M	Li_2SO_4	0.1	M	MES	30	% w/v	PEG 4000
D07	6				0.1	M	MES	5	% w/v	PEG 8000
D08	6				0.1	M	MES	10	% w/v	PEG 8000
D09	6				0.1	M	MES	15	% w/v	PEG 8000
D10	6				0.1	M	MES	20	% w/v	PEG 8000
D11	6				0.1	M	MES	25	% w/v	PEG 8000
D12	6				0.1	M	MES	30	% w/v	PEG 8000
E01	7	0.2	M	Li_2SO_4	0.1	M	MOPS	5	% w/v	PEG 4000
E02	7	0.2	M	Li_2SO_4	0.1	M	MOPS	10	% w/v	PEG 4000
E03	7	0.2	M	Li_2SO_4	0.1	M	MOPS	15	% w/v	PEG 4000

E04	7	0.2	M	Li_2SO_4	0.1	M	MOPS	20	% w/v	PEG 4000
E05	7	0.2	M	Li_2SO_4	0.1	M	MOPS	25	% w/v	PEG 4000
E06	7	0.2	M	Li_2SO_4	0.1	M	MOPS	30	% w/v	PEG 4000
E07	7				0.1	M	MOPS	5	% w/v	PEG 8000
E08	7				0.1	M	MOPS	10	% w/v	PEG 8000
E09	7				0.1	M	MOPS	15	% w/v	PEG 8000
E10	7				0.1	M	MOPS	20	% w/v	PEG 8000
E11	7				0.1	M	MOPS	25	% w/v	PEG 8000
E12	7				0.1	M	MOPS	30	% w/v	PEG 8000
F01	8	0.2	M	Li_2SO_4	0.1	M	HEPES	5	% w/v	PEG 4000
F02	8	0.2	M	Li_2SO_4	0.1	M	HEPES	10	% w/v	PEG 4000
F03	8	0.2	M	Li_2SO_4	0.1	M	HEPES	15	% w/v	PEG 4000
F04	8	0.2	M	Li_2SO_4	0.1	M	HEPES	20	% w/v	PEG 4000
F05	8	0.2	M	Li_2SO_4	0.1	M	HEPES	25	% w/v	PEG 4000
F06	8	0.2	M	Li_2SO_4	0.1	M	HEPES	30	% w/v	PEG 4000
F07	8				0.1	M	HEPES	5	% w/v	PEG 8000
F08	8				0.1	M	HEPES	10	% w/v	PEG 8000
F09	8				0.1	M	HEPES	15	% w/v	PEG 8000
F10	8				0.1	M	HEPES	20	% w/v	PEG 8000
F11	8				0.1	M	HEPES	25	% w/v	PEG 8000
F12	8				0.1	M	HEPES	30	% w/v	PEG 8000
G01	9	0.2	M	Li_2SO_4	0.02	M	TAPS	5	% w/v	PEG 4000
G02	9	0.2	M	Li_2SO_4	0.02	M	TAPS	10	% w/v	PEG 4000
G03	9	0.2	M	Li_2SO_4	0.02	M	TAPS	15	% w/v	PEG 4000
G04	9	0.2	M	Li_2SO_4	0.02	M	TAPS	20	% w/v	PEG 4000
G05	9	0.2	M	Li_2SO_4	0.02	M	TAPS	25	% w/v	PEG 4000
G06	9	0.2	M	Li_2SO_4	0.02	M	TAPS	30	% w/v	PEG 4000
G07	9				0.02	M	TAPS	5	% w/v	PEG 8000
G08	9				0.02	M	TAPS	10	% w/v	PEG 8000
G09	9				0.02	M	TAPS	15	% w/v	PEG 8000
G10	9				0.02	M	TAPS	20	% w/v	PEG 8000
G11	9				0.02	M	TAPS	25	% w/v	PEG 8000
G12	9				0.02	M	TAPS	30	% w/v	PEG 8000
H01	10	0.2	M	Li_2SO_4	0.02	M	CAPS	5	% w/v	PEG 4000
H02	10	0.2	M	Li_2SO_4	0.02	M	CAPS	10	% w/v	PEG 4000
H03	10	0.2	M	Li_2SO_4	0.02	M	CAPS	15	% w/v	PEG 4000
H04	10	0.2	M	Li_2SO_4	0.02	M	CAPS	20	% w/v	PEG 4000
H05	10	0.2	M	Li_2SO_4	0.02	M	CAPS	25	% w/v	PEG 4000
H06	10	0.2	M	Li_2SO_4	0.02	M	CAPS	30	% w/v	PEG 4000
H07	10				0.02	M	CAPS	5	% w/v	PEG 8000
H08	10				0.02	M	CAPS	10	% w/v	PEG 8000
H09	10				0.02	M	CAPS	15	% w/v	PEG 8000
H10	10				0.02	M	CAPS	20	% w/v	PEG 8000
H11	10				0.02	M	CAPS	25	% w/v	PEG 8000
H12	10				0.02	M	CAPS	30	% w/v	PEG 8000

Table 5.5: Grid screen "GS002" used for primary screening of crystallization conditions.

		Salt			Buffer			Precipitant		
Well	**pH**	**Value**	**Units**	**Name**	**Value**	**Units**	**Name**	**Value**	**Units**	**Name**
A01	3				0.1	M	malonic acid	15	%	$(NH_4)_2SO_4$ (at 4°C saturated)
A02	3				0.1	M	malonic acid	20	%	$(NH_4)_2SO_4$ (at 4°C saturated)
A03	3				0.1	M	malonic acid	25	%	$(NH_4)_2SO_4$ (at 4°C saturated)
A04	3				0.1	M	malonic acid	30	%	$(NH_4)_2SO_4$ (at 4°C saturated)
A05	3				0.1	M	malonic acid	35	%	$(NH_4)_2SO_4$ (at 4°C saturated)
A06	3				0.1	M	malonic acid	40	%	$(NH_4)_2SO_4$ (at 4°C saturated)
A07	3				0.1	M	malonic acid	45	%	$(NH_4)_2SO_4$ (at 4°C saturated)
A08	3				0.1	M	malonic acid	50	%	$(NH_4)_2SO_4$ (at 4°C saturated)
A09	3				0.1	M	malonic acid	55	%	$(NH_4)_2SO_4$ (at 4°C saturated)
A10	3				0.1	M	malonic acid	60	%	$(NH_4)_2SO_4$ (at 4°C saturated)
A11	3				0.1	M	malonic acid	70	%	$(NH_4)_2SO_4$ (at 4°C saturated)
A12	3				0.1	M	malonic acid	80	%	$(NH_4)_2SO_4$ (at 4°C saturated)
B01	4				0.05	M	succinic acid	15	%	$(NH_4)_2SO_4$ (at 4°C saturated)
B02	4				0.05	M	succinic acid	20	%	$(NH_4)_2SO_4$ (at 4°C saturated)
B03	4				0.05	M	succinic acid	25	%	$(NH_4)_2SO_4$ (at 4°C saturated)
B04	4				0.05	M	succinic acid	30	%	$(NH_4)_2SO_4$ (at 4°C saturated)
B05	4				0.05	M	succinic acid	35	%	$(NH_4)_2SO_4$ (at 4°C saturated)
B06	4				0.05	M	succinic acid	40	%	$(NH_4)_2SO_4$ (at 4°C saturated)
B07	4				0.05	M	succinic acid	45	%	$(NH_4)_2SO_4$ (at 4°C saturated)
B08	4				0.05	M	succinic acid	50	%	$(NH_4)_2SO_4$ (at 4°C saturated)
B09	4				0.05	M	succinic acid	55	%	$(NH_4)_2SO_4$ (at 4°C saturated)
B10	4				0.05	M	succinic acid	60	%	$(NH_4)_2SO_4$ (at 4°C saturated)
B11	4				0.05	M	succinic acid	70	%	$(NH_4)_2SO_4$ (at 4°C saturated)
B12	4				0.05	M	succinic acid	80	%	$(NH_4)_2SO_4$ (at 4°C saturated)
C01	5				0.1	M	citric acid	15	%	$(NH_4)_2SO_4$ (at 4°C saturated)
C02	5				0.1	M	citric acid	20	%	$(NH_4)_2SO_4$ (at 4°C saturated)
C03	5				0.1	M	citric acid	25	%	$(NH_4)_2SO_4$ (at 4°C saturated)
C04	5				0.1	M	citric acid	30	%	$(NH_4)_2SO_4$ (at 4°C saturated)
C05	5				0.1	M	citric acid	35	%	$(NH_4)_2SO_4$ (at 4°C saturated)
C06	5				0.1	M	citric acid	40	%	$(NH_4)_2SO_4$ (at 4°C saturated)
C07	5				0.1	M	citric acid	45	%	$(NH_4)_2SO_4$ (at 4°C saturated)
C08	5				0.1	M	citric acid	50	%	$(NH_4)_2SO_4$ (at 4°C saturated)
C09	5				0.1	M	citric acid	55	%	$(NH_4)_2SO_4$ (at 4°C saturated)
C10	5				0.1	M	citric acid	60	%	$(NH_4)_2SO_4$ (at 4°C saturated)
C11	5				0.1	M	citric acid	70	%	$(NH_4)_2SO_4$ (at 4°C saturated)
C12	5				0.1	M	citric acid	80	%	$(NH_4)_2SO_4$ (at 4°C saturated)
D01	6				0.1	M	MES	15	%	$(NH_4)_2SO_4$ (at 4°C saturated)
D02	6				0.1	M	MES	20	%	$(NH_4)_2SO_4$ (at 4°C saturated)
D03	6				0.1	M	MES	25	%	$(NH_4)_2SO_4$ (at 4°C saturated)
D04	6				0.1	M	MES	30	%	$(NH_4)_2SO_4$ (at 4°C saturated)
D05	6				0.1	M	MES	35	%	$(NH_4)_2SO_4$ (at 4°C saturated)
D06	6				0.1	M	MES	40	%	$(NH_4)_2SO_4$ (at 4°C saturated)
D07	6				0.1	M	MES	45	%	$(NH_4)_2SO_4$ (at 4°C saturated)
D08	6				0.1	M	MES	50	%	$(NH_4)_2SO_4$ (at 4°C saturated)
D09	6				0.1	M	MES	55	%	$(NH_4)_2SO_4$ (at 4°C saturated)
D10	6				0.1	M	MES	60	%	$(NH_4)_2SO_4$ (at 4°C saturated)
D11	6				0.1	M	MES	70	%	$(NH_4)_2SO_4$ (at 4°C saturated)
D12	6				0.1	M	MES	80	%	$(NH_4)_2SO_4$ (at 4°C saturated)
E01	7				0.1	M	MOPS	15	%	$(NH_4)_2SO_4$ (at 4°C saturated)
E02	7				0.1	M	MOPS	20	%	$(NH_4)_2SO_4$ (at 4°C saturated)
E03	7				0.1	M	MOPS	25	%	$(NH_4)_2SO_4$ (at 4°C saturated)

E04	7	0.1	M	MOPS	30	%	$(NH_4)_2SO_4$ (at 4°C saturated)
E05	7	0.1	M	MOPS	35	%	$(NH_4)_2SO_4$ (at 4°C saturated)
E06	7	0.1	M	MOPS	40	%	$(NH_4)_2SO_4$ (at 4°C saturated)
E07	7	0.1	M	MOPS	45	%	$(NH_4)_2SO_4$ (at 4°C saturated)
E08	7	0.1	M	MOPS	50	%	$(NH_4)_2SO_4$ (at 4°C saturated)
E09	7	0.1	M	MOPS	55	%	$(NH_4)_2SO_4$ (at 4°C saturated)
E10	7	0.1	M	MOPS	60	%	$(NH_4)_2SO_4$ (at 4°C saturated)
E11	7	0.1	M	MOPS	70	%	$(NH_4)_2SO_4$ (at 4°C saturated)
E12	7	0.1	M	MOPS	80	%	$(NH_4)_2SO_4$ (at 4°C saturated)
F01	8	0.1	M	HEPES	15	%	$(NH_4)_2SO_4$ (at 4°C saturated)
F02	8	0.1	M	HEPES	20	%	$(NH_4)_2SO_4$ (at 4°C saturated)
F03	8	0.1	M	HEPES	25	%	$(NH_4)_2SO_4$ (at 4°C saturated)
F04	8	0.1	M	HEPES	30	%	$(NH_4)_2SO_4$ (at 4°C saturated)
F05	8	0.1	M	HEPES	35	%	$(NH_4)_2SO_4$ (at 4°C saturated)
F06	8	0.1	M	HEPES	40	%	$(NH_4)_2SO_4$ (at 4°C saturated)
F07	8	0.1	M	HEPES	45	%	$(NH_4)_2SO_4$ (at 4°C saturated)
F08	8	0.1	M	HEPES	50	%	$(NH_4)_2SO_4$ (at 4°C saturated)
F09	8	0.1	M	HEPES	55	%	$(NH_4)_2SO_4$ (at 4°C saturated)
F10	8	0.1	M	HEPES	60	%	$(NH_4)_2SO_4$ (at 4°C saturated)
F11	8	0.1	M	HEPES	70	%	$(NH_4)_2SO_4$ (at 4°C saturated)
F12	8	0.1	M	HEPES	80	%	$(NH_4)_2SO_4$ (at 4°C saturated)
G01	9	0.02	M	TAPS	15	%	$(NH_4)_2SO_4$ (at 4°C saturated)
G02	9	0.02	M	TAPS	20	%	$(NH_4)_2SO_4$ (at 4°C saturated)
G03	9	0.02	M	TAPS	25	%	$(NH_4)_2SO_4$ (at 4°C saturated)
G04	9	0.02	M	TAPS	30	%	$(NH_4)_2SO_4$ (at 4°C saturated)
G05	9	0.02	M	TAPS	35	%	$(NH_4)_2SO_4$ (at 4°C saturated)
G06	9	0.02	M	TAPS	40	%	$(NH_4)_2SO_4$ (at 4°C saturated)
G07	9	0.02	M	TAPS	45	%	$(NH_4)_2SO_4$ (at 4°C saturated)
G08	9	0.02	M	TAPS	50	%	$(NH_4)_2SO_4$ (at 4°C saturated)
G09	9	0.02	M	TAPS	55	%	$(NH_4)_2SO_4$ (at 4°C saturated)
G10	9	0.02	M	TAPS	60	%	$(NH_4)_2SO_4$ (at 4°C saturated)
G11	9	0.02	M	TAPS	70	%	$(NH_4)_2SO_4$ (at 4°C saturated)
G12	9	0.02	M	TAPS	80	%	$(NH_4)_2SO_4$ (at 4°C saturated)
H01	10	0.02	M	CAPS	15	%	$(NH_4)_2SO_4$ (at 4°C saturated)
H02	10	0.02	M	CAPS	20	%	$(NH_4)_2SO_4$ (at 4°C saturated)
H03	10	0.02	M	CAPS	25	%	$(NH_4)_2SO_4$ (at 4°C saturated)
H04	10	0.02	M	CAPS	30	%	$(NH_4)_2SO_4$ (at 4°C saturated)
H05	10	0.02	M	CAPS	35	%	$(NH_4)_2SO_4$ (at 4°C saturated)
H06	10	0.02	M	CAPS	40	%	$(NH_4)_2SO_4$ (at 4°C saturated)
H07	10	0.02	M	CAPS	45	%	$(NH_4)_2SO_4$ (at 4°C saturated)
H08	10	0.02	M	CAPS	50	%	$(NH_4)_2SO_4$ (at 4°C saturated)
H09	10	0.02	M	CAPS	55	%	$(NH_4)_2SO_4$ (at 4°C saturated)
H10	10	0.02	M	CAPS	60	%	$(NH_4)_2SO_4$ (at 4°C saturated)
H11	10	0.02	M	CAPS	70	%	$(NH_4)_2SO_4$ (at 4°C saturated)
H12	10	0.02	M	CAPS	80	%	$(NH_4)_2SO_4$ (at 4°C saturated)

Table 5.6: Grid screen "GS003" used for primary screening of crystallization conditions.

		Salt			Buffer			Precipitant		
Well	**pH**	**Value**	**Units**	**Name**	**Value**	**Units**	**Name**	**Value**	**Units**	**Name**
A01	3	0.2	M	Li_2SO_4	0.1	M	malonic acid	5	% w/v	PEG 4000
A02	3	0.2	M	Li_2SO_4	0.1	M	malonic acid	10	% w/v	PEG 4000
A03	3	0.2	M	Li_2SO_4	0.1	M	malonic acid	15	% w/v	PEG 4000
A04	3	0.2	M	Li_2SO_4	0.1	M	malonic acid	20	% w/v	PEG 4000
A05	3	0.2	M	Li_2SO_4	0.1	M	malonic acid	25	% w/v	PEG 4000
A06	3	0.2	M	Li_2SO_4	0.1	M	malonic acid	30	% w/v	PEG 4000
A07	3				0.1	M	malonic acid	5	% w/v	PEG 6000
A08	3				0.1	M	malonic acid	10	% w/v	PEG 6000
A09	3				0.1	M	malonic acid	15	% w/v	PEG 6000
A10	3				0.1	M	malonic acid	20	% w/v	PEG 6000
A11	3				0.1	M	malonic acid	25	% w/v	PEG 6000
A12	3				0.1	M	malonic acid	30	% w/v	PEG 6000
B01	4	0.2	M	Li_2SO_4	0.05	M	succinic acid	5	% w/v	PEG 4000
B02	4	0.2	M	Li_2SO_4	0.05	M	succinic acid	10	% w/v	PEG 4000
B03	4	0.2	M	Li_2SO_4	0.05	M	succinic acid	15	% w/v	PEG 4000
B04	4	0.2	M	Li_2SO_4	0.05	M	succinic acid	20	% w/v	PEG 4000
B05	4	0.2	M	Li_2SO_4	0.05	M	succinic acid	25	% w/v	PEG 4000
B06	4	0.2	M	Li_2SO_4	0.05	M	succinic acid	30	% w/v	PEG 4000
B07	4				0.05	M	succinic acid	5	% w/v	PEG 6000
B08	4				0.05	M	succinic acid	10	% w/v	PEG 6000
B09	4				0.05	M	succinic acid	15	% w/v	PEG 6000
B10	4				0.05	M	succinic acid	20	% w/v	PEG 6000
B11	4				0.05	M	succinic acid	25	% w/v	PEG 6000
B12	4				0.05	M	succinic acid	30	% w/v	PEG 6000
C01	5	0.2	M	Li_2SO_4	0.1	M	citric acid	5	% w/v	PEG 4000
C02	5	0.2	M	Li_2SO_4	0.1	M	citric acid	10	% w/v	PEG 4000
C03	5	0.2	M	Li_2SO_4	0.1	M	citric acid	15	% w/v	PEG 4000
C04	5	0.2	M	Li_2SO_4	0.1	M	citric acid	20	% w/v	PEG 4000
C05	5	0.2	M	Li_2SO_4	0.1	M	citric acid	25	% w/v	PEG 4000
C06	5	0.2	M	Li_2SO_4	0.1	M	citric acid	30	% w/v	PEG 4000
C07	5				0.1	M	citric acid	5	% w/v	PEG 6000
C08	5				0.1	M	citric acid	10	% w/v	PEG 6000
C09	5				0.1	M	citric acid	15	% w/v	PEG 6000
C10	5				0.1	M	citric acid	20	% w/v	PEG 6000
C11	5				0.1	M	citric acid	25	% w/v	PEG 6000
C12	5				0.1	M	citric acid	30	% w/v	PEG 6000
D01	6	0.2	M	Li_2SO_4	0.1	M	MES	5	% w/v	PEG 4000
D02	6	0.2	M	Li_2SO_4	0.1	M	MES	10	% w/v	PEG 4000
D03	6	0.2	M	Li_2SO_4	0.1	M	MES	15	% w/v	PEG 4000
D04	6	0.2	M	Li_2SO_4	0.1	M	MES	20	% w/v	PEG 4000
D05	6	0.2	M	Li_2SO_4	0.1	M	MES	25	% w/v	PEG 4000
D06	6	0.2	M	Li_2SO_4	0.1	M	MES	30	% w/v	PEG 4000
D07	6				0.1	M	MES	5	% w/v	PEG 6000
D08	6				0.1	M	MES	10	% w/v	PEG 6000
D09	6				0.1	M	MES	15	% w/v	PEG 6000
D10	6				0.1	M	MES	20	% w/v	PEG 6000
D11	6				0.1	M	MES	25	% w/v	PEG 6000
D12	6				0.1	M	MES	30	% w/v	PEG 6000
E01	7	0.2	M	Li_2SO_4	0.1	M	MOPS	5	% w/v	PEG 4000
E02	7	0.2	M	Li_2SO_4	0.1	M	MOPS	10	% w/v	PEG 4000
E03	7	0.2	M	Li_2SO_4	0.1	M	MOPS	15	% w/v	PEG 4000

E04	7	0.2	M	Li_2SO_4	0.1	M	MOPS	20	% w/v	PEG 4000
E05	7	0.2	M	Li_2SO_4	0.1	M	MOPS	25	% w/v	PEG 4000
E06	7	0.2	M	Li_2SO_4	0.1	M	MOPS	30	% w/v	PEG 4000
E07	7				0.1	M	MOPS	5	% w/v	PEG 6000
E08	7				0.1	M	MOPS	10	% w/v	PEG 6000
E09	7				0.1	M	MOPS	15	% w/v	PEG 6000
E10	7				0.1	M	MOPS	20	% w/v	PEG 6000
E11	7				0.1	M	MOPS	25	% w/v	PEG 6000
E12	7				0.1	M	MOPS	30	% w/v	PEG 6000
F01	8	0.2	M	Li_2SO_4	0.1	M	HEPES	5	% w/v	PEG 4000
F02	8	0.2	M	Li_2SO_4	0.1	M	HEPES	10	% w/v	PEG 4000
F03	8	0.2	M	Li_2SO_4	0.1	M	HEPES	15	% w/v	PEG 4000
F04	8	0.2	M	Li_2SO_4	0.1	M	HEPES	20	% w/v	PEG 4000
F05	8	0.2	M	Li_2SO_4	0.1	M	HEPES	25	% w/v	PEG 4000
F06	8	0.2	M	Li_2SO_4	0.1	M	HEPES	30	% w/v	PEG 4000
F07	8				0.1	M	HEPES	5	% w/v	PEG 6000
F08	8				0.1	M	HEPES	10	% w/v	PEG 6000
F09	8				0.1	M	HEPES	15	% w/v	PEG 6000
F10	8				0.1	M	HEPES	20	% w/v	PEG 6000
F11	8				0.1	M	HEPES	25	% w/v	PEG 6000
F12	8				0.1	M	HEPES	30	% w/v	PEG 6000
G01	9	0.2	M	Li_2SO_4	0.02	M	TAPS	5	% w/v	PEG 4000
G02	9	0.2	M	Li_2SO_4	0.02	M	TAPS	10	% w/v	PEG 4000
G03	9	0.2	M	Li_2SO_4	0.02	M	TAPS	15	% w/v	PEG 4000
G04	9	0.2	M	Li_2SO_4	0.02	M	TAPS	20	% w/v	PEG 4000
G05	9	0.2	M	Li_2SO_4	0.02	M	TAPS	25	% w/v	PEG 4000
G06	9	0.2	M	Li_2SO_4	0.02	M	TAPS	30	% w/v	PEG 4000
G07	9				0.02	M	TAPS	5	% w/v	PEG 6000
G08	9				0.02	M	TAPS	10	% w/v	PEG 6000
G09	9				0.02	M	TAPS	15	% w/v	PEG 6000
G10	9				0.02	M	TAPS	20	% w/v	PEG 6000
G11	9				0.02	M	TAPS	25	% w/v	PEG 6000
G12	9				0.02	M	TAPS	30	% w/v	PEG 6000
H01	10	0.2	M	Li_2SO_4	0.02	M	CAPS	5	% w/v	PEG 4000
H02	10	0.2	M	Li_2SO_4	0.02	M	CAPS	10	% w/v	PEG 4000
H03	10	0.2	M	Li_2SO_4	0.02	M	CAPS	15	% w/v	PEG 4000
H04	10	0.2	M	Li_2SO_4	0.02	M	CAPS	20	% w/v	PEG 4000
H05	10	0.2	M	Li_2SO_4	0.02	M	CAPS	25	% w/v	PEG 4000
H06	10	0.2	M	Li_2SO_4	0.02	M	CAPS	30	% w/v	PEG 4000
H07	10				0.02	M	CAPS	5	% w/v	PEG 6000
H08	10				0.02	M	CAPS	10	% w/v	PEG 6000
H09	10				0.02	M	CAPS	15	% w/v	PEG 6000
H10	10				0.02	M	CAPS	20	% w/v	PEG 6000
H11	10				0.02	M	CAPS	25	% w/v	PEG 6000
H12	10				0.02	M	CAPS	30	% w/v	PEG 6000

Table 5.7: Grid screen "GS007" used for primary screening of crystallization conditions.

		Salt			Buffer			Precipitant			
Well	**pH**	**Value**	**Units**	**Name**	**Value**	**Units**	**Name**	**Value**	**Units**	**Name**	
A01	5.5	0.3	M	Na-Acetate	0.1	M	Na-Acetate	25	%	PEG 2K MME	
A02	5.5	0.2	M	Li_2SO_4	0.1	M	Na-Acetate	25	%	PEG 2K MME	
A03	5.5	0.2	M	$MgCl_2$	0.1	M	Na-Acetate	25	%	PEG 2K MME	
A04	5.5	0.2	M	KBr	0.1	M	Na-Acetate	25	%	PEG 2K MME	
A05	5.5	0.2	M	KSCN	0.1	M	Na-Acetate	25	%	PEG 2K MME	
A06	5.5	0.8	M	Na-Formate	0.1	M	Na-Acetate	25	%	PEG 2K MME	
A07	5.5	0.3	M	Na-Acetate	0.1	M	Na-Acetate	15	%	PEG 4K	
A08	5.5	0.2	M	Li_2SO_4	0.1	M	Na-Acetate	15	%	PEG 4K	
A09	5.5	0.2	M	$MgCl_2$	0.1	M	Na-Acetate	15	%	PEG 4K	
A10	5.5	0.2	M	KBr	0.1	M	Na-Acetate	15	%	PEG 4K	
A11	5.5	0.2	M	KSCN	0.1	M	Na-Acetate	15	%	PEG 4K	
A12	5.5	0.8	M	Na-Formate	0.1	M	Na-Acetate	15	%	PEG 4K	
B01	5.5	0.3	M	Na-Acetate	0.1	M	Na-Acetate	10	%	PEG 8K	PEG 1K
B02	5.5	0.2	M	Li_2SO_4	0.1	M	Na-Acetate	10	%	PEG 8K	PEG 1K
B03	5.5	0.2	M	$MgCl_2$	0.1	M	Na-Acetate	10	%	PEG 8K	PEG 1K
B04	5.5	0.2	M	KBr	0.1	M	Na-Acetate	10	%	PEG 8K	PEG 1K
B05	5.5	0.2	M	KSCN	0.1	M	Na-Acetate	10	%	PEG 8K	PEG 1K
B06	5.5	0.8	M	Na-Formate	0.1	M	Na-Acetate	10	%	PEG 8K	PEG 1K
B06								10	%	PEG 1K	
B07	5.5	0.3	M	Na-Acetate	0.1	M	Na-Acetate	8	%	PEG 20K	PEG550 MME
B08	5.5	0.2	M	Li_2SO_4	0.1	M	Na-Acetate	8	%	PEG 20K	PEG550 MME
B09	5.5	0.2	M	$MgCl_2$	0.1	M	Na-Acetate	8	%	PEG 20K	PEG550 MME
B10	5.5	0.2	M	KBr	0.1	M	Na-Acetate	8	%	PEG 20K	PEG550 MME
B11	5.5	0.2	M	KSCN	0.1	M	Na-Acetate	8	%	PEG 20K	PEG550 MME
B12	5.5	0.8	M	Na-Formate	0.1	M	Na-Acetate	8	%	PEG 20K	PEG550 MME
C01	5.5				0.1	M	Na-Acetate	1.5	M	$(NH_4)_2SO_4$	
C02	5.5	0.8	M	Li_2SO_4	0.1	M	Na-Acetate				
C03	5.5				0.1	M	Na-Acetate	2	M	Na-Formate	
C04	5.5	0.5	M	KH_2PO_4	0.1	M	Na-Acetate				
C05	5.5	0.2	M	Ca-Acetate	0.1	M	Na-Acetate	25	%	PEG 2KMME	
C06	5.5	0.2	M	Ca-Acetate	0.1	M	Na-Acetate	15	%	PEG 4K	
C07	5.5				0.1	M	Na-Acetate	2.7	M	$(NH_4)_2SO_4$	
C08	5.5				0.1	M	Na-Acetate	1.8	M	Li2SO4	
C09	5.5				0.1	M	Na-Acetate	4	M	Na-Formate	
C10	5.5				0.1	M	Na-Acetate	1	M	KH2PO4	
C11	5.5	0.2	M	Ca-Acetate	0.1	M	Na-Acetate	10	%	PEG 8K	
C11								10	%	PEG 1K	
C12	5.5	0.2	M	Ca-Acetate	0.1	M	Na-Acetate	8	%	PEG 20K	
C12								8	%	PEG 550MME	
D01	5.5				0.1	M	Na-Acetate	40	%	MPD	
D02	5.5				0.1	M	Na-Acetate	40	%	Butane-diol	
D03	5.5	0.005	M	$CdCl_2$	0.1	M	Na-Acetate	20	%	PEG 4K	
D04	5.5	0.15	M	KSCN	0.1	M	Na-Acetate	20	%	PEG 550 MME	
D05	5.5	0.15	M	KSCN	0.1	M	Na-Acetate	20	%	PEG 600	
D06	5.5	0.15	M	KSCN	0.1	M	Na-Acetate	20	%	PEG 1.5K	
D07	5.5				0.1	M	Na-Acetate	35	%	Isopropanol	
D08	5.5				0.1	M	Na-Acetate	30	%	Jeffamine 600M	
D09	5.5	0.005	M	$NiCl_2$	0.1	M	Na-Acetate	20	%	PEG 4K	
D10	5.5	0.15	M	KSCN	0.1	M	Na-Acetate	18	%	PEG 3350	
D11	5.5	0.15	M	KSCN	0.1	M	Na-Acetate	18	%	PEG 5K MME	

D12	5.5	0.15	M	KSCN	0.1	M	Na-Acetate	15	%	PEG 6K	
E01	6.5	0.3	M	Na-Acetate	0.1	M	Na-Cacodylate	25	%	PEG 2K MME	
E02	6.5	0.2	M	Li_2SO_4	0.1	M	Na-Cacodylate	25	%	PEG 2K MME	
E03	6.5	0.2	M	$MgCl_2$	0.1	M	Na-Cacodylate	25	%	PEG 2K MME	
E04	6.5	0.2	M	KBr	0.1	M	Na-Cacodylate	25	%	PEG 2K MME	
E05	6.5	0.2	M	KSCN	0.1	M	Na-Cacodylate	25	%	PEG 2K MME	
E06	6.5	0.8	M	Na-Formate	0.1	M	Na-Cacodylate	25	%	PEG 2K MME	
E07	6.5	0.3	M	Na-Acetate	0.1	M	Na-Cacodylate	15	%	PEG 4K	
E08	6.5	0.2	M	Li_2SO_4	0.1	M	Na-Cacodylate	15	%	PEG 4K	
E09	6.5	0.2	M	$MgCl_2$	0.1	M	Na-Cacodylate	15	%	PEG 4K	
E10	6.5	0.2	M	KBr	0.1	M	Na-Cacodylate	15	%	PEG 4K	
E11	6.5	0.2	M	KSCN	0.1	M	Na-Cacodylate	15	%	PEG 4K	
E12	6.5	0.8	M	Na-Formate	0.1	M	Na-Cacodylate	15	%	PEG 4K	
F01	6.5	0.3	M	Na-Acetate	0.1	M	Na-Cacodylate	10	%	PEG 8K	PEG 1K
F02	6.5	0.2	M	Li_2SO_4	0.1	M	Na-Cacodylate	10	%	PEG 8K	PEG 1K
F03	6.5	0.2	M	$MgCl_2$	0.1	M	Na-Cacodylate	10	%	PEG 8K	PEG 1K
F04	6.5	0.2	M	KBr	0.1	M	Na-Cacodylate	10	%	PEG 8K	PEG 1K
F05	6.5	0.2	M	KSCN	0.1	M	Na-Cacodylate	10	%	PEG 8K	PEG 1K
F06	6.5	0.8	M	Na-Formate	0.1	M	Na-Cacodylate	10	%	PEG 8K	PEG 1K
F07	6.5	0.3	M	Na-Acetate	0.1	M	Na-Cacodylate	8	%	PEG 20K	PEG550 MME
F08	6.5	0.2	M	Li_2SO_4	0.1	M	Na-Cacodylate	8	%	PEG 20K	PEG550 MME
F09	6.5	0.2	M	$MgCl_2$	0.1	M	Na-Cacodylate	8	%	PEG 20K	PEG550 MME
F10	6.5	0.2	M	KBr	0.1	M	Na-Cacodylate	8	%	PEG 20K	PEG550 MME
F11	6.5	0.2	M	KSCN	0.1	M	Na-Cacodylate	8	%	PEG 20K	PEG550 MME
F12	6.5	0.8	M	Na-Formate	0.1	M	Na-Cacodylate	8	%	PEG 20K	PEG550 MME
G01	6.5				0.1	M	Na-Cacodylate	1.5	M	(NH4)2SO4	
G02	6.5	0.8	M	Li_2SO_4	0.1	M	Na-Cacodylate				
G03	6.5				0.1	M	Na-Cacodylate	2	M	Na-Formate	
G04	6.5	0.5	M	KH_2PO_4	0.1	M	Na-Cacodylate				
G05	6.5	0.2	M	Ca-Acetate	0.1	M	Na-Cacodylate	25	%	PEG 2KMME	
G06	6.5	0.2	M	Ca-Acetate	0.1	M	Na-Cacodylate	15	%	PEG 4K	
G07	6.5				0.1	M	Na-Cacodylate	2.7	M	$(NH_4)_2SO_4$	
G08	6.5				0.1	M	Na-Cacodylate	1.8	M	Li_2SO_4	
G09	6.5				0.1	M	Na-Cacodylate	4	M	Na-Formate	
G10	6.5				0.1	M	Na-Cacodylate	1	M	KH_2PO_4	
G11	6.5	0.2	M	Ca-Acetate	0.1	M	Na-Cacodylate	10	%	PEG 8K	
G11								10	%	PEG 1K	
G12	6.5	0.2	M	Ca-Acetate	0.1	M	Na-Cacodylate	8	%	PEG 20K	PEG 550MME
H01	6.5				0.1	M	Na-Cacodylate	40	%	MPD	
H02	6.5				0.1	M	Na-Cacodylate	40	%	Butane-diol	
H03	6.5	0.005	M	$CdCl_2$	0.1	M	Na-Cacodylate	20	%	PEG 4K	
H04	6.5	0.15	M	KSCN	0.1	M	Na-Cacodylate	20	%	PEG 550 MME	
H05	6.5	0.15	M	KSCN	0.1	M	Na-Cacodylate	20	%	PEG 600	
H06	6.5	0.15	M	KSCN	0.1	M	Na-Cacodylate	20	%	PEG 1.5K	
H07	6.5				0.1	M	Na-Cacodylate	35	%	Isopropanol	
H08	6.5				0.1	M	Na-Cacodylate	30	%	Jeffamine 600M	
H09	6.5	0.005	M	$NiCl_2$	0.1	M	Na-Cacodylate	20	%	PEG 4K	
H10	6.5	0.15	M	KSCN	0.1	M	Na-Cacodylate	18	%	PEG 3350	
H11	6.5	0.15	M	KSCN	0.1	M	Na-Cacodylate	18	%	PEG 5K MME	
H12	6.5	0.15	M	KSCN	0.1	M	Na-Cacodylate	15	%	PEG 6K	

Table 5.8: Grid screen "GS008" used for primary screening of crystallization conditions.

		Salt			Buffer			Precipitant			
Well	**pH**	**Value**	**Units**	**Name**	**Value**	**Units**	**Name**	**Value**	**Units**	**Name**	
A01	7.5	0.3	M	Na-Acetate	0.1	M	TRIS	25	%	PEG 2K MME	
A02	7.5	0.2	M	Li_2SO_4	0.1	M	TRIS	25	%	PEG 2K MME	
A03	7.5	0.2	M	$MgCl_2$	0.1	M	TRIS	25	%	PEG 2K MME	
A04	7.5	0.2	M	KBr	0.1	M	TRIS	25	%	PEG 2K MME	
A05	7.5	0.2	M	KSCN	0.1	M	TRIS	25	%	PEG 2K MME	
A06	7.5	0.8	M	Na-Formate	0.1	M	TRIS	25	%	PEG 2K MME	
A07	7.5	0.3	M	Na-Acetate	0.1	M	TRIS	15	%	PEG 4K	
A08	7.5	0.2	M	Li_2SO_4	0.1	M	TRIS	15	%	PEG 4K	
A09	7.5	0.2	M	$MgCl_2$	0.1	M	TRIS	15	%	PEG 4K	
A10	7.5	0.2	M	KBr	0.1	M	TRIS	15	%	PEG 4K	
A11	7.5	0.2	M	KSCN	0.1	M	TRIS	15	%	PEG 4K	
A12	7.5	0.8	M	Na-Formate	0.1	M	TRIS	15	%	PEG 4K	
B01	7.5	0.3	M	Na-Acetate	0.1	M	TRIS	10	%	PEG 8K	PEG 1K
B02	7.5	0.2	M	Li_2SO_4	0.1	M	TRIS	10	%	PEG 8K	PEG 1K
B03	7.5	0.2	M	$MgCl_2$	0.1	M	TRIS	10	%	PEG 8K	PEG 1K
B04	7.5	0.2	M	KBr	0.1	M	TRIS	10	%	PEG 8K	PEG 1K
B05	7.5	0.2	M	KSCN	0.1	M	TRIS	10	%	PEG 8K	PEG 1K
B06	7.5	0.8	M	Na-Formate	0.1	M	TRIS	10	%	PEG 8K	PEG 1K
B07	7.5	0.3	M	Na-Acetate	0.1	M	TRIS	8	%	PEG 20K	PEG550 MME
B08	7.5	0.2	M	Li_2SO_4	0.1	M	TRIS	8	%	PEG 20K	PEG550 MME
B09	7.5	0.2	M	$MgCl_2$	0.1	M	TRIS	8	%	PEG 20K	PEG550 MME
B10	7.5	0.2	M	KBr	0.1	M	TRIS	8	%	PEG 20K	PEG550 MME
B11	7.5	0.2	M	KSCN	0.1	M	TRIS	8	%	PEG 20K	PEG550 MME
B12	7.5	0.8	M	Na-Formate	0.1	M	TRIS	8	%	PEG 20K	PEG550 MME
C01	7.5				0.1	M	TRIS	1.5	M	$(NH_4)_2SO_4$	
C02	7.5	0.8	M	Li_2SO_4	0.1	M	TRIS				
C03	7.5				0.1	M	TRIS	2	M	Na-Formate	
C04	7.5	0.5	M	KH_2PO_4	0.1	M	TRIS				
C05	7.5	0.2	M	Ca-Acetate	0.1	M	TRIS	25	%	PEG 2KMME	
C06	7.5	0.2	M	Ca-Acetate	0.1	M	TRIS	15	%	PEG 4K	
C07	7.5				0.1	M	TRIS	2.7	M	$(NH_4)_2SO_4$	
C08	7.5				0.1	M	TRIS	1.8	M	Li_2SO_4	
C09	7.5				0.1	M	TRIS	4	M	Na-Formate	
C10	7.5				0.1	M	TRIS	1	M	KH2PO4	
C11	7.5	0.2	M	Ca-Acetate	0.1	M	TRIS	10	%	PEG 8K	PEG 1K
C12	7.5	0.2	M	Ca-Acetate	0.1	M	TRIS	8	%	PEG 20K	PEG 550MME
D01	7.5				0.1	M	TRIS	40	%	MPD	
D02	7.5				0.1	M	TRIS	40	%	Butane-diol	
D03	7.5	0.005	M	$CdCl_2$	0.1	M	TRIS	20	%	PEG 4K	
D04	7.5	0.15	M	KSCN	0.1	M	TRIS	20	%	PEG 550 MME	
D05	7.5	0.15	M	KSCN	0.1	M	TRIS	20	%	PEG 600	
D06	7.5	0.15	M	KSCN	0.1	M	TRIS	20	%	PEG 1.5K	
D07	7.5				0.1	M	TRIS	35	%	Isopropanol	
D08	7.5				0.1	M	TRIS	30	%	Jeffamine 600M	
D09	7.5	0.005	M	$NiCl_2$	0.1	M	TRIS	20	%	PEG 4K	
D10	7.5	0.15	M	KSCN	0.1	M	TRIS	18	%	PEG 3350	
D11	7.5	0.15	M	KSCN	0.1	M	TRIS	18	%	PEG 5K MME	
D12	7.5	0.15	M	KSCN	0.1	M	TRIS	15	%	PEG 6K	
E01	8.5	0.3	M	Na-Acetate	0.1	M	TRIS	25	%	PEG 2K MME	
E02	8.5	0.2	M	Li_2SO_4	0.1	M	TRIS	25	%	PEG 2K MME	

E03	8.5	0.2	M	$MgCl_2$	0.1	M	TRIS	25	%	PEG 2K MME	
E04	8.5	0.2	M	KBr	0.1	M	TRIS	25	%	PEG 2K MME	
E05	8.5	0.2	M	KSCN	0.1	M	TRIS	25	%	PEG 2K MME	
E06	8.5	0.8	M	Na-Formate	0.1	M	TRIS	25	%	PEG 2K MME	
E07	8.5	0.3	M	Na-Acetate	0.1	M	TRIS	15	%	PEG 4K	
E08	8.5	0.2	M	Li_2SO_4	0.1	M	TRIS	15	%	PEG 4K	
E09	8.5	0.2	M	$MgCl_2$	0.1	M	TRIS	15	%	PEG 4K	
E10	8.5	0.2	M	KBr	0.1	M	TRIS	15	%	PEG 4K	
E11	8.5	0.2	M	KSCN	0.1	M	TRIS	15	%	PEG 4K	
E12	8.5	0.8	M	Na-Formate	0.1	M	TRIS	15	%	PEG 4K	
F01	8.5	0.3	M	Na-Acetate	0.1	M	TRIS	10	%	PEG 8K	PEG 1K
F02	8.5	0.2	M	Li_2SO_4	0.1	M	TRIS	10	%	PEG 8K	PEG 1K
F03	8.5	0.2	M	$MgCl_2$	0.1	M	TRIS	10	%	PEG 8K	PEG 1K
F04	8.5	0.2	M	KBr	0.1	M	TRIS	10	%	PEG 8K	PEG 1K
F05	8.5	0.2	M	KSCN	0.1	M	TRIS	10	%	PEG 8K	PEG 1K
F06	8.5	0.8	M	Na-Formate	0.1	M	TRIS	10	%	PEG 8K	PEG 1K
F07	8.5	0.3	M	Na-Acetate	0.1	M	TRIS	8	%	PEG 20K	PEG550 MME
F08	8.5	0.2	M	Li_2SO_4	0.1	M	TRIS	8	%	PEG 20K	PEG550 MME
F09	8.5	0.2	M	$MgCl_2$	0.1	M	TRIS	8	%	PEG 20K	PEG550 MME
F10	8.5	0.2	M	KBr	0.1	M	TRIS	8	%	PEG 20K	PEG550 MME
F11	8.5	0.2	M	KSCN	0.1	M	TRIS	8	%	PEG 20K	PEG550 MME
F12	8.5	0.8	M	Na-Formate	0.1	M	TRIS	8	%	PEG 20K	PEG550 MME
G01	8.5				0.1	M	TRIS	1.5	M	$(NH_4)_2SO_4$	
G02	8.5	0.8	M	Li_2SO_4	0.1	M	TRIS				
G03	8.5				0.1	M	TRIS	2	M	Na-Formate	
G04	8.5	0.5	M	KH_2PO_4	0.1	M	TRIS				
G05	8.5	0.2	M	Ca-Acetate	0.1	M	TRIS	25	%	PEG 2KMME	
G06	8.5	0.2	M	Ca-Acetate	0.1	M	TRIS	15	%	PEG 4K	
G07	8.5				0.1	M	TRIS	2.7	M	$(NH_4)_2SO_4$	
G08	8.5				0.1	M	TRIS	1.8	M	Li_2SO_4	
G09	8.5				0.1	M	TRIS	4	M	Na-Formate	
G10	8.5				0.1	M	TRIS	1	M	KH2PO4	
G11	8.5	0.2	M	Ca-Acetate	0.1	M	TRIS	10	%	PEG 8K	
G11								10	%	PEG 1K	
G12	8.5	0.2	M	Ca-Acetate	0.1	M	TRIS	8	%	PEG 20K	
G12								8	%	PEG 550MME	
H01	8.5				0.1	M	TRIS	40	%	MPD	
H02	8.5				0.1	M	TRIS	40	%	Butane-diol	
H03	8.5	0.005	M	$CdCl_2$	0.1	M	TRIS	20	%	PEG 4K	
H04	8.5	0.15	M	KSCN	0.1	M	TRIS	20	%	PEG 550 MME	
H05	8.5	0.15	M	KSCN	0.1	M	TRIS	20	%	PEG 600	
H06	8.5	0.15	M	KSCN	0.1	M	TRIS	20	%	PEG 1.5K	
H07	8.5				0.1	M	TRIS	35	%	Isopropanol	
H08	8.5				0.1	M	TRIS	30	%	Jeffamine 600M	
H09	8.5	0.005	M	$NiCl_2$	0.1	M	TRIS	20	%	PEG 4K	
H10	8.5	0.15	M	KSCN	0.1	M	TRIS	18	%	PEG 3350	
H11	8.5	0.15	M	KSCN	0.1	M	TRIS	18	%	PEG 5K MME	
H12	8.5	0.15	M	KSCN	0.1	M	TRIS	15	%	PEG 6K	

Table 5.9: Grid screen "GS027" used for primary screening of crystallization conditions.

		Salt			Buffer			Precipitant		
Well	**pH**	**Value**	**Units**	**Name**	**Value**	**Units**	**Name**	**Value**	**Units**	**Name**
A01	4.5	0.2	M	Li_2SO_4	0.1	M	$NaCH_3COO$	50	%	PEG 400
A02	5.5				0.1	M	tri-sodium citrate	20	%	PEG 3000
A03		0.2	M	ammonium citrate				20	%	PEG 3350
A04	4.6	0.02	M	$CaCl_2$	0.1	M	$NaCH_3COO$	30	%	MPD
A05		0.2	M	$Mg(HCO_2)_2$				20	%	PEG 3350
A06	4.2	0.2	M	Li_2SO_4	0.1	M	$C_6H_5K_3O_7$	20	%	PEG 1000
A07	9.5				0.1	M	CHES	20	%	PEG 8000
A08		0.2	M	NH_4HCO_2				20	%	PEG 3350
A09		0.2	M	NH_4Cl				20	%	PEG 3350
A10		0.2	M	$KHCO_2$				20	%	PEG 3350
A11	8.5	0.2	M	$(NH_4)_3PO_4$	0.1	M	TRIS	50	%	MPD
A12		0.2	M	potassium nitrate				20	%	PEG 3350
B01	4				0.1	M	Citric acid	0.8	M	$NH_4(SO_4)_2$
B02		0.2	M	NaSCN				20	%	PEG 3350
B03	9				0.1	M	BICINE	20	%	PEG 6000
B04	7.5				0.1	M	HEPES	10	%	PEG 8000
B04								8	%	Ethylene glycol
B05	6.5				0.1	M	$Na(CH_3)_2AsOO$	40	%	MPD
B05								5	%	PEG 8000
B06	4.2				0.1	M	phosphate-citrate	40	%	Ethanol
B06								5	%	PEG 1000
B07	4.6				0.1	M	$NaCH_3COO$	8	%	PEG 4000
B08	7	0.2	M	$MgCl_2$	0.1	M	TRIS	10	%	PEG 8000
B09	5				0.1	M	Citric acid	20	%	PEG 6000
B10	6.5	0.2	M	$MgCl_2$	0.1	M	$Na(CH_3)_2AsOO$	50	%	PEG 200
B11								1.6	M	tri-sodium citrate
B12		0.2	M	tri-potassium citrate				20	%	PEG 3350
C01	4.2	0.2	M	NaCl	0.1	M	$C_6H_5K_3O_7$	20	%	PEG 8000
C02	4	1	M	Li_2SO_4	0.1	M	Citric acid	20	%	PEG 6000
C03		0.2	M	ammonium nitrate				20	%	PEG 3350
C04	7				0.1	M	HEPES	10	%	PEG 6000
C05	7.5				0.1	M	HEPES	0.8	M	Na_3PO_4
C05					0.1			0.8	M	K_3PO_4
C06	4.2				0.1	M	phosphate-citrate	40	%	PEG 300
C07	4.5	0.2	M	$Zn(CH_3COO)_2$	0.1	M	$NaCH_3COO$	10	%	PEG 3000
C08	8.5				0.1	M	TRIS	20	%	Ethanol
C09	6.2				0.1	M	Na/K phosphate	25	%	1,2 propandiol + Glycerol (10%)
C10	9				0.1	M	BICINE	10	%	PEG 20000
C10								2	%	Dioxane
C11	4.6				0.1	M	$NaCH_3COO$	2	M	$NH_4(SO_4)_2$
C12								10	%	PEG 1000 PEG 8000
D01								24	%	PEG 1500
D01								20	%	Glycerol
D02	7.5	0.2	M	$MgCl_2$	0.1	M	HEPES	30	%	PEG 400
D03	6.2	0.2	M	NaCl	0.1	M	Na_3PO_4	50	%	PEG 200
D04	4.5	0.2	M	Li_2SO_4	0.1	M	$NaCH_3COO$	30	%	PEG 8000
D05	7.5				0.1	M	HEPES	70	%	MPD
D06	8.5	0.2	M	$MgCl_2$	0.1	M	TRIS	20	%	PEG 8000
D07	8.5	0.2	M	Li_2SO_4	0.1	M	TRIS	40	%	PEG 400
D08	8				0.1	M	TRIS	40	%	MPD

D09		0.17	M	$NH_4(SO_4)_2$				25.5	%	PEG 4000 + Glycerol (15%)
D10	6.5	0.2	M	$Ca(CH_3COO)_2$	0.1	M	$Na(CH_3)_2AsOO$	40	%	PEG 300
D11	4.6	0.14	M	$CaCl_2$	0.07	M	$NaCH_3COO$	14	%	Isopropanol + Glycerol (30%)
D12		0.04	M	K_3PO_4				16	%	PEG 8000 + Glycerol (20%)
E01	6.5				0.1	M	$Na(CH_3)_2AsOO$	1	M	tri-sodium citrate
E02	6.5	0.2	M	NaCl	0.1	M	$Na(CH_3)_2AsOO$	2	M	$NH_4(SO_4)_2$
E03	7.5	0.2	M	NaCl	0.1	M	HEPES	10	%	Isopropanol
E04	8.5	0.2	M	Li_2SO_4	0.1	M	TRIS	1.26	M	$NH_4(SO_4)_2$
E05	10				0.1	M	CAPS	40	%	MPD
E06	8	0.2	M	$Zn(CH_3COO)_2$	0.1	M	Imidazole	20	%	PEG 3000
E07	6.5	0.2	M	$Zn(CH_3COO)_2$	0.1	M	$Na(CH_3)_2AsOO$	10	%	Isopropanol
E08	4.5				0.1	M	Na acetate	1	M	di-ammonium phosphate
E09	6.5				0.1	M	MES	1.6	M	$Mg(SO_4)_2$
E10	9				0.1	M	BICINE	10	%	PEG 6000
E11	6.5	0.16	M	$Ca(CH_3COO)_2$	0.08	M	$Na(CH_3)_2AsOO$	14.4	%	PEG 8000
E11								20	%	Glycerol
E12	8				0.1	M	Imidazole	10	%	PEG 8000
F01	6.5	0.05	M	$CsCl_2$	0.1	M	MES	30	%	Jeffamine M-600
F02	5				0.1	M	Citric acid	3.2	M	$NH_4(SO_4)_2$
F03	8				0.1	M	TRIS	20	%	MPD
F04	7.5				0.1	M	HEPES	20	%	Jeffamine M-600
F05	8.5	0.2	M	$MgCl_2$	0.1	M	TRIS	50	%	Ethylene glycol
F06	9				0.1	M	BICINE	10	%	MPD
F07	7							0.8	M	Succinic acid
F08	7							2.1	M	DL-Malic acid
F09	7							2.4	M	Sodium malonate
F10	7	0.5	%	Jeffamine ED-2001	0.1	M	HEPES	1.1	M	Sodium malonate
F11	7	1	%	PEG 2000 MME	0.1	M	HEPES	1	M	Succinic acid
F12	7				0.1	M	HEPES	30	%	Jeffamine M-600
G01	7				0.1	M	HEPES	30	%	Jeffamine ED-2001
G02	7.5	0.02	M	$MgCl_2$	0.1	M	HEPES	22	%	Polyacrylic acid 5100
G03	8.5	0.01	M	$CoCl_2$	0.1	M	TRIS	20	%	Polyvinylpyrrolidone
G04	8.5	0.2	M	Trimethylamine N-oxide	0.1	M	TRIS	20	%	PEG 2000 MME
G05	7.5	0.005	M	CoCl, CdCl, $MgCl_2$, $NiCl_2$	0.1	M	HEPES	12	%	PEG 3350
G06	7	0.2	M	Sodium malonate pH 7.0				20	%	PEG 3350
G07	7	0.1	M	Succinic acid pH 7.0				15	%	PEG 3350
G08	7	0.15	M	DL-Malic acid pH 7.0				20	%	PEG 3350
G09		0.1	M	KSCN				30	%	PEG 2000 MME
G10		0.15	M	KBr				30	%	PEG 2000 MME
G11	5.5				0.1	M	Bis-TRIS	2	M	$NH_4(SO_4)_2$
G12	5.5				0.1	M	Bis-TRIS	3	M	NaCl
H01	5.5				0.1	M	Bis-TRIS	0.3	M	$Mg(HCO_2)_2$
H02	5.5	1	%	PEG 3350	0.1	M	Bis-TRIS	1	M	$NH_4(SO_4)_2$
H03	5.5				0.1	M	Bis-TRIS	25	%	PEG 3350
H04	5.5	0.2	M	$CaCl_2$	0.1	M	Bis-TRIS	45	%	MPD
H05	5.5	0.2	M	NH_4CH_3COO	0.1	M	Bis-TRIS	45	%	MPD
H06	5.5	0.1	M	NH_4CH_3COO	0.1	M	Bis-TRIS	17	%	10,000
H07	5.5	0.2	M	NH_4CH_3COO	0.1	M	Bis-TRIS	25	%	PEG 3350
H08	5.5	0.2	M	NaCl	0.1	M	Bis-TRIS	25	%	PEG 3350
H09	5.5	0.2	M	Li_2SO_4	0.1	M	Bis-TRIS	25	%	PEG 3350
H10	5.5	0.2	M	NH_4CH_3COO	0.1	M	Bis-TRIS	25	%	PEG 3350
H11	5.5	0.2	M	$MgCl_2$	0.1	M	Bis-TRIS	25	%	PEG 3350
H12	7.5	0.2	M	NH_4CH_3COO	0.1	M	HEPES	45	%	MPD

Table 5.10: Grid screen "GS034" used for primary screening of crystallization conditions.

		Salt			Buffer			Precipitant		
Well	**pH**	**Value**	**Units**	**Name**	**Value**	**Units**	**Name**	**Value**	**Units**	**Name**
A01	2.5				0.1	M	citric acid	15	%	Na_2SO_4
A02	2.5				0.1	M	citric acid	25	%	Na_2SO_4
A03	2.5				0.1	M	citric acid	35	%	Na_2SO_4
A04	2.5				0.1	M	citric acid	50	%	Na_2SO_4
A05	2.5				0.1	M	citric acid	65	%	Na_2SO_4
A06	2.5				0.1	M	citric acid	80	%	Na_2SO_4
A07	2.5				0.1	M	citric acid	10	%	MPD
A08	2.5				0.1	M	citric acid	20	%	MPD
A09	2.5				0.1	M	citric acid	30	%	MPD
A10	2.5				0.1	M	citric acid	45	%	MPD
A11	2.5				0.1	M	citric acid	60	%	MPD
A12	2.5				0.1	M	citric acid	80	%	MPD
B01	2.9				0.1	M	citric acid	15	%	Na_2SO_4
B02	2.9				0.1	M	citric acid	25	%	Na_2SO_4
B03	2.9				0.1	M	citric acid	35	%	Na_2SO_4
B04	2.9				0.1	M	citric acid	50	%	Na_2SO_4
B05	2.9				0.1	M	citric acid	65	%	Na_2SO_4
B06	2.9				0.1	M	citric acid	80	%	Na_2SO_4
B07	2.9				0.1	M	citric acid	10	%	MPD
B08	2.9				0.1	M	citric acid	20	%	MPD
B09	2.9				0.1	M	citric acid	30	%	MPD
B10	2.9				0.1	M	citric acid	45	%	MPD
B11	2.9				0.1	M	citric acid	60	%	MPD
B12	2.9				0.1	M	citric acid	80	%	MPD
C01	3.3				0.1	M	citric acid	15	%	Na_2SO_4
C02	3.3				0.1	M	citric acid	25	%	Na_2SO_4
C03	3.3				0.1	M	citric acid	35	%	Na_2SO_4
C04	3.3				0.1	M	citric acid	50	%	Na_2SO_4
C05	3.3				0.1	M	citric acid	65	%	Na_2SO_4
C06	3.3				0.1	M	citric acid	80	%	Na_2SO_4
C07	3.3				0.1	M	citric acid	10	%	MPD
C08	3.3				0.1	M	citric acid	20	%	MPD
C09	3.3				0.1	M	citric acid	30	%	MPD
C10	3.3				0.1	M	citric acid	45	%	MPD
C11	3.3				0.1	M	citric acid	60	%	MPD
C12	3.3				0.1	M	citric acid	80	%	MPD
D01	3.7				0.1	M	citric acid	15	%	Na_2SO_4
D02	3.7				0.1	M	citric acid	25	%	Na_2SO_4
D03	3.7				0.1	M	citric acid	35	%	Na_2SO_4
D04	3.7				0.1	M	citric acid	50	%	Na_2SO_4
D05	3.7				0.1	M	citric acid	65	%	Na_2SO_4
D06	3.7				0.1	M	citric acid	80	%	Na_2SO_4
D07	3.7				0.1	M	citric acid	10	%	MPD
D08	3.7				0.1	M	citric acid	20	%	MPD
D09	3.7				0.1	M	citric acid	30	%	MPD
D10	3.7				0.1	M	citric acid	45	%	MPD
D11	3.7				0.1	M	citric acid	60	%	MPD
D12	3.7				0.1	M	citric acid	80	%	MPD
E01	2.5				0.1	M	citric acid	10	%	PEG 400
E02	2.5				0.1	M	citric acid	15	%	PEG 400
E03	2.5				0.1	M	citric acid	20	% v/v	PEG 400

E04	2.5	0.1	M	citric acid	25	% v/v	PEG 400
E05	2.5	0.1	M	citric acid	35	% v/v	PEG 400
E06	2.5	0.1	M	citric acid	50	% v/v	PEG 400
E07	2.5	0.1	M	citric acid	5	% w/v	PEG 6000
E08	2.5	0.1	M	citric acid	10	% w/v	PEG 6000
E09	2.5	0.1	M	citric acid	15	% w/v	PEG 6000
E10	2.5	0.1	M	citric acid	20	% w/v	PEG 6000
E11	2.5	0.1	M	citric acid	25	% w/v	PEG 6000
E12	2.5	0.1	M	citric acid	30	% w/v	PEG 6000
F01	2.9	0.1	M	citric acid	10	% v/v	PEG 400
F02	2.9	0.1	M	citric acid	15	% v/v	PEG 400
F03	2.9	0.1	M	citric acid	20	% v/v	PEG 400
F04	2.9	0.1	M	citric acid	25	% v/v	PEG 400
F05	2.9	0.1	M	citric acid	35	% v/v	PEG 400
F06	2.9	0.1	M	citric acid	50	% v/v	PEG 400
F07	2.9	0.1	M	citric acid	5	% w/v	PEG 6000
F08	2.9	0.1	M	citric acid	10	% w/v	PEG 6000
F09	2.9	0.1	M	citric acid	15	% w/v	PEG 6000
F10	2.9	0.1	M	citric acid	20	% w/v	PEG 6000
F11	2.9	0.1	M	citric acid	25	% w/v	PEG 6000
F12	2.9	0.1	M	citric acid	30	% w/v	PEG 6000
G01	3.3	0.1	M	citric acid	10	% v/v	PEG 400
G02	3.3	0.1	M	citric acid	15	% v/v	PEG 400
G03	3.3	0.1	M	citric acid	20	% v/v	PEG 400
G04	3.3	0.1	M	citric acid	25	% v/v	PEG 400
G05	3.3	0.1	M	citric acid	35	% v/v	PEG 400
G06	3.3	0.1	M	citric acid	50	% v/v	PEG 400
G07	3.3	0.1	M	citric acid	5	% w/v	PEG 6000
G08	3.3	0.1	M	citric acid	10	% w/v	PEG 6000
G09	3.3	0.1	M	citric acid	15	% w/v	PEG 6000
G10	3.3	0.1	M	citric acid	20	% w/v	PEG 6000
G11	3.3	0.1	M	citric acid	25	% w/v	PEG 6000
G12	3.3	0.1	M	citric acid	30	% w/v	PEG 6000
H01	3.7	0.1	M	citric acid	10	% v/v	PEG 400
H02	3.7	0.1	M	citric acid	15	% v/v	PEG 400
H03	3.7	0.1	M	citric acid	20	% v/v	PEG 400
H04	3.7	0.1	M	citric acid	25	% v/v	PEG 400
H05	3.7	0.1	M	citric acid	35	% v/v	PEG 400
H06	3.7	0.1	M	citric acid	50	% v/v	PEG 400
H07	3.7	0.1	M	citric acid	5	% w/v	PEG 6000
H08	3.7	0.1	M	citric acid	10	% w/v	PEG 6000
H09	3.7	0.1	M	citric acid	15	% w/v	PEG 6000
H10	3.7	0.1	M	citric acid	20	% w/v	PEG 6000
H11	3.7	0.1	M	citric acid	25	% w/v	PEG 6000
H12	3.7	0.1	M	citric acid	30	% w/v	PEG 6000

Table 5.11: Grid screen "GS048" used for primary screening of crystallization conditions.

		Salt			Buffer			Precipitant		
Well	**pH**	**Value**	**Units**	**Name**	**Value**	**Units**	**Name**	**Value**	**Units**	**Name**
A01	4.6	0.02	M	$CaCl_2(H_2O)_2$	0.1	M	$NaCH_3COO{\cdot}3H_2O$	30	%	MPD
A02								0.4	M	$NaKC_4H_4O_6{\cdot}4H_2O$
A03								0.4	M	$NH_4H_2PO_4$
A04	8.5				0.1	M	TRIS	2.0	M	$(NH_4)_2SO_4$
A05	7.5	0.2	M	$NaH_2C_6H_5O_7$	0.1	M	HEPES	30	%	MPD
A06	8.5	0.2	M	$MgCl_2{\cdot}6H_2O$	0.1	M	TRIS	30	%	PEG 4,000
A07	6.5				0.1	M	$Na(CH_3)_2AsOO{\cdot}3H_2O$	1.4	M	$NaCH_3COO{\cdot}3H_2O$
A08	6.5	0.2	M	$NaH_2C_6H_5O_7$	0.1	M	$Na(CH_3)_2AsOO{\cdot}3H_2O$	30	%	2-Propanol
A09	5.6	0.2	M	NH_4CH_3COO	0.1	M	$Na(CH_3)_2AsOO{\cdot}3H_2O$	30	%	PEG 4,000
A10	4.6	0.2	M	NH_4CH_3COO	0.1	M	$NaCH_3COO{\cdot}3H_2O$	30	%	PEG 4,000
A11	5.6				0.1	M	$NaH_2C_6H_5O_7$	1.0	M	$NH_4H_2PO_4$
A12	7.5	0.2	M	$MgCl_2{\cdot}6H_2O$	0.1	M	HEPES	30	%	2-Propanol
B01	8.5	0.2	M	$NaH_2C_6H_5O_7$	0.1	M	TRIS	30	%	PEG 400
B02	7.5	0.2	M	$CaCl_2 \cdot 2H_2O$	0.1	M	HEPES	28	%	PEG 400
B03	6.5	0.2	M	$(NH_4)_2SO_4$	0.1	M	$Na(CH_3)_2AsOO{\cdot}3H_2O$	30	%	PEG 8,000
B04	7.5				0.1	M	HEPES	1.5	M	$(Li)_2SO_4(H_2O)$
B05	8.5	0.2	M	$(Li)_2SO_4(H_2O)$	0.1	M	TRIS	30	%	PEG 4,000
B06	6.5	0.2	M	$Mg(CH_3COO)_2{\cdot}4H_2O$	0.1	M	$Na(CH_3)_2AsOO{\cdot}3H_2O$	20	%	PEG 8,000
B07	8.5	0.2	M	$(NH_4)_2SO_4$	0.1	M	TRIS	30	%	2-Propanol
B08	4.6	0.2	M	$(NH_4)_2SO_4$	0.1	M	$NaCH_3COO{\cdot}3H_2O$	25	%	PEG 4,000
B09	6.5	0.2	M	$Mg(CH_3COO)_2{\cdot}4H_2O$	0.1	M	$Na(CH_3)_2AsOO{\cdot}3H_2O$	30	%	MPD
B10	8.5	0.2	M	$NaCH_3COO{\cdot}3H_2O$	0.1	M	TRIS	30	%	PEG 4,000
B11	7.5	0.2	M	$MgCl_2{\cdot}6H_2O$	0.1	M	HEPES	30	%	PEG 400
B12	4.6	0.2	M	$CaCl_2{\cdot}2H_2O$	0.1	M	$NaCH_3COO(H_2O)_3$	20	%	2-Propanol
C01	6.5				0.1	M	Imidazole	1	M	$NaCH_3COO{\cdot}3H_2O$
C02	5.6	0.2	M	NH_4CH_3COO	0.1	M	Na citrate tribasic $\cdot 2H_2O$	30	%	MPD
C03	7.5	0.2	M	Na citrate tribasic ·2H2O	0.1	M	HEPES	20	%	2-Propanol
C04	6.5	0.2	M	$NaCH_3COO{\cdot}3H_2O$	0.1	M	$Na(CH_3)_2AsOO{\cdot}3H_2O$	30	%	PEG 8,000
C05	7.5				0.1	M	HEPES	0.8	M	$NaKC_4H_4O_6{\cdot}4H_2O$
C06		0.2	M	$(NH_4)_2SO_4$				30	%	PEG 8,000
C07		0.2	M	$(NH_4)_2SO_4$				30	%	PEG 4,000
C08								2.0	M	$(NH_4)_2SO_4$
C09								4.0	M	Sodium formate
C10	4.6				0.1	M	$NaCH_3COO(H_2O)_3$	2.0	M	Sodium formate
C11	7.5				0.1	M	HEPES	0.8	M	$NaH_2PO_4{\cdot}H_2O$
C11								0.8	M	$NH_4H_2PO_4$
C12	8.5				0.1	M	TRIS	8	%	PEG 8,000
D01	4.6				0.1	M	$NaCH_3COO(H_2O)_3$	8	%	PEG 4,000
D02	7.5				0.1	M	HEPES	1.4	M	Na citrate tribasic dihydrate
D03	7.5				0.1	M	HEPES	2	%	PEG 400
D03								2.0	M	$(NH_4)_2SO_4$
D04	5.6				0.1	M	Na citrate tribasic ·2H2O	20	%	2-Propanol
D04								20	%	PEG 4,000
D05	7.5				0.1	M	HEPES	10	%	2-Propanol
D05								20	%	PEG 4,000
D06		0.05	M	$NH_4H_2PO_4$				20	%	PEG 8,000
D07								30	%	PEG 1,500
D08								0.2	M	Mg formate dihydrate
D09	6.5	0.2	M	$Zn(CH_3COO)_2{\cdot}2H_2O$	0.1	M	$Na(CH_3)_2AsOO{\cdot}3H_2O$	18	%	PEG 8,000
D10	6.5	0.2	M	$Ca(CH_3COO)_2{\cdot}H_2O$	0.1	M	$Na(CH_3)_2AsOO{\cdot}3H_2O$	18	%	PEG 8,000
D11	4.6				0.1	M	$NaCH_3COO{\cdot}3H_2O$	2.0	M	$(NH_4)_2SO_4$

D12	8.5				0.1	M	TRIS	2.0	M	$NH_4H_2PO_4$
E01		2	M	NaCl						
E02		0.5	M	NaCl						
E02		0.01	M	$MgCl_2 \cdot 6H_2O$						
E03								25	%	Ethylene glycol
E04								35	%	1,4-Dioxane
E05		2.0	M	$(NH_4)_2SO_4$				5	%	2-Propanol
E06								1.0	M	Imidazole pH 7.0
E07								10	%	PEG 1000 PEG 8000
E08		1.5	M	NaCl				10	%	Ethanol
E09	4.6				0.1	M	$NaCH_3COO \cdot 3H_2O$	2.0	M	NaCl
E10	4.6	0.2	M	NaCl	0.1	M	$NaCH_3COO \cdot 3H_2O$	30	%	MPD
E11	4.6	0.01	M	$CoCl_2 \cdot 6H_2O$	0.1	M	$NaCH_3COO \cdot 3H_2O$	1.0	M	1,6-Hexanediol
E12	4.6	0.1	M	$CaCl_2 \cdot H_2O$	0.1	M	$NaCH_3COO \cdot 3H_2O$	30	%	PEG 400
F01	4.6	0.2	M	$(NH_4)_2SO_4$	0.1	M	$NaCH_3COO \cdot 3H_2O$	30	%	PEG MME 2,000
F02	5.6	0.2	M	$NaKC_4H_4O_6 \cdot 4H_2O$	0.1	M	$NaH_2C_6H_5O_7$	2.0	M	$(NH_4)_2SO_4$
F03	5.6	0.5	M	$(NH_4)_2SO_4$	0.1	M	$NaH_2C_6H_5O_7$	1.0	M	$(Li)_2SO_4 \cdot H_2O$
F04	5.6	0.5	M	NaCl	0.1	M	$NaH_2C_6H_5O_7$	2	%	Ethylene imine polymer
F05	5.6				0.1	M	$NaH_2C_6H_5O_7$	35	%	tert-Butanol
F06	5.6	0.01	M	$FeCl_3 \cdot 6H_2O$	0.1	M	$NaH_2C_6H_5O_7$	10	%	Jeffamine M-600
F07	5.6				0.1	M	$NaH_2C_6H_5O_7$	2.5	M	1,6-Hexanediol
F08	6.5				0.1	M	$MES \cdot H_2O$	1.6	M	$MgSO_4 \cdot 7H_2O$
F09	6.5	0.1	M	$NaH_2PO_4 \cdot H_2O$	0.1	M	$MES \cdot H_2O$	2.0	M	NaCl
F09		0.1	M	KH_2PO_4						
F10	6.5				0.1	M	$MES \cdot H_2O$	12	%	PEG 20,000
F11	6.5	1.6	M	$(NH_4)_2SO_4$	0.1	M	$MES \cdot H_2O$	10	%	1,4-Dioxane
F12	6.5	0.05	M	CsCl	0.1	M	$MES \cdot H_2O$	30	%	Jeffamine M-600
G01	6.5	0.01	M	$CoCl_2 \cdot 6H_2O$	0.1	M	$MES \cdot H_2O$	1.8	M	$(NH_4)_2SO_4$
G02	6.5	0.2	M	$(NH_4)_2SO_4$	0.1	M	$MES \cdot H_2O$	30	%	PEG MME 5,000
G03	6.5	0.01	M	$Zn(SO4)_2 \cdot 7H_2O$	0.1	M	$MES \cdot H_2O$	25	%	PEG MME 550
G04								1.6	M	Na citrate tribasic dihydrate
G05	7.5	0.5	M	$(NH_4)_2SO_4$	0.1	M	HEPES	30	%	MPD
G06	7.5							10	%	PEG 6,000 + MPD (5%)
G07	7.5				0.1	M	HEPES	20	%	Jeffamine M-600
G08	7.5	0.1	M	NaCl	0.1	M	HEPES	1.6	M	$(NH_4)_2SO_4$
G09	7.5				0.1	M	HEPES	2.0	M	$(NH_4)_2SO_4$
G10	7.5	0.05	M	$CdSO_4 \cdot H_2O$	0.1	M	HEPES	1.0	M	$NaCH_3COO \cdot 3H_2O$
G11	7.5				0.1	M	HEPES	70	%	MPD
G12	7.5				0.1	M	HEPES	4.3	M	NaCl
H01	7.5				0.1	M	HEPES	10	%	PEG 8,000
H01								8	%	Ethylene glycol
H02	7.5				0.1	M	HEPES	20	%	PEG 10,000
H03	8.5	0.2	M	$MgCl_2 \cdot 6H_2O$	0.1	M	TRIS	3.4	M	1,6-Hexanediol
H04	8.5				0.1	M	TRIS	25	%	tert-Butanol
H05	8.5	0.01	M	$NiCl_2 \cdot 6H_2O$	0.1	M	TRIS	1.0	M	$(Li)_2SO_4 \cdot H_2O$
H06	8.5	1.5	M	$(NH_4)_2SO_4$	0.1	M	TRIS	12	%	Glycerol
H07	8.5	0.2	M	$NH_4H_2PO_4$	0.1	M	TRIS	50	%	MPD
H08	8.5				0.1	M	TRIS	20	%	Ethanol
H09	8.5	0.01	M	$NiCl_2 \cdot 6H_2O$	0.1	M	TRIS	20	%	PEG MME 2,000
H10	9.0	0.1	M	NaCl	0.1	M	BICINE	20	%	PEG MME 550
H11	9.0				0.1	M	BICINE	2.0	M	$MgCl_2(H_2O)_6$
H12	9.0				0.1	M	BICINE	2	%	1,4-Dioxane
H12								10	%	PEG 20,000

3.5 Preliminary work and cloning for Sf9-expression

Previous to the Sf9 production of the different recombinant HER2-subdomains used for epitope mapping and crystallization experiments (as described in the Supplementary Text of **Chapter 3**), the respective baculoviral genome (bacmid) had to be prepared. We made use of the donor vector pFLmLIC (**Figure 5.11**:) to introduce the recombinant subdomain coding sequences into the bacmid EmBacY (**Figure 5.12**:). The donor vector pFLmLIC can be equipped with the respective subdomain-sequence via ligation-independent cloning (LIC) of the PCR-amplified insert (replacing a SacB-cassette and thereby allowing for negative selection on sucrose containing plates). The LIC-protocol was performed using chemocompetent *E. coli* XL1-blue cells and the pFLmLIC-derivatives were purified using a standard plasmid purification kit ("QIAprep Spin", Qiagen). Integration of parts of the donor vector into the bacmid is performed in bacteria as well. For this purpose, we made use of the *E. coli* strain DH10 EmBacY that carries the EmBacY bacmid and a helper plasmid encoding the transposase required for the Tn7 transposition of the gene of interest (GOI) from the donor vector to the bacmid. Transfection of chemocompetent *E. coli* EmBacY cells with pFLmLIC, followed by overnight recovery at 37°C in the absence of antibiotics (to allow for the transposition to occur) and plating on 2YT agar (containing 0.1 g/l XGal, 200 μM IPTG and all antibiotics for which pFLmLIC and EmBacY encode resistences) allowed for blue/white screening of clones containing bacmid DNA coding for the respective HER2 domain.

The bacmid DNA from bacterial cultures, inoculated with single white clones, was purified via isopropyl alcohol precipitation as described elsewhere (Fitzgerald *et al.* (2006)).

Baculoviruses were obtained via transfection of adherent Sf9 cells with bacmid DNA (Fitzgerald *et al.* (2006)) and used for infection for expression like described in the SI-Text of **Chapter 3**.

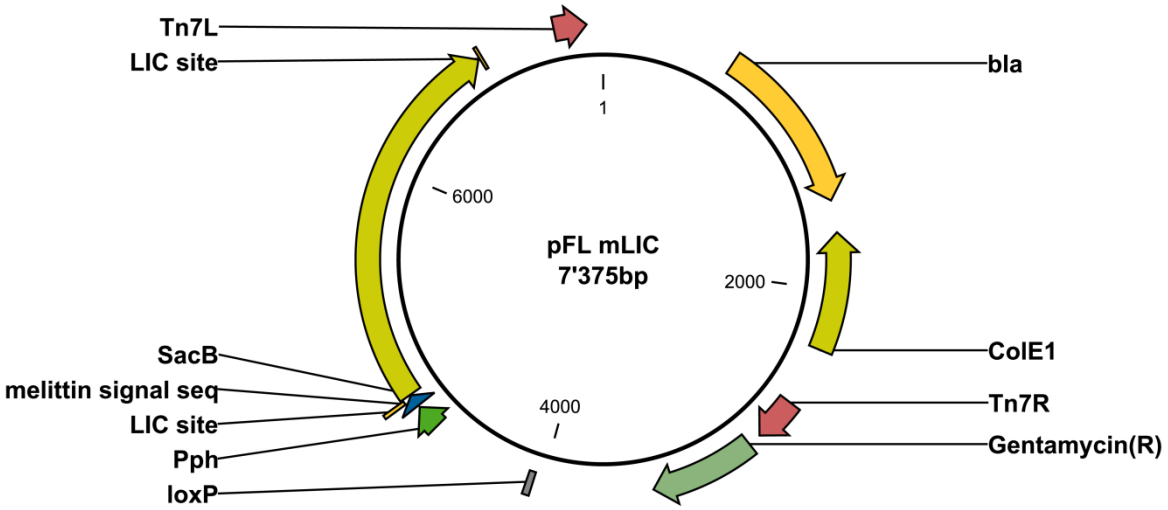

Figure 5.11: Schematic representation of the donor vector pFlmLIC. The plasmid contains an expression cassette comprising LIC sites, a polyhedrin promoter (Pph) and a melittin signal sequence. A beta lactamase gene (bla) is used for selection after initial transformation into *E. coli* XL1 blue. Transposon elements (Tn7L, Tn7R) and the resistance marker for gentamycin are used to assure and monitor the successful transposition into the bacmid in *E. coli* DH10 EmBacY.

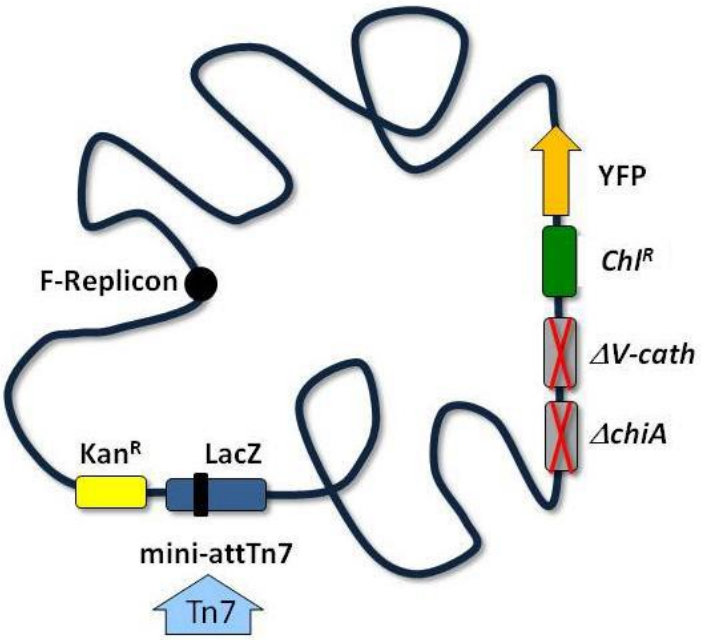

Figure 5.12: Schematic presentation of bacmid EmBacY used for the production of HER2 subdomains in Sf9 insect cells. The modified viral genome is shown in a schematic representation. The Tn7 attachment site is located within a LacZα gene; insertion of Tn7 elements from e.g. pFl derivatives therefore produces a white phenotype when plated on agar containing XGal and IPTG. The viral genes *v-cath* and *chiA* are disrupted by replacement with an antibiotic marker and a non-functional LoxP sequence (both not shown for reasons of clarity) (see Craig and Berger (2011)).

3.6 Immunoprecipitation with DARPins

It is very informative to monitor the alterations in the phosphorylation pattern of HER2 in the course of the treatment with the different anti-proliferative or even cytotoxic HER2-binding DARPin formats discussed within this thesis (like e.g. discussed in **Chapter 4,** using immunoblotting of phosphorylated HER2-residues).

Another method besides immunoblotting, that could be used to monitor phosphorylated HER2-residues, is mass spectrometry. One prerequisite to perform this method in a quantitative way is the purification of HER2 from the treated cells. Furthermore, the use of SILAC (stable isotope labelling by amino acids in cell culture) is needed, which means that the cells need to be grown for at least 4 generations in isotopically labelled medium (we used K8R10 labeled RPMI-1640 from Cambridge Isotope Laboratories which contains Lys with 8 D atoms and Arg with 10 D atoms). Mass spectrometry of immunoprecipitated HER2 from cells grown under SILAC-conditions can be used to quantify the changes in the phosphorylation patterns of the cytoplasmic tail of HER2 upon treatment with the DARPin constructs.

In order to perform such SILAC experiments for the quantification of the intracellular phosphorylation levels of HER2 from untreated, DARPin- and trastuzumab-treated cells, we developed an immunoprecipitation method using a bispecific DARPin-Affibody-fusion protein as affinity reagent. This affinity reagent, the construct 9_01_20_zHER2 (thereafter reffered to as "01_zHER2") was used to generate immunoprecipitation resins. These matrices were then used to immunoprecipitate and purify HER2 protein from BT474 cells that had been grown either untreated or treated with either DARPins or trastuzumab.

Generation of 01_zHER2-coated Ultralink Biosupport immunoprecipitation matrices (Thermo Scientific) was initially performed according to the instructions given by the supplier. Briefly, 2 mg of 01_zHER2 at a concentration of about 5 g/l was added to 10 mg of the immunoprecipitation resin and shaken at room temperature overnight. The reaction was then quenched overnight by addition of 1 ml of 1 M TRIS, pH 7.6 and subsequently washed with 1 M NaCl and PBS.

Per immunoprecipitation-aliquot, 2 × 10^6 BT474 cells were washed with cold PBS, scraped in ice-cold buffer IP_L (PBS containing 1% Triton X-100) and lysed in this buffer. In addition, “cOmplete” protease inhibitors (Roche), “PhosSTOP” phosphatase inhibitors (Roche), 25 mM NaF, 1 mM $NaVO_4$ and 10 mM β-glycerophosphate were added to inhibit protease and phosphatase activities and all procedures were performed on ice. The supernatant of the lysed cells (obtained by centrifugation (20,000 × g, 30 min, 4°C)) was applied to 20 mg of 01_zHER2-coupled resin and shaken for 2 h at 4°C. After washing the resin three times with buffer IP_L, bound HER2 was eluted in four fractions by shaking the resin for 15 min at 4°C in 400 µl buffer IP_E each (10 mM glycine, pH 1.0). The elutions were individually precipitated by adding 1.2 ml of ice-cold acetone, vortexing and incubating the fractions overnight at -20°C. The mixtures were then centrifuged in a tabletop centrifuge (20,000 × g, 30 min, , 4°C) and the supernatant discarded. The resulting pellets were dryed on ice and then subjected to analysis by mass spectroscopy by Yibo Wu (group of Prof. R. Aebersold, ETH Zürich). For a general overview of the IP-aliquots prepared for one SILAC-experiment see **Figure 5.13**:.

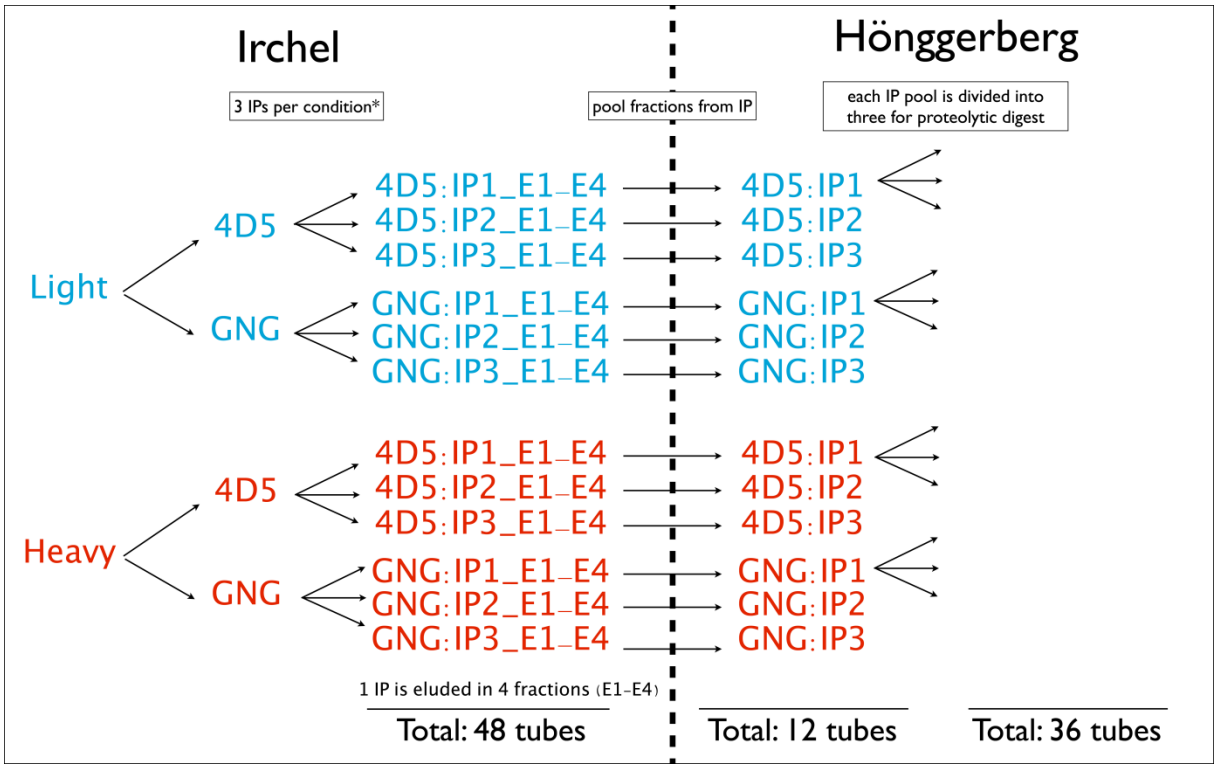

Figure 5.13: List of the IP-aliquots prepared for quantitative phosphomapping of HER2 by mass spectrometry. In this particular experimental set up, BT474 cells treated with either trastuzumab (4D5) or DARPin G3_N6C_G3 (GNG) were compared. In general, all samples were prepared in duplicates both from cells grown in unlabeled medium (Light, blue) and isotopically labeled medium (Heavy, red). Each treatment condition was performed in biological triplicates (IP1–IP3), each stemming from 2 × 10^6 cells. The protein precipitates E1–E4 were pooled and subjected to three different proteolytic digests using Glu-C, Asp-N or trypsin, followed by analysis by mass spectrometry.

3.7 Cell proliferation assays with further interesting constructs

One of the big advantages of the DARPin-fold, namely the possibility to easily generate and test multivalent binders in different formats, led to cell proliferation tests with further constructs, besides the rigidly linked homo-bivalent constructs discussed in **Chapter 2** and the flexibly linked bispecific constructs detailed in **Chapter 3** and **Chapter 4**.

Since DARPins binding to the HER2-homologues EGFR and HER4 had been selected recently (Steiner *et al.* (2008)), it seemed likely to produce further bispecific DARPin constructs that would not only recognize two different subdomains of one receptor-homologue (like described in **Chapters 3** and **4**) but different receptor-homologues, per se.

This section is meant to give a brief outline of the most interesting hetero-bispecific DARPin-constructs (i.e. constructs specific for two different HER-homologs), that could be identified in XTT-assays on BT474 cells. The bivalent binders were constructed from DARPins E.01 (α-EGFR), E.69 (α-EGFR), G3 (α-HER2) or B4.50 (α-HER4) lacking any anti-proliferative effect on BT474 cells in the monovalent format (**Figure 5.14**:). As seen with homo-bispecific HER2-binding constructs (i.e. constructs bivalently binding HER2), the most interesting hetero-bispecific constructs tested were the ones with flexible linkers. Furthermore, in agreement with the results obtained with the bispecific HER2-binding DARPins (**Chapter 3**), shortening of the linker improved the anti-proliferative effect (**Figure 5.15**: and **Figure 5.16**:). In general, the most effective hetero-bispecific constructs were those composed of the HER2_IV-binding DARPin G3 in combination with either HER4-binding DARPin B4.50 or one of the EGFR-binding DARPins E.01 or E.69. Hetero-bispecific constructs with a HER2_I-binding DARPin could not be found to show significant effects on BT474 cell proliferation (cf. construct 9.26_11_E.01 in **Figure 5.14**:).

The main part of this work was performed in collaboration with Jakob Stüber and further details (and constructs that proved to be of no further interest) can be found in his master's thesis. **Figure 5.17:** is added in addition to the data discussed in **Chapter 2**. Interestingly,

bivalent fusion of scFv 4D5 via a double helix motive (4D5-scdHLX) abolishes the slight antiproliferative effect caused by the monovalent scFv 4D5.

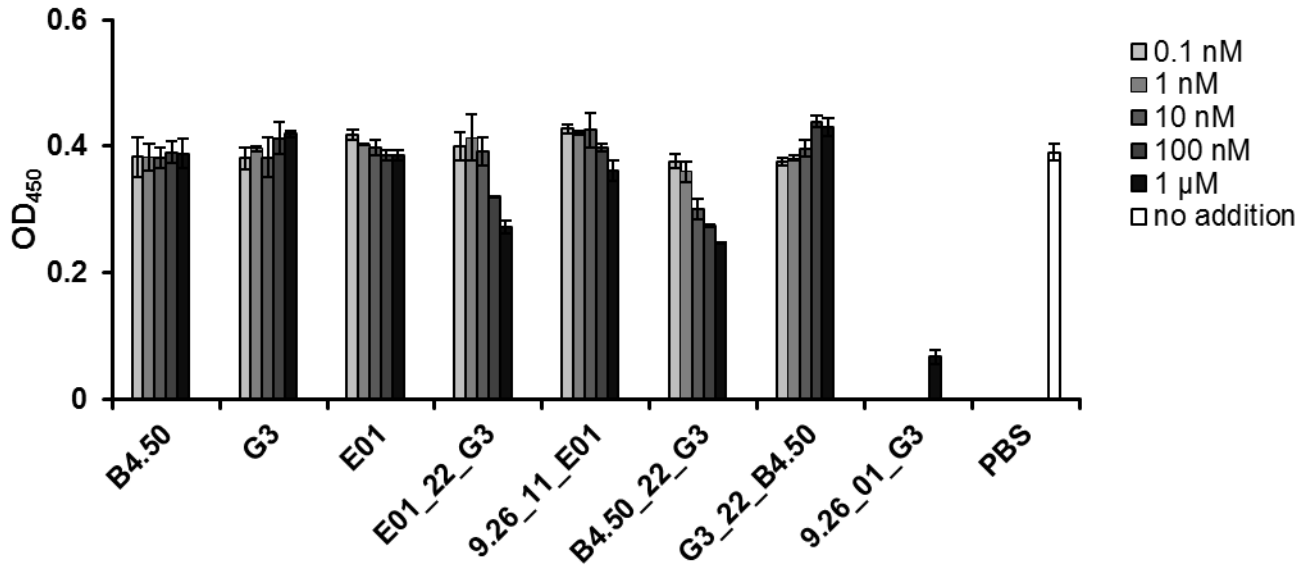

Figure 5.14: Cell proliferation assay (XTT) on BT474 cells with dilution series of different monovalent DARPins or different hetero-bispecific DARPins (_22_, _11_ or _01_ indicate linker length of 20, 10 or 5 aa). Cells were seeded with 10,000 cells × cm^{-2} and allowed to attach for 24 hours. Cell viability after an additional four days of growth with or without treatment (PBS) was measured by XTT-assays (indicated as OD_{450}). Cells grown in the presence of 1 µM 9.26_01_G3 (cf. Chapter 2) served as control.

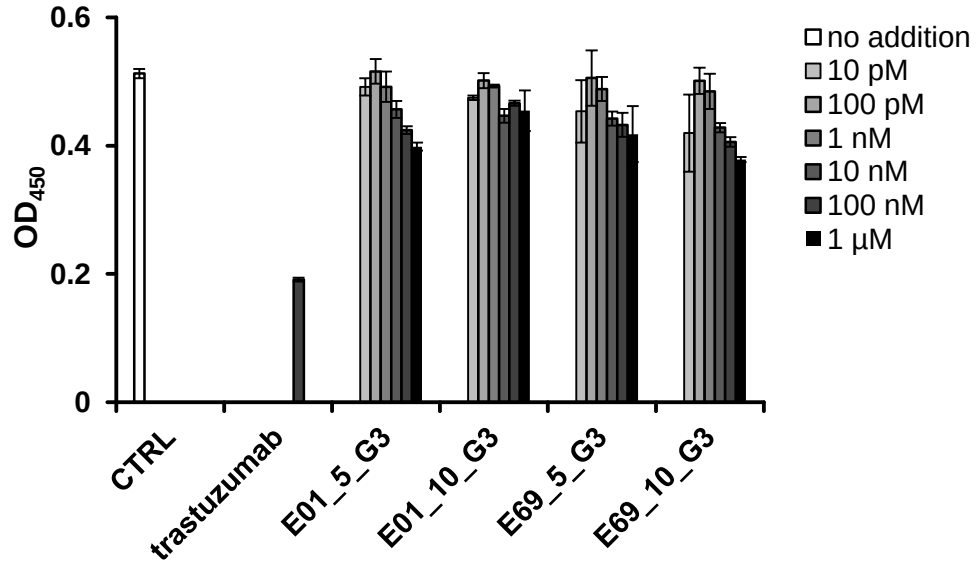

Figure 5.15: Cell proliferation assay (XTT) with dilution series of hetero bispecific DARPins composed of DARPins E01 or E69 (α-EGFR) and DARPin G3 (α-HER2) on BT474 cells. Cells were seeded with 10,000 cells × cm^{-2} and allowed to attach for 24 hours. Cell viability after additional four days of growth with or without treatment (Ctrl) was measured by XTT-assays (indicated as OD_{450}). Cells grown without treatment (CTRL) or in the presence of 100 nM trastuzumab served as control.

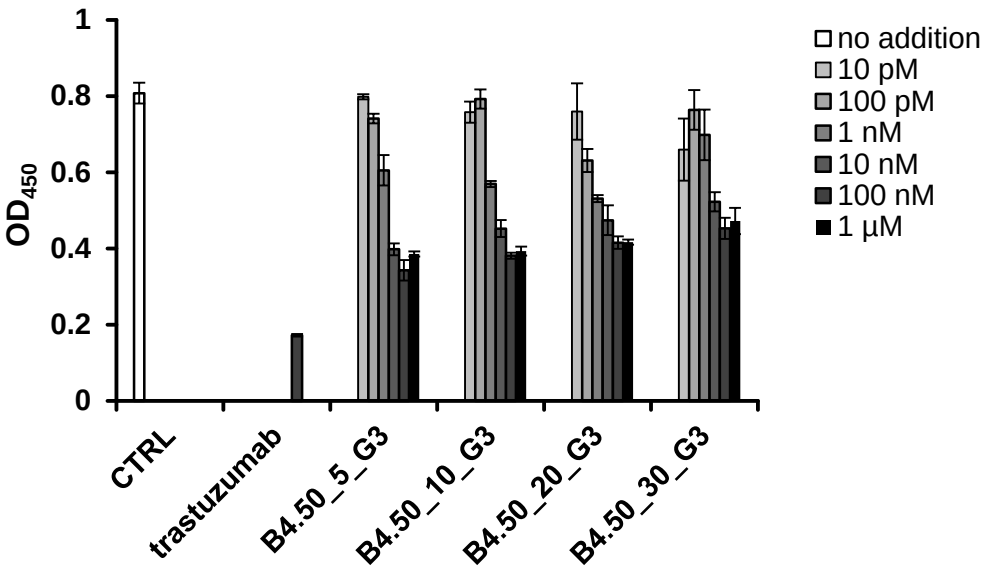

Figure 5.16: Cell proliferation assay on BT474 cells with dilution series of hetero bispecific DARPins composed of DARPin B4.50 (α-HER4) and DARPin G3 (α-HER2). The constructs differ in linker length (5, 10, 20 or 30 aa). Cells were seeded with 10,000 cells × cm^{-2} and allowed to attach for 24 hours. Cell viability after additional four days of growth with or without treatment was measured by XTT-assays (indicated as OD_{450}). Cells grown without treatment (CTRL) or in the presence of 100 nM trastuzumab served as control.

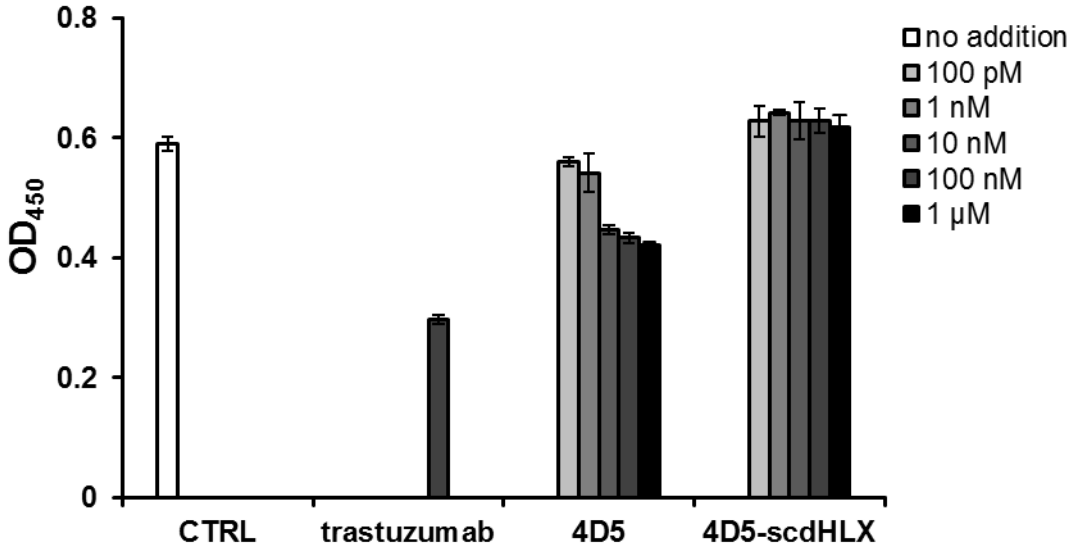

Figure 5.17: Cell proliferation assay with dilution series of monovalent scFv 4D5 and bivalent 4D5-scdHLX on BT474 cells. Cells were seeded with 10,000 cells × cm^{-2} and allowed to attach for 24 hours. Cell viability after additional four days of growth with or without treatment (Ctrl) was measured by XTT-assays (indicated as OD_{450}). Cells grown without treatment (CTRL) or in the presence of 100 nM trastuzumab served as control.

4 References

1. de Noronha CM & Mullins JI (1992) Amplimers with 3'-terminal phosphorothioate linkages resist degradation by vent polymerase and reduce Taq polymerase mispriming. *PCR Methods Appl.* 2:131-136.
2. Fitzgerald DJ*, et al.* (2006) Protein complex expression by using multigene baculoviral vectors. *Nat. Methods* 3:1021-1032.
3. Forrer P & Jaussi R (1998) High-level expression of soluble heterologous proteins in the cytoplasm of Escherichia coli by fusion to the bacteriophage lambda head protein D. *Gene* 224:45-52.
4. Hansen RE, Østergaard H, Nørgaard P, & Winther JR (2007) Quantification of protein thiols and dithiols in the picomolar range using sodium borohydride and 4,4'-dithiodipyridine. *Anal. Biochem.* 363:77-82.
5. Lange C & Rudolph R (2008) Production of Recombinant Proteins for Therapy, Diagnostics, and Industrial Research by in Vitro Folding. in *Protein Folding Handbook (eds J. Buchner and T. Kiefhaber)* (Wiley-VCH Verlag GmbH, Weinheim, Germany).
6. Pack P*, et al.* (1993) Improved bivalent miniantibodies, with identical avidity as whole antibodies, produced by high cell density fermentation of Escherichia coli. *Biotechnology. (N. Y).* 11:1271-1277.
7. Pack P & Plückthun A (1992) Miniantibodies: use of amphipathic helices to produce functional, flexibly linked dimeric FV fragments with high avidity in Escherichia coli. *Biochemistry (Mosc).* 31:1579-1584.
8. Stefan N*, et al.* (2011) DARPins recognizing the tumor-associated antigen EpCAM selected by phage and ribosome display and engineered for multivalency. *J. Mol. Biol.* 413:826-843.
9. Steiner D, Forrer P, & Plückthun A (2008) Efficient selection of DARPins with sub-nanomolar affinities using SRP phage display. *J. Mol. Biol.* 382:1211-1227.
10. Timmerman P, Beld J, Puijk WC, & Meloen RH (2005) Rapid and quantitative cyclization of multiple peptide loops onto synthetic scaffolds for structural mimicry of protein surfaces. *ChemBioChem* 6:821-824.

Chapter 6

Discussion, Conclusions and Outlook

Content

1 Discussion and Conclusions 204

2 Outlook 206

3 References 209

1 Discussion and Conclusions

During the last two decades, targeted tumor therapy has gained and still increases importance in the treatment of breast cancer. The prevailing class of binding molecules currently used are undoubtedly immunoglobulins (antibodies); nonetheless, antibody therapy of patients with metastatic breast cancer has been shown to be largely insufficient (Cobleigh *et al.* (1999)). Furthermore, the rather complex molecular architecture, limited stability and their tendency to aggregate make antibodies rather difficult (and expensive) to produce. This clearly argues for new, complementary approaches of targeted tumor therapy, making use of new, complementary binding scaffolds.

The ideal alternative to antibodies as tumor targeting and tumoricidal molecules would have to improve all of the above mentioned limitations, meaning it would have to be a molecular format of binders that have a simple fold (preferably produceable in bacteria), thermodynamically stable and non-aggregating. Such ideal binders would furthermore have to bind their respective targets with high affinity and specificity, and exhibit a long serum half life and good tolerance *in vivo*. The tumoricidal effects should either be caused by binding alone or should be attachable to the binder by easy fusion of effector molecules (either genetically or via simple directed chemistry).

Designed Ankyrin Repeat Proteins (DARPins) that have been developed within the last decade as a new class of binding proteins (cf. **Section 1.10**) fulfill nearly all of the above mentioned demands on ideal tumor targeting molecules. Solely the serum half life of DARPins is by far not as good as the serum half life of immunoglobulins, but can in principle be improved by making use of one of the DARPin-advantages, namely the feasible genetic fusion of another serum albumin binding DARPin, the chemical fusion of serum albumin itself or of a PEG moiety.

The question whether DARPins binding HER2 could be used for efficient tumor targeting of HER2 overexpressing cancer cells was the starting point of my diploma thesis, and the question how to improve the tumoricidal effects found for the monovalent HER2-binding DARPin H14 was consequentially the starting point of my PhD thesis.

With anti-HER2 DARPin constructs bivalently bridging pairs of HER2 molecules in a rigid manner (**Chapter 2**) and with DARPin constructs bispecifically binding HER2 molecules at subdomains I and IV (**Chapters 3** and **4**), we were able to develop HER2-binding DARPins with cytostatic and even cytotoxic effects on HER2 overexpressing and HER2 addicted cancer cells. Since these cancer cells are dependent on HER2 signaling for proliferation, the DARPin-induced interference with the receptor steady state leads to anti-proliferative effects that are caused by binding only. The reason for the observed difference in effectiveness of the homo-bivalent rigid constructs in comparison to the (more potent) flexibly linked bispecific constructs lies most likely in the difference in DARPin-induced interference with the conformation of the HER2_ECD. Whereas the homo bivalent rigid constructs just bridge HER2 molecules in the (still) open confirmation, binding of the flexibly linked bispecific constructs induces at least half of the bound HER2 ECDs to "bow down". Therefore the latter DARPin constructs prevent HER2 dimerization, both canonical and lateral, and both homo- and heterodimerization, far more effectively than the homo-bivalent rigid constructs.

The crystal structures of three different HER2-binding DARPins provided within this thesis are crucial for the explanation of the observed tumoricidal effects. In addition, the obtained information on the DARPin epitopes on HER2 did stimulate and affect several fruitful collaborations aiming to use DARPins as a targeting domain for lentiviral vectors (**Appendix 1**), as binding moieties in proximity ligation (**Appendix 2**) and for ligand based receptor identification on living cells (**Appendix 3**).

The success in developing bivalent and bispecific HER2-binding DARPin constructs with antiproliferative effects on HER2 addicted cancer cells raises the question whether the lessons lerned within this project might be applicable to other binders or other oncogenes.

In fact we are quite certain that the strategy to abolish HER2 signaling e.g by binding HER2_I and HER2_IV with one binding molecule should be applicable to other formats like antibody fragments or affibodies. We believe that the "blueprint" provided here is neither

limited to certain epitopes on HER2, nor to the DARPin format, which is why we have applied for a patent protecting the principle of causing strong tumoricidal effects on HER2 addicted cells with bispecific binders against HER2_I and _IV.

The final goal of the overall project, that is to elicit cytotoxic effects on HER2 overexpressing tumors in human, obviously still awaits to be reached, hopefully by an industrial partner capable to undertake this final step. Like described above, crucial aspects like the constructs' immunogenicity in human and means to improve serum half life will have to be taken into account. The final DARPin-constructs for *in vivo* tests in human will most probably have to be redesigned (e.g. removing T-cell epitopes), which should however be easily doable thanks to the rigid DARPin fold and the well defined blueprint for tumoricidal anti-HER2-constructs.

2 Outlook

The effort to obtain a complex structure of DARPin H14 which has been discussed in **Chapter 2** is currently ongoing and we are still busy with screening e.g. rigid DARPin-betalactamase-fusions and DARPin-DARPin-fusions for crystal formation in complex with HER2_IV (a project performed as the master's thesis work of Ms. Ye Xie).

Likewise ongoing is the SILAC project described in Section 3.6 of **Chapter 5**.

One interesting continuation of the here presented study is of course the attempt to transfer the blueprints for effective antiproliferative DARPin constructs onto constructs composed of alternative binding scaffolds on the one hand, and onto constructs binding other targets than HER2 on the other hand. The hetero-bispecific constructs described in Section 3.7 of **Chapter 5**, that is constructs composed of DARPins binding EGFR and HER2 or HER4 and HER2, have so far mainly been tested on the HER2 overexpressing cell line BT474. It would of course be interesting to test such heterospecific constructs on other cell lines with other patterns of

overexpressed ErbB receptors. Furthermore, it would be interesting to screen for further binders, e.g. to HER3 to then use such new monovalent binders for the incorporation into further bispecific constructs. Obviously, the feasibility of easy molecular construction made possible by the DARPin fold allows for nearly too many things to think of at one time.

The hetero-bispecific constructs binding HER4 and HER2 await further characterization. Different from the EGFR binding DARPins E.01 and E.69, that have been mapped to bind to subdomains III and I, respectively (Boersma *et al.* (2011)), the epitope of DARPin B4.50 has so far not been mapped on HER4_I-III (which had been used for panning). The required expression of single HER4 domains I, II and III for an approximate epitope mapping on domain level is currently ongoing.

The detailed knowledge on the epitopes of the DARPins best suited for the assembly of efficient bispecific constructs, in combination with the possibility to produce "tailor-made" parts of the target subdomain in Sf9 cell expression established within this thesis, would allow to select new binders by means of ribosome or phage display.

Along the same lines it would be possible to select for further DARPins binding to new epitopes, e.g. on the lateral site of HER2, to preclude non-canonical receptor dimers like shown for the DNA aptamer A30 (Chen *et al.* (2003)).

Again, production of "tailor-made" target protein in Sf9 cells could allow to direct the DARPin selection to the epitope of highest interest.

One project that has recently been started as collaboration with the lab of Prof. David Baker aims for the *ab initio in silico* design of an HER3 binding DARPin. Inspired by the high accuracy with which computational docking could be used to predict the binding of DARPin G3 to HER2_IV (**Apendix 4**) we would like to do the reverse and use computational docking and homology modeling to design a DARPin that binds to HER3_IV in a similar way like DARPin G3 binds to HER2_IV. The rigid nature of both the binder and the target and the high homology between the respective epitope on HER2 and HER3 are prerequisites that should facilitate this endeavor.

Certainly such homology modeling will not directly come up with an *ab initio* blueprint for a high affinity binder, but affinity can of course always be improved by means of affinity maturation and prescibing the epitope and the direction of binding would be a very interesting new achievement.

Another far simpler follow-up study could make further use of the crystal structures of DARPins 9.29 and 9.26. The complex structures presented in **Chapter 3** interestingly show that both N3C DARPins bind via their N-cap and first two internal repeat modules only. As the third internal repeat module and the C-cap do not make interactions with the target, one could either think of removing the third internal module, or elongating the DARPin as a C-terminally elongated chimeric DARPin (using the protocol for the assembly of chimeric DARPins given in **Section 2.2** of **Chapter 5**).

Incorporating such a shortened or elongated DARPin 9.29 into the bispecific constructs discussed in **Chapters 3** and **4** would of course be interesting as well.

3 References

1. Boersma YL, Chao G, Steiner D, Wittrup KD, & Plückthun A (2011) Bispecific designed ankyrin repeat proteins (DARPins) targeting epidermal growth factor receptor inhibit A431 cell proliferation and receptor recycling. *J. Biol. Chem.* 286:41273-41285.
2. Chen CH, Chernis GA, Hoang VQ, & Landgraf R (2003) Inhibition of heregulin signaling by an aptamer that preferentially binds to the oligomeric form of human epidermal growth factor receptor-3. *Proc. Natl. Acad. Sci. U. S. A.* 100:9226-9231.
3. Cobleigh MA*, et al.* (1999) Multinational study of the efficacy and safety of humanized anti-HER2 monoclonal antibody in women who have HER2-overexpressing metastatic breast cancer that has progressed after chemotherapy for metastatic disease. *J. Clin. Oncol.* 17:2639-2648.

Appendix 1

DARPins: An Efficient Targeting Domain for Lentiviral Vectors

Münch RC, Mühlebach MD, Schaser T, Kneissl S, Jost C, Plückthun A, Cichutek K, Buchholz CJ

(My contribution: screening and characterization of the utilized anti-HER2-DARPins)

original article

© The American Society of Gene & Cell Therapy

DARPins: An Efficient Targeting Domain for Lentiviral Vectors

Robert C Münch[1], Michael D Mühlebach[1], Thomas Schaser[1], Sabrina Kneissl[1], Christian Jost[2], Andreas Plückthun[2], Klaus Cichutek[1] and Christian J Buchholz[1]

[1]*Division of Medical Biotechnology, Paul-Ehrlich-Institut, Langen, Germany;* [2]*Department of Biochemistry, University of Zurich, Zurich, Switzerland.*

We have recently developed a retargeting system for lentiviral vectors (LVs) that relies on the pseudotyping of LVs with engineered measles virus (MV) glycoproteins (hemagglutinin (H) and fusion protein (F)). Specificity is provided through display of a single-chain antibody (scFv) as targeting domain by fusion to the MV-H protein. As an alternative to scFv, designed ankyrin repeat proteins (DARPins) can be selected to become high-affinity binders to any kind of target molecule. In this study six HER2/*neu*-specific DARPins exhibiting different affinities and binding to different HER2/*neu* epitopes were applied as targeting domains. All H-DARPin fusion proteins were efficiently expressed on the cell surface. Upon coexpression with F, syncytia formation was observed in HER2/*neu* positive cells only and correlated directly with the HER2/*neu* receptor density. All H-DARPin proteins incorporated into LVs, albeit at different levels. The vectors only transduced HER2/*neu*-positive cells, while HER2/*neu*-negative cells remained untransduced. Highest titers were observed with one particular DARPin binding to the membrane distal domain of HER2/*neu* with medium affinity. When applied *in vivo* systemically, HER2/*neu*-targeted LVs showed exclusive gene expression in HER2/*neu* positive tumor tissue, while vesicular stomatitis virus-glycoprotein (VSV-G) pseudotyped vectors mainly transduced cells in spleen and liver. Thus, DARPins are a promising alternative to scFvs for retargeting of LVs.

Received 1 November 2010; accepted 10 December 2010; published online 11 January 2011. doi:10.1038/mt.2010.298

INTRODUCTION

Virus-derived vectors have become one of the most promising gene delivery systems for human cells. Especially lentiviral vectors (LVs) provide an outstanding therapeutic potential by stable long-term transgene expression in nondividing cells.[1,2] The particle surface design of γ-retroviral vectors and LVs has been constantly improved during the last 20 years, starting with the use of murine leukemia virus envelope proteins, those of other γ-retroviruses and finally the glycoprotein (G) of the vesicular stomatitis virus (VSV), which mediates efficient transduction of basically all human cell types.[3] More recent developments aim at restricting the vector tropism at the level of cell entry to the target cell population defined by a specific surface antigen. It is expected that this will facilitate *in vivo* gene transfer strategies and reduce the vector dose required for successful therapy. Promising progress in this direction has recently been obtained by engineering viral envelope proteins that have the receptor attachment and membrane fusion functions separated into two glycoproteins.[4–7]

The measles virus (MV) glycoproteins, namely, hemagglutinin (H) and fusion protein (F), mediate cell entry directly at the cell membrane in a pH-independent manner.[8] The H-protein attaches the virus to the natural MV receptors CD46 and signaling lymphocyte-activation molecule and forms a complex with F protein to accomplish its fusion helper function. We have recently demonstrated that F and H can be incorporated into LVs, provided their N-terminal cytoplasmic tails are truncated.[9] Such MV–LVs were then retargeted to various cell types using a mutant of the H-protein with 4 point mutations that lost use of its natural receptors and fusing a cell type-specific single-chain antibody (scFv) to the C-terminus of the H-protein extracellular domain.[9,10]

The aim of this study was to evaluate designed ankyrin repeat proteins (DARPins) as an alternative targeting domain to scFvs for MV–LVs. DARPins are based on naturally occurring ankyrin repeat proteins—a ubiquitously expressed protein family that mediates specific protein–protein interactions.[11] By a consensus-design approach an ankyrin repeat module comprising 33 amino acid residues was derived in which residues that potentially can interact with the target are randomized. By combining 2–3 of these repeats and flanking them by N- and C-capping repeats (termed N2C or N3C), combinatorial libraries of DARPins have been obtained. These libraries can be selected against almost any kind of ligand using ribosome display (library diversities $>10^{12}$) or phage display (library diversity $>10^{10}$).[12,13] Specific binders with affinities in the pmol/l range have been obtained at high frequency. These molecules have no cysteines, and show very low tendencies of aggregation. They may thus have great promise in their application as fusion proteins to membrane proteins as the ones investigated here, where other fused targeting proteins, such as some aggregation-prone scFv fragments, would compromise the efficiency of correct assembly and thereby lead to low display levels.

Here, we report that DARPins can be used to re-target LVs to HER2/*neu* positive cancer cells. Belonging to the epidermal growth

Correspondence: *Christian J Buchholz, Division of Medical Biotechnology, Paul-Ehrlich-Institut, Paul-Ehrlich-Street 51-53, 63225 Langen, Germany. E-mail: bucch@pei.de*

© The American Society of Gene & Cell Therapy

factor family HER2/*neu* is a type-I receptor tyrosine kinase, which is highly expressed on breast, ovarian, colon and pancreatic cancer cells but shows low level or no expression on all normal human tissue.[14] By using a panel of six DARPins exhibiting distinct affinities for HER2/*neu* and using different binding sites, we could show that chimeric H-DARPin proteins are well expressed and incorporated in LVs and able to redirect membrane fusion via HER2/*neu*. The data suggest that a membrane distal binding site for HER2/*neu* mediates optimal cell entry of DARPin displaying LVs. By systemic application in a bilateral xenograft mouse model we demonstrate the *in vivo* targeting potential of these alternative binding molecules.

RESULTS

H-DARPin surface expression levels

Starting from plasmid pCG-H-α-CD20 encoding an H-protein mutated in its receptor binding sites and fused to a CD20-specific scFv,[9] we substituted the scFv coding sequence for that of six HER2/*neu*-specific DARPins[15,16] resulting in constructs pH-D9.29, pH-D9.26, pH-D9.16, pH-D9.01, pH-DH14R, and pH-DG3 (**Figure 1a**). As controls, we also generated an expression plasmid for an H-protein displaying the HER2/*neu*-specific scFv 4D5 (pH-scFv4D5)[17] and scFv 7A5, which does not allow cell surface expression as H fusion protein.[18] As sufficient surface expression of H fusion proteins is a critical prerequisite for the efficient pseudotyping of LVs, we transfected cells with the H-DARPin expression plasmids and determined the cell surface expression levels by fluorescence-activated cell sorter analysis. All six H-DARPin proteins showed high surface expression rates in a similar range (mean fluorescence intensity 1,500–3,200) (**Figure 1b**). H-DARPin-9.29 exhibited the highest surface expression (mean fluorescence intensity = 3,200), which was about twice that of the H-scFvCD20 protein (mean fluorescence intensity = 1,600) and almost three times higher than that of H-scFv4D5 (MFI = 1,100).

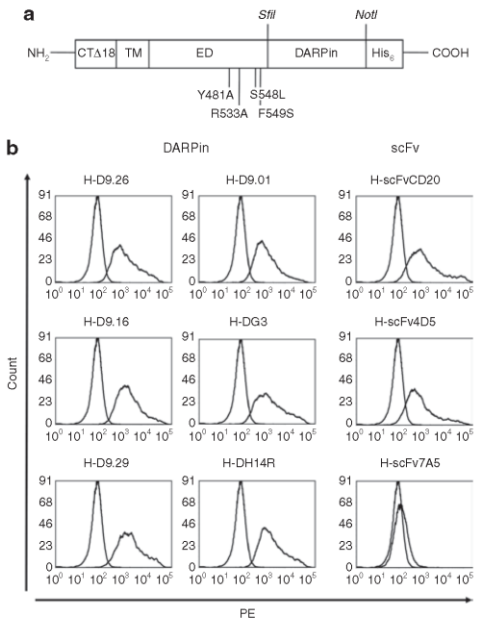

Figure 1 Organisation of hemagglutinin (H)-designed ankyrin repeat proteins (DARPins) and cell surface expression. (**a**) Schematic drawing of the modified MV-H used for retargeting, derived from strain Edmonston B (SwissProt P08362).[31] Four point mutations in the ectodomain (ED) ablating binding to CD46 and signaling lymphocyte-activation molecule (the natural receptors) are indicated.[9] An N-terminal cytoplasmic tail truncation by 18 amino acids (CTΔ18) allows stable incorporation into lentiviral particles.[9] The C-terminus of H is fused via a *Sfi*I site to the DARPin, resulting in the sequence EDGTNAAQPADLGKKL where the first underlined sequence is the C-terminus of H and the second is the N-cap of the DARPin. The DARPin terminates in the sequence EILQKLNAAARGSHHHHHH (DARPin C-cap is underlined). The transmembrane domain (TM) and the His-tag are indicated. (**b**) Expression plasmids for six different H-DARPin and three H-scFv fusion proteins were transfected into HEK-293T cells. Surface expression was analyzed after 48 hours using a His-tag-specific antibody (PE-labeled). H-scFvCD20 and H-scFv7A5 were used as positive and negative controls.

H-DARPin fusion helper function

Besides high surface expression levels of the H-DARPin proteins, it is essential that their fusion helper function is maintained for successful retargeting of LVs. To assess the fusion helper function of the H-DARPin proteins, the corresponding expression plasmids were co-transfected with pCG-FΔ30 (encoding a C-terminally truncated F protein,[9] **Figure 1a**) into SK-OV-3 cells, which express high levels of HER2/*neu* (**Table 1**). Membrane fusion can then be followed by the formation of syncytia through fusion of adjacent cells. All tested H-DARPin proteins caused syncytia formation. Quantification revealed that the H-DH14R and the H-DG3 proteins exhibited the strongest fusion helper function reaching almost 70% of that of the unmodified H-protein (**Figure 2a**).

To investigate the influence of the HER2/*neu* receptor density on cell–cell fusion, we generated a panel of stably transfected CHO clones expressing different HER2/*neu* surface levels (**Table 1**). The membrane fusion activity mediated by the H-DG3 and H-DH14R proteins on these cells was compared to that of the H-scFv4D5 protein. All three proteins mediated syncytia formation on cells with high (2×10^5 receptors/cell) and medium (4×10^4 receptors/cell) receptor levels. Low levels (8×10^2 receptors/cell) were not sufficient for syncytia formation to proceed (**Figure 2b**).

Table 1 HER2/*neu* surface density of applied cell lines

Cell line	HER2/*neu*-density[a]
CHO-Her2-k6	2.1×10^5
SK-OV-3	1.3×10^5
CHO-Her2-k13	3.7×10^4
HEK-293T	4.2×10^3
HT1080	2.3×10^3
CHO-Her2-k7	7.7×10^2
CHO-K1	$<1.0 \times 10^{2b}$
U87MG	$<1.0 \times 10^{2b}$

[a]Number of HER2/*neu* molecules per cell. [b]Background level as determined by isotype control.

© The American Society of Gene & Cell Therapy

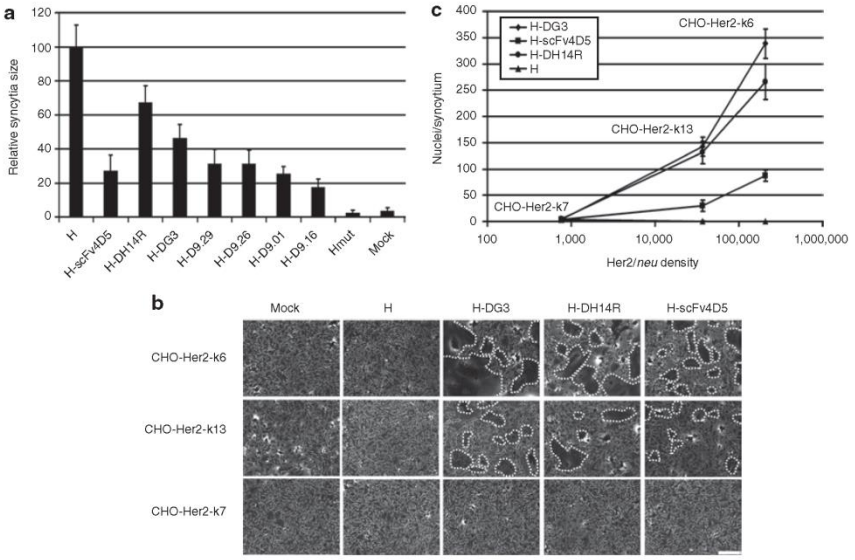

Figure 2 Fusion helper function of hemagglutinin (H)-designed ankyrin repeat proteins (DARPins). (**a**) SK-OV-3 cells were co-transfected with pCG-FΔ30 and each of the H-DARPin or H-scFv4D5 fusion protein encoding plasmids. pCG-HcΔ18 and pCG-HcΔ18mut (blinded for CD46 and signaling lymphocyte-activation molecule binding) coding for cytoplasmic tail truncated H proteins without fused DARPin were used as controls. Syncytia formation was normalized to that observed for pCG-HcΔ18 transfected cells (i.e., H). The results are expressed as mean values of 20 syncytia analysed for each sample. (**b**) H-DG3, H-DH14R and H-scFv4D5 mediated syncytia formation on CHO-Her2-k6, CHO-Her2-k13 and CHO-Her2-k7 cells. Untransfected and pCG-HcΔ18 transfected cells served as controls. Syncytia are indicated with dashed lines. Scale bar corresponds to 500 µm. (**c**) Correlation between syncytia size mediated by H-DG3, H-DH14R or H-scFv4D5 and HER2/*neu* receptor density. The results are expressed as mean values of 20 syncytia analyzed.

Likewise, HER2/*neu* negative cells did not form syncytia, demonstrating the HER2/*neu* specificity of the process. Plotting the membrane fusion activities of the proteins against the receptor densities demonstrated a direct correlation between both parameters (Figure 2c). Independent from the receptor levels, the fusion helper function of H-DG3 and H-H14R proteins was about fourfold more efficient than the function of the H-scFv4D5 protein (Figure 2c).

Generation and characterization of HER2/*neu*-targeted LVs

Having demonstrated HER2/*neu*-specific membrane fusion helper function, the H-DARPin proteins were next used for pseudotyping LVs. The corresponding vector particles (D9.29-LV, D9.26-LV, D9.16-LV, D9.01-LV, DH14R-LV, DG3-LV) were first assayed for the incorporation levels of the H-DARPin proteins. All six H-DARPin proteins were detectable in the particles albeit at different levels. There were only very low levels of the proteins H-D9.01 and H-scFv4D5 incorporated, while H-D9.16 showed moderate incorporation levels (Figure 3, Table 2). High incorporation levels were observed for the proteins H-DG3, H-D9.26 and H-DH14R, and the strongest incorporation for H-DARPin-9.29 (Figure 3, Table 2).

Next, we determined the targeting potential of the DARPin-LV particles by transducing a set of cell lines expressing different

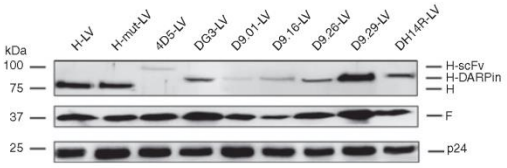

Figure 3 H-DARPin and F incorporation into HER2/*neu* targeting vectors. Western Blot analysis of the indicated LVs. Particle amounts loaded onto 10% sodium dodecyl sulfate–polyacrylamide gels were equivalent to 30 ng of p24 for each vector type. Proteins were detected utilizing anti-F, anti-H, or anti-p24 antibodies. Vector particles pseudotyped with unmodified or mutated H-protein (MV–LV, MVmut-LV) were used as controls.

HER2/*neu* levels, i.e., HER2/*neu* negative CHO-K1, low level HER2/*neu* expressing HEK-293T and high level HER2/*neu* expressing CHO-Her2-k6 and SK-OV-3 cells (see Table 1 for receptor densities). None of the DARPin-LVs transduced CHO-K1 cells, while some green fluorescent protein expressing cells were detected on HEK-293T cells (Figure 4a). Many more green fluorescent protein-positive cells were detectable on CHO-Her2-k6 and SK-OV-3 cells, especially upon incubation with D9.29-LV (Figure 4a). Calculation of vector titers revealed that on HEK-293T cells maximal titers of 1×10^4 t.u./ml were reached by vectors D9.29-LV, D9.26-LV, and DG3-LV (Figure 4b). On SK-OV-3

© The American Society of Gene & Cell Therapy

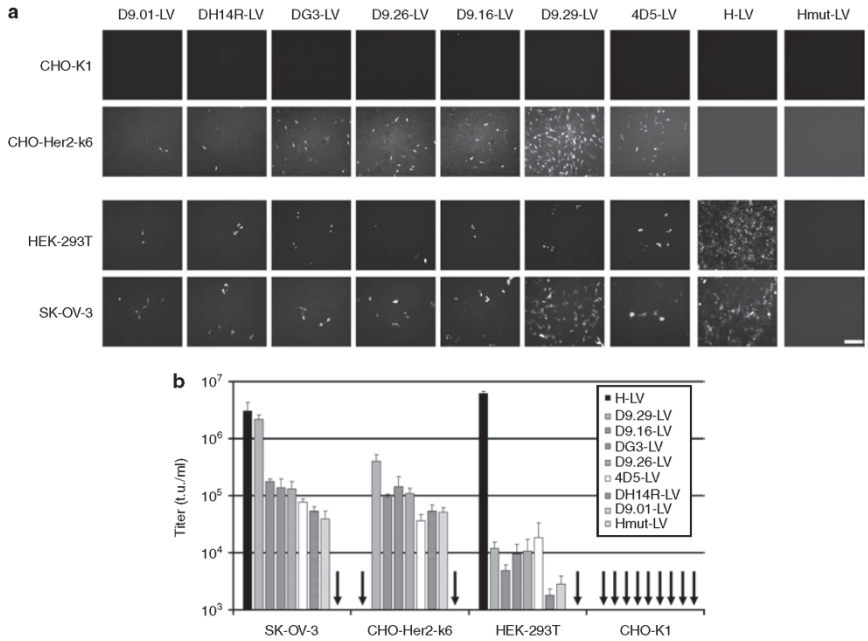

Figure 4 Selective transduction of HER2/*neu* positive cell lines. (**a**) CHO-K1, CHO-Her2-k6, HEK-293T, or SKOV-3 cells were incubated with vector particle supernatant. Transduced cells were visualized by fluorescence microscopy 48 hours after transduction. Scale bar corresponds to 500 µm. (**b**) The indicated cell lines were transduced with serial dilutions of each vector stock. Titers (t.u./ml) were calculated upon quantification of green fluorescent protein-positive cells by fluorescence-activated cell sorter analysis. Mean values of three independent transduction experiments are presented.

and CHO-Her2-k6 cells, all vectors reached at least tenfold higher titers. Moreover, most DARPin displaying LVs were considerably more efficient in mediating gene transfer via HER2/*neu* than 4D5-LV, which was 10–30 times less efficient. D9.29-LV was especially effective on SK-OV-3 cells where it showed the highest titers of all vector types tested (Figure 4b).

Transduction of mixed cell populations and *in vivo* application of HER2/*neu*-targeted LVs

After demonstration of HER2/*neu* receptor specificity and identification of the most effective H-DARPin protein (i.e., H-DARPin-9.29), we assessed the target cell specificity in co-cultures of CHO-Her2-k6 and CHO-K1 cells. VSV-G–pseudotyped LV (VSV-G-LV) transduced both cell lines at equal efficiency (Figure 5). In contrast, D9.29-LV only transduced CHO-Her2-k6 cells, even when these were clearly underrepresented (Figure 5).

The *in vivo* targeting potential of D9.29-LV was assessed in a xenograft mouse model carrying a HER2/*neu*-positive (SK-OV-3 cells) and a HER2/*neu*-negative tumor (U87MG cells). After both tumors were fully vascularized the luciferase transferring vectors D9.29-LV^{luc} and VSV-G-LV^{luc} were injected systemically through the tail vein and mice were analyzed using charged-coupled device imaging. D9.29-LV^{luc} showed strong luciferase activity in the SK-OV-3 tumor already 3 days after injection while luciferase activity was below the level of detection in the U87MG tumor or

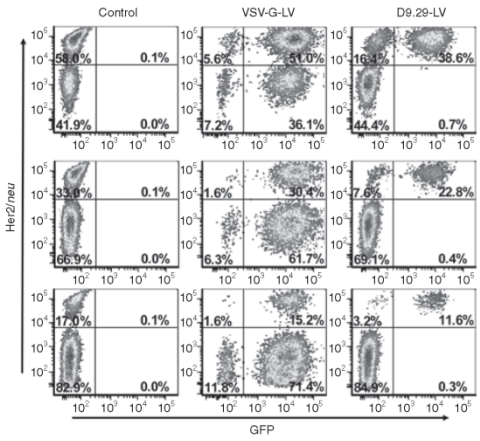

Figure 5 Target cell specificity of D9.29-LV in mixed cell cultures. CHO-Her2-k6 and CHO-K1 cells were mixed in three different ratios (see percentages in left gates in control panel) and then transduced with D9.29-LV (0.2 µg p24) or VSV-G-LV (0.02 µg p24) at a multiplicity of infection of 2.5, or left untransduced (control). Forty-eight hours after transduction, cells were analyzed by fluorescence-activated cell sorter analysis for green fluorescent protein fluorescence and HER2/*neu* expression. HER2/*neu* positive target cells were identified with a PE-labeled HER2/*neu*-specific antibody.

© The American Society of Gene & Cell Therapy

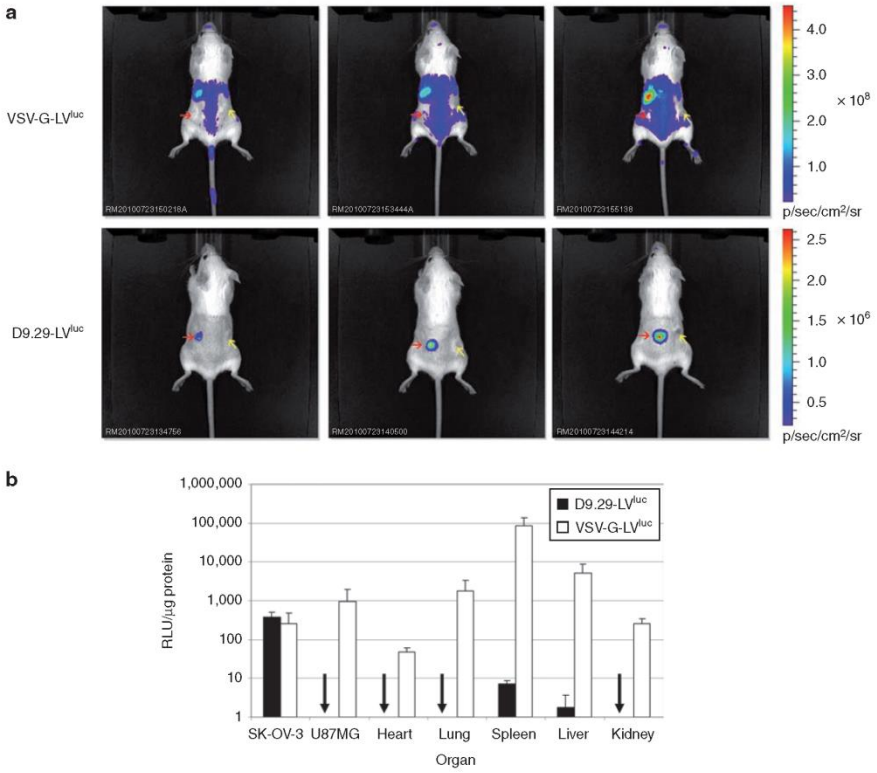

Figure 6 *In vivo* targeting of HER2/*neu* positive tumors. (**a**) Luciferase signals analyzed by *in vivo* imaging. Six- to 8-week-old CB17 SCID mice were injected with U87MG cells (right flank, yellow arrow) and SK-OV-3 cells (left flank, red arrow). After 11 days, 50 μg p24 of D9.29-LV^{luc} or 5 μg of VSV-G-LV^{luc} were injected into the tail vein. Two weeks postinjection, *in vivo* imaging data were monitored. Luciferase signal intensity is expressed as photons/second/square centimeter/steradian (p/sec/cm^2/sr). (**b**) Immediately after imaging, organs were isolated and homogenized. Luciferase activities were quantified and normalized to protein content. D9.29-LV^{luc} $n = 3$; mean ± SD; VSV-G-LV^{luc} $n = 4$; mean ± SD.

elsewhere in the mouse body (data not shown). Also after 2 weeks, luciferase activity could only be detected in the SK-OV-3 tumor, but not in the U87MG tumor or in spleen and liver (Figure 6a). In contrast VSV-G-LV^{luc} injected mice showed the most prominent signals in spleen and liver, whereas both tumors emitted a comparably low signal indistinguishable from other tissues (Figure 6a). Because the intensity of the charged-coupled device imaging can be influenced by variables such as depth of tissue and positioning of the animal during imaging, mice were killed and luciferase activitiy in organ lysates was quantified. D9.29-LV^{luc} injected mice showed the strongest luciferase activity in SK-OV-3 tumor lysates (4.0×10^2 RLU/μg protein), whereas the activity in U87MG tumor lysates was >1000-fold lower and remained at background level (3.0×10^{-1} RLU/μg protein) (Figure 6b). Besides the target tumor, a significant activity just above background was only detected in spleen (0.7×10^1 RLU/μg protein). In contrast, VSV-G-LV^{luc} injected mice revealed by far the most prominent signal in spleen (8.5×10^4 RLU/μg protein) and liver (5.1×10^3 RLU/μg protein), but comparably low luciferase activity in both tumor lysates (2.5×10^2 RLU/μg protein for SKOV and 9.3×10^2 RLU/μg protein for U87MG) (Figure 6b).

DISCUSSION

Here, we present proof of principle for applying DARPins as targeting domain of LV vectors. While adenovirus has recently been retargeted with DARPins[19] to our knowledge, this is the first description and *in vivo* demonstration of this type of application for DARPins for lentiviral gene transfer vector. Six different HER2/*neu*-specific DARPins, previously selected from DARPin libraries by ribosome or phage display,[15,16] were fused to the H-protein ectodomain at its C-terminus. A critical parameter for efficient LV particle incorporation of H proteins fused to targeting domains is their efficient cell surface expression. It was remarkable that all six H-DARPin proteins tested were readily expressed at the surface of HEK-293T cells. We did not observe any difference in surface expression between DARPins consisting of two or of three ankyrin repeats between the capping repeats. In each case, the surface expression levels were higher than those of H

© The American Society of Gene & Cell Therapy

Table 2 Properties of applied designed ankyrin repeat proteins (DARPins) and the corresponding vector particles

	DARPin-G3	DARPin-H14R	DARPin-9.29	DARPin-9.26	DARPin-9.16	DARPin-9.01	scFv4D5
K_D (nmol/l)[15,16]	0.09	0.20	3.80	1.40	6.90	N/A[a]	0.19
DARPin type[b]	N2C	N3C	N3C	N3C	N3C	N3C	-
Her2 binding domain[c]	IV	IV	I–III	I–III	I–III	N/A[a]	IV
Surface expression[d]	++	++	+++	++	++	++	+
Membrane fusion[e]	++	+++	++	++	+	++	+
Incorporation[f]	++	+++	++++	+++	++	+	+
Titer (t.u./ml)[g]	1.0×10^5	5.0×10^4	2.0×10^6	2.0×10^5	2.0×10^5	4.0×10^4	7.0×10^4

K_D, dissociation constant.
[a]Not available. [b]Number of ankyrin repeats, N is the N-capping repeat, the number the internal binding repeats and C is the C-terminal capping repeat.[15,16] [c]Her2/*neu* domains used for selection of the DARPins[15,16] [d]Mean fluorescence intensities from **Figure 1b**: +: 500–1,000; ++: 1,000–3,000; +++: >3,000. [e]Syncytia size on SK-OV-3 cells +: small syncytia up to 15 nuclei, ++: medium syncytia up to 50 nuclei, +++: large syncytia >50 nuclei. [f]Incorporation of H-DARPin proteins into vector particles normalized to p24 levels as determined by densitometric analysis of Western Blot shown in **Figure 3**, +: <1, ++: 1-2, +++: 2-3, ++++: 5.2; the data are representative for in total three independent Western Blots. [g]Mean titers of three independent vector production and titration experiments (see **Figure 4c**).

proteins fused to an scFv fragment, the HER2/*neu*-specific 4D5 or the CD20-specific scFv,[20] previously used to establish this targeting system.[9] Accordingly, all the H-DARPin fusion proteins were detected in vector particles, most of them at higher levels than H-scFv proteins. Moreover, while six out of six tested H-DARPin proteins were expressed at the cell surface and incorporated into vector particles, this was the case for only 12 of in total 25 H-scFv proteins tested so far (Schneider and Buchholz, unpublished results). When directly compared to a specific-scFv (4D5),[17] which recognized the same domain (IV) of HER/*neu* with a similar high affinity as DARPins G3 and H14R, between ten and 30-fold higher gene transfer efficiencies were observed for the DARPin displaying vectors (**Table 2**). Thus, DARPins seem to be better suited as targeting domain in context of the MV H-protein than scFv fragments. Even though in the current comparison only one scFv fragment was included, 4D5 scFv is known to be stable and well expressed,[21] and thus one with already above-average biophysical properties. DARPins have no disulfide bonds and are very resistant to aggregation, and thus probably more compatible with the folding and assembly of integral membrane proteins.

Most retrovirus receptors are multiple transmembrane spanning integral membrane proteins with rather small extracellular domains thus mediating binding in close proximity to the cell membrane.[22] For MV, it was shown that the distance between the viral binding site and the cell membrane correlates reciprocally with membrane fusion efficiency.[23] However, in such a receptor protein, the virus binding site is well accessible. If a membrane protein with a large, multi-domain extracellular region is used as receptor for the virus, it is essential that the epitope is accessible for the targeting domain within the context of the viral surface protein, in this case the MV H-protein. Unlike other members of the epidermal growth factor -receptor family, HER2/*neu* dimerises in absence of ligand contact.[24] This results in an exposed dimerisation domain, but covers partially the membrane proximal domain IV,[25] which therefore may be difficult to access by LVs binding to this domain. This may explain why DARPins binding to the membrane distal domains I–III of HER2/*neu* mediated more efficient gene transfer than those binding to the membrane proximal domain IV. It appears that affinity plays a smaller role, as gene transfer efficiency did not correlate with affinity (**Table 2**). One explanation for this finding would be multivalent binding, which would increase the functional affinity of the viral particle.

To assess the influence of the HER2/*neu* density on membrane fusion and gene transfer efficiency we analyzed a panel of cell lines expressing HER2/*neu* in a range of three orders of magnitude. We found that HER2/*neu* densities below 1,000 molecules per cell were insufficient to allow efficient membrane fusion and particle entry. With increasing densities, both syncytia formation and particle entry increased. Optimal gene transfer efficiency was observed above a density of 10^5 molecules per cell. Such an expression level of HER2/*neu* is found in certain types of cancer cells, such as e.g., the ovarian cancer cell line SK-OV-3. Thus, targeting specificity of these vectors critically depends on receptor density, which will facilitate the discrimination between cancer cells and noncancer cells.

Recently, a panel of recombinant MVs displaying HER2/*neu*-specific scFvs that ranged in their affinities from 10^{-6} to 10^{-11} mol/l have been described.[26] An affinity threshold of 1.6×10^{-8} mol/l for the displayed scFv was identified at which cell–cell fusion and cell entry of the virus proceeded efficiently. The affinities of the DARPins we used ranged from 7×10^{-8} mol/l to 10^{-10} mol/l, and thus were all above this threshold level. Our data are thus in line with those of Hasegawa *et al.* and extend them by demonstrating that, at least for MV–LV vector particles, above the threshold level, the location of the targeting domain binding site on HER2/*neu* is more important than affinity.

A surprising outcome of our study is the high tumor target specificity of D9.29-LV when applied by tail vein injection. It is well established that VSV-G-LV mainly accumulates in spleen and liver.[6,27] Our results are well in line with this revealing at least 100-fold more luciferase activity in spleen than in tumor tissue for VSV-G-LV. Previous attempts to detarget LVs from spleen and liver by surface engineering had limited success. Morizono *et al.* targeted lung tumor cells applying LVs pseudotyped with Sindbis virus envelope proteins bound to a tumor cell surface antigen-specific monoclonal antibody. They achieved a threefold higher luciferase activity in target compared to nontarget tissue.[5] D9.29-LV in contrast results in at least 40-fold more luciferase activity in the target

© The American Society of Gene & Cell Therapy

tumor than in off-target tissue. It is important to mention that off-target tissue was not only of murine origin, which is devoid of MV receptors, but also included a human cell–based tumor expressing the MV receptor CD46 at high density. Thus, targeted MV–LV vectors are not only highly specific *in vitro*[9,10] or after local *in vivo* application[10] but also when applied systemically. The possibility to apply DARPins for LV targeting further broadens the applicability of MV–LV vectors. DARPins can be generated with specificity for essentially any surface molecule, and many such DARPins are already available.[16,28]

MATERIALS AND METHODS

Cell culture. HEK-293T (ATCC CRL-11268), SK-OV-3 (ATCC HTB-77), HT1080 (ATCC CCL-121), and CHO-K1 (ATCC CCL-61) cells were grown in Dulbecco's modified Eagle's medium supplemented with 10% fetal calf serum and 1% glutamine at 37 °C in a humidified atmosphere containing 5% CO_2. CHO–Her2 clones expressing different densities of HER2/*neu* were established by stable transfection of CHO-K1 cells with pEX-Z2866-MO2 (GeneCopoeia, Germantown, MD), followed by G418 (Invitrogen, Karsruhe, Germany) selection and single cell cloning (1.2 mg/ml for CHO-Her2-k6 and CHO-Her2-k7; 0.5 mg/ml for CHO-Her2-k13).

Plasmids. The DARPin-coding sequences[15,16] have been PCR amplified as *Sfi*I/*Not*I fragments using the primers D1-for (5′-GCTTGGCCCAGC CGGCCGACCTGGGTAAGAAACTAC-3′) and D1-rev (5′-TTTTCCTT TTGCGGCCGCATTAAGCTTTTGCAGGATTTC-3′) for DARPins G3 and 9.26 and D2-for (5′-GCTTGGCCCAGCCGGCCGACCTGGGTAA GAAACTGC-3′) and D1-rev for all other DARPins. PCR products were ligated in-frame via *Sfi*I/*Not*I into the plasmid pCG-H-α-CD20.[9] The coding sequences for the scFv fragments 4D5[17] and 7A5[18] were subcloned from plasmids pIG6_4D5++ and pTC53-7A5neo, respectively, into pCG-H-α-CD20.

Vector particle production. Vector particles were generated as described previously.[9] Briefly, HEK-293T cells were transfected using calcium phosphate transfection. For transfection, 3.0 µg of pCG-FcΔ30, 1.0 µg of the H-protein variants encoding plasmids, 10.72 µg of the HIV-1 packaging plasmid pCMVΔR8.9,[29] and 11.27 µg of the green fluorescent protein transfer vector plasmid pSEW[30] were used for transfection of cells in T75 flasks. Vector particles pseudotyped with the VSV-G protein were produced by co-transfection of 4.55 µg of the plasmid pMD.G2 along with 8.45 µg of pCMVΔR8.9 and 13.00 µg of transfer plasmid. For vector particles transferring the luciferase gene, the luc coding sequence was cloned from the pGL4.50 vector system (Promega, Mannheim, Germany) into the pSEW transfer vector and the resulting transfer vector was used for vector production. Twenty-four hours after transfection, the cell supernatant was filtered (0.45 µm filter) and concentrated and purified by centrifugation at 25,000*g* and 4 °C over a 20% sucrose cushion for at least 3 hours. The pellet was resuspended in 200 µl fetal calf serum-free medium.

Transduction of cell lines. For transduction, 5×10^4 cells were seeded into a single well of a 12-well plate. Forty-eight hours later, vector particles were serially diluted in 1:10 steps and a total of 500 µl of the dilutions were added per well, incubated for 7 hours, and then replaced with 1 ml of fresh medium. After 48 hours, titers were calculated by determining the number of green fluorescent protein-positive cells under the fluorescence microscope. Alternatively, titers were determined by fluorescence-activated cell sorter analysis based on the indicated percentage of green fluorescent cells.

Flow cytometry. Flow cytometry was performed on a Becton Dickinson LSRII flow cytometry system (Becton Dickinson, Heidelberg, Germany) as described preciously.[9] Briefly, for surface expression experiments, 1×10^6 HEK-293T cells were transfected with H-DARPin expression plasmids (p-H-DARPin) using Lipofectamin 2000 transfection reagent (Invitrogen) according to manufacturers' instructions. After 48 hours, cells were detached and separated. Cells were washed and incubated with a 1:20 dilution in phosphate-buffered saline (PBS) of the mouse antihuman His-PE antibody (Miltenyi Biotec, Bergisch Gladbach, Germany) to detect the His-tagged H-DARPin protein. The data were analyzed using the BD FACSDiva software version 6.0 (Becton Dickinson).

HER2/*neu* expression levels were determined as described previously[26] using a phycoerythrin-conjugated anti-HER2/*neu* antibody (Becton Dickinson). HER2/*neu* receptor density was determined using the QuantiBrite phycoerythrin quantitation kit (Becton Dickinson), according to the manufacturers' instructions.

Quantification of syncytia size. To demonstrate functional surface expression of H-DARPin fusion proteins, the level of cell-to-cell fusion was quantified by counting the number of nuclei in each syncytium after co-transfection of 0.5 µg H-DARPin and 0.5 µg pCG-FcΔ30[9] into 5×10^5 HER2/*neu*-expressing cells using Lipofectamin 2000 transfection reagent (Invitrogen). Twelve hours after transfection, cells were washed with PBS and fixed with 10% formaldehyde in PBS for 12 hours at 4 °C. Subsequently, cells were stained using 1 ml of 0.1% methylrosanilium and 18% ethanol in PBS.

Quantification of p24. The quantity of p24 gag in purified vector suspensions was determined using the Innotest HIV antigen mAb (Innogenetics, Gent, Belgium) according to the manufacturers' instructions.

Immunoblotting. Concentrated vector particles were denatured by incubation for 10 minutes at 95 °C in 2× urea sample buffer (5% sodium dodecyl sulfate, 8 mol/l urea, 200 mmol/l Tris–HCl, 0.1 mmol/l EDTA, 0.03% bromphenol blue, 2.5% dithiothreitol, pH 8.0), separated by electrophoresis on 10% sodium dodecyl sulfate–polyacrylamide electrophoresis gels, and electrotransferred onto nitrocellulose membranes (Amersham Biosciences, Freiburg, Germany). The membranes were incubated with rabbit anti-F (F 431, 1:2,000) serum, rabbit anti-H (H 606, 1:1,000) serum, or mouse anti-p24 (clone 38/8.7.47, 1:1,000; Gentaur, Aachen, Germany) monoclonal antibody, to detect F, H, and p24 gag, respectively. Subsequently, the corresponding secondary antibodies conjugated to horseradish peroxidase (1:2,000; DakoCytomation, Hamburg, Germany) were used. Signals were detected using ECL Plus Western Blotting Detection System (GE Healthcare, München, Germany). The F and H specific sera had been raised by immunization of rabbits with peptides CTVTREDGTNRR (H606) or QVGSRRYPDAVYLHRC (F431), respectively (Eurogentec, Köln, Germany).

In vivo analysis of HER2/neu-specific vectors. Experimental mouse work was carried out in compliance with the regulations of the German animal protection law. CB17 SCID female mice (6- to 8-week-old) were obtained from Harlan Laboratories (Eystrup, Germany) and maintained under pathogen-free conditions. Tumors were established by subcutaneous injections of 2×10^6 U87MG cells or 5×10^6 SK-OV-3 cells, respectively, in 100 µl of PBS into the right or left flank of mice. Systemic vector application was performed 2 weeks later by injection of vector particles (50 µg p24/mouse for D9.29-LV^{luc}, 5 µg p24/mouse for VSV-G-LV^{luc}) into the tail vein in a volume of 100 µl diluted in PBS. After 2 weeks, mice were intraperitoneally injected with 150 mg D-Luciferin/kg body weight (Caliper Life Sciences, Mainz, Germany) and anesthetized. Imaging data were obtained 10 minutes after substrate injection using a noninvasive cooled charged-coupled device (IVIS Spectrum; Caliper Life Sciences). Data were analyzed using the Living Image Software (Caliper Life Sciences). Mice were killed after charged-coupled device imaging and organ excision was performed immediately. Organs were homogenized (FastPrep System; MP Biomedicals, Illkirch, France) and cell lysates were

© The American Society of Gene & Cell Therapy

analyzed for luciferase signals using the Dual-Luciferase Reporter Assay System (Promega).

ACKNOWLEDGMENTS

This work was supported by grants of the Priority Programme "Mechanisms of gene vector entry and persistence" (SPP 1230) of the Deutsche Forschungsgemeinschaft to C.J.B. and K.C. and of the 7th European Community programme project "PERSIST" to C.J.B. S.K., K.C., and C.J.B. are listed as inventors in an international Patent Cooperation Treaty European patent application (PCT/EP2007/008384) assigned to the Paul Ehrlich Institut, which includes as claims the generation of targeted lentiviral vectors.

REFERENCES

1. Cockrell, AS and Kafri, T (2007). Gene delivery by lentivirus vectors. *Mol Biotechnol* **36**: 184–204.
2. Naldini, L (2009). Medicine. A comeback for gene therapy. *Science* **326**: 805–806.
3. Frecha, C, Szécsi, J, Cosset, FL and Verhoeyen, E (2008). Strategies for targeting lentiviral vectors. *Curr Gene Ther* **8**: 449–460.
4. Buchholz, CJ, Mühlebach, MD and Cichutek, K (2009). Lentiviral vectors with measles virus glycoproteins - dream team for gene transfer? *Trends Biotechnol* **27**: 259–265.
5. Morizono, K, Xie, Y, Ringpis, GE, Johnson, M, Nassanian, H, Lee, B *et al.* (2005). Lentiviral vector retargeting to P-glycoprotein on metastatic melanoma through intravenous injection. *Nat Med* **11**: 346–352.
6. Morizono, K, Xie, Y, Helguera, G, Daniels, TR, Lane, TF, Penichet, ML *et al.* (2009). A versatile targeting system with lentiviral vectors bearing the biotin-adaptor peptide. *J Gene Med* **11**: 655–663.
7. Morizono, K, Pariente, N, Xie, Y and Chen, IS (2009). Redirecting lentiviral vectors by insertion of integrin-tageting peptides into envelope proteins. *J Gene Med* **11**: 549–558.
8. Yanagi, Y, Takeda, M and Ohno, S (2006). Measles virus: cellular receptors, tropism and pathogenesis. *J Gen Virol* **87**(Pt 10): 2767–2779.
9. Funke, S, Maisner, A, Mühlebach, MD, Koehl, U, Grez, M, Cattaneo, R *et al.* (2008). Targeted cell entry of lentiviral vectors. *Mol Ther* **16**: 1427–1436.
10. Anliker, B, Abel, T, Kneissl, S, Hlavaty, J, Caputi, A, Brynza, J *et al.* (2010). Specific gene transfer to neurons, endothelial cells and hematopoetic progenitors with lentiviral vectors. *Nat Methods* **7**: 929–935.
11. Sedgwick, SG and Smerdon, SJ (1999). The ankyrin repeat: a diversity of interactions on a common structural framework. *Trends Biochem Sci* **24**: 311–316.
12. Kohl, A, Binz, HK, Forrer, P, Stumpp, MT, Plückthun, A and Grütter, MG (2003). Designed to be stable: crystal structure of a consensus ankyrin repeat protein. *Proc Natl Acad Sci USA* **100**: 1700–1705.
13. Binz, HK, Amstutz, P, Kohl, A, Stumpp, MT, Briand, C, Forrer, P *et al.* (2004). High-affinity binders selected from designed ankyrin repeat protein libraries. *Nat Biotechnol* **22**: 575–582.
14. Yarden, Y (2001). Biology of HER2 and its importance in breast cancer. *Oncology* **61** Suppl 2: 1–13.
15. Zahnd, C, Wyler, E, Schwenk, JM, Steiner, D, Lawrence, MC, McKern, NM *et al.* (2007). A designed ankyrin repeat protein evolved to picomolar affinity to Her2. *J Mol Biol* **369**: 1015–1028.
16. Steiner, D, Forrer, P and Plückthun, A (2008). Efficient selection of DARPins with sub-nanomolar affinities using SRP phage display. *J Mol Biol* **382**: 1211–1227.
17. Ramm, K, Gehrig, P and Plückthun, A (1999). Removal of the conserved disulfide bridges from the scFv fragment of an antibody: effects on folding kinetics and aggregation. *J Mol Biol* **290**: 535–546.
18. Engelstädter, M, Bobkova, M, Baier, M, Stitz, J, Holtkamp, N, Chu, TH *et al.* (2000). Targeting human T cells by retroviral vectors displaying antibody domains selected from a phage display library. *Hum Gene Ther* **11**: 293–303.
19. Dreier, B, Mikheeva, G, Belousova, N, Parizek, P, Boczek, E, Jelesarov, I *et al.* (2010). Her2-specific multivalent adapters confer designed tropism to adenovirus for gene targeting. *J Mol Biol* (epub ahead of print).
20. Bucheit, AD, Kumar, S, Grote, DM, Lin, Y, von Messling, V, Cattaneo, RB *et al.* (2003). An oncolytic measles virus engineered to enter cells through the CD20 antigen. *Mol Ther* **7**: 62–72.
21. Jäger, M, Gehrig, P and Plückthun, A (2001). The scFv fragment of the antibody hu4D5-8: evidence for early premature domain interaction in refolding. *J Mol Biol* **305**: 1111–1129.
22. Overbaugh, J, Miller, AD and Eiden, MV (2001). Receptors and entry cofactors for retroviruses include single and multiple transmembrane-spanning proteins as well as newly described glycophosphatidylinositol-anchored and secreted proteins. *Microbiol Mol Biol Rev* **65**: 371–89, table of contents.
23. Buchholz, CJ, Schneider, U, Devaux, P, Gerlier, D and Cattaneo, R (1996). Cell entry by measles virus: long hybrid receptors uncouple binding from membrane fusion. *J Virol* **70**: 3716–3723.
24. Moasser, MM (2007). The oncogene HER2: its signaling and transforming functions and its role in human cancer pathogenesis. *Oncogene* **26**: 6469–6487.
25. Baselga, J and Swain, SM (2009). Novel anticancer targets: revisiting ERBB2 and discovering ERBB3. *Nat Rev Cancer* **9**: 463–475.
26. Hasegawa, K, Hu, C, Nakamura, T, Marks, JD, Russell, SJ and Peng, KW (2007). Affinity thresholds for membrane fusion triggering by viral glycoproteins. *J Virol* **81**: 13149–13157.
27. Zhang, KX, Kim, C, Chow, E, Chen, IS, Jia, W and Rennie, PS (2011). Targeting trastuzumab-resistant breast cancer cells with a lentivirus engineered to bind antibodies that recognize HER-2. *Breast Cancer Res Treat* **125**: 89–97.
28. Stumpp, MT and Amstutz, P (2007). DARPins: a true alternative to antibodies. *Curr Opin Drug Discov Devel* **10**: 153–159.
29. Zufferey, R, Nagy, D, Mandel, RJ, Naldini, L and Trono, D (1997). Multiply attenuated lentiviral vector achieves efficient gene delivery in vivo. *Nat Biotechnol* **15**: 871–875.
30. Demaison, C, Parsley, K, Brouns, G, Scherr, M, Battmer, K, Kinnon, C *et al.* (2002). High-level transduction and gene expression in hematopoietic repopulating cells using a human immunodeficiency [correction of imunodeficiency] virus type 1-based lentiviral vector containing an internal spleen focus forming virus promoter. *Hum Gene Ther* **13**: 803–813.
31. Moll, M, Klenk, HD and Maisner, A (2002). Importance of the cytoplasmic tails of the measles virus glycoproteins for fusogenic activity and the generation of recombinant measles viruses. *J Virol* **76**: 7174–7186.

Appendix 2

Protein tag-mediated conjugation of oligonucleotides to recombinant affinity binders for proximity ligation

Gu GJ, Friedman M, Jost C, Johnsson K, Kamali-Moghaddam M, Plückthun A, Landegren U, Söderberg O

(My contribution: construction, purification and characterization of SNAP-tagged DARPins)

New Biotechnology • Volume 00, Number 00 • July 2012 RESEARCH PAPER

Research Paper

Protein tag-mediated conjugation of oligonucleotides to recombinant affinity binders for proximity ligation

Gucci Jijuan Gu[1,4], Mikaela Friedman[1,4], Christian Jost[2], Kai Johnsson[3], Masood Kamali-Moghaddam[1], Andreas Plückthun[2], Ulf Landegren[1] and Ola Söderberg[1,]

[1] Department of Immunology, Genetics and Pathology, Science for Life Laboratory, Uppsala University, SE-75185 Uppsala, Sweden
[2] Department of Biochemistry, University of Zürich, Winterthurerstrasse 190, CH-8057 Zürich, Switzerland
[3] Institute of Chemical Sciences and Engineering, École Polytechnique Fédérale de Lausanne (EPFL), CH-1015 Lausanne, Switzerland

While antibodies currently play a dominant role as affinity reagents in biological research and for diagnostics, a broad range of recombinant proteins are emerging as promising alternative affinity reagents in detection assays and quantification. DNA-mediated affinity-based assays, such as immuno-PCR and proximity ligation assays (PLA), use oligonucleotides attached to affinity reagents as reporter molecules. Conjugation of oligonucleotides to affinity reagents generally employs chemistries that target primary amines or cysteines. Because of the random nature of these processes neither the number of oligonucleotides conjugated per molecule nor their sites of attachment can be accurately controlled for affinity reagents with several available amines and cysteines. Here, we present a straightforward and convenient approach to functionalize recombinant affinity reagents for PLA by expressing the reagents as fusion partners with SNAP protein tags. This allowed us to conjugate oligonucleotides in a site-specific fashion, yielding precisely one oligonucleotide per affinity reagent. We demonstrate this method using designed ankyrin repeat proteins (DARPins) recognizing the tumor antigen HER2 and we apply the conjugates in different assay formats. We also show that SNAP or CLIP tags, expressed as fusion partners of transfected genes, allow oligonucleotide conjugations to be performed in fixed cells, with no need for specific affinity reagents. The approach is used to demonstrate induced interactions between the fusion proteins FKBP and FRB by allowing the *in situ* conjugated oligonucleotides to direct the production of templates for localized rolling circle amplification reactions.

Introduction

For biomedical research and diagnostics, there is a need for standardized high-performance assays to analyze proteins and their interactions and modifications *in situ*, in cell lysates, or in body fluids. Such assays are likely to play increasing roles in medical practice by revealing diagnostic protein patterns, and supporting the selection of optimal therapy. These applications will require high-performance protein assays and broadly available repertoires of well-characterized affinity reagents for proteins of interest [1].

Currently, polyclonal or monoclonal antibodies are used in most affinity-based protein analyses, but several classes of recombinant affinity reagents are under development such as nanobodies [2], affibody [3], DARPins and others [4–6]. Such reagents can offer important advantages in terms of engineered specificity and affinity, and also in production. Because of properties such as excellent stability, small size and the possibility to engineer them

Corresponding author: Söderberg, O. (ola.soderberg@igp.uu.se)
[4] These authors contributed equally to the work.

1871-6784/$ - see front matter © 2012 Elsevier B.V. All rights reserved. http://dx.doi.org/10.1016/j.nbt.2012.05.005

Please cite this article in press as: Gu, G.J. et al., Protein tag-mediated conjugation of oligonucleotides to recombinant affinity binders for proximity ligation, New Biotechnol. (2012), http://dx.doi.org/10.1016/j.nbt.2012.05.005

NBT-510; No of Pages 9 ARTICLE IN PRESS

RESEARCH PAPER New Biotechnology • Volume 00, Number 00 • July 2012

for convenient application in specific assay formats, they can extend the range of applications of affinity reactions beyond those of antibodies. Examples of recombinant affinity reagents include molecules that represent fragments of antibodies and a range of scaffold proteins designed to exhibit contact surfaces that can be varied for binding to putative target proteins [4,5]. A scaffold protein with attractive properties for high-affinity protein binding is the designed ankyrin repeat proteins (DARPins) [6]. These are approximately 15–20 kDa in size (compared to 150 kDa for intact IgG antibodies) and they exhibit impressive stability, surviving for months at 37°C. Because the DARPins have no cysteines and fold well in the cytoplasm, they can also be expressed within the cell. A repertoire of DARPins directed against extracellular and intracellular target proteins is now available [6], and a particular effort has been devoted to generating DARPins against the ErbB receptor family, with affinities in the low nM to pM range [7–9].

Proximity ligation assay (PLA) can provide improved opportunities for measuring proteins [10] or more complex targets such as interacting or aggregated proteins [11] and exosomes [12] in blood samples and cell lysates [13]. The technique can also be applied to visualize endogenous protein interactions [14–16] and post-translational modifications [17] in cells and tissues. Detection of proteins or protein complexes using PLA requires binding by two or more affinity reagents that are equipped with DNA oligonucleotides, and referred to as PLA probes. Upon proximal binding by a set of PLA probes amplifiable DNA strands, representative of proximal binding events, are formed by DNA ligation. The reaction provides high selectivity due to the requirement for multiple recognitions and good sensitivity of detection is ensured via amplified detection. For localized detection using *in situ* PLA, the DNA strands (*priming* and *non-priming*) coupled to affinity reagents serve first as templates for ligation, creating circular DNA molecules and then the *priming* acts as primer for localized amplification via rolling circle amplification (RCA) to form RCA products, containing hundreds copies of the same oligonucleotide sequence. The RCA products are easily detected as bright fluorescent spots using fluorophore-labeled hybridization probes (Fig. 1A). These spots can then be digitally recorded using dedicated software [18]. Real-time PCR is generally used to measure ligation products representing proteins detected in solution phase such as in cell lysates (Fig. 1B).

The first demonstration of PLA reactions made use of DNA aptamers as affinity reagents for the targeted proteins [10], but in subsequent work poly- or monoclonal antibodies have generally been used. Several different chemistries are available to conjugate DNA strands to proteins. For antibodies, random coupling of oligonucleotides to primary amines is most commonly used

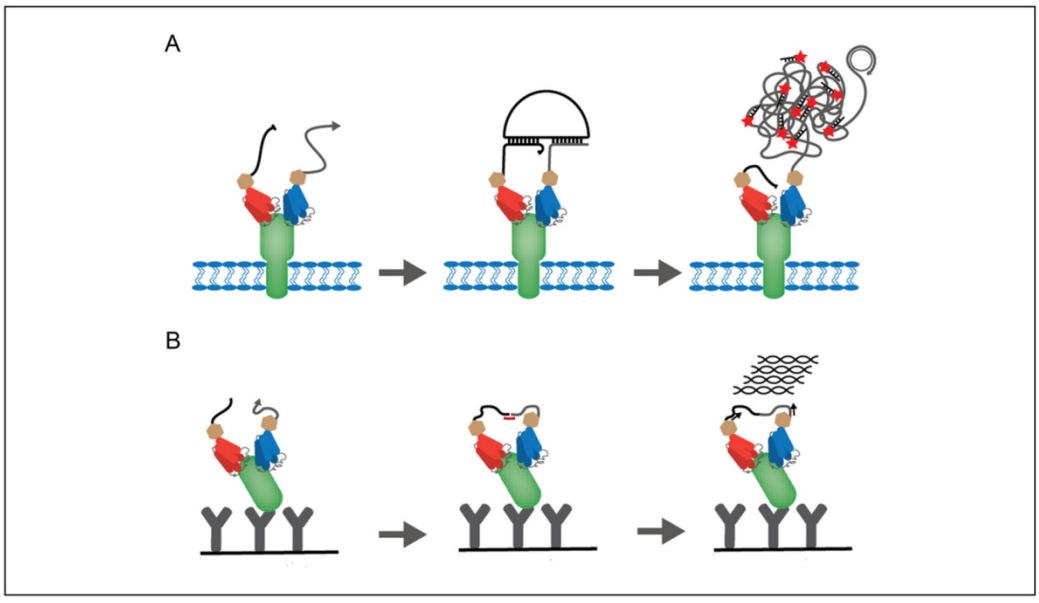

FIGURE 1

Schematic illustration of *in situ* PLA and solid-phase PLA using DARPin PLA probes. **(A)** In *in situ* PLA, targeted proteins or protein pairs are simultaneously bound by two DARPin PLA probes to which oligonucleotides (*priming* (with arrow) and *non-priming* (without arrow)) have been attached; circularization oligonucleotides are then hybridized to PLA probes in close proximity and enzymatically ligated to form amplifiable DNA circles. The circularized DNA is replicated with one of the PLA probes serving as a primer, forming an RCA product. Fluorophore-labeled detection oligonucleotides are then hybridized to the repeated sequence of the rolling circle products, resulting in bright sub-micrometer-sized DNA bundles. **(B)** In solid-phase PLA a sample (in this case cell lysate) is incubated with a target-specific antibody-coated solid phase. Upon simultaneous recognition of the target protein by a pair of DARPin PLA probes, the attached oligonucleotides are brought in close proximity and can be joined by enzymatic ligation in the presence of a connector oligonucleotide complementary to the free ends of the oligonucleotides. A DNA template is generated that can be exponentially amplified and quantified by quantitative PCR.

Please cite this article in press as: Gu, G.J. et al., Protein tag-mediated conjugation of oligonucleotides to recombinant affinity binders for proximity ligation, New Biotechnol. (2012), http://dx.doi.org/10.1016/j.nbt.2012.05.005

NBT-510; No of Pages 9 ARTICLE IN PRESS
New Biotechnology • Volume 00, Number 00 • July 2012 RESEARCH PAPER

[11,13,19]. Conjugation of oligonucleotides to larger affinity reagents is relatively straightforward, but the process is poorly defined and target binding may be affected. It is therefore desirable to conjugate oligonucleotides in a site-directed fashion and preferably in a one-to-one ratio. For small proteins, where a significant fraction of the surface is potentially involved in binding to the target, random coupling of oligonucleotides is unsuitable. For DARPins, protocols have been reported for stoichiometric site-specific coupling of ligands such as polyethylene glycol (PEG) and fluorophore at the N-terminal amino group, at engineered cysteines or at modified amino acids capable of undergoing click chemistry [20]. These reactions require purification of the ligand (here an oligonucleotide) and the protein, as well as some considerations about buffer and reaction conditions. For high-throughput protein–oligonucleotide couplings, alternative strategies with lower demands on reagent purity are thus of interest. A mutant form of the human DNA repair protein O^6-alkylguanine-DNA alkyltransferase reacts rapidly and specifically with O^6-benzylguanine (BG) and also with derivatives that carry a large moiety linked to the benzyl group [21]. With guanine as the leaving group, the benzyl moiety becomes covalently attached to a cysteine in the active site of the enzyme. The enzyme has also been mutagenized to become specific for O^6-benzylcytosine (BC) in a similar manner [22]. Both enzyme domains (about 20 kDa) are commercially available as SNAP and CLIP tags, respectively [22–24].

Here we have investigated the coupling of BG-modified DNA oligonucleotides to DARPin-SNAP fusion proteins. Using anti-HER2 DARPins [7–9] as a test case the resulting PLA probes were validated by visualizing expression and interactions of endogenous HER2 proteins in cells, and by measuring HER2 levels in cell lysates. Furthermore, we illustrated the possibility to demonstrate protein interactions *in situ* using BG- and BC-modified DNA oligonucleotides as probes for *in situ* PLA detection of SNAP or CLIP fusion proteins, expressed in transfected cells. The transfected cells were fixed and permeabilized and interactions were analyzed by adding BG- and BC-modified DNA oligonucleotides as PLA probes. The oligonucleotides coupled *in situ* guided the circularization of two other DNA strands that were then amplified by RCA and visualized via hybridization of fluorophore-labeled oligonucleotides. We show that this form of *in situ* PLA could successfully demonstrate induced interactions between FKBP and FRB proteins fused to SNAP- and CLIP-domains, respectively, with no need for specific affinity reagents.

Materials and methods

Cloning, expression and purification of DARPin-SNAP fusion proteins

The ORFs for the anti-HER2 DARPins 9.01 [8] and G3 [7] were digested with *Bam*HI and *Hin*dIII (New England Biolabs, Ipswich, MA) and ligated into the compatible expression vectors pQiBi_11_SNAP or pQiBi_SNAP_11, which had been constructed by inserting the SNAP domain into vectors made for creating DARPin fusion proteins [9] (C. Gehringer *et al.*, unpublished). This encodes DARPins N- or C-terminally fused to the SNAP-tag via an $(G_4S)_2$-linker. Fusion proteins were overexpressed in *Escherichia coli* XL1-Blue and purified via their N-terminal $MRGSH_6$ tag with nickel-nitrilotriacetic acid superflow resin (Qiagen, Hilden, Germany) giving yields of 25–40 mg of purified protein per liter expression culture [7,8].

Plasmid construction of FKBP-SNAP and FRB-CLIP gene fusion constructs

Gene construct encoding a fusion protein of FKBP (FK506-binding protein) and the SNAP-tag, or construct encoding a fusion protein of FRB (FKBP12/rapamycin-binding domain) and the CLIP-tag were each cloned in a pNuc vectors as previously described [25], hereafter, referred to as FKBP-SNAP and FRB-CLIP. To identify transfected cells, a GFP-encoding vector, the pLPS-AcGFP1-N vector (Cat. No. 632472; Clontech), was co-transfected with the FKBP-SNAP and FRB-CLIP gene fusion constructs.

Preparation of PLA probes

50 μL of 100 μM aldehyde-modified oligonucleotides (*priming*, *non-priming*, *biovic 1* and *biovic 2*, Table 1) were incubated for 3 hours at

TABLE 1
Oligonucleotide sequences

Name	Sequence	Modification	Company
Priming	AAAAAAAAAAGACGCTAATAGTTAAGACGCTT	5′-Aldehyde, or 5′-thiol	Trilink Biotechnology
Non-priming	AAAAAAAAAATATGACAGAACTAGACACTCTT	5′-Aldehyde	Trilink Biotechnology
Circularization oligonucleotide 1	CTATTAGCGTCCAGTGAATGCGAGTCCGTCTAA-GAGAGTAGTACAGCAGCCGTCAAGAGTGTCTA	5′-Phosphate	Integrated DNA Technology
Circularization oligonucleotide 2	GTTCTGTCATATTTAAGCGTCTTAA	5′-Phosphate	Integrated DNA Technology
Detection oligonucleotide	CAGTGAATGCGAGTCCGTCT	5′-Alexa fluor 555	Trilink Biotechnology
Biovic 1	CGCATCGCCCTTGGACTACGACTGACGAACCG-CTTTGCCTGACTGATCGCTAAATCGTG	5′-Aldehyde	Eurogentec
Biovic 2	TCGTGTCTAAAGTCCGTTACCTTGATTCCCCTA-ACCCTCTTGAAAAATTCGGCATCGGTGA	5′-Phosphate, 3′-aldehyde	Eurogentec
Fwdprimer	CATCGCCCTTGGACTACGA		Integrated DNA Technology
Revprimer	GGGAATCAAGGTAACGGACTTTAG		Integrated DNA Technology
Connector	TACTTAGACACGACACGATTTAGTTT		Integrated DNA Technology
Taqman probe	TGACGAACCGCTTTGCCTGA	5′-FAM, 3′-MGB	Applied Biosystems

Please cite this article in press as: Gu, G.J. et al., Protein tag-mediated conjugation of oligonucleotides to recombinant affinity binders for proximity ligation, New Biotechnol. (2012), http://dx.doi.org/10.1016/j.nbt.2012.05.005

TABLE 2

PLA probes

PLA probe	DARPin	Target protein	Oligonucleotide
Probe 1	SNAP_G3	HER2	*Non-priming*
Probe 2	G3_SNAP	HER2	*Priming*
Probe 3	SNAP_9.01	HER2	*Priming*
Probe 4	SNAP_G3	HER2	*Biovic 1*
Probe 5	SNAP_9.01	HER2	*biovic 2*
PLA probe	**5′ modification**	**Specific for**	**Oligonucleotide**
Probe 6	BC-maleimide	CLIP-tag	*Priming*
Probe 7	BG-hydrazine	SNAP-tag	*Non-priming*

37°C with a 30-fold molar excess of BG-hydrazine (5 mM in dimethylformamide (DMF); Covalys, Switzerland) in conjugation buffer (100 mM MES, 150 mM NaCl, pH 4.8). The BG-modified oligonucleotides were purified by reverse-phase high-performance liquid chromatography (RP-HPLC) using a 4.6 mm × 250 mm silica matrix column with a particle size of 5 μm (Lichrosphere RP18 column; Supelco. Inc.), a 60-min gradient of 2–60% B (A: 0.1 M triethylamine acetate (pH 7.0); B: acetonitrile) and a flow rate of 1 mL/min. The reactive cysteine in the SNAP-tag-DARPin fusion proteins (G3 and 9.01) were reduced in 20 mM DTT, and incubated overnight at 4°C in 1 mM DTT with a 3-fold molar excess of BG-modified oligonucleotides, resulting in PLA probes G3-SNAP-*priming*, *non-priming*-SNAP-G3, *priming*-SNAP-9.01, *biovic1*-SNAP-G3 and *biovic2*-SNAP-9.01 (Table 2). No purifications of the conjugates were undertaken, because remaining unconjugated oligonucleotides were removed by washes in the *in situ* and solid phase PLA reactions. The formation of conjugates was validated by separating the products in a SDS polyacrylamide gel (GeneGel Excel 12.5%; GE Healthcare), followed by protein silver staining (PlusOne™ silver staining kit; GE Healthcare) (Fig. 1A), band intensities were measured using Image J and the conjugation efficiency was calculated via the intensity of the conjugate band divided by the intensity of the non-conjugated SNAP-DARPin band. The anti-HER2 antibody pertuzumab and the anti-HER2 polyclonal antibody (AF1129, R&D Systems) were conjugated separately with aldehyde-modified *priming* and *non-priming* oligonucleotides and with aldehyde-modified *biovic 1* and *biovic 2* oligonucleotides (Table 1), respectively, as previously described [26]. In preparing probes for *in situ* analysis of FKBP and FRB interaction, 50 μL of 100 μM thiol-modified *priming* oligonucleotide was reduced in 20 mM DTT for 1 hour at 37°C. The reduced oligonucleotide was purified by MicroSpin G-50 column (GE healthcare) and incubated for 2 hours at room temperature (RT) with a 30-fold molar excess of BC-maleimide, followed by RP-HPLC purification as described above. The preparation of *non-priming-BG* was performed in the same way as for aldehyde-modified *non-priming* oligonucleotide (Table 2).

Cell cultures

The HER2 expressing breast cancer cell line (SK-BR-3) and ovarian cancer cell line (SK-OV-3) were grown in RPMI1640 medium and the human embryonic kidney cell line HEK 293T was grown in Dulbecco's modified Eagle's medium (DMEM). All media were supplemented with 10% fetal bovine serum (FBS), 2 mM L-glutamine and 1% penicillin-streptomycin (all reagents from Sigma Aldrich). The cells were grown at 37°C in a humidified 5% CO_2 environment.

Detection of HER2 in cells by in situ *PLA*

10,000 cells were seeded per well and cultivated overnight on Lab-Tek Chamber Slides (Nalge Nunc International). Cells fixed in EtOH were blocked in blocking buffer (1 mg/mL BSA, 20 μg/mL salmon sperm DNA, 2 mM cysteine, 0.05% Tween20 in TBS buffer) for 1 hour at 37°C, followed by incubation with 40 μL of DARPin PLA probes (*non-priming*-SNAP-G3 (2.4 nM) + G3-SNAP-*priming* (2.4 nM), *non-priming*-SNAP-G3 (4.8 nM) + *priming*-SNAP-9.01 (23 nM), Table 2) diluted in blocking buffer ON at 4°C. Circularization oligonucleotide 1 and 2 (125 nM each, Table 1) in ligation buffer (0.25 mg/mL BSA, T4 ligase buffer, 1 mM ATP, 250 mM NaCl, 0.05% Tween20, 0.05 U/μL T4 DNA ligase (Fermentas)) were incubated at 37°C for 30 min. After ligation rolling circle amplification (RCA) was performed (0.25 mg/mL BSA, phi29 polymerase buffer, 0.25 mM dNTP, 0.125 U/μL phi29 polymerase (Thermo Scientific)) for 90 min at 37 °C followed by hybridization of 250 nM detection oligonucleotide (Table 1) in detection buffer (2 × SSC, 0.25 μg/μL BSA, 75 ng/μL polyA, 0.05% Tween20) to the single-stranded RCA product for 30 min at 37°C. All steps were separated by two washes in TBS + 0.05% Tween20 (TBST). The slides were counterstained with DAPI (100 μg/mL) in Vectashield mounting medium (Vector Laboratory). The same protocol was used for the pertuzumab PLA probe (10 nM of each probe).

Detection of HER2 in cell lysate by solid-phase PLA

1.2×10^5 SK-BR-3 cells or HEK 293T cells were lysed in 150 μL cold lysis buffer (10 mM Tris, 150 mM NaCl, 1 mM EDTA, 1 mM EGTA, 0.5% Nonidet P-40, 0.5% Triton X-100, pH 7.4) supplemented with a Complete Protease Inhibitor Cocktail Tablet (Roche). Tubes (Robostrip®, AJ Roboscreen) were coated with pertuzumab (1 ng/μL) in carbonate buffer (50 mM Na_2CO_3, 50 mM $NaHCO_3$, pH 9.6) for 1 hour at 37°C. After blocking for 1 hour at 37°C in PBS containing 1% BSA, 0.1% salmon sperm DNA and 0.05% Tween20, the tubes were incubated with 50 μL of cell lysate at 4°C ON. Subsequently, 50 μL of DARPin PLA probes (2 nM, *biovic1*-SNAP-G3 and *biovic2*-SNAP-9.01) or anti-HER2 antibody PLA probes (1 nM) was added to the tubes and incubated for 1.5 hours at 37°C. All steps were separated by three washes in PBS with 0.05% Tween20 (PBST). Thereafter, 50 μL ligation and PCR mix (PCR buffer (Invitrogen)), 100 nM connector oligonucleotide (Table 1), 2.5 mM $MgCl_2$, 0.4 units of T4 DNA ligase (Fermentas), 0.1 U uracil-DNA-glycosylase (Fermentas), 80 μM ATP, 0.2 mM dNTPs containing dUTP, 0.1 μM primers (*fwdprimer* and *revprimer*, Table 1), 220 nM Taqman probe (Table 1) were added. The real-time PCR was performed in a Mx-3000 instrument (Stratagene), with an initial incubation at 95°C for 2 min, followed by 45 cycles of 95°C for 15 s and 60°C for 1 min. Solid-phase PLA was also performed with lysate buffer alone as a negative control. The results are presented as threshold cycle (Ct) values [27], reflecting the amount of PLA ligation products, and as ΔCt value where the Ct values for lysate buffer have been subtracted from the Ct value for the cell lysate.

Detection of FKBP and FRB interaction

FKBP-SNAP and FRB-CLIP fusion encoding plasmids were co-transfected together with a GFP-expressing vector and transiently

Please cite this article in press as: Gu, G.J. et al., Protein tag-mediated conjugation of oligonucleotides to recombinant affinity binders for proximity ligation, New Biotechnol. (2012), http://dx.doi.org/10.1016/j.nbt.2012.05.005

NBT-510; No of Pages 9 ARTICLE IN PRESS
New Biotechnology • Volume 00, Number 00 • July 2012 RESEARCH PAPER

expressed in HEK 293T cells. Transfection using Lipofectamine® 2000 (Invitrogen) was carried out according to manufacturer's protocol using 2.5 μg of plasmid and 7.5 μL Lipofectamine and incubation of 50 μL of plasmid-Lipofectamine complex for 24 hours. In this study, the FKBP-SNAP expressing plasmid (1.125 μg) and the FRB-CLIP expressing plasmid (1.125 μg) were co-transfected together with the GFP expressing vector (0.25 μg) into HEK 293T cells. Thereafter, 15,000 cells/well were seeded on collagen-type 1-coated slides (BD Biocoat) and cultivated for 4 hours. Rapamycin (dissolved in DMSO, Sigma–Aldrich) was diluted in 200 μL of antibiotics-free growth medium to concentrations 0.2 μM, 1 μM, 5 μM, 20 μM and 40 μM and incubated with cells for 6 hours at 37°C in a humidified incubator with 5% CO_2, keeping the final concentration of DMSO at 0.1% (v/v). In parallel, 0.1% DMSO was included as a control for the effect of DMSO on the FKBP/FRB interaction. Cells were then fixed in 3% paraformaldehyde (PFA) (Sigma–Aldrich) for 15 min at RT, permeabilized for 15 min in 0.1% Triton X-100 (Sigma–Aldrich) in PBS, and briefly washed in PBS. 20 nM of *priming*-BC and 20 nM *non-priming*-BG in PBS was applied to the cells and incubation for 1 hour at 37°C was followed by 3× 5 min washing in TBST. The *in situ* PLA was performed as described above by steps of hybridization of circularization oligonucleotides, RCA and detection.

Image analysis

Images of all cell experiments were taken in a Zeiss Axioplan II epifluorescence microscope, using an AxioCam MRm CCD sensor and a 40x/1.3 Oil PlanNeofluar objective together with filters for

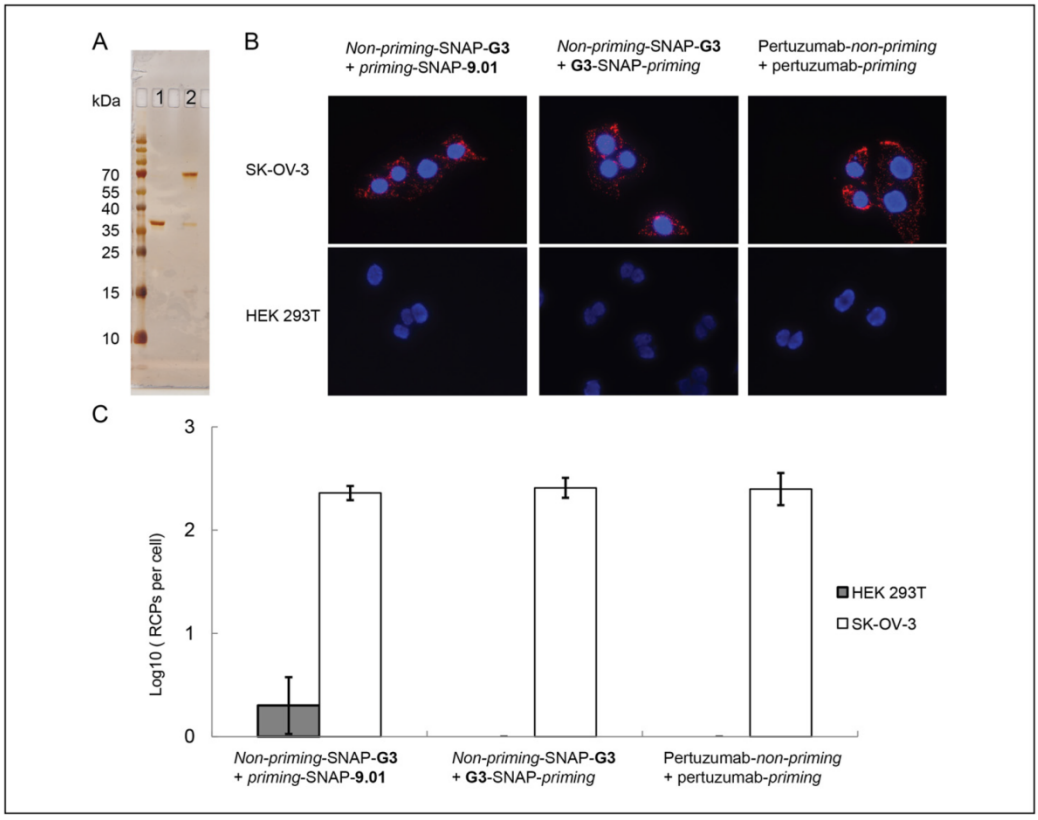

FIGURE 2

Detection of HER2 in cells using DNA-modified DARPins and antibodies. **(A)** SDS-PAGE gel demonstrating the conjugation of SNAP-9.01 (37.9 kDa) (lane 1) with the *biovic 1* oligonucleotide, for production of a PLA probe (lane 2). Molecular weights of marker proteins (Fermentas) are shown in kDa. Proteins were visualized by protein silver staining, and the conjugation efficiency was estimated using Image J. **(B)** *In situ* PLA showing HER2 proteins in SK-OV-3 and HEK 293T cells using two different DARPins, one binding to domain IV (*non-priming*-SNAP-G3) and another one binding to domain I (*priming*-SNAP-9.01) (left panel), both DARPins binding to domain IV (*non-priming*-SNAP-G3 and G3-SNAP-*priming*) (middle panel), and pertuzumab PLA probes (right panel). Red dots are RCA products representing HER2 proteins. **(C)** Numbers of RCA products representing HER2 proteins in SK-OV-3 cells (white bars) and HEK 293T cells (grey bars) detected using *in situ* PLA, as described in (**B**). Data were generated in triplicates and the quantification was performed in Duolink ImageTool (Olink Bioscience). *Y*-axis of the plot is in log scale and error bars indicate standard deviations.

Please cite this article in press as: Gu, G.J. et al., Protein tag-mediated conjugation of oligonucleotides to recombinant affinity binders for proximity ligation, New Biotechnol. (2012), http://dx.doi.org/10.1016/j.nbt.2012.05.005

NBT-510; No of Pages 9 ARTICLE IN PRESS

RESEARCH PAPER New Biotechnology • Volume 00, Number 00 • July 2012

DAPI, FITC and Cy3. PLA signals from HER2 detection in cells were digitally quantified using Duolink ImageTool (Olink Bioscience, Sweden). For quantification of the number of PLA signals derived from FKBP/FRB interactions, only cells displaying signals both in the FITC channel (GFP transfected cells) and in the Cy3 channel (from the RCA products) were counted digitally using the Duolink ImageTool.

Results and discussion

Preparation of PLA probes using SNAP- and CLIP-tag technology and verification by in situ and solid-phase PLA

Simple and efficient methods to attach DNA strands to recombinant affinity proteins are needed to functionalize the reagents for use in methods such as immuno-PCR and PLA [28]. Here, we demonstrate a straightforward approach to convert recombinant affinity reagents into PLA probes by using SNAP-tag fusions of DARPin affinity reagents for site-specific and stoichiometrically controlled conjugation of oligonucleotides. We wished to evaluate if the reactivity of the 20 kDa SNAP and CLIP tags, engineered to react covalently with benzyl-guanine or benzyl-cytosine derivatives, could be exploited to attach oligonucleotides to proteins. Two different approaches were used to obtain BG- (or BC-) derivatized oligonucleotides. Aldehyde-oligonucleotide was first coupled to hydrazine-BG and the product was purified via RP-HPLC. An analogous reaction was also carried out between thiol-modified oligonucleotide and the corresponding maleimide-BC derivative. The BG-coupled oligonucleotides were then incubated with DARPins fused to the SNAP domain tag, resulting in conjugates with a one-to-one ratio of oligonucleotides to affinity reagents. In this manner, 75–85% of total DARPin-SNAP-tag fusion proteins were successfully coupled to an oligonucleotide each, as exemplified by the DARPin PLA probe shown in Fig. 2A. Because the BG- and BC-modified oligonucleotides are stable for long periods they can be prepared in large batches, facilitating DNA conjugation to many SNAP- or CLIP-labeled reagents. Two DARPins were used in these studies that both recognize the extracellular part of the human HER2 membrane protein, frequently overexpressed in, for example, breast cancer [29]. G3 has a K_D of about 100 pM to domain IV of HER2 [7,9], and 9.01 [8] binds domain I with a K_D of about 80 nM (C. Jost *et al.*, unpublished). Because it was not clear *a priori* whether the 20-kDa SNAP domain might interfere with binding by the DARPin to HER2 on the cell, constructs were prepared with the SNAP domain either at the N- or C-termini of the DARPins. All products were obtained from *E. coli* at the same high yield as unfused DARPins.

The HER2-specific DARPin-SNAP conjugates (PLA probes) were applied for HER2 expression analyses both by *in situ* PLA (schematic illustration of *in situ* PLA in Fig. 1A), and in solid-phase PLA of cell lysates with quantitative PCR readout (schematic illustration of solid-phase PLA in Fig. 1B). When two different DARPins are used to bind different epitopes of HER2, then both mono- and dimeric HER2 can be detected, while with DARPins binding to the same epitope (conjugated to different oligonucleotides), only homo-dimeric or clustered forms of HER2 would be detected. With HER2-overexpressing SK-OV-3 cells, the signals obtained using two different DARPin-based PLA probes (referred to as *non-priming*-SNAP-G3 and *priming*-SNAP-9.01) or only one DARPin (*non-priming*-SNAP-G3 and G3-SNAP-*priming*) are about the same. This suggests that most of the HER2 proteins are in a clustered state on this cell line (Fig. 2B,C). Clustering of highly overexpressed HER2 on tumor cells is consistent with previous observations [30]. Using pairs of PLA probes based on the therapeutic monoclonal antibody pertuzumab, similar results were obtained (Fig. 2B,C). By contrast, HEK 293T cells are known to express low but still measurable amounts of HER2 [31]. In these cells, HER2 is not expected to be oligomeric. Indeed, PLA signals were only seen when two different DARPins were used (Fig. 2B,C), but not with only one DARPin or with pertuzumab.

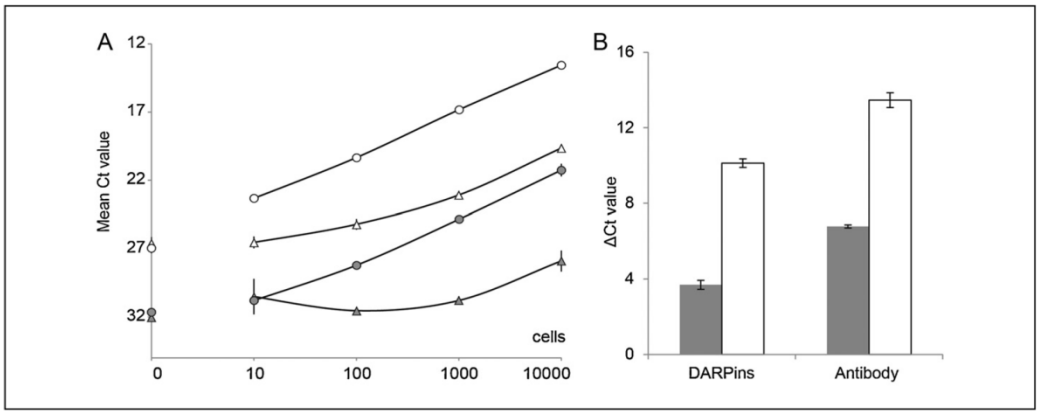

FIGURE 3

Comparison of HER2 detection in cell lysates using DARPins and antibody by solid-phase PLA. **(a)** Performance of solid-phase PLA in cell lysates using two different DARPins, one binding to domain IV (*biovic1*-SNAP-G3), the other binding to domain I (*biovic2*-SNAP-9.01) (in SK-BR-3 cell lysate, filled circles; in HEK 293T, filled triangles), or polyclonal antibody against HER2 (in SK-BR-3 cell lysate, open circles; in HEK 293T, open triangles). **(b)** Calculation of ΔCt from the data shown in (a) by subtracting the Ct value of lysis buffer from the Ct value of cell lysates (10^4 cells). Lysates from SK-BR-3 cells are shown in white bars and from HEK 293T cells in dark grey bars. Mean values with standard deviations for triplicate measurements are shown.

Please cite this article in press as: Gu, G.J. et al., Protein tag-mediated conjugation of oligonucleotides to recombinant affinity binders for proximity ligation, New Biotechnol. (2012), http://dx.doi.org/10.1016/j.nbt.2012.05.005

NBT-510; No of Pages 9 ARTICLE IN PRESS
New Biotechnology • Volume 00, Number 00 • July 2012 RESEARCH PAPER

The DARPin-SNAP PLA probes were also applied for protein measurements in cell lysates by solid-phase PLA with quantitative PCR readout. Here, HER2 levels in cell lysates from HER2 expressing SK-BR-3 cells and low HER2-expressing HEK 293T cells were compared. HER2 proteins were captured by pertuzumab immobilized on solid support and assayed using either two different DARPin PLA probes, one binding to domain IV (*biovic1*-SNAP-G3) and the other binding to domain I (*biovic2*-SNAP-9.01), or an anti-HER2 polyclonal antibody divided in two aliquots, each conjugated to one of two different oligonucleotides. Both experiments revealed the expected difference in levels of HER2 proteins between the two lysates (Fig. 3). It should be pointed out that the two DARPins used both recognize conformational epitopes, and thus lysate preparations that even partially denature HER2 risk decreasing assay sensitivity. The polyclonal anti-HER2 antibody (AF1129, RnD systems) that was used in this assay, together with pertuzumab as capture antibody on solid support, has been shown to detect HER2 in Western blots and must thus be able to detect denatured forms of HER2, or unfolded regions. The polyclonal antibody might simultaneously bind different epitopes of HER2 and there may be several oligonucleotides attached per antibody. By contrast, the DARPins are monoclonal and strictly contain only one oligonucleotide each, and will therefore produce less signals overall than the antibody-based assay, both for lysates from SK-BR-3 cells expressing high levels of HER2 and from HEK 293T cells (Fig. 3A). The differences in HER2 detection signals between SK-BR-3 and HEK 293T cells were similar, however, using the two classes of affinity reagents (ΔCts of 6.4 and 6.7, for DARPins and antibodies respectively) (Fig. 3B).

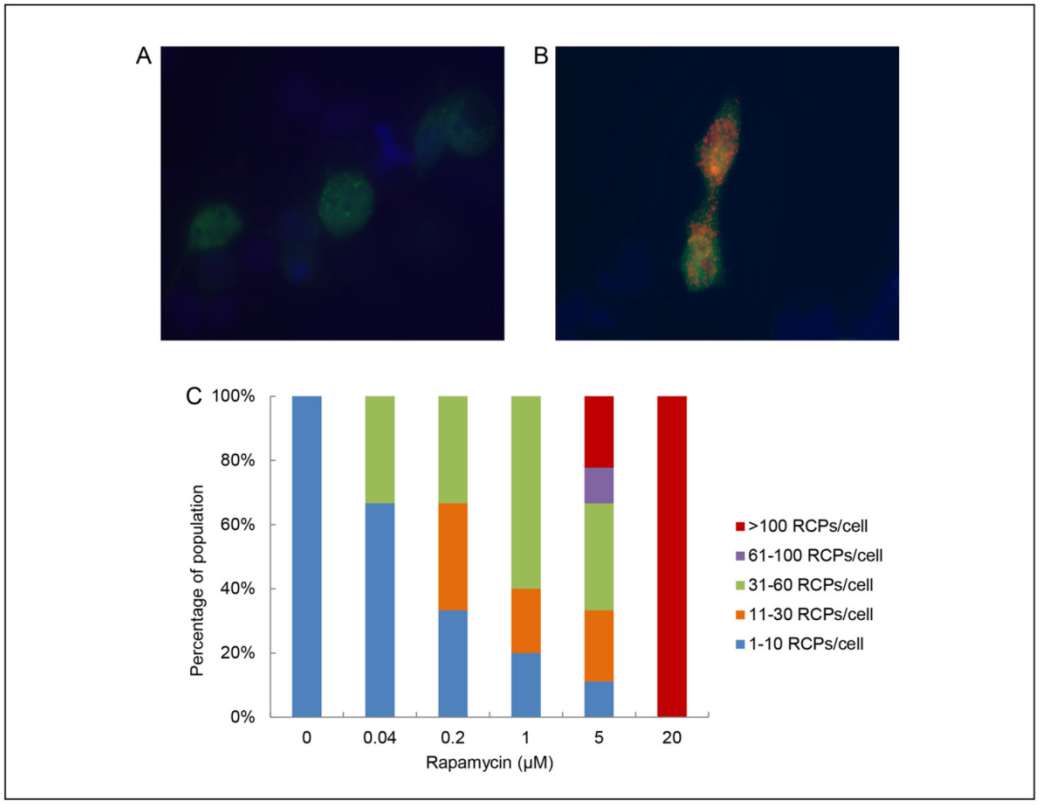

FIGURE 4

In situ detection of rapamycin-mediated interactions between FKBP and FRB fusion proteins via their fused SNAP and CLIP domains. HEK 293T cells were co-transfected with plasmids expressing FKBP-SNAP and FRB-CLIP fusion and with GFP-expressing plasmids. After 24 hours the cells were analyzed without **(A)** and with treatment with 20 μM of rapamycin **(B)** for 6 hours. *In situ* PLA with PLA probes (*priming*-BC and *non-priming*-BG) was applied for detection of interaction of FKBP and FRB fusion proteins in the absence and presence of rapamycin, and the RCA product detected with Alexa 555-labeled oligonucleotide (red) in GFP expressing cells (green). The cells were counterstained with DAPI (blue) to visualize the nuclei. GFP (green) served as an indicator of successful co-transfection and expression in cells. (**C**) Bar graph demonstrating the frequency of cells with the indicated numbers of RCA products (RCPs), as a function of the concentration of rapamycin in the culture media. On average 50 cells were investigated for each concentration of rapamycin in three experiments and analyzed using automated image analysis (Duolink ImageTool).

Please cite this article in press as: Gu, G.J. et al., Protein tag-mediated conjugation of oligonucleotides to recombinant affinity binders for proximity ligation, New Biotechnol. (2012), http://dx.doi.org/10.1016/j.nbt.2012.05.005

NBT-510; No of Pages 9 ARTICLE IN PRESS

RESEARCH PAPER New Biotechnology • Volume 00, Number 00 • July 2012

In situ conjugation of SNAP- and CLIP-fusion proteins

At times it is desirable to measure binding to and interactions among proteins for which no suitable affinity reagents exist. We investigated the possibility of transfecting cells with SNAP- and CLIP-fusion gene constructs to study protein interactions with no need for antibodies or any other specific protein-binding reagents. We tested this strategy using FKBP and FRP as model system, as interaction between these proteins can be induced by rapamycin. Rapamycin binds with high affinity (K_D = 0.2 nM) to the 12-kDa FK506 binding protein (FKBP) as well as to a 100-amino acid domain of the mammalian target of rapamycin (mTOR), known as the FKBP-rapamycin binding domain (FRB), thereby forming a FKBP·rapamycin·FRB ternary complex [32,33].

In cells transfected with SNAP- and CLIP-domains fused to FKBP and FRB proteins, respectively, the fusion proteins were conjugated *in situ* with BG- and BC-modified DNA oligonucleotides. Colocalization of the two oligonucleotides was investigated, by addition of two connector oligonucleotides, capable of being ligated into a DNA circle in reactions templated by the BG- and BC-oligonucleotides. We demonstrated successfully circularized oligonucleotides via RCA, followed by detection of the amplification products using fluorophore-labeled oligonucleotides, complementary to the repeated sequence of the RCA products. In the absence of rapamycin, the transfected HEK 293T cells, expressing FKBP-SNAP and FRB-CLIP, gave rise to only very few *in situ* PLA reaction products (1–10 RCPs per cell) (Fig. 4A), whereas upon incubation with 20 μM rapamycin the numbers of signals per cell increased to greater than 100 per cell (Fig. 4B,C).

This approach provides a way to use *in situ* PLA where proteins of interest can be expressed as fusion proteins with the SNAP or CLIP domains after transfection. This strategy could also be combined with the use of specific affinity reagents in situation where such a reagent is only available against one partner in a protein interaction. The procedure, which works on cells that have been fixed and permeabilized, provides a complementary method *to in situ* interaction analysis of genetically modified living cells via Förster resonance energy transfer (FRET) of pairs of fluorescent protein domains that are expressed as fusions to the proteins of interest [34,35] or by using complementing protein domains on fusion proteins [36]. Although the *in situ* PLA approach, unlike FRET and protein complementation techniques, is limited to fixed cells, the strong signal amplification can be of value because it enables detection of individual interaction events using standard microscopy.

Conclusion

Because the reaction of BG- or BC-modified oligonucleotides with SNAP or CLIP tags is a robust and specific procedure, this strategy will be helpful to functionalize a large range of recombinant affinity reagents for proteomics investigation through the addition of DNA strands. It thus provides a general means for production of highly stable, renewable DNA-conjugated affinity reagents with one oligonucleotide added in a site-specific fashion per affinity reagent molecule. This was demonstrated for HER2-specific DARPin PLA probes. We also demonstrate that BG- and BC-modified oligonucleotides can be used as general affinity reagents directly in cells transfected with fusion gene constructs.

Conflicts of interest

Ulf Landegren is a co-founder and stockholder of Olink Bioscience, having rights to the PLA technology. Andreas Plückthun is a co-founder and stockholder of Molecular Partners AG, having rights to the DARPin technology.

Acknowledgments

The authors thank Dr Karl-Johan Leuchowius and Dr Irene Weibrecht for valuable advice and discussions and Swedish Research Council, Knut and Alice Wallenberg Foundation, Uppsala Berzelii Technology Centre for Neurodiagnostics, the European Community's 7th Framework Program (FP7/2007-2013) under grant agreement no. 222635 (AffinityProteome) and 241481 (Affinomics) and China Scholarship Council.

References

1 Landegren, U. *et al.* (2012) Opportunities for sensitive plasma proteome analysis. *Anal Chem* 84, 1824–1830
2 Hamers-Casterman, C. *et al.* (1993) Naturally occurring antibodies devoid of light chains. *Nature* 363, 446–448
3 Nord, K. *et al.* (1997) Binding proteins selected from combinatorial libraries of an alpha-helical bacterial receptor domain. *Nat Biotechnol* 15, 772–777
4 Gebauer, M. and Skerra, A. (2009) Engineered protein scaffolds as next-generation antibody therapeutics. *Curr Opin Chem Biol* 13, 245–255
5 Binz, H.K. *et al.* (2005) Engineering novel binding proteins from nonimmunoglobulin domains. *Nat Biotechnol* 23, 1257–1268
6 Boersma, Y.L. and Plückthun, A. (2011) DARPins and other repeat protein scaffolds: advances in engineering and applications. *Curr Opin Biotechnol* 22, 849–857
7 Zahnd, C. *et al.* (2007) A designed ankyrin repeat protein evolved to picomolar affinity to Her2. *J Mol Biol* 369, 1015–1028
8 Steiner, D. *et al.* (2008) Efficient selection of DARPins with sub-nanomolar affinities using SRP phage display. *J Mol Biol* 382, 1211–1227
9 Zahnd, C. *et al.* (2010) Efficient tumor targeting with high-affinity designed ankyrin repeat proteins: effects of affinity and molecular size. *Cancer Res* 70, 1595–1605
10 Fredriksson, S. *et al.* (2002) Protein detection using proximity-dependent DNA ligation assays. *Nat Biotechnol* 20, 473–477
11 Kamali-Moghaddam, M.v *et al.* (2010) Sensitive detection of Abeta protofibrils by proximity ligation – relevance for Alzheimer's disease. *BMC Neurosci* 11, 124–130
12 Tavoosidana, G. *et al.* (2011) Multiple recognition assay reveals prostasomes as promising plasma biomarkers for prostate cancer. *Proc Natl Acad Sci USA* 108, 8809–8814
13 Liu, Y. *et al.* (2011) Western blotting via proximity ligation for high performance protein analysis. *Mol Cell Proteomics* 10, O111–O011031
14 Söderberg, O. *et al.* (2006) Direct observation of individual endogenous protein complexes in situ by proximity ligation. *Nat Methods* 3, 995–1000
15 Clausson, C.M. *et al.* (2011) Increasing the dynamic range of in situ PLA. *Nat Methods* 8, 892–893
16 Weibrecht, I. *et al.* (2012) Visualising individual sequence-specific protein–DNA interactions in situ. *N Biotechnol* 29, 589–598
17 Jarvius, M. *et al.* (2007) In situ detection of phosphorylated platelet-derived growth factor receptor beta using a generalized proximity ligation method. *Mol Cell Proteomics* 6, 1500–1509
18 Allalou, *et al.* (2009) a tool for fluorescence microscopy image cytometry. *Comput Methods Programs Biomed* 94, 58–65
19 Söderberg, O. *et al.* (2008) Characterizing proteins and their interactions in cells and tissues using the in situ proximity ligation assay. *Methods* 45, 227–232
20 Tamaskovic, R. *et al.* (2012) Designed ankyrin repeat proteins (DARPins): from research to therapy. *Methods Enzymol* 503, 101–134
21 Gronemeyer, T. *et al.* (2005) Adding value to fusion proteins through covalent labelling. *Curr Opin Biotechnol* 16, 453–458
22 Gautier, A. *et al.* (2008) An engineered protein tag for multiprotein labeling in living cells. *Chem Biol* 15, 128–136

Please cite this article in press as: Gu, G.J. et al., Protein tag-mediated conjugation of oligonucleotides to recombinant affinity binders for proximity ligation, New Biotechnol. (2012), http://dx.doi.org/10.1016/j.nbt.2012.05.005

23 Maurel, D. *et al.* (2008) Cell-surface protein-protein interaction analysis with time-resolved FRET and SNAP-tag technologies: application to GPCR oligomerization. *Nat Methods* 5, 561–567
24 Kindermann, M. *et al.* (2003) Covalent and selective immobilization of fusion proteins. *J Am Chem Soc* 125, 7810–7811
25 Gautier, A. *et al.* (2009) Selective cross-linking of interacting proteins using self-labeling tags. *J Am Chem Soc* 131, 17954–17962
26 Leuchowius, K.J. *et al.* (2009) Flow cytometric in situ proximity ligation analyses of protein interactions and post-translational modification of the epidermal growth factor receptor family. *Cytometry A* 75, 833–839
27 Gibson, U.E. *et al.* (1996) A novel method for real time quantitative RT-PCR. *Genome Res* 6, 995–1001
28 Nong, R.Y. *et al.* (2012) DNA-assisted protein detection technologies. *Expert Rev Proteom* 9, 21–32
29 Wolff, A.C. *et al.* (2007) American Society of Clinical Oncology/College of American Pathologists guideline recommendations for human epidermal growth factor receptor 2 testing in breast cancer. *J Clin Oncol* 25, 118–145
30 Kaufmann, R. (2011) Analysis of Her2/neu membrane protein clusters in different types of breast cancer cells using localization microscopy. *J Microsc* 242, 46–54
31 Gensler, M. *et al.* (2004) Negative regulation of HER2 signaling by the PEST-type protein-tyrosine phosphatase BDP1. *J Biol Chem* 279, 12110–12116
32 Banaszynski, L.A. *et al.* (2005) Characterization of the FKBP.rapamycin.FRB ternary complex. *J Am Chem Soc* 127, 4715–4721
33 Muthuswamy, S.K. *et al.* (1999) Controlled dimerization of ErbB receptors provides evidence for differential signaling by homo- and heterodimers. *Mol Cell Biol* 19, 6845–6857
34 Pollok, B.A. and Heim, R. (1999) Using GFP in FRET-based applications. *Trends Cell Biol* 9, 57–60
35 Rizzo, M.A. *et al.* (2004) An improved cyan fluorescent protein variant useful for FRET. *Nat Biotechnol* 22, 445–449
36 Hu, C.D. *et al.* (2002) Visualization of interactions among bZIP and Rel family proteins in living cells using bimolecular fluorescence complementation. *Mol Cell* 9, 789–798

Please cite this article in press as: Gu, G.J. et al., Protein tag-mediated conjugation of oligonucleotides to recombinant affinity binders for proximity ligation, New Biotechnol. (2012), http://dx.doi.org/10.1016/j.nbt.2012.05.005

Appendix 3

Direct identification of ligand-receptor interactions on living cells and tissues

Frei PA, Jeon OY, Kilcher S, Moest H, Henning L, Jost C, Plückthun A, Mercer J, Aebersold R, Carreira EM, Wollscheid B

(My contribution: epitope characterization of the utilized anti-HER2-DARPins)

LETTERS

nature biotechnology

Direct identification of ligand-receptor interactions on living cells and tissues

Andreas P Frei[1–3], Ock-Youm Jeon[4,10], Samuel Kilcher[3,5,10], Hansjoerg Moest[1,2,6], Lisa M Henning[1,2], Christian Jost[3,7], Andreas Plückthun[7,8], Jason Mercer[5], Ruedi Aebersold[1,8,9], Erick M Carreira[4] & Bernd Wollscheid[1,2]

Many cellular responses are triggered by proteins, drugs or pathogens binding to cell-surface receptors, but it can be challenging to identify which receptors are bound by a given ligand. Here we describe TRICEPS, a chemoproteomic reagent with three moieties—one that binds ligands containing an amino group, a second that binds glycosylated receptors on living cells and a biotin tag for purifying the receptor peptides for identification by quantitative mass spectrometry. We validated this ligand-based, receptor-capture (LRC) technology using insulin, transferrin, apelin, epidermal growth factor, the therapeutic antibody trastuzumab and two DARPins targeting ErbB2. In some cases, we could also determine the approximate ligand-binding sites on the receptors. Using TRICEPS to label intact mature vaccinia viruses, we identified the cell surface proteins AXL, M6PR, DAG1, CSPG4 and CDH13 as binding factors on human cells. This technology enables the identification of receptors for many types of ligands under near-physiological conditions and without the need for genetic manipulations.

Identifying the receptors of key ligands can often lead to new research directions and provide valuable mechanistic information about signal transduction, drug action or off-target effects. However, the unbiased and unambiguous identification of ligand-receptor interactions remains a daunting task despite the emergence of mass spectrometry–based technologies for the identification of protein-protein[1,2] and small molecule–protein[3–5] interactions in cell lysates. This is mostly due to the transient nature of such interactions and the problems inherent in the analysis of plasma membrane proteins that are often hydrophobic and present in relatively low abundance[6,7]. Furthermore, cell surface proteins typically need to be embedded in their natural environment, that is, within living cells or tissues, to exhibit their characteristic binding properties[8,9].

We and others have previously used bifunctional reagents containing hydrazide and aminooxy active groups to label carbohydrate-containing proteins on the surface of live cells with biotin[10,11]. Subsequently, the purification and mass spectrometric analysis of corresponding peptides allows for the characterization of the cell surface proteome[11,12]. As an extension of this strategy, we hypothesized that specifically designed trifunctional reagents would allow the capture of ligand-based receptors bound to ligands on the surface of live cells followed by identification of the captured receptors using quantitative mass spectrometry. We designed and synthesized biocompatible chemoproteomic reagents (**Fig. 1a** and **Supplementary Note**) incorporating three independent functionalities: an *N*-hydroxysuccinimide ester for conjugating the reagent to a ligand containing a free amino group; a protected hydrazine that reacts with aldehydes in carbohydrates on glycoprotein receptors; and a biotin group for the affinity purification of the captured glycopeptides for mass spectrometric analysis[13]. Special emphasis was also placed on water solubility, conformational flexibility, spacer length and compatibility with gentle yet selective conditions for the ligand coupling and receptor-capture reactions. We call these trifunctional chemoproteomic reagents 'TRICEPS'.

The *N*-hydroxysuccinimide ester on TRICEPS nonspecifically couples the reagent to primary amines, the α-NH_2 group of the N terminus or the ε-NH_2 group of lysine side chains, in protein or peptide ligands of interest, under physiological conditions[14]. Typically, several primary amines are present in ligands. Simultaneous coupling to all or most available groups might interfere with subsequent receptor binding, whereas lower labeling ratios are expected to minimally impair the majority of ligands (**Supplementary Fig. 1**). After reaction of the *N*-hydroxysuccinimide ester, TRICEPS retained the ability to efficiently capture aldehydes on the surface of living cells (**Fig. 1b**). Aldehydes are generally absent from cell surfaces but can be introduced into the carbohydrates of cell surface glycoproteins through exposure of cells to gentle oxidizing conditions with sodium-metaperiodate[10,11,15]. In contrast to other combinations of reactive and protecting groups, the trifluoroacetylated hydrazines used in TRICEPS can undergo condensation with carbohydrate-derived aldehydes under essentially neutral conditions without prior removal of the protecting group. This is one of the key features of TRICEPS as the trifluoroacetamide protective group prevents unwanted side reactions

[1]Department of Biology, Institute of Molecular Systems Biology, ETH Zurich, Switzerland. [2]NCCR Neuro Center for Proteomics, University of Zurich, Switzerland. [3]PhD Program in Molecular Life Sciences (MLS), University of Zurich/ETH Zurich, Switzerland. [4]Department of Chemistry and Applied Biosciences, Laboratory of Organic Chemistry, ETH Zurich, Switzerland. [5]Department of Biology, Institute of Biochemistry, ETH Zurich, Switzerland. [6]Department of Health and Technology, Institute of Food, Nutrition and Health, ETH Zurich, Switzerland. [7]Department of Biochemistry, University of Zurich, Switzerland. [8]Faculty of Science, University of Zurich, Switzerland. [9]Competence Center for Systems Physiology and Metabolic Diseases, Zurich, Switzerland. [10]These authors contributed equally to this work. Correspondence should be addressed to B.W. (bernd.wollscheid@imsb.biol.ethz.ch).

Received 6 April; accepted 8 August; published online 16 September 2012; doi:10.1038/nbt.2354

LETTERS

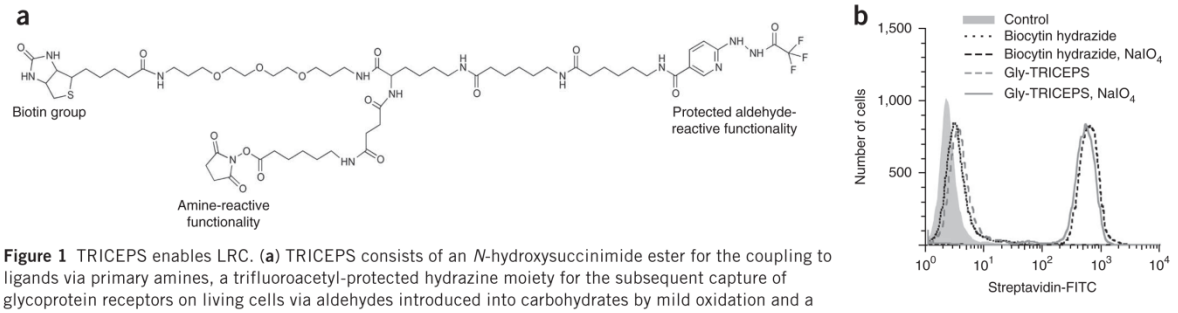

Figure 1 TRICEPS enables LRC. (**a**) TRICEPS consists of an *N*-hydroxysuccinimide ester for the coupling to ligands via primary amines, a trifluoroacetyl-protected hydrazine moiety for the subsequent capture of glycoprotein receptors on living cells via aldehydes introduced into carbohydrates by mild oxidation and a biotin moiety for the affinity purification of captured glycopeptides. Flexibility is provided by the stochastic coupling of TRICEPS to topologically different sites on ligands, the long (~48 Å) and flexible spacer between the reactive moieties and the presence of typically more than one aldehyde in a single carbohydrate structure after mild oxidation. Alternative ligand-reactive functionalities may be implemented to further broaden the possible application (e.g., for small-molecule ligands). (**b**) Labeling of living cells with TRICEPS through the aldehyde-reactive functionality. Commercially available biocytin hydrazide (an unprotected aldehyde-reactive biotin derivative) was used as a reference. Amine-reactive moieties of TRICEPS were quenched with glycine and reagents were reacted with Jurkat T lymphocytes with or without prior oxidation of the cells with sodium metaperiodate. Biotinylation was detected by flow cytometric analysis of ungated cell populations after staining with streptavidin-FITC.

between the nucleophilic hydrazine and electrophiles such as active ester groups in the reagent itself. As the condensation reaction can occur under neutral conditions, this eliminates the need to remove the protective groups under harsh conditions, which would be incompatible with protein ligands maintaining their native structures.

We next established a TRICEPS-based workflow to identify receptors for ligands using two samples (**Fig. 2**). In one sample, the TRICEPS-labeled ligand predominantly directed the carbohydrate-reactive element of the reagents toward ligand-specific glycoprotein receptors. In parallel, an equimolar amount of TRICEPS was either quenched with glycine or coupled to a control ligand with known or no binding preferences. This control allowed us to account for nonspecific binding based on the relative abundance of a given target protein on a cell line or tissue. The two TRICEPS-containing samples were then incubated with previously oxidized cells or tissues under near-physiological conditions. During this phase, transient and stable ligand-receptor interactions were expected to lead to increased covalent capture events between TRICEPS and nearby carbohydrates. In general, the reactivity between hydrazine and carbohydrates is advantageous because it targets TRICEPS away from polypeptide domains that are important for ligand binding. After the receptor-capture reaction, the cells were lysed and enzymatically digested with trypsin, and TRICEPS-labeled peptides were isolated using streptavidin beads. This circumvents problems inherent in the affinity purification of intact plasma membrane proteins, such as limited solubility and unspecific interactions through exposed hydrophobic domains. Captured N-glycopeptides were specifically released from the beads through an enzymatic cleavage with PNGase F. This endoglycosidase cleaves between the proximal *N*-acetylglucosamine and the asparagine of the glycopeptide in the N-X-S/T glycosylation site motif (where N stands for asparagine, X stands for any amino acid except proline and S/T for serine or threonine, respectively). Besides releasing the glycosylated peptides, PNGase F treatment also results in the enzymatic deamidation of the glycosylated asparagine to aspartic acid. This generates a +0.984 Da mass shift at the asparagine residue and thus introduces the specific N[115]-X-S/T signature (where 115 is the mass of the deamidated Asn residue) in formerly glycosylated cell surface peptides. This protocol leads to the generation of two virtually identical peptide samples that can be analyzed with a high mass accuracy mass spectrometer. The identified peptides were filtered for the presence of N[115]-X-S/T motifs, and the relative concentrations of cell surface glycopeptides in the ligand sample were compared to those in the control sample using MS1-based label-free quantification. Identified peptides of random cell surface proteins were expected to have equal concentrations in both samples, whereas peptides of the corresponding receptors were specifically enriched in the ligand sample.

In the first application of this approach, we coupled human insulin to TRICEPS and then added it to murine adipocytes at a concentration routinely used in cell culture applications (1.7 μM). In the parallel control reaction, an equimolar amount of TRICEPS was quenched with glycine and added to an equal number of cells. Mass spectrometric analysis led to the identification of 117 formerly glycosylated peptides with similar abundance in both samples. These were derived from 69 random, but highly abundant, cell surface glycoproteins and represented nonspecific capture events. Owing to the comparatively low abundance of the insulin receptor (INSR) on the target cells, INSR peptide signals were weak or not detectable above background in the control sample. In contrast, INSR peptides were highly enriched in the sample that had been generated with insulin providing selectivity for the capture reaction (**Fig. 3a** and **Supplementary Table 1**). These results show that TRICEPS-bound ligands can be used to guide the hydrazine reaction toward specific receptors on living cells. Furthermore, this experiment led to the immediate and unbiased detection of the interaction of human insulin with the murine INSR on the target cells. Notably, the INSR was identified with six unique enriched peptides. This added confidence to the specific receptor identification because every peptide provided independent enrichment information owing to the peptide-level affinity purification. In a similar experiment using human Jurkat T lymphocytes, the enrichment of the human INSR was prevented by pre-incubating cells with a tenfold molar excess of uncoupled insulin (**Supplementary Fig. 2** and **Supplementary Table 2**), again highlighting the robustness and specificity of the approach.

To demonstrate the versatility of the LRC technology, we used transferrin (a secreted glycoprotein) and apelin-17 (a G protein–coupled receptor (GPCR) binding peptide) as ligands to capture receptors on human U-2 OS osteosarcoma cells. This experiment simultaneously identified the transferrin receptor protein 1 and the apelin receptor as interaction partners of the respective ligands (**Fig. 3b** and **Supplementary Table 3**). The identification of the transferrin receptor shows that LRC technology is also compatible with glycosylated

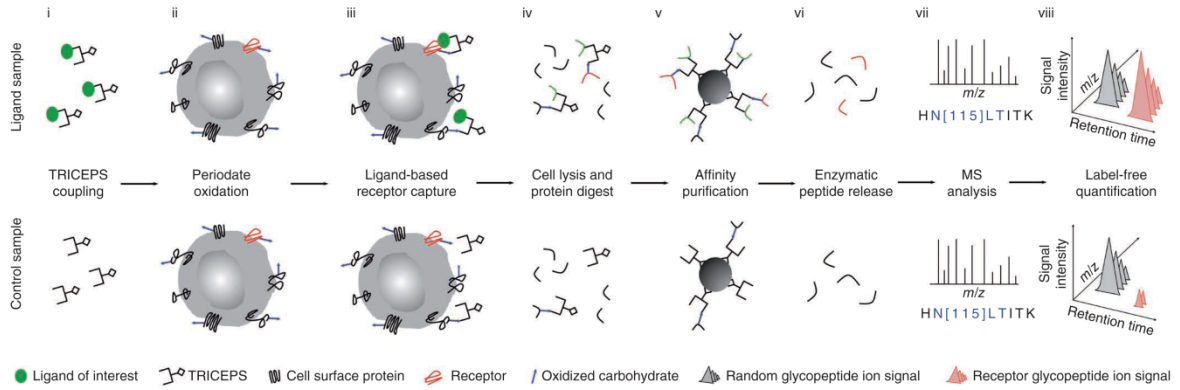

Figure 2 Workflow for the LRC and identification on living cells. (i) Conjugation of a purified ligand of interest to TRICEPS and quenching of an equimolar amount of TRICEPS with glycine (or coupling to a control ligand with known or no binding preferences) in the control reaction. (ii) Mild periodate oxidation of target cells or tissue to introduce aldehydes into carbohydrate structures for TRICEPS capture. (iii) LRC and stochastic biotinylation of random cell surface glycoproteins according to their abundance. (iv) Cell lysis and tryptic digest of proteins. (v) Biotin-mediated affinity enrichment of captured glycopeptides on streptavidin beads. (vi) Cell surface N-glycopeptide release by PNGase F treatment, which introduces the N[115]-X-S/T motif (N[115], deamidated asparagine; X, any amino acid except proline; S/T, serine or threonine, respectively) in formerly N-glycosylated peptides. (vii) Glycopeptide identification by high mass accuracy MS and peptide filtering for the presence of the N[115]-X-S/T motif. (viii) Relative label-free quantification of formerly glycosylated cell surface peptides to identify specific LRC events.

ligands such as transferrin. Furthermore, this experiment demonstrates the potential of LRC technology to identify interactions of peptide ligands with GPCRs. Such interactions are particularly difficult to capture by other means owing to the small size of peptide ligands and the typically low abundance and integral membrane nature of the corresponding seven-transmembrane domain receptors.

Next, we explored the utility of LRC technology to identify pharmaceutically interesting targets of growth factors, therapeutic antibodies and engineered affinity binders. The first experiment was performed with the therapeutic antibody trastuzumab (Herceptin), which binds to ErbB2, and the epidermal growth factor (EGF) on U251 human glioblastoma cells. To allow for statistical evaluation, we performed these experiments in biological triplicates. This application was of particular interest as the two ligands are very different in nature (trastuzumab is a 150-kDa glycoprotein, whereas EGF is a small 6-kDa protein), and they each bind to a single site on different members of the EGF receptor (EGFR) superfamily[16,17]. Using trastuzumab as a ligand, ErbB2 was unambiguously identified through the consistent enrichment of corresponding ErbB2 glycopeptides (**Fig. 3c** and **Supplementary Table 4**). As another positive control, the EGF experiment yielded enriched glycopeptides from domain III of the EGFR. Because the molecular size of the EGFR by far exceeds that of its ligand and the enriched peptides matched only two of the more than ten EGFR glycosylation sites, this result also suggests that the approximate localization of the EGF binding site is on this particular domain of the receptor.

We further explored the capability of LRC technology to map binding sites in a subsequent experiment with two 18 kDa designed ankyrin repeat proteins (DARPins), DARPin 9.01 and DARPin H14. These two DARPins were selected by phage display as antibody mimetic proteins targeting the full-length ectodomain of the ErbB2 protein[18]. We applied LRC to BT-474 human breast cancer cells and confirmed binding of both DARPins to the ErbB2 protein in its native environment on living cells. Furthermore, the specific enrichment of corresponding glycosylation sites confirmed that DARPin 9.01 binds to domain I in ErbB2, whereas DARPin H14 binds to domain IV (**Fig. 3d** and **Supplementary Table 5**). These epitopes were independently determined *in vitro* using enzyme-linked immunosorbent assays (ELISA) with different recombinant extracellular domains of ErbB2 (**Supplementary Fig. 3**). These results demonstrate the potential of the LRC technology to identify targets and binding sites at domain-level resolution for established and prospective clinical binding proteins. Small molecule–based LRC applications are also technically feasible through direct derivatization of ligands or the prior attachment of chemical functionalities to TRICEPS. Because such strategies typically lead to a uniform modification of coupled ligands at a particular site, ligands should be tested for functionality after derivatization. In addition, the number of receptor glycosylation sites that can be reached on average is likely to be reduced compared to LRC applications with protein ligands.

In contrast to homogenous cell populations, such as immortalized clonal cell lines, complex primary tissues contain different cell types, each of which is expected to express a quantitatively and qualitatively different set of cell surface proteins. We thus did an LRC experiment with trastuzumab on primary breast cancer tissue. This tissue had been classified as immunohistochemically ErbB2 negative with a diagnostic antibody and was therefore expected to contain only low levels of the target protein (**Supplementary Fig. 4**). Nevertheless, a single LRC experiment unambiguously confirmed the ErbB2 protein as the primary target and several high- and low-affinity immunoglobulin Fcγ receptors as additional interaction partners of this IgG antibody in the tissue (**Fig. 3e** and **Supplementary Table 6**). These results underscore the sensitivity of the approach and indicate that trastuzumab binds to multiple proteins on subpopulations of cells within complex target tissues, in contrast to the comparatively simple scenario on U251 cells. Thus, the LRC technology has the potential to detect multiple intended, as well as off-target, interactions of almost any specific binding protein on clinically relevant primary tissues inaccessible to genetic engineering.

This particular capability of the LRC technology also holds great potential for the identification of receptor panels for more complex ligands. As biological particles, viruses often depend on multiple host cell surface proteins to mediate binding and subsequent internalization[19], thus representing a unique class of complex ligands.

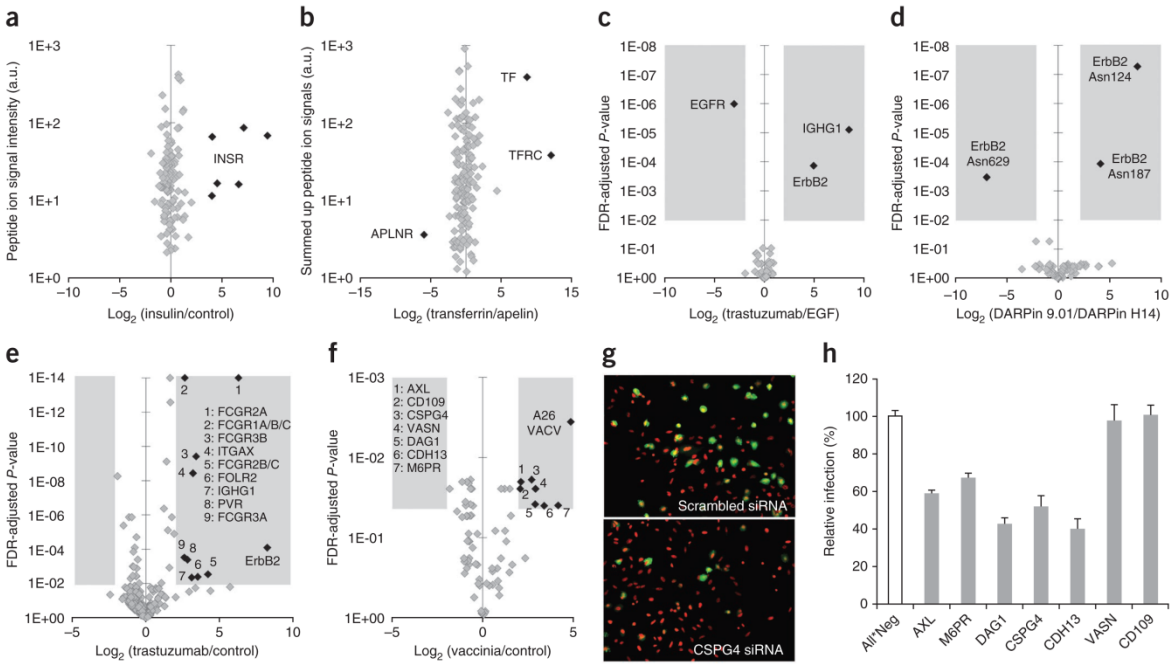

Figure 3 LRC identifies receptors and receptor panels for ligands ranging from peptides to intact viruses on living cells and tissues. (**a**) LRC with human insulin on differentiated murine visceral adipocytes. Data are shown on the peptide level. (**b**) LRC with transferrin and apelin on U-2 OS cells. Data are shown on the protein level. Two glycopeptides of transferrin were captured and identified as well without prior exposure of the ligand to oxidative conditions, which was also observed with other glycoprotein ligands used later on. APLNR, apelin receptor; TF, transferrin; TFRC, transferrin receptor. (**c**) LRC with epidermal growth factor and trastuzumab on U251 cells in biological triplicates. The receptor candidate space highlighted in gray is defined by an enrichment factor of fourfold or greater and an FDR-adjusted *P*-value less than or equal to 0.01. IGHG1, immunoglobulin heavy constant gamma 1. (**d**) LRC with DARPins on BT-474 cells in biological triplicates. Data are shown on the glycosylation site level. Identified ErbB2 glycosylation sites: Asn124, Asn187 (ErbB2 domain I), Asn629 (ErbB2 domain IV). (**e**) LRC with trastuzumab on primary breast cancer tissue in technical (multiple LC-MS/MS runs of the same sample) triplicates. (**f**) LRC with intact vaccinia viruses on HeLa CCL2 cells in biological triplicates. Receptor candidates with a fold enrichment ≥4 and a *P* value ≤ 0.05 were tested for effects on viral infectivity in follow-up investigations. Identified peptides and proteins are shown in gray. Ligands, receptors and receptor candidates are shown in black. (**g**) Representative images of siRNA-treated HeLa cells infected with vaccinia virus (red, nuclei; green, vaccinia virus early protein expression). (**h**) Percentage of vaccinia virus–infected HeLa cells after siRNA knockdown of the receptor candidates identified in the LRC experiment with intact viruses. Infection rates were calculated relative to control cells transfected with AllStars Negative Control siRNAs (All*Neg). Error bars indicate s.d.

As such, virus receptor identification remains a daunting task, with the vast majority of specific virus receptors remaining undefined. For instance, vaccinia virus (VACV) was used for the eradication of smallpox and is the most intensively studied poxvirus, yet little is known about the cell surface receptors used by VACV for infection. Competition assays suggest that VACV mature virions attach to host cells through interactions between viral proteins (A27 and D8) and glycosaminoglycans (heparin and chondroitin sulfates)[20,21], or A26 and the extracellular matrix protein laminin[22]. For internalization, phosphatidylserine in the viral membrane[23], EGFR[24], the lipid raft component CD98 (ref. 25) and the phosphatidylserine receptor AXL[26] have all been implicated. However, no direct *in vivo* interaction between mature virions and these proposed binding and internalization factors has been demonstrated. Thus, to better understand the complex interactions between these viruses and their host cells, we used LRC technology to identify the cell surface factors to which VACV mature virions bind.

Preliminary experiments demonstrated that only very high TRICEPS coupling ratios affected mature virion infectivity (**Supplementary Fig. 5**). Subsequently, LRC with intact mature virions on HeLa CCL2 cells revealed a defined set of seven cellular VACV binding factor candidates: AXL, M6PR, DAG1, CSPG4, CDH13, CD109 and VASN (**Fig. 3f** and **Supplementary Table 7**). Identification of chondroitin sulfate proteoglycan 4 (CSPG4), laminin binding protein dystroglycan 1 (DAG1) and AXL was consistent with previous independent findings[21,22,26]. The candidate VACV receptors were then subjected to short interfering RNA (siRNA)-mediated silencing to determine their functional relevance with regard to virus infection (**Supplementary Fig. 6** and **Supplementary Table 8**). Of the seven candidates tested, five (AXL, M6PR, DAG1, CSPG4 and CDH13) reduced VACV infection by 40–60% (**Fig. 3g**,**h**). That silencing of a single factor did not completely attenuate infection was not surprising. This likely reflects the complex nature of VACV-host cell interactions in which multiple virus and cellular factors each contribute to successful and potentially cooperative binding and infection. Collectively, these five factors are likely to represent the earliest set of cell surface proteins that the virus binds to and uses to infect a cell. Although LRC technology provided a unique opportunity to identify this defined set of host receptor candidates, the enrichments of individual receptors were generally weaker than in the comparatively simple one-to-one or one-to-many types of interactions addressed previously. This was expected owing to the comparatively large size of this promiscuous ligand and the many-to-many

types of interactions involved between multiple viral and host factors. Nevertheless, this discovery-driven application with a complex ligand demonstrated the potential of LRC technology to define a set of receptor candidates, after which the functional relevance can be investigated in targeted and combinatorial follow-up experiments. In summary, we are confident that LRC technology can be used to map the mostly uncharted territory of cell surface interactions.

METHODS

Methods and any associated references are available in the online version of the paper.

Accession code. The data associated with this manuscript may be downloaded from https://proteomecommons.org/ Tranche using the following hash:4rCLZMX5zYWApQjYpivFhKVrxCjTJji6V/CCyxjZYqqs1d6AMwIAR0bq1utGVuQEoj9+B8C64rQbHBNjCHWhkT464A4AAAAAAAACSw = =.

Note: Supplementary information is available in the online version of the paper.

ACKNOWLEDGMENTS

We greatly acknowledge T. Clough and O. Vitek at Purdue University for help with statistical data analysis. We are grateful to A. Hofmann, T. Bock, D. Bausch-Fluck, F. Cerciello, A. Jacobs and A. Leitner for suggestions and support at all stages of the project. We acknowledge S. Dettwiler, P. Schraml, M. Tinguely, H. Moch and the Laboratory for *In situ* Technologies, University Hospital Zurich, for preparation and staining of breast cancer tissues. This work was supported by funding from National Center of Competence in Research (NCCR) Neural Plasticity and Repair (to B.W.), Swiss National Science Foundation (SNSF) (to B.W.), SystemsX.ch/InfectX (to B.W.), SNSF Ambizione (to J.M.), SystemsX.ch and European Research Council (ERC) (to R.A.) and SystemsX.ch/InfectX and ERC (to S.K. on behalf of A. Helenius). Immortalized murine pre-adipocytes were kindly provided by M. Rosenwald and C. Wolfrum (ETH Zurich). ErbB2-negative breast carcinoma tissue cut into 50 µm slices was kindly provided by the tissue biobank of the Institute of Surgical Pathology, University Hospital Zurich.

AUTHOR CONTRIBUTIONS

A.P.F. and B.W. designed the project and wrote the paper. A.P.F. performed experiments and analyzed all data. A.P.F., B.W., O.-Y.J. and E.M.C. designed TRICEPS and O.-Y.J. synthesized the reagents. J.M. and S.K. designed and performed vaccinia virus experiments and J.M. edited the manuscript. C.J. and A.P. designed DARPin experiments and performed ELISAs. R.A., H.M. and L.M.H. contributed ideas and performed experiments. All authors discussed the results and implications and commented on the manuscript at all stages.

COMPETING FINANCIAL INTERESTS

The authors declare no competing financial interests.

Published online at http://www.nature.com/doifinder/10.1038/nbt.2354.
Reprints and permissions information is available online at http://www.nature.com/reprints/index.html.

1. Hubner, N.C. *et al.* Quantitative proteomics combined with BAC TransgeneOmics reveals *in vivo* protein interactions. *J. Cell Biol.* **189**, 739–754 (2010).
2. Glatter, T., Wepf, A., Aebersold, R. & Gstaiger, M. An integrated workflow for charting the human interaction proteome: insights into the PP2A system. *Mol. Syst. Biol.* **5**, 237 (2009).
3. Bantscheff, M. & Drewes, G. Chemoproteomic approaches to drug target identification and drug profiling. *Bioorg. Med. Chem.* **20**, 1973–1978 (2012).
4. Lenz, T., Fischer, J.J. & Dreger, M. Probing small molecule-protein interactions: A new perspective for functional proteomics. *J. Proteomics* **75**, 100–115 (2011).
5. Barglow, K.T. & Cravatt, B.F. Activity-based protein profiling for the functional annotation of enzymes. *Nat. Methods* **4**, 822–827 (2007).
6. Elschenbroich, S., Kim, Y., Medin, J.A. & Kislinger, T. Isolation of cell surface proteins for mass spectrometry-based proteomics. *Expert Rev. Proteomics* **7**, 141–154 (2010).
7. Helbig, A.O., Heck, A.J.R. & Slijper, M. Exploring the membrane proteome–challenges and analytical strategies. *J. Proteomics* **73**, 868–878 (2010).
8. Savas, J.N., Stein, B.D., Wu, C.C. & Yates, J.R. Mass spectrometry accelerates membrane protein analysis. *Trends Biochem. Sci.* **36**, 388–396 (2011).
9. Lee, A. How lipids affect the activities of integral membrane proteins. *Biochim. Biophys. Acta.* **1666**, 62–87 (2004).
10. Zeng, Y., Ramya, T.N.C., Dirksen, A., Dawson, P.E. & Paulson, J.C. High-efficiency labeling of sialylated glycoproteins on living cells. *Nat. Methods* **6**, 207–209 (2009).
11. Wollscheid, B. *et al.* Mass-spectrometric identification and relative quantification of N-linked cell surface glycoproteins. *Nat. Biotechnol.* **27**, 378–386 (2009).
12. Hofmann, A. *et al.* Proteomic cell surface phenotyping of differentiating acute myeloid leukemia cells. *Blood* **116**, e26–e34 (2010).
13. Frei, A., Jeon, O.Y., Carreira, E. & Wollscheid, B. Trifunctional crosslinking reagents. European Patent Application No. 11000731 (2012).
14. Mädler, S., Bich, C., Touboul, D. & Zenobi, R. Chemical cross-linking with NHS esters: a systematic study on amino acid reactivities. *J. Mass Spectrom.* **44**, 694–706 (2009).
15. Sletten, E.M. & Bertozzi, C.R. Bioorthogonal chemistry: fishing for selectivity in a sea of functionality. *Angew. Chem. Int. Edn Engl.* **48**, 6974–6998 (2009).
16. Ferguson, K.M. Structure-based view of epidermal growth factor receptor regulation. *Annu. Rev. Biophys.* **37**, 353–373 (2008).
17. Cho, H.-S. *et al.* Structure of the extracellular region of HER2 alone and in complex with the Herceptin Fab. *Nature* **421**, 756–760 (2003).
18. Steiner, D., Forrer, P. & Plückthun, A. Efficient selection of DARPins with sub-nanomolar affinities using SRP phage display. *J. Mol. Biol.* **382**, 1211–1227 (2008).
19. Marsh, M. & Helenius, A. Virus entry: open sesame. *Cell* **124**, 729–740 (2006).
20. Chung, C., Hsiao, J., Chang, Y. & Chang, W. A27L protein mediates vaccinia virus interaction with cell surface heparan sulfate. *J. Virol.* **72**, 1577–1585 (1998).
21. Hsiao, J.C., Chung, C.S. & Chang, W. Vaccinia virus envelope D8L protein binds to cell surface chondroitin sulfate and mediates the adsorption of intracellular mature virions to cells. *J. Virol.* **73**, 8750–8761 (1999).
22. Chiu, W.-L., Lin, C.-L., Yang, M.-H., Tzou, D.-L.M. & Chang, W. Vaccinia virus 4c (A26L) protein on intracellular mature virus binds to the extracellular cellular matrix laminin. *J. Virol.* **81**, 2149–2157 (2007).
23. Mercer, J. & Helenius, A. Vaccinia virus uses macropinocytosis and apoptotic mimicry to enter host cells. *Science* **320**, 531–535 (2008).
24. Mercer, J. *et al.* Vaccinia virus strains use distinct forms of macropinocytosis for host-cell entry. *Proc. Natl. Acad. Sci. USA* **107**, 9346–9351 (2010).
25. Schroeder, N., Chung, C.-S., Chen, C.-H., Liao, C.-L. & Chang, W. The lipid raft-associated protein CD98 is required for vaccinia virus endocytosis. *J. Virol.* **86**, 4868–4882 (2012).
26. Morizono, K. *et al.* The soluble serum protein Gas6 bridges virion envelope phosphatidylserine to the TAM receptor tyrosine kinase Axl to mediate viral entry. *Cell Host Microbe* **9**, 286–298 (2011).

ONLINE METHODS

Mammalian cell cultures. All cells were grown at 37 °C and 5% ambient CO_2. Adherent U-2 OS osteosarcoma cells, U251 glioblastoma cells and HeLa CCL2 adenocarcinoma cells were grown to near 100% confluence from initial addition to 140 × 20 mm Nunclon dishes (Thermo Scientific) in Dulbecco's Modified Eagle's Medium (DMEM, Sigma-Aldrich) completed with 10% Fetal Bovine Serum (Sigma-Aldrich) and penicillin-streptomycin-glutamine (Invitrogen). BT-474 human breast cancer cells were grown accordingly in complete RPMI medium (Sigma-Aldrich). Jurkat T suspension cells were grown in 175 cm^2 Nunclon flasks (Thermo Scientific) to an approximate concentration of 400,000 cells/ml in complete RPMI medium (Sigma-Aldrich). Immortalized murine pre-adipocytes were kindly provided by Matthias Rosenwald and Christian Wolfrum (ETH Zurich) and originally obtained by Johannes Klein (University of Lübeck). Murine cells were grown in DMEM 4.5 g/l glucose (Invitrogen) completed with 20% fetal bovine serum and penicillin-streptomycin-glutamine. Pre-adipocytes were differentiated into white adipocytes by the addition of a differentiation cocktail (115 µg/ml 3-isobutyl-1-methylxanthine (Sigma-Aldrich), 1 µM dexamethasone (Sigma-Aldrich), 1 µg/ml insulin (Sigma-Aldrich) in medium) on day 0, removal of medium and addition of new medium containing the same cocktail on day 1, removal of medium and addition of new medium containing insulin on day 2, and removal of medium and addition of standard medium on day 4. Cells were harvested on day 7 after they had adopted a rounded phenotype and accumulated lipids in the form of intracellular lipid droplets.

Flow cytometric analyses. *Aldehyde capture with TRICEPS.* Reagents were incubated with a tenfold molar excess of glycine in 25 mM HEPES pH 8.2 for 60 min to quench the amine reactive moieties of the reagents. Jurkat T cells were collected and resuspended in labeling buffer (PBS, pH adjusted to 6.5 with H_3PO_4) and cooled down to 4 °C for all of the following steps. Half of the cells were subjected to mild periodate oxidation with 1.5 mM $NaIO_4$ (Pierce) for 15 min in the dark and cell pellets were washed once with labeling buffer. Subsequently, cells were reacted with 100 µM TRICEPS or biocytin hydrazide (Biotium) in labeling buffer for 60 min on a slow rotator. Cells were washed twice and stained with streptavidin-FITC (BD Biosciences, 554060) in FACS buffer (1% Fetal Bovine Serum in PBS) for 20 min. Labeled cells were washed once and analyzed with a FACSCalibur flow cytometer (BD Biosciences) in combination with Flowjo (version 8.8.4) software.

Transferrin uptake. 50 µg AlexaFluor-488 labeled transferrin (Invitrogen) was coupled to TRICEPS or incubated in coupling buffer (25 mM HEPES pH 8.2) without reagent. After coupling, the labeled protein was diluted in DMEM to a final concentration of 8.3 µg/ml. Confluent 12 wells of HeLa ATCC cells were starved in DMEM for 2 h. Transferrin was bound to cells for 30 min at 4 °C (750 µl/well) and cells were shifted to 37 °C for 15 min (water-bath). Cells were washed once with cold PBS and treated with acid washing buffer (0.1 M NaCl, 0.1 M glycine, pH 3.0) for 2 min. Samples were detached with 0.05% trypsin, fixed (4% formaldehyde in PBS, 20 min) and analyzed by flow cytometry.

VACV infection. Confluent 24 wells of HeLa ATCC cells were infected with VACV strain Western Reserve expressing EGFP from an early viral promoter (WR Early-EGFP) at different multiplicities of infection (MOI) in 250 µl DMEM. After 30 min at 37 °C, DMEM was replaced with full medium (DMEM, 10% FBS, NEAA and Glutamax). Five hours after infection, cells were detached with 0.05% trypsin, fixed (4% formaldehyde in PBS, 20 min) and analyzed by flow cytometry.

LRC. 100 µg insulin (Sigma-Aldrich), 100 µg holo-transferrin (Sigma-Aldrich), 30 µg apelin-17 (Tocris Bioscience), 50 µg EGF (Sigma-Aldrich), 100 µg trastuzumab (Roche), 5×10^8 plaque-forming units of vaccinia virus or 100 µg glycine (Sigma-Aldrich) were reacted with 40 µg TRICEPS in 40–100 µl 25 mM HEPES pH 8.2 for 60 min. Typically, coupling reactions do not need to be optimized and we recommend using 40 µg TRICEPS per 100 µg ligand for all applications. Higher coupling ratios can be applied in cases where a limited amount of ligand is available. Hydrolyzed TRICEPS and the fraction of ligands that are compromised by the coupling to reagents will simply contribute to the random capture of cell surface proteins, so there is no need to purify coupled ligands. Using intact viruses as ligands in LRC experiments, true receptors will be captured and enriched by TRICEPS coupled to viral proteins that interact with these host factors. At the same time, reagents that are coupled to other viral proteins may contribute to the stochastic capture of cell surface proteins (the majority of capture events in every LRC experiment) in the vicinity of actual binding events. On HeLa CCL2 cells no binding of insulin to the INSR was detected in preliminary LRC experiments and the peptide hormone was used to quench reagents. 5×10^7 cells (murine adipocytes, U-2 OS, U251, BT-474, HeLa CCL2) per experiment were harvested by gentle scraping in PBS and cooled down to 4 °C for all of the following steps. Frozen ErbB2-negative breast carcinoma tissue cut into 50-µm slices was kindly provided by the tissue biobank of the Institute of Surgical Pathology, University Hospital Zurich (approved by the local ethics committee: StV12-2005). The procedure for freezing and cutting tissues has been previously described[27]. Tissue slices were processed without further dissociation to partly conserve the three-dimensional tissue structure during incubation with trastuzumab. Cells or tissue slices were resuspended in 50 ml labeling buffer (PBS pH 6.5) and subjected to mild periodate oxidation with 1.5 mM $NaIO_4$ (Pierce) on a slow rotator in the dark for 15 min (30 min for tissue slices). Subsequently, cells were washed once with 50 ml labeling buffer and resuspended in 10 ml labeling buffer for incubation with the ligands or quenched reagents. LRC was carried out for 60 min (90 min for tissue slices) on a slow rotator. Cells were collected by centrifugation and the cell pellet was resuspended in 1 ml 50 mM ammonium bicarbonate (Sigma-Aldrich). Cells were lysed by indirect sonication (100% amplitude, 0.8 cycle, 2 × 30 s) in a VialTweeter (Hielscher) and the subsequent addition of RapiGest surfactant (Waters). Tissue slices were subjected to additional sonication cycles and vigorous pipetting after the addition of RapiGest to completely dissociate the tissue. After centrifugation (2,500*g*, 10 min), the supernatant was collected after which proteins were reduced by adding 5 mM TCEP (Pierce) at 20 °C for 30 min and then alkylated by adding 10 mM iodoacetamide (Fluka) in the dark at 20 °C for 30 min. Trypsin (Sigma) was added to a 1:50 trypsin to protein ratio and protein digestion was carried out overnight at 37 °C. After digestion, peptide mixtures were heated to 96 °C for 10 min to inactivate proteases and undigested particles were removed by centrifugation (13,000*g* for 10 min). TRICEPS-captured cell surface glycopeptides were bound to streptavidin by addition of 60 µl washed Streptavidin Plus UltraLink Resin (Pierce) and incubated for 60 min on a slow rotator at 4 °C. Beads were washed extensively in Mobicols (Boca Scientific) connected to a Vac-Man Laboratory Vacuum Manifold (Promega) with a variety of buffers: 5 M NaCl, followed by 100 mM NaCl, 100 mM glycerol, 50 mM Tris, 1% Triton X-100, followed by 100 mM $NaHCO_3$ pH 11, followed by 50 mM ammonium bicarbonate. Washed beads were incubated with 300 µl 50 mM ammonium bicarbonate containing 1.5 µl PNGase F (New England Biolabs) in a head-over-head shaker overnight at 37 °C. Peptides were eluted by spinning of the Mobicol and subsequent addition of another 500 µl 50 mM ammonium bicarbonate. Combined eluates were acidified with 40 µl 10% formic acid and subjected to C18 purification using 3–30 µg UltraMicroSpin Columns (The Nest Group) according to the manufacturer's instructions.

Liquid chromatography–tandem mass spectrometry (LC-MS/MS) analysis. Peptide samples were separated by reversed-phase chromatography on a high-performance liquid chromatography (HPLC) column (75-µm inner diameter, New Objective) that was packed in-house with a 10-cm stationary phase (Magic C18AQ, 200 Å, 3 µm, Michrom Bioresources) and connected to a nano-flow HPLC (nanoLC-Ultra 1D plus, Eksigent) and an autosampler (nanoLC AS-2, Eksigent). The HPLC was coupled to a LTQ-Orbitrap XL mass spectrometer (Thermo Scientific) equipped with a nanoelectrospray ion source (Thermo Scientific). Peptides were loaded onto the column with 95% buffer A (98% H_2O, 2% acetonitrile, 0.1% formic acid) and eluted with 300 nl/min over a 40-min linear gradient from 5–35% buffer B (2% H_2O, 98% acetonitrile, 0.1% formic acid). After the gradient, the column was washed with 95% buffer B and re-equilibrated with buffer A. Mass spectra were acquired in a data-dependent manner, with an automatic switch between MS and MS/MS scans. High-resolution MS scans were acquired in the Orbitrap (60,000 FWHM, target value 10^6) to monitor peptide ions in the mass range of 350–1,650 m/z, followed by collision-induced dissociation MS/MS scans in the ion trap (minimum signal threshold 150, target value 10^4, isolation width 2 m/z) of the five most

doi:10.1038/nbt.2354

intense precursor ions. To avoid multiple scans of dominant ions, the precursor ion masses of scanned ions were dynamically excluded from MS/MS analysis for 10 s. Singly charged ions and ions with unassigned charge states were excluded from MS/MS fragmentation.

MS data analysis and quantification. Raw data were converted to the open mzXML format with ReAdW (version 4.3.1). mzXML files were searched by the SEQUEST search engine against UniProtKB/Swiss-Prot protein databases (version 57.15 of *Homo sapiens*, *Mus musculus* and vaccinia virus strain Western Reserve) concatenated with the sequences of common contaminants. Search parameters for the peptide identification included a precursor mass tolerance of 0.05 Da, a minimum of one tryptic terminus and a maximum of two internal trypsin cleavage sites. Cysteine carbamidomethylation (+57.021 Da) was set as a static amino acid modification and methionine oxidation (+15.995 Da) as well as asparagine deamidation (+0.9840 Da) were set as differential modifications. The PeptideProphet and ProteinProphet tools of the Trans-Proteomic Pipeline (TPP version 4.5) were used for the probability scoring of peptides and proteins, and protein identifications were filtered to a false-discovery rate of ≤1%. For label-free quantification of the identified peptides, Thermo. RAW files were imported into the Progenesis LC-MS software (Nonlinear Dynamics) to detect and extract ion signals corresponding to peptide features. Peptide features matched to ion signals were filtered for the presence of the N[115]-X-S/T motif (wherein N[115] stands for a deamidated asparagine residue, X stands for any amino acid except proline and S/T for serine or threonine, respectively). This filtering step assured that only formerly N-glycosylated cell surface peptides and proteins that had been specifically captured and purified were considered for the quantitative sample comparison (typically 40–70% of the identified proteins). Peptide ion signals with high fold changes between samples were manually inspected to assure correct feature picking and extraction. The different enrichment factors obtained for potential receptor peptides can typically be explained by differences in the efficiency of the LRC reaction; for example, due to the spatial arrangement of the captured carbohydrates in relation to the ligand binding site. Furthermore, the virtual absence of some receptor peptide signals in the control sample can make ratios susceptible to the response of individual peptides in the mass spectrometer and background integration in the quantification process. Peptide signal intensities were exported on the feature level for the statistical analysis.

Statistical analysis. As described above, the output of a LRC experiment is a list of quantified spectral features. For the statistical analysis, the intensities for peptide features with multiple charge states and differential modifications were summed up and constant normalization was performed on the log-transformed intensities across samples. To make protein-level conclusions based on those measurements, a previously described fixed effects Analysis of Variance (ANOVA) model[28] was applied using the publicly available R-based software MSStats (http://www.stat.purdue.edu/~ovitek/Software.html) according to instructions in the package documentation. This model views individual features as replicate measurements of a protein's abundance and explicitly accounts for this redundancy, which increases the sensitivity and specificity of testing. Thus, it was used to test each protein for differential abundance in all pairwise comparisons of ligand and control samples and to report the *P*-values of the tests. Subsequently, *P*-values were adjusted for multiple comparisons using the approach by Benjamini and Hochberg to control the experiment-wide false-discovery rate at a desired level.

ErbB2-binding DARPin selection and ELISA. Selection of ErbB2-binding DARPins has been described previously[18]. In brief, Signal Recognition Particle Phage Display was used to select DARPins recognizing the complete ecto-domain (domains I-IV) of ErbB2. To determine the binding specificity at the domain level in ELISAs, recombinant ErbB2-ectodomains carrying an N-terminal melittin signal sequence (MKFLVNVALVFMVVYISYIYA) and an N-terminal His_6 tag were expressed in *Spodoptera frugiperda* (*Sf*9) cells using baculoviral vectors. *Sf*9 cells were grown to a density of 4×10^6 cells/mL and co-infected with the respective virus at a MOI of 1. 72 h post-infection, cells were harvested by centrifugation (30 min, 5,000*g*, 4 °C) and the cleared medium was subjected to immobilized metal ion affinity chromatography (IMAC) purification with Ni-NTA Superflow (Qiagen) purification resin. The purified ErbB2 domains (200 nM, 100 µl/well) in PBS were immobilized on MaxiSorp plates (Thermo Scientific) by overnight incubation at 4 °C. For ELISAs, wells were blocked with 300 µl of PBSTB (PBS, 0.1% Tween-20, 0.2% BSA) for 1 h at room temperature. 50 nM of purified DARPins were incubated with the target domains for 1 h at room temperature followed by three washing steps with 300 µl of PBSTB. For detection of bound DARPins, an anti RGS-His IgG1 mouse antibody (Qiagen) was added (1:5,000 in PBSTB, 1 h at room temperature), which recognizes the N-terminal MRGS-His_6 tag of the DARPins, and wells were washed as described above. After incubation with a secondary anti-mouse-IgG antibody alkaline phosphatase conjugate (Sigma-Aldrich) (1:10,000 in PBSTB, 1 h at room temperature), pNPP substrate (Fluka) was added to measure alkaline phosphatase activity.

siRNA knockdown and infection assays. HeLa cells were reverse-transfected with pooled Qiagen siRNAs (3 siRNAs/gene, **Supplementary Table 8**) at a final concentration of 20 nM in 96-well flat-bottom microscopy plates (Greiner Bio-One). siRNAs in ddH_2O were mixed with Lipofectamine RNAiMax (Invitrogen) in DMEM to a final volume of 30 µl according to the manufacturer's instructions (0.1 µl RNAiMax/well). 1,800 cells were seeded onto the Lipofectamine mixture and transfected for 72 h. Transfected cells were infected with VACV Western Reserve Early-EGFP with a target infection index of ~20% to allow for a dynamic measurement of possible enhancing and inhibiting effects on infection. Virus was bound to cells at 37 °C in 50 µl DMEM for 30 min, inoculum was replaced with full medium and cells were infected for an additional 6 h. Samples were fixed (4% formaldehyde, 20 min) and permeabilized (0.5% Triton X-100), and nuclei were stained with Hoechst 33258 (Molecular Probes). EGFP was stained with rabbit antiserum and an Alexa-Fluor-488 goat anti-rabbit secondary antibody (Invitrogen) to increase the signal of inherently weak early viral gene expression levels. Primary antibody staining was done in permeabilization buffer, secondary staining in PBS. Automated image acquisition (16 images/well) was done with a 10× objective using an ImageXpress Micro high content screening system (Molecular Devices). Cell numbers and raw infection indices for each well were determined using a MATLAB-based infection-scoring program (InfectionCounter V, Thomas Heger, ETH Zurich). Infection rates were calculated relative to the control wells transfected with AllStars Negative (All*Neg) Control siRNAs (Qiagen). An internal checkerboard assay was performed for each plate to normalize for the negative correlation between cell number and infection index. Increasing cell numbers (500–1,800 cells, 18 data points/plate) were transfected (All*Neg) and infected as described. The correlation between the number of nuclei and infection index was determined using logarithmic regression (% infection = a*ln(nuclei)+b). Relative infection rates of target siRNAs were calculated in relation to the negative control at the corresponding nuclei number. For the verification of siRNA-mediated protein depletion, HeLa ATCC cells were transfected with 20 nM nontargeting All*Neg siRNAs or pooled siRNAs targeting receptor candidate proteins for 72 h. Cells were detached (500 µM EDTA in PBS), lysed in RIPA buffer (50 mM Tris pH7.4, 150 mM NaCl, 0.5% Na-deoxycholate, 1.0% Triton X-100) and protein levels were analyzed by western blot using primary AXL (Cell Signaling, 4566), CDH13 (R&D Systems, AF3264), M6PR (Novus Biologicals, NB100-93413) and α-tubulin (Sigma, T9026) antibodies. To monitor CD109 cell surface expression, detached cells were stained with a PE-coupled CD109 antibody (BD Biosciences, 556040) for 30 min, washed with PBS and analyzed by flow cytometry.

27. Steu, S. *et al.* A procedure for tissue freezing and processing applicable to both intra-operative frozen section diagnosis and tissue banking in surgical pathology. *Virchows Arch.* **452**, 305–312 (2008).
28. Clough, T. *et al.* Protein quantification in label-free LC-MS experiments. *J. Proteome Res.* **8**, 5275–5284 (2009).

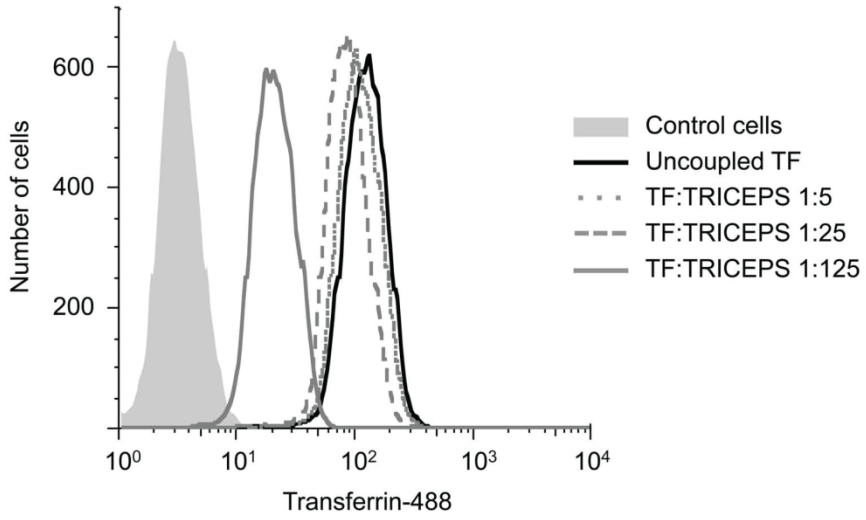

Supplementary Figure 1: Uptake of fluorescently labeled transferrin-488 (TF) into HeLa cells after coupling to TRICEPS. Coupling reactions were set up with the indicated ratios of TF:TRICEPS. Notably, the actual coupling ratios (average number of TRICPES attached to a TF protein) are substantially lower since hydrolysis of the NHS ester is a major competing reaction of the coupling reaction in solution. In every LRC experiment, a fraction of ligands is compromised by the attachment of TRICEPS to particular lysines that are sterically or otherwise important for the respective ligand-receptor interaction. Since the coupling of TRICEPS to lysine side chains is unspecific and several lysines are typically present in protein ligands, only high TRICEPS:protein ratios lead to an impairment of the majority of ligands.

e Biotechnology: doi:10.1038/nbt.2354

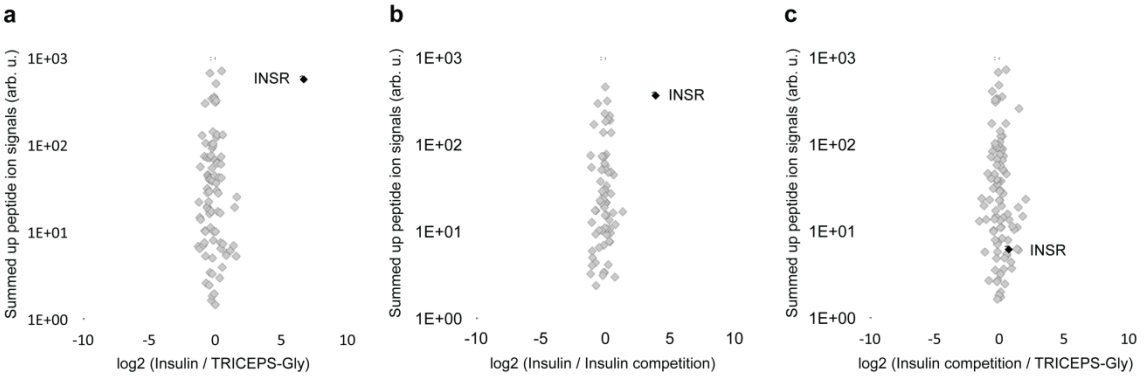

Supplementary Figure 2: LRC competition experiment with insulin. (**a**) Jurkat T lymphocytes were incubated with TRICEPS-coupled insulin or Glycine-quenched TRICEPS, respectively. (**b** and **c**) For the insulin competition sample, cells were incubated with a 10-fold molar excess of uncoupled insulin prior to the addition of TRICEPS-coupled insulin. Data are shown on the protein level.

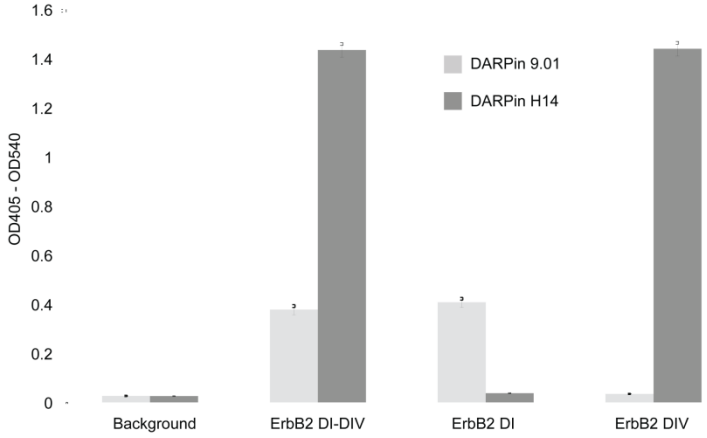

ErbB2 DI
HHHHHHQVCTGTDMKLRLPASPETHLDMLRHLYQGCQVVQGNLELT
NASLSFLQDIQEVQGYVLIAHNQVRQVPLQRLRIVRGTQLFEDNYALA
GDPLNNTTPVTGASPGGLRELQLRSLTEILKGGVLIQRNPQLCYQDTIL
FHKNNQLALTLIDTNRSRACHPCSPMCKGSRCWGE SSEDCQSLTRTV

ErbB2 DIV
HHHHHHVNCSQFLRGQECVEECRVLQGLPREYVNARHCLPCHPECQ
GSVTCFGPEADQCVACAHYKDPPFCVARCPSGVKPDLSYMPIWKFPD
ACQP

ErbB2 DI-DIV
HHHHHHQVCTGTDMKLRLPASPETHLDMLRHLYQGCQVVQGNLELT
NASLSFLQDIQEVQGYVLIAHNQVRQVPLQRLRIVRGTQLFEDNYALA
GDPLNNTTPVTGASPGGLRELQLRSLTEILKGGVLIQRNPQLCYQDTIL
FHKNNQLALTLIDTNRSRACHPCSPMCKGSRCWGESSEDCQSLTRTV
GCARCKGPLPTDCCHEQCAAGCTGPKHSDCLACLHFNHSGICELHCP
YNTDTFESMPNPEGRYTFGASCVTACPYNYLSTDVGSCTLVCPLHNQ
EDGTQRCEKCSKPCARVCYGLGMEHLREVRAVTSANIQEFAGCKKIF
FLPESFDGDPASNTAPLQPEQLQVFETLEEITGYLYISAWPDSLPDLSV
QVIRGRILHNGAYSLTLQGLGISWLGLRSLRELGSGLALIHHNTHLCFV
WDQLFRNPHQALLHTANRPEDECVGEGLACHQLCARGHCWGPGPT
CSQFLRGQECVEECRVLQGLPREYVNARHCLPCHPECQPQNGSVTC
ADQCVACAHYKDPPFCVARCPSGVKPDLSYMPIWKFPDEEGACQPA

Supplementary Figure 3: ELISA of the ErbB2 binding DARPins 9.01 and H14. The respective DARPins were tested for binding to the immobilized complete extracellular do of ErbB2 (ErbB2 DI-DIV), extracellular domain 1 (ErbB2 DI), and extracellular domain 4 (ErbB2 DIV), respectively. Amino acid sequences of the recombinant ErbB2 domains shown on the right. Higher signals for DARPin H14 (K_D = 200 pM) than for 9.01 (K_D ≈ 100 nM) can be explained by the difference in the affinities for ErbB2 as determine surface plasmon resonance and competition ELISA (data not shown). Error bars, s.d. (n=3)

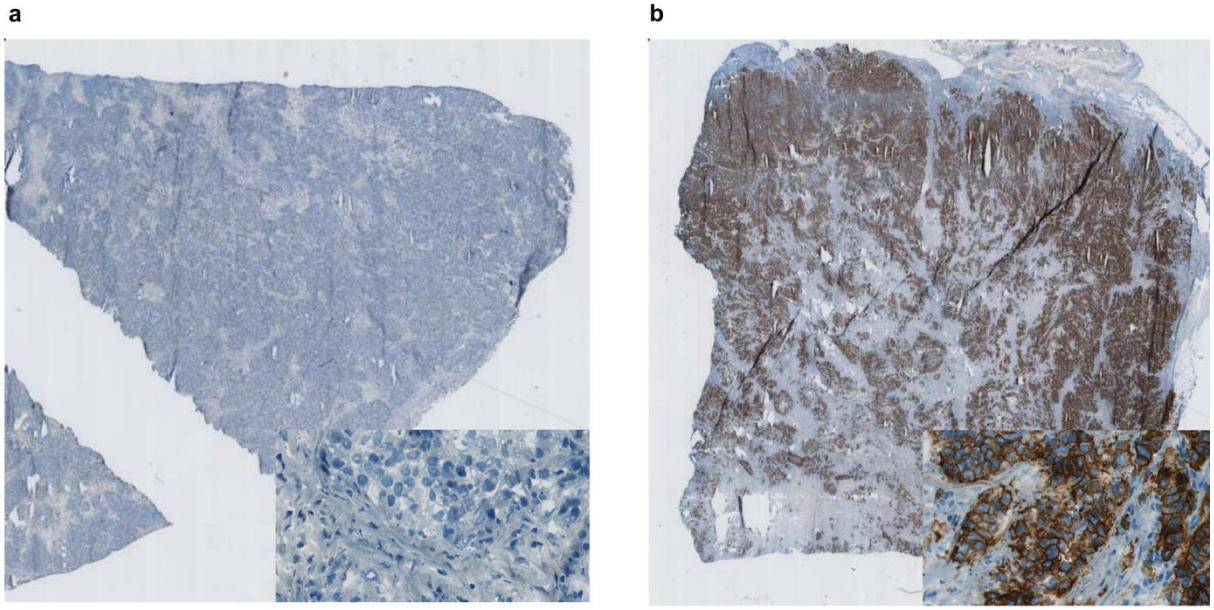

Supplementary Figure 4: ErbB2 immunohistochemical staining of two ductal breast carcinomas. (**a**) ErbB2-negative tissue section of the carcinoma used in the trastuzumab LRC experiment. (**b**) ErbB2-positive tissue section with comparatively high ErbB2 expression levels.

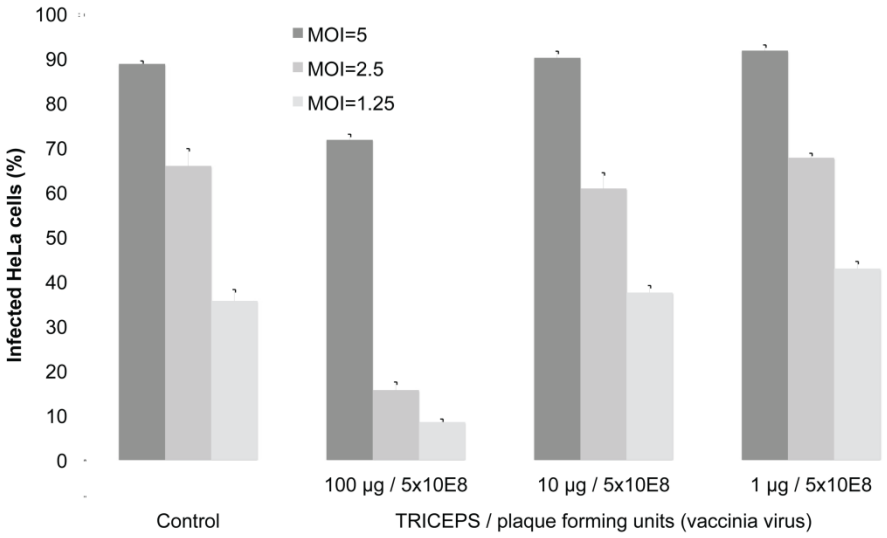

Supplementary Figure 5: Infection assay using vaccinia virus after coupling to TRICEPS at different ratios. Vaccinia virus (strain Western Reserve) Early-EGFP expression in HeLa cells was measured by flow cytometry. Multiplicities of infection (MOI) are indicated. Error bars, s.d. (n=3, technical triplicate)

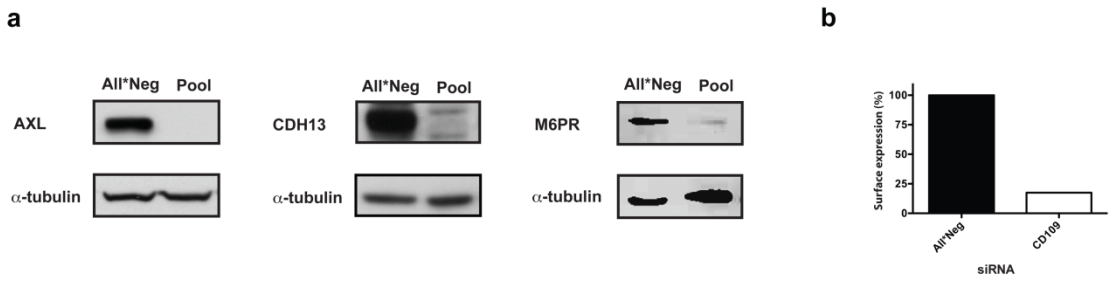

Supplementary Figure 6: Confirmation of siRNA-mediated protein depletion. (**a**) Western blots in total HeLa cell extracts after transfection of cells with targeting siRNAs against AXL, CDH13, and M6PR (Pool) or with non-targeting siRNAs (All*Neg). (**b**) Cell surface expression of CD109 as measured by flow cytometry after transfection of cells with targeting siRNAs against CD109 or with non-targeting siRNAs.

e Biotechnology: doi:10.1038/nbt.2354

Supplementary Note 1: Chemical synthesis description for TRICEPS.

Abbreviations: Boc, butoxycarbonyl; DCC, *N*,*N*'-dicyclohexylcarbodiimide; DIPEA, diisopropylethylamine; DMAP, 4-dimethylaminopyridine; DMSO, dimethylsulfoxide; EDCI, 1-(3-dimethylaminopropyl)-3-ethylcarbodiimide hydrochloride; Et_2O, diethylether; EtOH, ethanol; Fmoc, 9-fluorenylmethoxycarbonyl; HBTU, *N*,*N*,*N*',*N*'-tetramethyl-O-(1H-benzotriazol-1-yl) uronium hexafluoro-phosphate; Hex, hexane; *i*-PrOH, isopropanol; NHS, *N*-hydroxysuccinimide; TFA, trifluoroacetic acid; TFAA, trifluoroacetic anhydride.

Synthesis of compound 1:

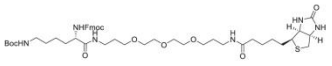

Fmoc-*N*-ε-Boc-L-Lysine (1.7 g, 3.7 mmol) was dissolved in DMF (20 ml) and mixed with DIPEA (0.63 ml, 3.7 mmol) and HBTU (1.7 g, 4.4 mmol). After 10 min, a solution of 1-*N*-biotinyl-4,7,10-trioxatridecane-1,13-diamine (1.8 g, 4.1 mmol) in DMF (5 ml) was added and stirred at room temperature for 1 h. The solvent was evaporated under reduced pressure and the product was purified by flash chromatography ($CHCl_3$:MeOH:H_2O = 10:6:1) providing the desired compound as a white viscous foam (2.6 g, 78%).

Synthesis of compound 2:

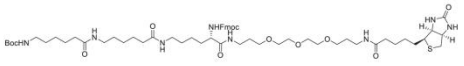

Compound 1 (2.6 g, 2.9 mmol) was stirred in a mixture of CH_2Cl_2:TFA (1:1, 20 ml). Subsequently, the reaction mixture was subjected to concentration and drying under high vacuum. The crude product (2.4 g, 3.0 mmol) and 2,5-dioxopyrrolidin-1-yl 6-({[(*tert*-butoxy)carbonyl]amino}hexanamido)hexanoate (1.5 g, 3.5 mmol; synthesized as described previously[1]) were dissolved in MeOH (6 ml). TEA was added (0.83 ml, 5.9 mmol) and the mixture was stirred at room temperature for 20 min. The solvent was evaporated under reduced pressure and the product was purified by flash chromatography (CH_2Cl_2:MeOH = 9:1 to $CHCl_3$:MeOH:H_2O = 85:15:1) providing the desired compound as a white viscous foam (2.8 g, 84%).

Synthesis of compound 3:

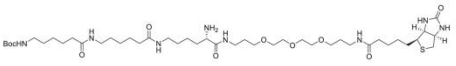

Compound 2 (0.39 g, 0.35 mmol) was dissolved in DMF (3 ml) and mixed with piperidine (0.2 ml) at room temperature for 5 min followed by the addition of Et_2O (100 ml). The ether layer was decanted and the oil crude mixture was dissolved in MeOH. The product was concentrated under reduced pressure and purified by flash chromatography ($CHCl_3$:MeOH:H_2O = 65:25:4 to 10:6:1) providing the desired compound as a white viscous foam (0.21 g, 67%).

Synthesis of compound 4:

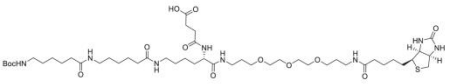

Compound 3 (2.1 g, 2.3 mmol) was dissolved in DMF (1 ml) followed by the addition of DIPEA (0.48 ml, 2.8 mmol) and succinic anhydride (0.28 g, 2.8 mmol) at room temperature for 1.5 h. The solvent was evaporated under reduced pressure and purified by flash chromatography (CH_2Cl_2:MeOH = 10:1 to $CHCl_3$:MeOH:H_2O = 65:25:4 to 10:6:1) providing the desired compound as a white viscous foam (1.4 g, 61%).

Synthesis of compound 5:

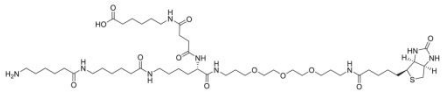

Compound 4 (1.3 g, 1.3 mmol), DIPEA (0.27 ml, 1.6 mmol) and HBTU (0.61 g, 1.6 mmol) were dissolved in DMF (15 ml). 6-aminocaproic acid (0.21 g, 1.6 mmol) was added and the mixture was stirred at room temperature for 1.5 h. The solvent was evaporated under reduced pressure and the product was purified by flash chromatography ($CHCl_3$:MeOH:H_2O = 85:15:1 to 65:25:4) providing the compound as a white viscous foam (1.5 g, quant.). Subsequently, the product (1.5 g, 1.3 mmol) was dissolved in a mixture of CH_2Cl_2:TFA (1:1, 20 ml) and stirred at 0°C for 10 min. The solvent was evaporated under reduced pressure and the product was purified by flash chromatography (CH_2Cl_2:MeOH = 10:1 to $CHCl_3$:MeOH:H_2O = 10:6:1) providing the desired compound as a white viscous foam (1.4 g, 61%).

Synthesis of compound 6:

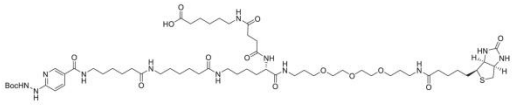

6-({[(*tert*-Butoxy)carbonyl]amino}amino)pyridine-3-carboxylic acid (0.43 g, 1.7 mmol, synthesized as described previously[2]), HBTU (0.51 g, 1.4 mmol), and DIPEA (0.23 ml, 1.4 mmol) were dissolved in DMF (10 ml). Compound 5 (1.1 g, 1.1 mmol) was added as a solution in DMF (10 ml) and the mixture was stirred at room temperature for 40 min. The solvent was evaporated under reduced pressure and the product was purified by flash chromatography (CH_2Cl_2:MeOH = 10:1 to $CHCl_3$:MeOH:H_2O = 65:25:4) providing the desired compound as a slightly yellow viscous foam (0.96 g, 68%).

Synthesis of compound 7:

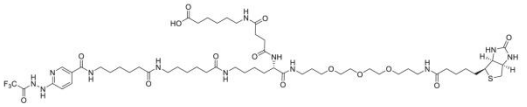

Compound 6 (0.16 g, 0.14 mmol) was dissolved in TFA (4 ml) and stirred at room temperature for 30 min. The solvent was evaporated and the product was purified on sephadex LH-20 resin and dried under vacuum. The resulting purple amorphous solid was dissolved in DMF (1.5 ml). TFAA (21 µL, 0.15 mmol) was added to the solution and the mixture was stirred at room temperature for 30 min. The crude mixture was evaporated under reduced pressure and purified on sephadex LH-20 ($CHCl_3$:MeOH = 95:5) providing the desired compound as a slightly yellow viscous foam (0.14 g, 90%).

Synthesis of compound 8 (TRICEPS):

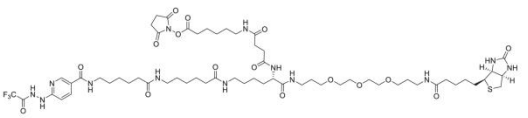

Compound 7 (28 mg, 23 µmol), NHS (3.1 mg, 27 µmol), and EDCI (5.6 mg, 27 µmol) were dissolved in DMF (0.3 ml) and the reaction mixture was stirred overnight. The crude mixture was concentrated under reduced pressure and purified on sephadex LH-20 ($CHCl_3$:MeOH = 95:5) providing the desired compound as a slightly green viscous foam (19 mg, 62%).

Supplementary References

1 Srinivasan, B. & Huang, X. Functionalization of magnetic nanoparticles with organic molecules: loading level determination and evalu linker length effect on immobilization. *Chirality* **20**, 265–277 (2008).

2 Abrams, M. *et al.* Technetium-99m-Human Polyclonal Igg Radiolabeled via the Hydrazino Nicotinamide Derivative for Imaging Focal Infection in Rats. *J Nucl Med* **31**, 2022–2028 (1990).

Appendix 4

Structural Model for the Interaction of a Designed Ankyrin Repeat Protein with the Human Epidermal Growth Factor Receptor 2

Epa VC, Dolezal O, Doughty L, Xiao X, Jost C, Plückthun A and Adams TE

OPEN ACCESS Freely available online

PLOS ONE

Structural Model for the Interaction of a Designed Ankyrin Repeat Protein with the Human Epidermal Growth Factor Receptor 2

V. Chandana Epa[1]*, Olan Dolezal[1], Larissa Doughty[1¤], Xiaowen Xiao[1], Christian Jost[2], Andreas Plückthun[2], Timothy E. Adams[1]

1 Commonwealth Scientific & Industrial Research Organization Materials Science & Engineering, Parkville, Victoria, Australia, **2** Biochemisches Institut der Universität Zürich, Zürich, Switzerland

Abstract

Designed Ankyrin Repeat Proteins are a class of novel binding proteins that can be selected and evolved to bind to targets with high affinity and specificity. We are interested in the DARPin H10-2-G3, which has been evolved to bind with very high affinity to the human epidermal growth factor receptor 2 (HER2). HER2 is found to be over-expressed in 30% of breast cancers, and is the target for the FDA-approved therapeutic monoclonal antibodies trastuzumab and pertuzumab and small molecule tyrosine kinase inhibitors. Here, we use computational macromolecular docking, coupled with several interface metrics such as shape complementarity, interaction energy, and electrostatic complementarity, to model the structure of the complex between the DARPin H10-2-G3 and HER2. We analyzed the interface between the two proteins and then validated the structural model by showing that selected HER2 point mutations at the putative interface with H10-2-G3 reduce the affinity of binding up to 100-fold without affecting the binding of trastuzumab. Comparisons made with a subsequently solved X-ray crystal structure of the complex yielded a backbone atom root mean square deviation of 0.84–1.14 Ångstroms. The study presented here demonstrates the capability of the computational techniques of structural bioinformatics in generating useful structural models of protein-protein interactions.

Citation: Epa VC, Dolezal O, Doughty L, Xiao X, Jost C, et al. (2013) Structural Model for the Interaction of a Designed Ankyrin Repeat Protein with the Human Epidermal Growth Factor Receptor 2. PLoS ONE 8(3): e59163. doi:10.1371/journal.pone.0059163

Editor: Paul Taylor, University of Edinburgh, United Kingdom

Received January 1, 2013; **Accepted** February 12, 2013; **Published** March 19, 2013

Copyright: © 2013 Epa et al. This is an open-access article distributed under the terms of the Creative Commons Attribution License, which permits unrestricted use, distribution, and reproduction in any medium, provided the original author and source are credited.

Funding: This work was funded by the Commonwealth Scientific and Industrial Research Organization. The funder had no role in study design, data collection and analysis, decision to publish, or preparation of the manuscript.

Competing Interests: The authors have declared that no competing interests exist.

* E-mail: Vidana.Epa@csiro.au

¤ Current address: St Vincent's Institute of Medical Research, Fitzroy, Victoria, Australia

Introduction

The human epidermal growth factor receptor 2 (HER2 or ErbB2) is over-expressed in several cancers, in particular in about 30% of breast tumors [1] and is indicative of a poor prognosis for these patients. Members of the HER/EGFR family are cell-surface receptors that have an intracellular tyrosine kinase domain and an ectodomain consisting of four distinct domains including the ligand-binding regions (domains 1 and 3) and two cysteine-rich domains (domains 2 and 4). HER2 plays a fundamental role in normal growth and development, eliciting a complex program of intracellular signaling and cellular responses, initiated by hetero-dimerization with other members of the HER family, in particular HER3 and HER4 [2], that become dimerization competent through ligand binding. Over-expression of HER2, usually the result of gene amplification, allows the constitutive dimerization of the receptor with HER3 devoid of ligand [3] and all liganded members of the EGFR family, and is thus a major factor in the development and maintenance of malignancy. Hence, HER2 is an important target for cancer therapeutic and diagnostic development. Of the HER2 binding monoclonal antibodies that are used in the clinic, trastuzumab (Herceptin^{TM}) binds to domain 4 [4] while pertuzumab (Perjeta^{TM}) binds to domain 2 [5].

Designed ankyrin repeat proteins (DARPins) [6,7,8] are a novel class of small, highly stable binding proteins that can be selected by ribosome display to bind target proteins with high affinity and can be expressed in bacteria in high yields. Because of their small size, DARPins targeting cell-surface proteins are expected to have much better tissue penetration and higher clearance than antibodies recognizing the same protein target when administered *in vivo*. The DARPin H10-2-G3 (hereafter referred to as 'G3') has been selected to bind HER2 with picomolar affinity [9]. This DARPin has been found to be as reliable and even more specific when compared to an FDA-approved anti-HER2 antibody used for testing the status of HER2 in paraffin-embedded breast cancer tissue [10]. G3 consists of only two ankyrin repeat motifs flanked by N-terminal and C-terminal capping regions. Each of the 33-residue ankyrin repeat motifs contain two antiparallel α-helices. G3 has been randomized at six positions in each of the repeats and contains four further mutations in the framework region. G3, while binding to domain 4 of HER2 [10], does not compete with trastuzumab in binding to HER2 (C. Jost and A. Plückthun, unpublished data). Tumor targeting experiments with mice bearing HER2-overexpressing human breast cancer xenografts have shown high tumor accumulation correlating with the affinity of the DARPins to HER2 [11].

Knowledge of the three-dimensional structure of the G3-HER2 complex would be very valuable in understanding the structural basis of the interaction between the DARPin and HER2 and would facilitate protein engineering approaches for anti-HER2 DARPins that contain G3. In the current paper, we use macromolecular computational docking methodology in combination with a number of different energetic and structural metrics to construct a 3-dimensional atomic structural model of the complex between G3 and HER2. We then selected putative interacting amino acid residues on HER2 to mutagenize. By analyzing the impact of these mutations on the interaction of G3, we provide evidence that validates the structural model of the G3-HER2 complex. Structural comparison with a subsequently solved X-ray crystal structure (PDB id: 4HRN) of the complex provides a quantitative measure of the accuracy of the computational model.

Results and Discussion

Modeling the Structure of the G3-HER2 Complex

The construction of the three-dimensional structure of the complex between HER2 and G3 commenced with the X-ray crystal structure of HER2 in complex with trastuzumab [4] and the X-ray crystal structure of the HER2-specific DARPin G3 [9]. G3 is one of the KEYL sequence family DARPins evolved by affinity maturation and exhibits affinity of 90 pM to HER2. As Cho et al. [4] describe in their crystal structure of the complex between trastuzumab-Fab and the HER2 ectodomain, trastuzumab binds to the domain 4 of HER2. While G3 also binds to domain 4 of HER2, it does not compete with trastuzumab in binding to the receptor (C. Jost and A. Plückthun, unpublished). For this reason we used only domain 4 (residues #508–607) in macromolecular docking to construct the structural model of the G3-HER2 complex. This also has the effect of making the computational task more tractable and facilitates the generation of more accurate results through the use of a finer grid mesh for the docking than otherwise would have been possible. Chain A (residues #12–135) of the G3 structure was used in the modeling. Prior to the macromolecular docking, the structure of the loop containing residues #581–590 of domain 4 of HER2 was modeled, since atomic coordinates of this region are missing in the crystal structure of Cho et al. Prior experience in loop modeling, both in our laboratory as well as elsewhere, has shown that *ab initio* modeling of loops of 10 residues in length may be done with reasonable reliability [12].

We performed rigid body macromolecular docking with these two structures using ZDOCK [13] as described in Methods. This suite of algorithms has performed quite well in the periodically held Critical Assessment of Prediction of Interactions (CAPRI) experiments [14]. Although we performed some limited energy minimization of the final structural model, this approach to modeling the complex excludes the possibility that significant conformational changes (with respect to the *apo* structures) may occur in either the HER2 or the G3 structure or both. Exclusion of such changes is a safe assumption to make for the following reasons: neither the X-ray crystal structure of trastuzumab bound to HER2 nor that of the bispecific antibody bH1 bound to HER2 [15] showed any significant conformational changes in domain 4 of HER2 due to the complexation. Furthermore, an analysis [16] of a number of X-ray crystal structures of DARPins bound to different proteins did not show any significant conformational changes in the DARPin structure. The grid size that we used in the docking translates to a grid spacing of 1.2 Å, which is a sufficiently fine resolution for the docking, and at the same time implicitly allows for some conformational 'flexibility' during the docking.

Numerous protein-protein docking studies over the past few years, including the CAPRI experiments, have shown that more accurate results are produced by using existing structural biological and biochemical experimental information to guide and filter the computational results [17]. Experimentally determined structures of complexes of DARPins with other proteins show that the concave face of the DARPin structure is used in binding the target [16]. This is consistent with expectations from the design [6] as this face is randomized and amino acids mediating tight binding are selected by ribosome display or phage display [7,18]. In DARPins, the "constant" convex face, distal to the randomized and selected concave face, is characterized by the presence of a number of acidic amino acid residues, i.e. Glu 61, Glu 64, Glu 97, Asp 127, and Glu 130. Hence, in our computational docking, we required that none of these acidic residues would be present in the interacting surface of the ZDOCK docking solutions, i.e. such docked solutions were 'blocked out'. The top 2000 docked solutions produced by this protocol were then scored and re-ranked by the secondary scoring function ZRANK [19]. The top ranked 20 solutions from this scoring step were selected for further analysis. This analysis consisted of diverse computational metrics as well as visual examination.

During the formation of a complex between two proteins, it can be reasonably expected that favorable interactions between the two molecules would be maximized, i.e. the thermodynamically most stable complex would be that with the optimum interaction energy. In protein-protein interactions this is largely achieved by maximizing the shape complementarity, and hence maximizing favorable van der Waals interactions between the two proteins. For this reason, we chose the total interaction energy (IE) and shape complementarity (Sc) between the two proteins as the primary metrics to select the 'best' solution from the top 20 ZRANKed solutions. The empirical force field FoldX [20] was used to evaluate IE. The FoldX force field contains parameters derived from experimental data, and had been developed for the purpose of evaluating the effects of mutations on protein and protein-protein complex stability in a rapid and accurate manner. We used the metric developed by Lawrence and Colman [21] to measure Sc at the interface of each of the top ranked solutions. This metric is easy to compute and was found by the developers to distinguish between different classes of protein-protein complexes. Table 1 lists the computed IE and Sc values for each of the top ranked 20 solutions.

On the basis of these metrics, we selected ZDOCK solution #45 as the optimal solution since it had both the highest shape complementarity (0.748) as well as the highest interaction energy (-19.37 kcal mol^{-1}) between the two protein components. While solutions #1 and #136 also have Sc greater than 0.7, visualizing these two solutions made it apparent that G3 in these instances was binding to the far C-terminal region of HER2 domain 4, such that their orientation made clashes with the cell membrane likely. We also considered the possibility of solution #195, which had the second highest interaction energy of -18.66 kcal mol^{-1}.

Two more metrics were considered in making the final decision: One was RPScore [22], which uses an empirically derived (from statistical analysis of non-homologous interfaces in the Protein Data Bank) amino acid residue pair potential matrix and gives the likelihood of the occurrence of the given residue pairs across the interface. The other was EC, the electrostatic complementarity at the interface [23] of the complex, computed by solving the linear Poisson-Boltzmann equation at the interface surfaces. These calculations gave a RPScore value of +2.40 and an EC (Pearson)

Table 1. Top ZRANKed docking solutions and their computed metrics shape complementarity (Sc) and interaction energy (IE).

ZRANK #	ZDOCK solution #	Sc	IE (kcal mol^{-1})
1	1698	0.425	−6.35
2	1	0.704	−15.40
3	566	0.663	−8.51
4	**45**[a]	**0.748**	**−19.37**
5	431	0.668	−3.61
6	20	0.673	−14.29
7	1094	0.414	−3.72
8	41	0.672	−13.46
9	380	0.658	−10.42
10	136	0.710	−13.33
11	240	0.400	−0.99
12	88	0.444	−10.98
13	21	0.520	−15.42
14	24	0.557	−13.65
15	1235	0.492	−8.29
16	268	0.386	−3.19
17	6	0.610	−15.75
18	195	0.550	−18.66
19	491	0.365	−6.15
20	8	0.529	−12.72

[a]This ZDOCK solution was selected as the optimal or preferred solution for the structural model of the G3 - HER2 complex.

doi:10.1371/journal.pone.0059163.t001

value of +0.35 for the solution #45 while for solution #195 these values were +1.80 and +0.29, respectively. These additional metrics confirmed our selection of solution #45 as the preferred solution of the structure of the complex. (We note here that using EC as a metric for filtering docked solutions in general is impracticable as this calculation is very compute-intensive in nature). This structure was then further refined to the final model (see Text S1 for the coordinates of this model in Protein Data Bank format) by performing a limited amount of constrained energy minimization as described in Methods.

Analysis of the Structural Model

The resultant three-dimensional atomic structure of the complete (all four domains) HER2 ectodomain – G3 complex is shown in Figure 1 in a molecular surface representation. (This was obtained by superimposing our computational structural model with the HER2 crystal structure of Cho et al. [4]). Figure 1 also depicts the structure of trastuzumab bound to HER2 (as given by the X-ray crystal structure of Cho et al. [4]) superimposed on the structural model of the complex. While the HER2 epitopes for the DARPin G3 and trastuzumab are adjacent and very close to each other, they do not overlap, in agreement with the experimental observation that trastuzumab and G3 binding to HER2 are not competitive with each other. It can also be seen that G3 does not make any contacts with HER2 domains 1–3 (in agreement with experimental observations), despite the fact that the latter were not considered at all by our modeling of the complex.

The interface between HER2 domain 4 and G3 buries 961.8 Å^2 of total surface area. Figure 2 depicts the interactions between HER2 and G3 present at the interface in a LigPlot figure [24]. With the exception of a backbone hydrogen bond between Ala 535 of HER2 and Asn 123 of G3, all the interactions are of van der Waals in nature. The largest number of interactions across the interface are by the HER2 amino acid residues Phe 555 (with G3 amino acid residues Ile 79, Phe 81, Phe 112, and Ile 119), Val 552 (with G3 residues Phe 81, Leu 86, and Phe 89), Ser 551 (with G3 residues Asp 77, Ala 78, and Ile 79), Val 563 (with G3 residues Ile 79 and Phe 112), Gly 550 (with G3 residues Tyr 46 and Leu 48), and Leu 525 (with G3 residues Tyr 52 and Ala 56). We note that of the interacting residues depicted in Figure 2, a relatively large number of residues on the part of G3, and a relatively small number of residues on the part of HER2, are aromatic. This characteristic of DARPin-antigen complexes has been commented on previously [6,7,16], and especially exposed Tyr residues are well-known for facilitating protein-protein interactions in antibodies and other complexes [25]. Five of the G3 interacting residues are from the first ankyrin repeat, six residues are from the second repeat, and three residues are from the C-cap region while none are from the N-cap region. The interacting G3 amino acid residues Tyr 46, Leu 48, Ala 56, His 57, Ala 78, Ile 79, Phe 81, and Phe 89 are all at randomized positions on the DARPin.

Validation of the Structural Model

To validate our structural model of the HER2-G3 complex we mutated HER2 amino acid residues at the interface predicted by the model structure to make important interactions and stabilize the complex. We chose to mutate to alanine the HER2 amino acid residues Leu 525, Ser 551, Val 552, and Phe 555. According to our structural model each of these residues makes interactions with several G3 amino acids at the interface which are primarily van der Waals in nature. Hence mutating these residues to alanine would be expected to have a detrimental effect on G3-binding. These expectations were further supported by analyzing the complex structural model with the DrugScore^{PPI} [26] web server, which predicted that the Leu 525→Ala, Ser 551→Ala, Val 552→Ala, and Phe 555→Ala mutations should decrease the binding free energy by 0.87, 0.6, 1.92, and 0.77 kcal mol^{-1}, respectively. DrugScore^{PPI} is a knowledge-based scoring function for computational alanine scanning, derived from experimental structures of complexes and alanine scanning results. Finally, we utilized PROSA [27] to estimate whether the proposed mutations in the HER2 structure were stabilizing or destabilizing. PROSA is most frequently used to assess the quality of structural models of proteins. The computation using the knowledge-based potentials in PROSA, derived from 1352 high-resolution X-ray structures of proteins, concluded that the mutations Leu 525→Ala and Phe 555→Ala should be stabilizing to the HER2 protein structure while the mutations Ser 551→Ala and Val 552→Ala would not cause any significant changes to the stability. Since none of these amino acid residues are part of the epitope for trastuzumab, we anticipated that the introduction of alanine mutations at each position should not affect trastuzumab binding to the mutant HER2 isoforms.

Site-directed mutagenesis was used to introduce the selected mutations into a mammalian expression vector encoding residues 1–623 of the mature extracellular domain of HER2 and incorporating a C-terminal Flag tag. The introduction of the mutations had no effect on the expression yield and secretion of soluble HER2, established by western blotting using an anti-Flag monoclonal antibody on immune blotted cell culture supernatants derived from HEK-293 T cells transiently transfected with

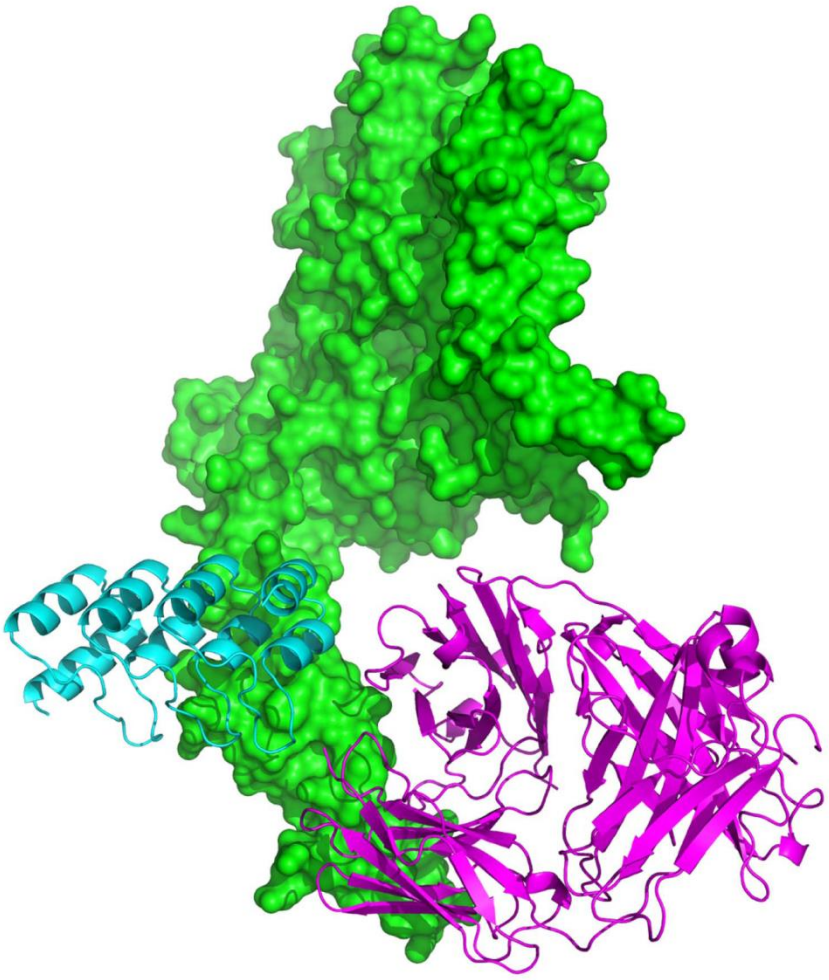

Figure 1. Structural model of the DARPin G3 (cyan) in complex with the human epidermal growth factor receptor 2 HER2 (green). In magenta the structure of trastuzumab Fab bound to HER2 is shown superimposed on the G3-HER2 complex.
doi:10.1371/journal.pone.0059163.g001

plasmid vectors encoding either wild-type or mutant HER2 isoforms (data not shown). Purified recombinant HER2 was isolated from supernatants of scaled-up transiently transfected cultures of HEK-293F cells by immunoaffinity chromatography.

Surface Plasmon Resonance

Surface Plasmon Resonance (SPR) was utilized for the kinetic interaction analyses of the HER2 wild type and mutant constructs. A concentration series of each HER2 mutant was injected over chip surfaces coated with either DARPin G3 or trastuzumab. Binding sensorgrams shown in Figure 3 and the corresponding binding rate parameters and overall affinity estimates listed in Table 2 clearly indicated that none of the introduced alanine mutations affected the binding of HER2 to immobilized trastuzumab. This provided further evidence that none of these mutations compromised structural integrity of the HER2 protein.

DARPin G3 has been analyzed in SPR using both BIAcore [9] and ProteOn instruments (Nagy-Davidescu and Plückthun, unpublished). In many repeated measurements K_D values of 90–100 pM were obtained under all conditions, and this is consistent with measurements on cells as well [1]. For these previous SPR measurements, HER2 was coupled to the sensor, since amine coupling of the DARPin may interfere with the HER2 interaction of this very small protein. Indeed, a 30-fold lower affinity was observed here when amine-coupling the wild type DARPin G3 (Table 2). However, since only relative affinities of HER2 mutants were needed, this can still be used for comparisons.

More importantly, when compared with HER2 wild-type, estimated binding parameters for interactions of the HER2 mutants with DARPin G3 showed very clear differences. Thus, the Val 552→Ala mutation generated the most significant difference of the four mutant constructs tested with the measured affinity being more than 100-fold weaker. Similarly, Leu 525→Ala and Phe 555→Ala were also shown to significantly affect the binding to G3 DARPin resulting in an 80-fold and 63-fold reduction in affinity, respectively. The Ser 551→Ala mutation proved to change the binding least, generating only a 4-fold reduction in affinity. In all four cases the dissociation rate constant (k_d) was most significantly affected and corresponded with the overall affinity. In contrast, the association rate constant (k_a) was

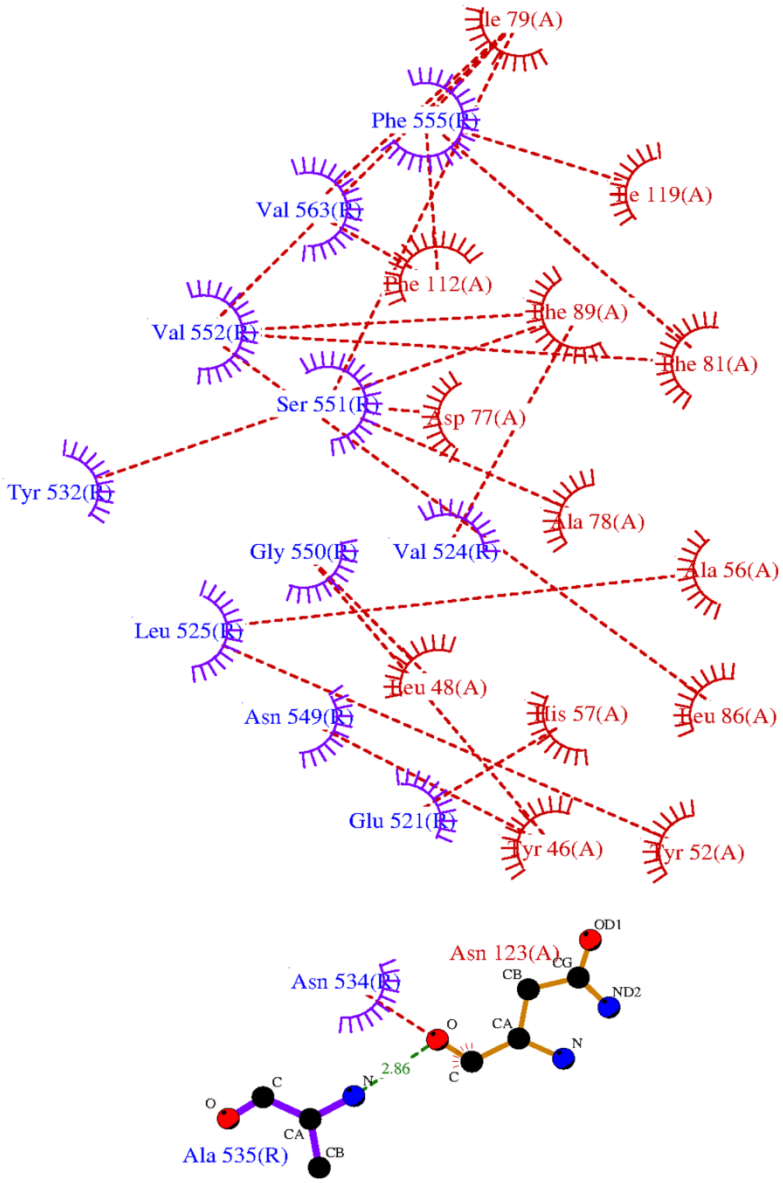

Figure 2. LigPlot diagram of all G3 (red) - HER2 (blue) residue interactions in the model.
doi:10.1371/journal.pone.0059163.g002

little affected, and it typically falls in a narrow window for protein-protein interactions [28] as it is mainly influenced by translational and rotational diffusion, which was little affected by the mutations.

Structural Comparison with the X-ray Crystallographic Structure

During the preparation of this manuscript the X-ray crystallographic structure of the complex between H10-2-G3 and a construct of HER2 domain 4 was solved at a resolution of 2.65 Å (C. Jost et al., submitted). After obtaining the coordinates of the crystal structure (PDB id: 4HRN), we compared the structure with that of the computational model.

The X-ray crystal structure has two complex molecules in the asymmetric unit with each consisting of the complex between the DARPin H10-2-G3 (chain A with residues #13–133 and chain B with residues #13–135) and HER2 (chain C with residues #509–579, and chain D with residues #509–578). Thus we shall refer to the 2 complexes in the crystal structure as 'ADxray' and 'BCxray'. Superimposing the backbone atoms of the G3 residues #13–133 and HER2 residues #509–578 of ADxray and BCxray on the corresponding atoms of the computational model (hereafter referred to as the 'model') gives a root mean square deviation (rmsd) value of 1.14 Å between ADxray and model and a value of 0.84 Å between BCxray and model. In the more detailed

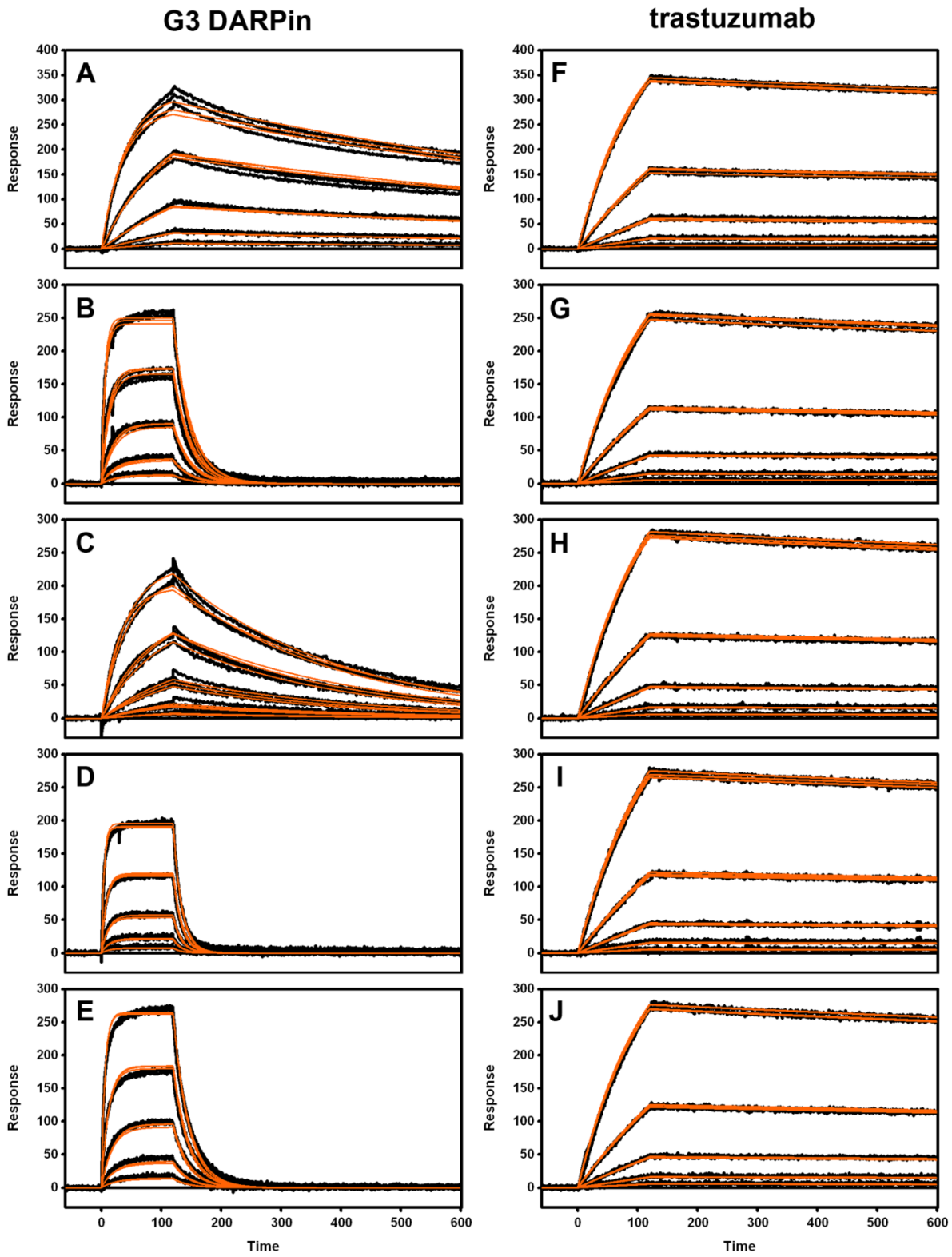
G3 DARPin
trastuzumab
A
B
C
D
E
F
G
H
I
J
Response
Time
0
100
200
300
400
500
600

Figure 3. SPR binding sensorgrams for the interaction of HER2 wild type and mutant proteins with immobilized DARPin G3 (left panels) and trastuzumab (right panels). Injected analyte (HER2) protein construct: wild type (A and F), Leu 525→Ala (B and G), Ser 551→Ala (C and H), Val 552→Ala (D and I) and Phe 555→Ala (E and J). Typically, injected HER 2 protein concentrations were diluted three-fold in running buffer from 81 nM to 1 nM except in B, D and E where the concentration series were diluted from 729 nM down to 9 nM. Overlayed triplicate binding responses are shown (black lines). Binding data were globally fit to a simple 1:1 interaction model (orange lines).
doi:10.1371/journal.pone.0059163.g003

comparisons discussed below we shall restrict ourselves to the comparison between the model and BCxray. Figure 4 depicts the model superimposed (as described above) on BCxray.

The CAPRI experiments [14] use a number of standard metrics to assess the structural models that are submitted. These include f_{nat} (the fraction of native contacts present in the model), $f_{non\text{-}nat}$ (the fraction of non-native contacts), L-RMSD (the ligand rmsd after the receptor, defined as the larger of the two proteins, is superimposed), and I-RMSD (the rmsd for the interface residues). The interface in BCxray (analyzed with PDBsum [29]) consists of amino acid residues Tyr 46, Leu 48, Tyr 52, Ala 56, His 57, Asp 77, Ala 78, Ile 79, Phe 81, Phe 89, Ile 90, His 92, Phe 112, Gly 122, Asn 123, and Gly 124 of the DARPin, and residues Phe 512, Glu 521, Leu 525, Gln 526, Tyr 532, Val 533, Asn 534, Ala 535, Asp 549, Gly 550, Ser 551, Cys 554, Phe 555, and Val 563 of HER2. In the complex BCxray, these interface residues contribute to a total of 26 residue-residue contacts, out of which 24 are present in the model. This gives a f_{nat} value of 0.92 for the model. The $f_{non\text{-}nat}$ value for the model is 0.47. The I-RMSD value (i.e. for the interface residues) is 0.92 Å, while the L-RMSD value for the model is 1.84 Å. (We note here that in deriving the L-RMSD value we followed the CAPRI convention and treated the HER2 chains as the 'ligand'. If instead, we take HER2 as the 'receptor' the 'L-RMSD' value is 1.38 Å.) The CAPRI assessment classifies models with $f_{nat} \geq 0.5$ *and* (L_RMSD ≤ 1.0 *or* I_RMSD ≤ 1.0) as 'highly accurate' models. Accordingly, this model can be classed as 'highly accurate'. This however, should also be tempered by possible 'false positive' interactions indicated by the $f_{non\text{-}nat}$ value, likely caused by the energy minimization in the final refinement.

In summary, we have, in this work, constructed a three-dimensional atomic model of the complex between HER2 and the DARPin G3 using computational methodologies and metrics. It utilized the *apo* crystal structures of HER2 and the DARPin as well as information on the binding face of the DARPin. The model was tested with HER2 mutants selected from the structurally characterized interface of the complex, showing reduced binding to G3. The work described here not only resulted in a structural model of reasonably good accuracy for the interaction between HER2 and G3, but also provided a validated examination of the capabilities of the computational methodologies.

Materials and Methods

Modeling

Preparation of the starting structures. The starting structures for the protein-protein docking were derived from the X-ray crystal structure of HER2 (i.e. ErbB2) in complex with trastuzumab [4] (PDB id 1N8Z), and the X-ray crystal structure of the DARPin H10-2-G3 [9] (PDB id 2JAB), referred to as 'G3'. Chain A (residues # 12–135) of the G3 structure was used in the modeling. Only domain 4 of HER2 was utilized in the docking calculations. In this domain, the atomic coordinates of the residues # 581–590 are missing due to disorder. Hence, prior to the macromolecular docking, the structure of this loop was modeled using Modeller v. 7.6 [30]. From the 20 loops constructed for this region, model #12, the one with the lowest value of $-\log_e$PDF (where PDF is the molecular probability density function), was selected as the optimal model.

Table 2. SPR binding parameters for HER2 constructs binding to the DARPin G3 and trastuzumab.

	DARPin G3			
HER2 protein	**$k_a \times 10^5$ ($M^{-1}s^{-1}$)**	**$k_d \times 10^{-3}$ (s^{-1})**	**K_D (nM)**	**fold difference in K_D**
wild-type[a]	3.22±0.20	1.07±0.01	3.3±0.2	1.0
Leu525-Ala	1.49±0.03	39.3±4.2	265±30	79.7
Ser551-Ala	2.85±0.59	3.5±2.1	12.8±3.1	3.8
Val552-Ala	1.69±0.16	64.0±3.7	380±39	114.4
Phe555-Ala	1.84±0.09	38.4±1.0	210±15	63.2
	trastuzumab			
HER2 protein	**$k_a \times 10^5$ ($M^{-1}s^{-1}$)**	**$k_d \times 10^{-4}$ (s^{-1})**	**K_D (nM)**	**fold difference in K_D**
wild-type	1.19±0.09	1.56±0.03	1.31±0.13	1.0
Leu525-Ala	1.04±0.01	1.32±0.05	1.26±0.03	1.0
Ser551-Ala	1.07±0.03	1.47±0.01	1.38±0.04	1.0
Val552-Ala	0.96±0.02	1.28±0.08	1.33±0.06	1.0
Phe555-Ala	1.06±0.01	1.48±0.02	1.39±0.03	1.1

Note 1: The values given are the average values for three separate measurements and the uncertainties represent one standard deviation.
[a]Note 2: About 30-fold higher affinities are obtained when avoiding random amine coupling of this very small DARPin [9,36], (Nagy-Davidescu and Plückthun, unpublished).
doi:10.1371/journal.pone.0059163.t002

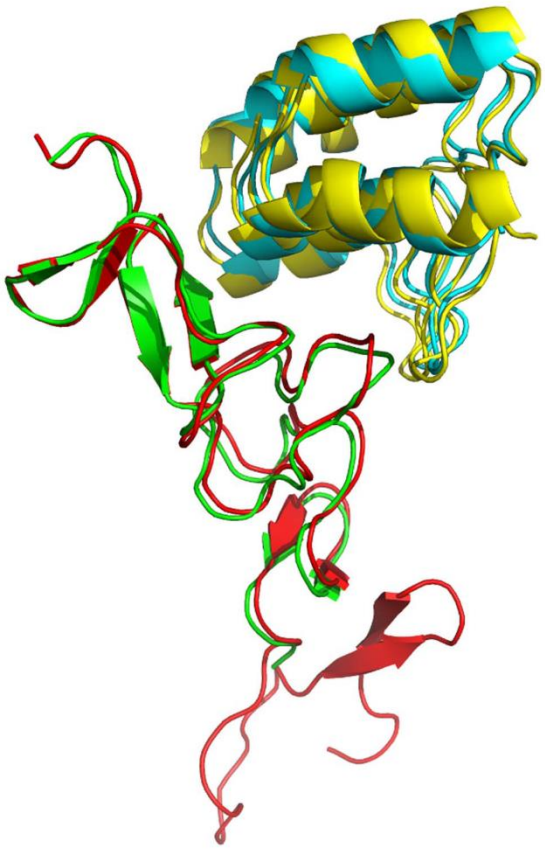

Figure 4. The computational model of the complex superimposed on the B and C chains of the X-ray crystal structure (BCxray). The G3 chains of the model and BCxray are in yellow and cyan, respectively, while the HER2 chains of the model and BCxray are shown in red and green, respectively.
doi:10.1371/journal.pone.0059163.g004

Macromolecular docking. For the docking of these two protein structures we used the macromolecular docking program ZDOCK v. 3.0.1 [13]. ZDOCK is a grid-based rigid body docking algorithm, which discretizes the two proteins (labeled the "receptor" and the "ligand") into grids, and performs global scans of the rotational and translational space of the ligand with respect to the receptor, with each relative orientation scored by a shape complementarity function. In our docking, we designated domain 4 of HER2 as the "receptor" and the DARPin G3 as the "ligand". Our grid size of 128 yielded a grid spacing of 1.2 Å, while the rotational sampling was done with an interval of 6 degrees. The search space for ZDOCK was effectively reduced by requiring that the docking solutions excluded the convex face of G3. This was done by specifying that the amino acid residues Glu 61, Glu 64, Glu 97, Asp 127, and Glu 130 that are on the convex face of G3 be absent from the interacting surface of the ZDOCK docking solutions, i.e. these residues were 'blocked out' during the docking.

The top 2000 docked solutions produced by this protocol were then scored and re-ranked by the secondary scoring function ZRANK [19]. This function is a linear weighted sum of van der Waals, Coulomb, and desolvation energy terms, where the optimal weights had been obtained by training the function on a benchmark set of protein-protein complexes. The top ranked 20 solutions from this step were selected for further analysis.

We used the total interaction energy (IE) and shape complementarity (Sc) between the two proteins as the primary metrics to select the 'best' solution from the top 20 ZRANKed solutions. The empirical force field FoldX [20] was used to evaluate the interaction IE. This force field free energy consists of a linear combination of terms due to van der Waals energy, solvation, hydrogen bonding, Coulomb electrostatics, and entropy changes. We used the metric developed by Lawrence and Colman [21] to measure the shape complementarity Sc at the interface of each of the top ranked solutions.

We also used the computed metrics RPScore and EC in the final choice of the optimal solution. RPScore [22] uses an empirically derived (from statistical analysis of non-homologous interfaces in the Protein Data Bank) amino acid residue pair potential matrix and gives the likelihood of the occurrence of the given residue pairs across the interface. EC, the electrostatic complementarity at the interface [23] of the complex, was computed by solving the linear Poisson-Boltzmann equation at the interface surfaces.

Refinement and analysis of the model. Prior to the structural characterization of the final optimal solution, the selected top solution of the complex structure was further refined by performing a limited amount of constrained energy minimization with the program Discover v. 2.98 within InsightII v.2005 (Accelrys, Inc.). After adding hydrogen atoms to the structure, the energy was first minimized with 500 steps of steepest descents, holding the backbone of HER2 domain 4 fixed and tethering the backbone of G3 with a force constant of 10.0 kcal $Å^{-2}$. Next, 100 steps of steepest descents were performed by tethering the backbone of HER2 domain 4 with a force constant of 5.0 kcal $Å^{-2}$. The CVFF force field was used with a distance-dependant dielectric and no Morse or cross terms in the application of the force field. The resultant structure of the complex was analyzed and the interface between HER2 and G3 was characterized using LigPlot [24].

Molecular and Cell Biology

The mammalian expression vector pME18s.HER2-623, encoding the natural signal peptide and residues 1–623 of the extracellular domain of HER2, and incorporating a C-terminal Flag tag, was used as a template for site-directed mutagenesis. Selected residues were mutated using the QuikChange site-directed mutagenesis protocol (Stratagene) and the mutagenic primer pairs listed in Table S1. The successful incorporation of mutations was confirmed by DNA sequencing.

The culture and transient transfection of human 293 T fibroblasts was performed as previously described [31]. The successful biosynthesis and secretion of wild-type and mutant HER2 isoforms was established by western blotting of culture supernatants using an anti-Flag tag-specific monoclonal antibody. For the purification of recombinant HER2 ectodomain, suspension-adapted cultures (200 ml) of Freestyle 293-F cells (Invitrogen) grown in Freestyle 293 Expression Medium were transiently transfected with plasmid DNA using polyethylenimine (PEI; [32]). Following culture for 7–9 days, supernatants were harvested and recombinant HER2 purified by anti-Flag immunoaffinity chromatography [33].

Surface Plasmon Resonance

All SPR experiments were performed at 25°C using Bio-Rad's ProteOn XPR36 array biosensor [34]. A standard amine-coupling protocol was employed to immobilize G3 DARPin on a GLC chip

surface in 1× HBS-P buffer (10 mM HEPES, 150 mM NaCl, 0.05% (v/v) Tween 20) at a constant flow rate of 30 µl/min. Briefly, with instrumental fluidics oriented in the "vertical" direction, a single lane on the chip surface was activated by a 5-min injection of a freshly prepared mixture consisting of 2.5 mM sulfo-NHS and 10 mM EDC. G3 DARPin solution (15 µg/ml in 10 mM sodium acetate, pH 5.0) was then injected for 5 min and any residual reactive sites deactivated by a final 5-min injection of 1 M ethanolamine (pH 8.5). Approximately 1,200 RU (1 RU = 1 pg of protein/mm^2) of G3 DARPin was coupled using this method. Trastuzumab was captured onto the SPR sensor chip surface using a previously described Protein G' capture method [35]. Briefly, Protein G' (Sigma-Aldrich) was coupled in a single lane on a GLC chip at 2,200 RU using an identical amine coupling method described for G3 DARPin except that Protein G' was injected at 50 µg/ml in 10 mM sodium acetate, pH 4.0. A single injection of trastuzumab at (5 µg/ml, 100 µl/min for 30 sec) in the vertical orientation resulted in a consistent capture of approximately 1,300 RU of protein across entire Protein G' lane. No significant dissociation (drift) of trastuzumab from the Protein G' surface was observed (drift ≤1 RU/600 sec).

The 'One-Shot Kinetics' approach of Bravman et al. [34] was utilized for binding analyses of HER2 proteins. Binding assays were performed in 1× HBS-EBP+ buffer (10 mM HEPES, 150 mM NaCl, 3 mM EDTA, 0.1% [w/v] BSA; 0.05% [v/v] Tween 20) with the instrumental fluidics oriented in "horizontal" direction. Six concentrations of HER2 (including "zero buffer blank") were injected simultaneously over amine-coupled G3 DARPin or Protein G'-captured trastuzumab at 30 µL/min for 120 sec. The dissociation phase was monitored until all of the bound HER2 protein had dissociated from the DARPin-coupled surface. This was possible, since random amine coupling of the DARPin lowered its known K_D of 90–100 pM about 30-fold to 3 nM (Table 2), while the reverse set-up leads to almost no dissociation. In case of the trastuzumab-HER2 complex, complete dissociation was not achievable in a practicable timeframe. Consequently, after each binding cycle, the Protein G' surface was regenerated in the vertical direction with a single injection of 10 mM glycine pH 1.5 (100 µl/min, 18 sec). Trastuzumab was recaptured for any subsequent binding cycles.

All SPR binding data were processed using the Scrubber-Pro software package (www.biologic.com.au). To determine the kinetic rate constants (k_a and k_d) of the binding interactions, binding data were fit globally to a 1:1 interaction model and the ratio of these rate constants (k_d/k_a) yielded the value for the equilibrium dissociation constant (K_D).

Structural Analysis

Structural superimposition and comparison was done with ProFit v. 2.5.3 (A.C.R. Martin, and C.T. Porter, www.bioinf.org.ac.uk/software/profit/) while the interface analysis was performed with PDBsum [29] (www.ebi.ac.uk/pdbsum). Figures 1 and 4 were prepared with PyMol v. 1.5.0.4 (Schrödinger, LLC.).

Supporting Information

Table S1 Oligonucleotide pairs for site-directed mutagenesis of HER2.
(DOCX)

Text S1 Coordinates of the computational model for the G3-HER2 complex in PDB format.
(DOCX)

Acknowledgments

We would like to thank Tram Phan and John Bentley for help with cell culture and protein purification.

Author Contributions

Conceived and designed the experiments: VCE TEA. Performed the experiments: VCE OD LD XX CJ AP TEA. Analyzed the data: VCE OD CJ AP TEA. Contributed reagents/materials/analysis tools: VCE OD XX AP TEA. Wrote the paper: VCE OD CJ AP TEA.

References

1. Ross JS, Fletcher JA (1998) The HER-2/neu oncogene in breast cancer: Prognostic factor, predictive factor, and target for therapy. Stem Cells 16: 413–428.
2. Yarden Y, Sliwkowski MX (2001) Untangling the ErbB signalling network. Nature Reviews Molecular Cell Biology 2: 127–137.
3. Junttila TT, Akita RW, Parsons K, Fields C, Phillips GDL, et al. (2009) Ligand-independent HER2/HER3/PI3K complex is disrupted by trastuzumab and is effectively inhibited by the PI3K inhibitor GDC-0941. Cancer Cell 15: 429–440.
4. Cho HS, Mason K, Ramyar KX, Stanley AM, Gabelli SB, et al. (2003) Structure of the extracellular region of HER2 alone and in complex with the Herceptin Fab. Nature 421: 756–760.
5. Franklin MC, Carey KD, Vajdos FF, Leahy DJ, de Vos AM, et al. (2004) Insights into ErbB signaling from the structure of the ErbB2-pertuzumab complex. Cancer Cell 5: 317–328.
6. Binz HK, Stumpp MT, Forrer P, Amstutz P, Plückthun A (2003) Designing repeat proteins: Well-expressed, soluble and stable proteins from combinatorial libraries of consensus ankyrin repeat proteins. Journal of Molecular Biology 332: 489–503.
7. Binz HK, Amstutz P, Kohl A, Stumpp MT, Briand C, et al. (2004) High-affinity binders selected from designed ankyrin repeat protein libraries. Nature Biotechnology 22: 575–582.
8. Boersma YL, Plückthun A (2011) DARPins and other repeat protein scaffolds: advances in engineering and applications. Current Opinion in Biotechnology 22: 849–857.
9. Zahnd C, Wyler E, Schwenk JM, Steiner D, Lawrence MC, et al. (2007) A designed ankyrin repeat protein evolved to picomolar affinity to Her2. Journal of Molecular Biology 369: 1015–1028.
10. Theurillat JP, Dreier B, Nagy-Davidescu G, Seifert B, Behnke S, et al. (2010) Designed ankyrin repeat proteins: a novel tool for testing epidermal growth factor receptor 2 expression in breast cancer. Modern Pathology 23: 1289–1297.
11. Zahnd C, Kawe M, Stumpp MT, de Pasquale C, Tamaskovic R, et al. (2010) Efficient tumor targeting with high-affinity designed ankyrin repeat proteins: effects of affinity and molecular size. Cancer Research 70: 1595–1605.
12. Choi Y, Deane CM (2010) FREAD revisited: Accurate loop structure prediction using a database search algorithm. Proteins: Structure, Function, and Bioinformatics 78: 1431–1440.
13. Chen R, Li L, Weng ZP (2003) ZDOCK: An initial-stage protein-docking algorithm. Proteins-Structure Function and Genetics 52: 80–87.
14. Lensink MF, Mendez R, Wodak SJ (2007) Docking and scoring protein complexes: CAPRI 3rd edition. Proteins-Structure Function and Bioinformatics 69: 704–718.
15. Bostrom J, Yu SF, Kan D, Appleton BA, Lee CV, et al. (2009) Variants of the antibody Herceptin that interact with HER2 and VEGF at the antigen binding site. Science 323: 1610–1614.
16. Sennhauser G, Grütter MG (2008) Chaperone-assisted crystallography with DARPins. Structure 16: 1443–1453.
17. Mendez R, Leplae R, Lensink MF, Wodak SJ (2005) Assessment of CAPRI predictions in rounds 3–5 shows progress in docking procedures. Proteins-Structure Function and Bioinformatics 60: 150–169.
18. Steiner D, Forrer P, Plückthun A (2008) Efficient selection of DARPins with sub-nanomolar affinities using SRP phage display. Journal of Molecular Biology 382: 1211–1227.
19. Pierce B, Weng ZP (2007) ZRANK: Reranking protein docking predictions with an optimized energy function. Proteins-Structure Function and Bioinformatics 67: 1078–1086.
20. Schymkowitz J, Borg J, Stricher F, Nys R, Rousseau F, et al. (2005) The FoldX web server: an online force field. Nucleic Acids Research 33: W382–W388.
21. Lawrence MC, Colman PM (1993) Shape complementarity at protein-protein interfaces. Journal of Molecular Biology 234: 946–950.
22. Moont G, Gabb HA, Sternberg MJE (1999) Use of pair potentials across protein interfaces in screening predicted docked complexes. Proteins-Structure Function and Genetics 35: 364–373.

23. McCoy AJ, Epa VC, Colman PM (1997) Electrostatic complementarity at protein/protein interfaces. Journal of Molecular Biology 268: 570–584.
24. Wallace AC, Laskowski RA, Thornton JM (1995) Ligplot - a program to generate schematic diagrams of protein ligand interactions. Protein Engineering 8: 127–134.
25. Jones S, Thornton JM (1996) Principles of protein-protein interactions. Proceedings of the National Academy of Sciences of the United States of America 93: 13–20.
26. Kruger DM, Gohlke H (2010) DrugScore(PPI) webserver: fast and accurate in silico alanine scanning for scoring protein-protein interactions. Nucleic Acids Research 38: W480–W486.
27. Wiederstein M, Sippl MJ (2005) Protein sequence randomization: Efficient estimation of protein stability using knowledge-based potentials. Journal of Molecular Biology 345: 1199–1212.
28. Northrup SH, Erickson HP (1992) Kinetics of protein protein association explained by Brownian dynamics computer-simulation. Proceedings of the National Academy of Sciences of the United States of America 89: 3338–3342.
29. Laskowski RA (2009) PDBsum new things. Nucleic Acids Research 37: D355–D359.
30. Eswar N, Webb B, Marti-Renom MA, Madhusudhan MS, Eramian D, et al. (2006) Comparative protein structure modeling using Modeller. Current Protocols in Bioinformatics/editoral board, Andreas D Baxevanis et al. Chapter 5: Unit 5.6.
31. Adams TE, Koziolek EJ, Hoyne PH, Bentley JD, Lu L, et al. (2009) A truncated soluble epidermal growth factor receptor-Fc fusion ligand trap displays anti-tumour activity in vivo. Growth Factors 27: 141–154.
32. Durocher Y, Perret S, Kamen A (2002) High-level and high-throughput recombinant protein production by transient transfection of suspension-growing human 293-EBNA1 cells. Nucleic Acids Research 30.
33. Garrett TPJ, McKern NM, Lou MZ, Elleman TC, Adams TE, et al. (2003) The crystal structure of a truncated ErbB2 ectodomain reveals an active conformation, poised to interact with other ErbB receptors. Molecular Cell 11: 495–505.
34. Bravman T, Bronner V, Lavie K, Notcovich A, Papalia GA, et al. (2006) Exploring "one-shot" kinetics and small molecule analysis using the ProteOn XPR36 array biosensor. Analytical Biochemistry 358: 281–288.
35. Nahshol O, Bronner V, Notcovich A, Rubrecht L, Laune D, et al. (2008) Parallel kinetic analysis and affinity determination of hundreds of monoclonal antibodies using the ProteOn XPR36. Analytical Biochemistry 383: 52–60.

Appendix 5

1 Abbreviations 260

2 Relevant *E. coli* strains 262

2.1 *E. coli* XL1-blue 262

2.2 *E. coli* DH10 EmBacY 262

3 Curriculum vitae 264

1 Abbreviations

2YT	2x concentrated yeast tryptone medium
aa	amino acid
AP	alkaline phosphatase
bp	base pairs
bla	beta lactamase
BSA	bovine serum albumin
CAPS	N-cyclohexyl-3-aminopropanesulfonic acid
CDR	complementarity determining region
cds	coding sequence / coding sequences
DARPin	designed ankyrin repeat protein
DPS	dithiodipyridine
DTT	dithiothreitol
ECD	extracellular domain
E. coli	*Escherichia coli*
EDTA	ethylenediaminetetraacetic acid
ELISA	enzyme-linked immunosorbent assay
FCS	fetal calf serum
GOI	gene of interest
GSH	glutathione
GSSG	glutathione disulfide
HEPES	4-(2-hydroxyethyl)-1-piperazineethanesulfonic acid
HER	human epidermal growth factor receptor
IB	immunoblot
IEX	ion exchange chromatography
Ig	immunoglobulin
IMAC	immobilized metal ion affinity chromatography
IPTG	isopropyl-β-D-thiogalactoside
K_D	equilibrium dissociation constant
kDa	kiloDalton
k_{off}	dissociation rate constant
k_{on}	association rate constant
mAb	monoclonal antibody
MBP	maltose binding protein
MES	2-(N-morpholino)ethanesulfonic acid
MFI	median fluorescence intensity

MMP	matrix metalloproteinase
MOPS	3-(N-morpholino)propanesulfonic acid
MW	molecular weight
Ni-NTA	nickel-nitrilotriacetic acid
OD	optical density
PBS	phosphate buffered saline
PCR	polymerase chain reaction
pD	protein D from phage lambda
PD	phage display
PDB	Protein Data Bank
PDB ID	Protein Data Bank identification number
PEG	polyethylene glycol
PNK	polynucleotide kinase
pNPP	4-nitrophenyl phosphate disodium salt
POI	protein of interest
PTO	phosphorothioate
RD	ribosome display
RT	room temperature
scFv	single-chain fragment variable
SDS-PAGE	sodium dodecylsulfate polyacrylamide gel electrophoresis
SEC	size exclusion chromatography
Sf9	*Spodoptera frugiperda* (clonal isolate cell line)
SILAC	stable isotope labelling by amino acid in cell culture
SPR	surface plasmon resonance
TBS	TRIS buffered saline
TM	transmembrane helix
TRIS	tris(hydroxymethyl)aminomethane
X-gal	5-bromo-4-chloro-indolyl-β-D-galactopyranoside
XTT	2,3-bis-(2-methoxy-4-nitro-5-sulfophenyl)-2H-tetrazolium-5-carboxanilide

2 Relevant *E. coli* strains

2.1 *E. coli* XL1-blue

This strain was used for cloning and expression of DARPins and DARPin-constructs, for cloning and expression of HER2 domains for *in vitro* refolding from IBs, and for preliminary cloning procedures of HER2 domains lateron expressed in Sf9 insect cells.

XL1-blue provides $lacI^q$ in trans and is thus suitable for expression of DARPins coded on pQE30_ss (pDST67) that does not have $lacI^q$ in cis. Chemocompetent cells were prepared according to a modified Inoue protocol.

Genotype: *endA1 gyrA96(*nal^R*) thi-1 recA1 relA1 lac glnV44 F'[::Tn10 proAB*$^+$ *lacI*^{q}*Δ(lacZ)M15] hsdR17(*r_K^- m_K^+*)*

2.2 *E. coli* DH10 EmBacY

This strain was used for the production of bacmids through transfection with pFLmLIC donor plasmids carrying the coding sequences for the HER2 domains intended for Sf9 expression. The strain is an *E. coli* DH10 derivative that carries the EmBacY baculoviral genome, an approx. 130 kb derivative of the *Autographa californica* nucleopolyhedrovirus (AcMNPV) genome. This bacmid has been genetically engineered for improved protein production and reduced protein degradation and contains a transposition acceptor site (mini-attTn7) for accepting donor DNA from pFLmLIC. The bacmid possesses the F replicon that keeps the plasmid copy number at 1.

The modified viral genome carries the coding sequences for YFP (as reporter), Kan^R, $Gent^R$ and Cml^R. It is further deficient in the viral genes *v-cath* and *chiA* (that code for the viral protease V-CATH and the viral chitinase chiA, repectively). The Tn7 attachment site is located within a *LacZα* gene; insertion of Tn7 elements from pFlmLIC derivatives therefore produces a white phenotype when plated on agar containing X-gal and IPTG. The Tn7 transposition functions are provided *in trans* by a helper plasmid (pMON7124 with Tet^R) encoding for the required transposase in *E. coli* DH10 EmBacY.

3 Curriculum vitae

Personal data

Name:	Jost
First Name:	Christian
Date of birth:	October 21st, 1982
Place of birth:	Giessen, Germany
Nationality:	German

Education:

09/2007 – spring 2013	Ph.D. studies in the laboratory of Prof. Dr. A. Plückthun, Institute of Biochemistry, University of Zürich, Switzerland (Title: "Tumor targeting with Designed Ankyrin Repeat Proteins")
10/2006 – 05/2007	Diploma thesis in the laboratory of Prof. Dr. A. Plückthun, Institute of Biochemistry, University of Zürich, Switzerland (Title: "Protein Engineering: Designed Ankyrin Repeat Proteins directed against human epidermal growth factor receptors")
10/2004 – 09/2006	postgraduate studies of biochemistry ("Hauptstudium") at the University of Witten/Herdecke, Germany
10/2002 - 08/2004	undergraduate studies of biology („Grundstudium") at the Justus-Liebig-University of Giessen, Germany
07/2002	„Abitur" at the Christian-Wirth-Schule Usingen, Germany

Practical training

07/2007	participation in the two-week International Summer School "Pathogen-Host-Interplay" at the Center of Infection Biology, Berlin, Germany
01/2006 – 04/2006	research project at the Max-Planck-Institute of Molecular Physiology, Dortmund, Germany, Dr. S. Eschenburg (Preparatory work for interaction studies on Cardinal and different members of the Nalp-family)
10/2005 – 12/2005	research project at the Institute of Virology, University of Witten/Herdecke, Prof. M. Wolff (Studies on modulation of PI3K-Akt-signalling in the course of VZV-infection)
07/2005 – 09/2005	research project in the Department of biochemistry, University of Cambridge, UK, Dr. M. Carrington (Characterization-studies on a VSG of *T.brucei*)
05/2005 – 07/2005	research project at the Institute of Cell Biology, University of Witten/Herdecke, Prof. H.J. Lipps (Work on developmentally regulated genes during macronuclear differentiation in *S.lemnae*)
04/2005 – 05/2005	research project at the Institute of Phytochemistry, University of Witten/Herdecke, Prof. U. Pfüller (Purification of different viscotoxine species)
03/2004 - 04/2004	research assistant at the University of Giessen, Department of medical virology, Dr. C. G. Schüttler
08/2002 - 09/2004	temporary job in a pet shop („aqua natura“, Leun, Germany)